The Influence of Dietary Nutrients on Intrahepatocellular Lipid Metabolism



Eloise Cross

Department: Oxford Centre for Diabetes, Endocrinology and Metabolism

University of Oxford

A thesis submitted for the degree of

Doctor of Philosophy

Michaelmas 2023

Acknowledgements

Thank-you to the Radcliffe Department of Medicine, for funding this studentship, and to the department of OCDEM to giving me a research base.

To my three supervisors, thank you for your continual support and for giving me this opportunity to carry out this work. Firstly, to Professor Leanne Hodson, a huge thank you, for supporting me every step of the way, and showing me what exceptional supervising looks like. For being there to celebrate the process, tell me when I need to pull my socks up and badger me into writing. To Dr Fabio Sanna, for helping me find my feet in the lab and getting this project up and running. To Professor Fredrik Karpe, for your support and guidance throughout this project.

I would also like to thank all past and present members of the Hodson group. I have immensely enjoyed my time within the group, surrounded by such helpful and hardworking individuals. Specifically, I would like to thank the members of the hepatocyte subgroup; Dr Shilpa Nagarajan, Felix Westcott and the others who have joined throughout the years for your insights and collaborations. To Elspeth Johnson, thank you for fielding the endless number of questions that have come your way over the last few years, amazingly always with a smile. To the wider OXLIP/MRG group, thank you for the support over the last few years.

To my fellow students, in the fellows room, thank you. Specifically to Ismael and Maria, for providing some sanity during the lockdowns where the office was the only allowed indoor space, for the post-work catch-ups, the Friday fish and chips and laughs. To the others, for making the office a nice place to be, albeit sometimes with a few extra distractions.

It would be amiss to not mention the many people outside of the lab. Completing this DPhil throughout the pandemic has not been so easy. So an extra thanks to my housemates at Ridgefield Road for the insanity sanity. I'll treasure the memories of babyfood, berry costumes and bust-bakes forever. To my DPhil funding friends, you're all incredible and I'm proud to call you my friends.

One of my bigger thanks goes out to the Oxford University Triathlon club, a collection of some of the most kind and helpful people and I know I've found many friends for life. Specific thanks goes out to those who have been on the committee alongside me for both the help and the friendship; so Jonny, Emma, Justin, Jenny, thank-you. OUTriC has been both a challenging experience but at the same time a home. I've learnt so much and I will be forever grateful for the new experiences and sport you've introduced me to.

Finally, to my parents, who have given me every opportunity to find my own path in life. I would not have gotten here without your unwavering support. Specifically, to Mum, for every time you've dropped everything and come running to Oxford to help me with my latest crisis, thank you. To Dad, for not quite managing to talk me out of this PhD. To Izzy, for never letting my pedestal get too large.

0.1 Declaration

I hereby declare that no part of this thesis has been submitted for any degree at this or any other university. The work presented herein is entirely my own except where stated in the text and below:

- Size exclusion chromatography protocols were carried out by Dr Camilla Pramfalk (Karolinska Institutet).
- RNA sequencing was completed by Novogene.
- Participant plasma samples were collected by nurses Sarah White and Diana Mantripp of OCDEM.

Supervision for the work was provided by Professor Leanne Hodson, Dr Fabio Sanna and Professor Fredrik Karpe and funding was provided by the University of Oxford, Radcliffe Department of Medicine Scholarship.

0.1.1 The impact of COVID-19 on my work

The period of my DPhil straddled the lockdowns associated with the COVID-19 pandemic and my work was affected as a result of that, despite the eventual award of a three month extension. During the required lockdowns, access to the laboratory was prohibited and consequently laboratory work was delayed.

Abstract

Pathological accumulation of intrahepatocellular triacylglycerol (IHTAG) is the first stage of metabolic dysfunction-associated steatotic liver disease (MASLD). Intervention studies have shown that diets rich in saturated fatty acids (SFA) compared to unsaturated fatty acids (UNSFA) increase IHTAG accumulation to a greater extent. Studying the underlying metabolic mechanisms driving these differences in IHTAG accumulation *in vivo* in humans remains challenging therefore, *in vitro* cellular models which recapitulate the effects of dietary alterations in hepatic metabolism are needed.

Huh7 cells, cultured with fatty acid (FA) treatments, enriched in either SFA or MUFA and given at either a high (800µM) or low (200µM) concentration, were used in combination with a low glucose (5.5mM) media to explore hepatic lipid metabolism: IHTAG composition reflected that of the provided treatments suggesting a lack of preferential uptake. Consequently, there were notable disparities in glucose production and cellular oxidation. Additionally, differences were seen in lipid droplet morphology with Huh7 cells treated with SFA accumulating small homogenous lipid droplets, compared to those treated with UNSFA which accumulated a heterogeneous pattern of large and small lipid droplets.

The response of primary human hepatocytes (PHH) to FA treatments enriched in SFA or UNSFA was also investigated, however, these cells proved challenging to study as results were confounded by pre-existing IHTAG accumulation and blunted metabolic responses. RNA sequencing showed divergence in the differentially expressed genes between Huh7 and PHH cells, however, both cells implicated SFA enriched treatment as being the more detrimental of the two FA compositions. Overall, the addition of FA compared to controls treated with no-fat showed a greater effect on the transcriptional profile when compared to FA composition or concentration changes in Huh7 cells and PHH.

Lifestyle changes are the primary suggested treatment for patients presenting with MASLD and involve the changing of both dietary quantity and composition. To attempt to understand these changes at an cellular level, cellular responses to changes in either the provided FA concentration or composition were analysed. Although Huh7 cells continued to non-selectively take up the FA provided, despite

significant previous FA accrual, results showed blunted responses to hormonal stimulation. Of interest, those Huh7 cells previous treated with FA enriched in SFA, which had displayed small homogeneous lipid droplet patterns, when treated with FA enriched in UNSFA took on the morphology of those cells treated with UNSFA for the whole treatment period.

Human derived TAG-rich remnants, an under-studied source of hepatic IHTAG, enriched in either SFA or UNSFA were labelled using a novel protocol with stable isotopes and Huh7 cells were found to take up these remnants non-selectively. TAG-rich remnants FA composition significantly effected glucose uptake and urea production although further work is required to explore the intrahepatic metabolic changes.

Overall, I developed physiologically-relevant models of hepatocellular metabolism and steatosis, reflecting differences in dietary composition. Data showed that although FA composition did not alter IHTAG accumulation, it did alter a number of metabolic pathways, including oxidation, glucose handling, and significantly it had a strong effect on lipid droplet morphology.

Contents

Acknowledgements **ii**
0.1 Declaration . . . iv
0.1.1 The impact of COVID-19 on my work . . . iv

Abstract **v**

List of Figures **xii**

List of Tables **xviii**

List of Abbreviations **xix**

1 Introduction **1**
1.1 Overview of the liver . . . 1
1.2 MASLD and risk of metabolic disease . . . 4
1.3 Fat metabolism . . . 10
1.3.1 Biochemistry of fatty acids . . . 10
1.3.2 Dietary fat metabolism . . . 11
1.3.3 Adipose tissue . . . 18
1.3.3.1 Adipose tissue metabolism in the fasted state . . . 19
1.3.3.2 Adipose tissue FA metabolism in the post-prandial state . . . 20
1.4 Intrahepatic fatty acid uptake, synthesis and metabolism . . . 22
1.4.1 Hepatic fat uptake . . . 22
1.4.2 Esterification pathways . . . 24
1.4.2.1 VLDL synthesis . . . 24
1.4.2.2 Lipid droplets . . . 26
1.4.2.3 DNL . . . 27
1.4.3 Oxidation pathways . . . 31
1.5 Influence of dietary composition on hepatic metabolism . . . 33
1.5.1 Carbohydrates . . . 35
1.5.1.1 Dietary fructose . . . 37
1.5.1.2 Dietary glucose . . . 37
1.6 Implicated cellular mechanisms in development of hepatic steatosis . 38

1.7 Current models of hepatic steatosis 42
1.8 Summary 44
1.9 Thesis aims 45
1.10 Scientific contributions 46

2 Characterisation of an *in vitro* model of IHTAG accumulation with FA treatments enriched in UNSFA or SFA 47
2.1 Introduction 47
2.2 Methods 50
2.2.1 Cell culture 50
2.2.1.1 Freezing and thawing 50
2.2.1.2 Passaging and seeding of Huh7 cells 50
2.2.1.3 Culturing of PHH cells 51
2.2.1.4 Treatment media 51
2.2.1.5 Experimental FA stock production 52
2.2.1.6 Treatment protocol 52
2.2.1.7 Reagent preparation 54
2.2.2 Cellular analysis 54
2.2.2.1 Protein analysis 54
2.2.2.2 Viability assay 54
2.2.2.3 ATP concentration 55
2.2.2.4 Single cell gel electrophoresis (comet assay) 55
2.2.3 Glucose methods 58
2.2.3.1 Glycogen 58
2.2.3.2 Glucose production 59
2.2.4 FA methods 61
2.2.4.1 Folch method 61
2.2.4.2 SPE column isolation and methylation 61
2.2.4.3 Gas chromatography 62
2.2.4.4 Gas chromatography - mass spectrometry 64
2.2.4.5 *De novo* lipogenesis quantification 64
2.2.4.6 Analysis of cellular oxidation 66
2.2.5 Biochemical Analysis 66
2.2.5.1 3-hydroxybutyrate concentration 67
2.2.5.2 Cholesterol concentration 67
2.2.5.3 Glucose concentration 67
2.2.5.4 Lactate concentration 68
2.2.5.5 TAG concentration 68
2.2.5.6 Urea concentration 68
2.2.5.7 NEFA concentration 69

2.2.5.8 Ubiquitin enrichment 69
2.2.6 Western blot 69
2.2.7 Size exclusion chromatography 70
2.2.8 Confocal imaging 71
2.2.9 Statistical analysis 72
2.2.9.1 General R packages used 72
2.3 Results 73
2.3.1 Cell viability and vitality 73
2.3.2 FA compositions in Huh7 cells 76
2.3.2.1 Huh7 TAG FA composition following treatment with FAs 76
2.3.2.2 Huh7 PL composition following FA treatments . . 81
2.3.3 Primary human hepatocyte TAG composition 86
2.3.3.1 Primary human hepatocyte phenotype effect 86
2.3.3.2 PHH TAG composition 88
2.3.3.3 Primary human hepatocyte PL profile 92
2.3.4 Glucose metabolism 96
2.3.5 *De novo* lipogenesis 100
2.3.6 Huh7 cellular oxidation 103
2.3.7 Quantification of media lipoproteins from Huh7 105
2.3.8 Confocal imaging of FA treated Huh7 cells 111
2.3.9 Quantification of ATGL in FA treated Huh7 cells 113
2.4 Discussion 114
2.5 Conclusion 118

3 Transcriptome analysis of mRNA in an *in vitro* Huh7 or PHH model of IHTAG using FA treatments enriched in UNSFA or SFA 119
3.1 Introduction 119
3.2 Methods 122
3.2.1 RNA extraction 122
3.2.1.1 Huh7 RNA extraction 122
3.2.1.2 Primary cell RNA extraction 123
3.2.1.3 RNA specifications 124
3.2.1.4 RNA clean-up 124
3.2.1.5 In-house quality control checks for Huh7 and PHH cell sequencing 124
3.2.1.6 Novogene protocols for Huh7 and PHH cell sequencing 125
3.2.2 Data analysis 126
3.2.2.1 Data normalisation 126
3.2.2.2 Data visualisation 128

3.2.2.3 Differential gene expression analysis 128
3.2.2.4 Pathway analysis 131
3.3 Results 132
3.3.1 RNA sequencing in Huh7 cells 132
3.3.1.1 Factor analysis 132
3.3.1.2 Differential gene expression 134
3.3.1.3 Go terms and KEGG pathways 137
3.3.1.4 Huh7 RNA sequencing pathway analysis 143
3.3.2 Results from PHH RNA sequencing analysis 147
3.3.2.1 Factor analysis 147
3.3.2.2 Differential gene expression 151
3.3.2.3 Hall mark and functional gene enrichment scores . 159
3.3.2.4 Top gene analysis 171
3.4 Discussion 175
3.5 Conclusions 183

4 Characterisation of IHTAG turnover *in vitro* in Huh7 cells cultured with FA enriched in UNSFA or SFA 184
4.1 Introduction 184
4.2 Method 186
4.2.1 Cellular experiment timeline 186
4.2.2 Gas chromatography 188
4.2.3 Cell profiler 189
4.3 Results 191
4.3.1 Quantification of Huh7 TAG following 14 days of FA treatment 191
4.3.2 Quantification of Huh7 PL following 14 days of FA treatment 201
4.3.3 Analysis of cellular treatment media 211
4.3.4 Contribution of DNL in to intrahepatocellular fat 213
4.3.5 Huh7 cellular oxidation 215
4.3.6 Huh7 glucose metabolism 217
4.3.7 Confocal imaging of Huh7 FA treated cells 219
4.4 Discussion 224
4.5 Conclusion 225

5 *In vitro* model of uptake of TAG-rich remnants enriched in either UNSFA or SFA by Huh7 cells 226
5.1 Introduction 226
5.2 Methods 231
5.2.1 Volunteers 231
5.2.2 Dietary intervention 231
5.2.3 Post-prandial study day 232

5.2.4 Remnant isolation . . . 233
5.2.5 LDL receptor expression . . . 233
5.2.6 Labeling of isolated fraction . . . 234
5.2.7 Cell treatment . . . 234
5.2.8 Quantification of ^{13}C tri-palmitin and U^{13}C palmitic acid . . 236
5.2.9 Imaging of uptake . . . 236
5.2.10 Breath analysis . . . 236
5.2.11 Plasma insulin concentration . . . 237
5.3 Results . . . 237
5.3.0.1 *Ex vivo* labelling of TAG-rich remnants . . . 237
5.3.1 Plasma lipoprotein composition . . . 240
5.3.2 Plasma biochemistry . . . 248
5.3.3 Culturing of cells with TAG-rich remnants . . . 250
5.3.4 Time lapse imaging of fluorescently stained TAG-rich remnants applied to flourescently stained Huh7 cells . . . 262
5.4 Discussion . . . 264
5.5 Conclusion . . . 265

6 General discussion and future directions 267
6.1 Improving and Developing *in vitro* hepatocyte models . . . 267
6.2 Future directions . . . 270
6.3 Conclusion . . . 271

Appendices

A 273
A.1 Supplementary Material for Chapter 2 . . . 273
A.1.1 PHH phenotypic factors . . . 273
A.1.2 Molar quantities of TAG in Huh7 cells . . . 274
A.1.3 Molar quantities of PL in Huh7 cells . . . 276
A.1.4 Molar quantities of TAG in PHH . . . 278
A.1.5 Molar quantities of PL in PHH . . . 280
A.2 Supplementary Material for Chapter 3 . . . 282
A.2.1 Publication by Novogene, describing their methods for RNA sequencing . . . 282
A.3 Supplementary Material for Chapter 4 . . . 288
A.3.1 Huh7 media lipid following 14 days of culturing with FA treatments . . . 289
A.4 Supplementary Material for Chapter 5 . . . 295
A.4.1 Participant post parandial breath samples . . . 295
A.4.2 Participant insulin concentration . . . 296

References 297

List of Figures

1.1 Structure of the liver 3
1.2 Development of MASLD 7
1.3 Overview of dietary lipid absorption in the intestine 15
1.4 Fatty acid uptake and release in adpiocytes. 21
1.5 Hepatic *de novo* lipogenesis 30

2.1 Cell culturing timeline for both Huh7 and PHH cells 53
2.2 Quantification of DNA damage using single cell gel electrophoresis (comet assay) 57
2.3 Inclusion of duterium into *de novo* lipogeneiss (DNL) derived palmitate in Huh7 cells 66
2.4 Huh7 cell viability following days treatment with fatty acids 75
2.5 Intrahepatocellular triacylglycerol (IHTAG) content and composition in Huh7 cells following treatment with different FA compositions. . 78
2.6 Ratio of intrahepatocellular triacylglycerol (IHTAG) derived fatty acids (FA) in Huh7 cells following treatment with FA. 80
2.7 Intrahepatocellular phospholipid (PL) content and composition in Huh7 cells following treatment with different FA compositions. . . . 83
2.8 Ratios of phospholipid (PL) derived fatty acids (FA) in Huh7 cells following treatment with FAs. 85
2.9 87
2.10 Intrahepatocellular Triacylglycerol (IHTAG) by donor 87
2.11 Intrahepatocellular Triacylglycerol (IHTAG) in primary human hepatocytes (PHH) cells following fatty acid (FA) treatment 89
2.12 Ratio of intrahepatocellular triacylglycerol (IHTAG) derived fatty acids (FAs) in primary human hepatocytes (PHH) cells following treatment with FAs. 91
2.13 Phospholipid (PL) profile of primary human hepatocytes (PHH) following treatment with FA 93
2.14 Ratio of phospholipid (PL) derived fatty acids (FA) in Huh7 cells following treatment with FA. 95
2.15 Media glucose and lactate in Huh7 cells and primary human hepatoctyes (PHH) 97

2.16 Huh7 quantification of glucose production and glycogen storage following treatment with fatty acids (FA). 99
2.17 *De novo* lipogenesis (DNL) in fatty acid (FA) treated Huh7 hepatocytes 101
2.18 *De novo* lipogenesis (DNL) in fatty acid (FA) treated primary human hepatocytes (PHH) 102
2.19 Cellular oxidation in fatty acid (FA) treated Huh7 hepatocytes. . . 104
2.20 Export of triacylglycerol (TAG) by fatty acid (FA) treated Huh7 cells 106
2.21 Export of cholesterol by fatty acid (FA) treated Huh7 cells 108
2.22 Export of triacylglycerol (TAG) and cholesterol by FA treated Huh7 cells adjusted for the intrahepatocellar TAG (IHTAG) or cholesterol concentration 110
2.23 Confocal imaging of fluorescent stained lipid droplets (LDs) in fatty acid (FA) treated Huh7 cells 112
2.24 Quantification of the amount of ubiquitinated adipose triglyceride lipase ATGL in fatty acid (FA) treated Huh7 cells. 113

3.1 TMM normalisation with the EdgeR (v3.42.4) package on PHH cells 127
3.2 Relationship between the standard errors and the average log-counts of the genes in the differential expression analysis of fatty acid (FA) treated Huh7 cells and primary human hepatocytes (PHH). 130
3.3 Factor analysis in RNA expression from fatty acid (FA) treated Huh7 cells 133
3.5 Volcano plots of extracted RNA from fatty acid (FA) treated Huh7 cells. 136
3.6 KEGG and GO pathway analysis of RNA extracted from fatty acid (FA) treatment versus no-fat control in Huh7 cells. 139
3.7 KEGG and GO pathway analysis for RNA extracted from Huh7 cells treated with OPLA fatty acids (FA) versus POLA FAs. 140
3.8 Heatmap of most differentially expressed genes RNA extracted from fatty acid (FA) treated Huh7 cells 142
3.9 Pathway enrichment for the unfolded protein response (UPR) in RNA extracted from fatty acid (FA) treated Huh7 cells. 144
3.10 Pathway enrichment for the compliment and coagulation pathway in RNA extracted from fatty acid (FA) treated Huh7 cells. 145
3.11 Pathway enrichment for p53 signalling in RNA extracted from fatty acid (FA) treated Huh7 cells. 146
3.12 Factor analysis in RNA expression from fatty acid (FA) treated primary human hepatocytes (PHH) 148
3.13 Principle component analysis (PCA) in RNA expression from fatty acid (FA) treated primary human hepatocytes (PHH) 150

3.14 Venn diagram of differentially expressed genes in RNA extracted from fatty acid (FA) treated primary human hepatocytes (PHH) . . 152
3.15 Volcano plots of extracted RNA from fatty acid (FA) treated primary human hepatocytes (PHH) comparing treatment with low fat concentration (LF) versus control, or high fat concentration (HF) versus control. 154
3.16 Volcano plots of extracted RNA from fatty acid (FA) treated primary human hepatocytes (PHH) comparing high fat concentration to low fat concentration and OPLA and POLA FA treatments. 156
3.17 Volcano plots of extracted RNA from fatty acid (FA) treated primary human hepatocytes (PHH) comparing treatment with low OPLA concentration (OL) versus low POLA concentration (PL), or high OPLA concentration (OH) versus high POLA concentration (PH). . 158
3.18 KEGG and GO pathway analysis of RNA extracted from fatty acid (FA) treatment versus no-fat control in primary human hepatocytes (PHH) comparing low FA concentration treatment with no-fat control 160
3.19 KEGG and GO pathway analysis of RNA extracted from fatty acid (FA) treatment versus no-fat control in primary human hepatocytes (PHH) comparing high FA (HF) concentration treatment with no-fat control 162
3.20 KEGG and GO pathway analysis of RNA extracted from fatty acid (FA) treatment versus no-fat control in primary human hepatocytes (PHH) comparing high FA (HF) concentration treatment with low FA (LF) concentration treatment. 164
3.21 KEGG and GO pathway analysis of RNA extracted from fatty acid (FA) treatment versus no-fat control in primary human hepatocytes (PHH) comparing OPLA FA treatment with POLA FA treatment. . 166
3.22 KEGG pathway analysis of RNA extracted from fatty acid (FA) treatment versus no-fat control in primary human hepatocytes (PHH) comparing low concentration OPLA (OL) FA treatment with low POLA (PL) FA treatment. 168
3.23 KEGG and GO pathway analysis of RNA extracted from fatty acid (FA) treatment versus no-fat control in primary human hepatocytes (PHH) comparing high concentration OPLA (OH) FA treatment with high POLA (PH) FA treatment. 170
3.24 Heatmap of most differentially expressed genes RNA extracted from fatty acid (FA) treated Huh7 cells comparing cells treated with OPLA FA treatment with POLA FA treatment and cells treated with high concentration of FAs versus those treated with low concentration of FAs. 172

3.25 Heatmap of most differentially expressed genes RNA extracted from fatty acid (FA) treated Huh7 cells comparing cells treated with low concentration of OPLA FA treatment with low concentration POLA FA treatment and cells treated with high concentration of OPLA FA treatment with high concentration POLA FA treatment 174

4.1 Experimental timeline for Chapter 4 187
4.2 Methodology for analysing lipid droplet size using Cell Profiler in Huh7 cells 190
4.3 Huh7 cells intrahepatic triacylglycerol (IHTAG) content in Huh7 cells following treatment with fatty acids (FA). 192
4.4 Huh7 intrahepatocellular triacylglycerol (TAG) derived oleic acid composition following treatment with fatty acids (FA) 194
4.5 Huh7 intrahepatocellular triacylglycerol (TAG) derived palmitic acid composition following treatment with fatty acids (FA) 196
4.6 Huh7 intrahepatocellular triacylglycerol (TAG) derived steatic acid composition following treatment with fatty acids (FA) 198
4.7 Huh7 intrahepatocellular triacylglycerol (TAG) derived palmitoleic acid composition following treatment with fatty acids (FA) 200
4.8 Huh7 cells intrahepatic phospholipid (PL) content in Huh7 cells following treatment with fatty acids (FA). 202
4.9 Huh7 intrahepatocellular phospholipid (PL) derived oleic acid composition following treatment with fatty acids (FA) 204
4.10 Huh7 intrahepatocellular phospholipid (PL) derived palmitic acid composition following treatment with fatty acids (FA) 206
4.11 Huh7 intrahepatocellular phospholipid (PL) derived stearic acid composition following treatment with fatty acids (FA) 208
4.12 Huh7 intrahepatocellular phospholipid (PL) palmitoleic acid composition following treatment with fatty acids (FA) 210
4.13 Huh7 media triacylglycerol (TAG) content in Huh7 cells following treatment with fatty acids (FA) 212
4.14 Huh7 contribution of *de novo* lipogenesis (DNL) to intrahepatic triacylglycerol (TAG) or phospholipid (PL) content following treatment with fatty acids (FA). 214
4.15 Huh7 cellular oxidation following treatment with fatty acids (FA). . 216
4.16 Huh7 quantification of glucose metabolism following treatment with fatty acids (FA). 218
4.17 Confocal imaging of fluorescent stained lipid droplets (LDs) in Huh7 cells treated for 2-weeks with OPLA of at either high concentration (OH), or high then low concentration (OL) 220

4.18 Confocal imaging of fluorescent stained lipid droplets (LDs) in Huh7 cells treated for 2-weeks with POLA of at either high concentration (PH), or high then low POLA concentration (PL) or low OPLA concentration (OL) 221
4.19 Confocal imaging of fluorescent stained lipid droplets (LDs) in Huh7 cells treated for 2-weeks with POLA of at a high concentration (PH) then OPLA at a high concentration (OH) 222
4.20 Huh7 quantification of lipid droplet (LD) size following treatment with fatty acids (FA). 223

5.1 Experimental protocol for Chapter 5 235
5.2 Analysis of the incorporation of a tripalmitin label into triacylglycerol (TAG) rich lipoproteins TTR and consequently into Huh7 cells . . . 239
5.3 Composition of triacylglycerol (TAG) within isolated TAG-rich remnants 241
5.4 Composition of triacylglycerol (TAG) within isolated TAG-rich remnants grouped by lipoprotein isolation fraction. 242
5.5 Composition of phospholipid (PL) within isolated triacylglycerol (TAG)-rich remnants 244
5.6 Composition of phospholipid (PL) within isolated triacylglycerol (TAG)-rich remnants grouped by lipoprotein isolation fraction. . . . 245
5.7 Analysis of the incorporation of dietary U^{13}C palmitic acid label into triacylglycerol (TAG) rich lipoproteins 247
5.8 Post parandial plasma TAG and NEFA concentration in participants following consumption of a diet enriched in unsaturated fatty acids (UNSFA) or saturated fatty acids (SFA). 249
5.9 Analysis of the incorporation of dietary U^{13}C palmitic acid label and ^{13}C tripalmitin into triacylglycerol (TAG) rich lipoproteins 251
5.10 Huh7 lipid composition after culturing with triacylclycerol (TAG)-rich remnants with or without additional free fatty acids (FA). . . . 253
5.11 Analysis of the incorporation of dietary U^{13}C palmitic acid label and ^{13}C tripalmitin into Huh7 cells after treatment with triacylglycerol (TAG) rich lipoproteins 255
5.12 Huh7 media lipid composition after culturing with triacylclycerol (TAG)-rich remnants with or without additional free fatty acids (FA).257
5.13 Huh7 media Apolipoprotein B (ApoB) concentration and lipid composition after culturing with triacylclycerol (TAG)-rich remnants with or without additional free fatty acids (FA). 259
5.14 Huh7 media glucose, lactate and urea concentration after culturing with triacylclycerol (TAG)-rich remnants with or without additional free fatty acids (FA). 261

5.15 Time-lapse images taken of Huh7 cells immediatly after treatment with fluorescently labelled triacyglycerol (TAG)-rich lipoproteins. . 263

A.1 Intrahepatocellular triacylglycerol (IHTAG) concentration and composition in Huh7 cells following treatment with different FA compositions. 274
A.2 Huh7 concentration of triacyglycerol (TAG) derived palmitoleic acid and stearic acid in fatty acid (FA) treated Huh7 cells 275
A.3 Intrahepatocellular phospholipid (PL) concentration and composition in Huh7 cells following treatment with different FA compositions. . 276
A.4 Huh7 concentration of phospholipid (PL) derived palmitoleic acid and stearic acid n fatty acid (FA) treated Huh7 cells 277
A.5 Intrahepatocellular triacylglycerol (IHTAG) concentration and composition in PHH following treatment with different FA compositions. 278
A.6 PHH concentration of triacyglycerol (TAG) derived palmitoleic acid and stearic acid in fatty acid (FA) treated Huh7 cells 279
A.7 Intrahepatocellular phospholipid (PL) concentration and composition in PHH following treatment with different FA compositions. 280
A.8 Huh7 concentration of phospholipid (PL) derived palmitoleic acid and stearic acid n fatty acid (FA) treated Huh7 cells 281
A.9 Media Oleic acid FA content in Huh7 cells 290
A.10 Media palmitic acid FA content in Huh7 cells 292
A.11 Media stearic acid FA content in Huh7 cells 294
A.12 Media Palmitoleate and linoleic acid 295
A.13 $^{13}CO_2$ in breath, postprandial study day. 295
A.14 Post-prandial plasma insulin 296

List of Tables

2.1 FA proportion for different FA treatment conditions and physiological ranges 52

5.1 Plasma Biochemistry of participants post diet 248

A.1 Primary human hepatocytes (PHH) donor phenotype 273

List of Abbreviations

A2M . . . . . Alpha 2-Macroglobulin

AADAC . . . . Arylacetamide Deacetylase

ACC . . . . . Acetyl CoA carboxylase

ASS . . . . . Argininosuccinate Synthase

ApoB . . . . . Apolipoprotein B

AR . . . . . Adrenergic Receptor

ATGL . . . . . Adipose Triacyclyceride Lipase

AU . . . . . Arbritry Units

AQP7 . . . . . Aquaporin 7

BAMBI . . . . BMP and Activin Membrane Bound Inhibitor

BSA . . . . . Bovine Serum Albumin

CCL . . . . . C-C motif chemokine ligand

CIDEB . . . . Cell Death Inducing DFFA Like Effector B

CHO . . . . . Chinese Hamster Ovary cells

CM . . . . . Chylomicron

CMR . . . . . Chylomicron Remnant

CoA . . . . . Coenzyme A

CPT . . . . . Carnitine Aalmitoyltransferase

CRP . . . . . C-Reactive Protein

CVD . . . . . Cardiovascular Disease

DAG . . . . . Diacylglyceride

DGAT . . . . . Diacylglyceride Acyltransferase

DMSO . . . . . Dimethylsulfoxide

DNL . . . . . *De Novo* Lipogenesis

ECM . . . . . Extracellular Matrix

EE . . . . . Energy Expenditure

ER . . . . . Endoplasmic Reticulum

EV . . . . . Extracellular Vesicles

FA . . . . . Fatty Acid

FABP . . . . . Fatty Acid Binding Protein

FAME . . . . . Fatty Acid Methyl Ester

FASN . . . . . Fatty Acid Synthase

FATP . . . . . Fatty Acid transport proteins

FBS . . . . . Foetal Bovine Serum

FFA . . . . . Free Fatty Acids

GC . . . . . Gas Chromatography

GCKR . . . . Glucokinase Regulatory Protein

GCMS . . . . . Gas Chromatography Mass Spectrometry

GLP . . . . . Glucagon Like Peptide

GPAT . . . . . Glycerol-3 Phosphate Acyl Transferase

GPC sn-glycero-3-phosphocholine

GPCR . . . . . G Protein Coupled Receptor

GWAS . . . . . Genome Wide Association Study

HCC . . . . . Hepatocellular Carcinoma

HDL . . . . . High density Lipoproteins

HIF . . . . . Hypoxia Inducible Factor

HS . . . . . Human Serum

HSD17B13 . . 17-Beta Hydroxysteroid Dehydrogenase 13.

HSL . . . . . Hormone Sensitive Lipase

HSPA5 . . . . Heat Shock Protein Family A (Hsp70) Member 5

IL . . . . . Interleukin

IHTAG . . . . Intrahepatic Triacylglyceride

INSIG2 . . . . Insulin Induced Gene 2

IR . . . . . Insulin Resistant

IRMS . . . . . Isotope Ratio Mass Spectrometry

IS . . . . . Insulin Sensitive

LCFA . . . . . Long Chain Fatty Acid

LD . . . . . Lipid Droplet

LDLR . . . . . Low Density Lipoprotein Receptor

LDL . . . . . Low Density Lipoprotein

LPL . . . . . Lipoprotein Lipase

MAFLD . . . . Metabolic Associated Fatty Liver Disease

MANF . . . . Mesencephalic Asterocyte-Derived Neutrophic Factor

MAG . . . . . Monoacylglyceride

MASLD . . . . Metabolic Associated Steatotic Liver Disease

MBOAT . . . Membrane Bound O-Acyl Transferase

MGAT . . . . Monoacylglyceride Acyl Transferase

MGL . . . . . Monoacylglyceride Lipase

MMP . . . . . Maximal Mappable Prefix

MRI . . . . . Magnetic Resonanace Imaging

mTORC . . . Mammalian Target Of Rapamycin

MTTP . . . . . Microsomal Triglyceride Transfer Protein

MUFA . . . . . Mono-Unsaturated Fatty Acid

NAFLD . . . . Non - Alcoholic Fatty Liver Disease

NASH . . . . . Non-Alcoholic Steatohepatitis

NAS . . . . . NAFLD Activity Score

NEFA . . . . . Non-Esterified Fatty Acids

OLFM2 . . . . Olfactomedin 2

OPLA . . . . . MUFA Enriched Fatty Acid Treatment

PARVB . . . . Parvin Beta

PBS . . . . . Phosphate Buffer Solution

PC . . . . . Phosphocholine

PCA . . . . . Principal Component Analysis

PDGF . . . . . Platelet derived Growth Factor

PEX2 . . . . . Peroxisomal Biogenesis Factor 2

PHH . . . . . Primary Human Hepatocytes

PIGR . . . . . Polymeric Immunoglobulin Receptor

PL . . . . . Phosholipid

PLIN . . . . . Perilipin

PNPLA . . . . Patatin-Like Phospholipase Domain-Containing Protein

POLA . . . . . SFA Enriched Fatty Acid Treatment

PPAR . . . . . Peroxisome Proliferator-Activated Receptors

PUFA . . . . . Poly-Unsatured Fatty Acids

RIN . . . . . RNA Integrity Number

ROS . . . . . Reactive Oxygen Species

SCAP . . . . . SREBP cleavage activating protein

SCGE . . . . . Single Cell Gel Electrophoresis

SCN . . . . . Suprachiasmatic Nucleus

SD . . . . . Standard Deviation

SEC . . . . . Size Exclusion Chromatography

SERCA . . . . SarcoEndoplasmic Reticulum Calcium ATPase

SFA . . . . . Saturated Fatty acids

SPE . . . . . Solid Phase Extraction

SSB . . . . . Sugar Sweetened Beverage

SREBP . . . . Sterol Regulatory Element Binding Proteins

T2DM . . . . . Type 2 Diabetes

TAG . . . . . Triacylglyceride

TCA . . . . . The Citric Acid Cycle aka Krebs Cycle

TGF . . . . . Transforming Growth Factor

TLR . . . . . Toll-Like Receptor

TTR . . . . . Tracer to Tracee Ratio

TM6SF2 . . . Transmembrane 6 Superfamily 2

TNF . . . . . Tumor Necrosis Factor

TRPV2 . . . . Transient Receptor Potential Vanilloid type 2

UNSFA . . . . Unsaturated Fatty Acid

UPR . . . . . Unfolded Protein Response

VLDL . . . . . Very Low Density Lipoprotein

VWF . . . . . Von Willebrand Factor

1 Introduction

1.1 Overview of the liver

Situated within the abdominal cavity, the liver undertakes many metabolic processes. Supplied directly by the portal vein, the liver has a key regulatory role in maintaining whole-body homeostasis, including regulation of: blood volume, immune system support, endocrine signalling and clearance of xenobiotic compounds (Trefts et al. 2017). Most relevant to this thesis, is the liver's influence on nutrient and energy metabolism and homeostasis. The liver provides a balance between exogenous (dietary) and endogenous energy and nutrient supply and is a key regulator of circulating lipids and blood glucose concentration.

The liver is composed of 4 major cell types: hepatocytes, kupffer cells (specialised immune cells), stellate cells and endothelial cells. The majority of cells are hepatocytes which form 80% of liver tissue volume and 60% of total cellular composition. Along with stellate cells (about 5% of total cells), hepatocytes carry out nutrient metabolism (Ding et al. 2016; Trefts et al. 2017; Vekemans et al. 2005; Yin et al. 2013). The liver is subdivided into metabolic zones, initiated in response to metabolic factors including nutrient availability and various hormones. Zonation, is primarily a mechanism to reduce futile cycling and competition for common substrates. Oxygen gradients facilitate zonation, signaled by hypoxia

inducible factors (HIFs). Metabolic processes which require more energy such as protein secretion and gluconeogenesis occur closer to the portal vein where more oxygen is available, whereas less energy demanding processes (for example, glycolysis or bile acid synthesis) occur in the pericentral region, where less oxygen is available (Cunningham et al. 2021; Manco et al. 2021). Indeed, a murine model of HIF-α knockdown, resulted in metabolic dysfunction of processes regulated by the liver; with increased gluconeogenesis and lipogenesis (glucose and lipid production respectively) and decreased ketone body production. These mice developed severe hepatic steatosis alongside impaired β-oxidation and increased lipogenic gene expression demonstrating the importance of these zones (Cunningham et al. 2021; Kietzmann 2017; Manco et al. 2021).

Liver lobules form both the functional and structural units of the liver. They consist of hexagonal arrangement of hepatocytes radiating outwards from a central vein, forming a polygonal shape. These hepatocytes are organised into plates of a single cell layer, allowing for the exchange of metabolites (Jungermann et al. 1989; Kietzmann 2017). Within each lobule, blood flows through the hepatic sinusoid (small blood vessels), which are lined by specialised endothelial cells, kuppfer cells and stellate cells providing an efficient structure for the exchange of nutrients and waste products. This structure also allows the liver to carry out detoxification functions and the secretion of essential proteins including albumin and clotting factors with blood draining from the liver to the body via a central vein (Figure 1.1)(Jungermann et al. 2000).

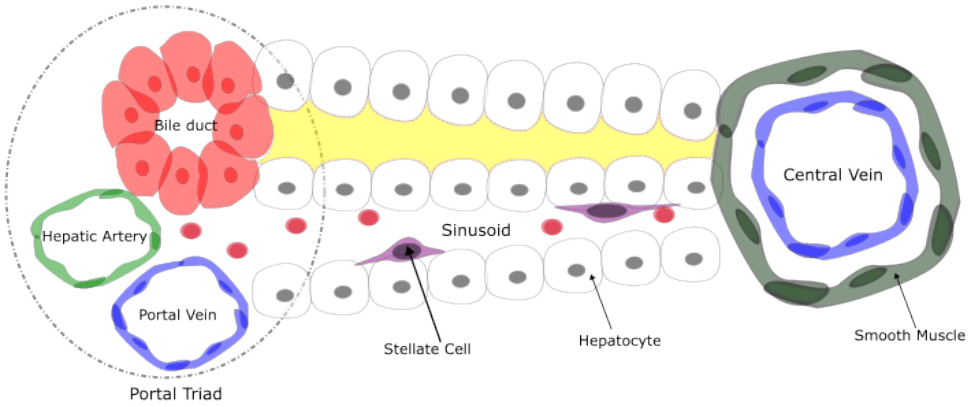


Figure 1.1: Structure of the liver. The liver is composed of hexagonal units made up of sinusoids radiating out from the central vein to the portal triad consisting of a bile duct, portal vein and hepatic artery. This figure shows the structure of one sinusoid. From one central vein many of these radiates forming a hexagonal structure. Figure redrawn and adapted from Cargnoni et al. 2018.

1.2 MASLD and risk of metabolic disease

As the liver plays a key role in maintaining metabolic homeostasis, perturbations in hepatic metabolism can impact widely on metabolic disease risk. The pathological accumulation of intrahepatic triacylglycerol (IHTAG), originally known as NAFLD (non-alcoholic fatty liver disease), or sometimes metabolic associated fatty liver disease (MAFLD), is now referred to as metabolic dysfunction-associated steatotic liver disease (MASLD) (Eslam et al. 2020; Rinella et al. 2023). This name change was solicited by an international Delphi consensus with the adjusted definition proposed to reduce stigmatisation and alter the diagnosis principles to be through positive selection rather than a process of elimination (Rinella et al. 2023). MASLD represents a spectrum of disease states starting with steatosis, through to cirrhosis and hepatocellular carcinoma (Mundi et al. 2020) (Figure 1.2). In 2019, it was estimated that 25% of the global population have some degree of MASLD, and that the prevalence was increasing. In 2016 a reported 32% of the population in the Middle East were diagnosed with MASLD, followed by: South America at 31%, Asia at 27%, the US at 24%, Europe at 24% and Africa at 14% (Younossi et al. 2016b) demonstrating the global prevalence of MASLD. Disease progression of MASLD is associated with significant complications, both liver specific and with an increased overall mortality, with those diagnosed with MASLD primarily dying from cardiovascular events (Ong et al. 2008). MASLD is one of the leading causes of necessary liver transplants (Pais et al. 2016). The consequential economic burden of MASLD in 2020 was already estimated to exceed $100 billion in the US alone (Mundi et al. 2020).

Why the liver starts to accumulate fat remains unclear but is likely to be due, in part, to an imbalance between fatty acid (FA) delivery to the liver, FA synthesis within the liver, removal of FA from the liver in either very low- density lipoproteins (VLDL) or oxidation. Accumulation of IHTAG is known as ectopic fat deposition which is defined as the aberrant storage of excess fat in non-adipose tissues including the liver, heart and skeletal muscle (Britton et al. 2011). Ectopic fat deposition, has been directly attributed to increased risk of insulin resistance, cardiovascular

disease (CVD) and type 2 diabetes mellitus (T2DM) (Snel et al. 2012; Britton et al. 2011). It has been proposed that MASLD develops following 'multiple hits' on the liver over a number of years with each 'hit' being a loss of metabolic homeostatic control or overload (Buzzetti et al. 2016).

MASLD, across all stages, is typically associated with: tissue insulin resistance, increased plasma TAG, reduced plasma high-density lipoproteins (HDL) and low plasma adiponectin (Luukkonen et al. 2016). The Pathology Committee of the MASH Clinical Research Network have outlined a histological feature scoring system for classifying hepatic lesions into a MASLD activity score (NAS). Using 14 histological markers, 4 of which are semi-quantitative: steatosis (0-3), lobular inflammation (0-2), hepatocellular ballooning (0-2), and fibrosis (0-4) (Kleiner et al. 2005). MASLD is diagnosed in 4 stages (Figure 1.2): i) steatosis, the pathological accrual of fat, defined as when fat accounts for more than 5% of the livers weight and presence of macrovesicular steatosis lipid droplets (LDs); ii) metabolic associated hepatitis (MASH), where a fatty liver has become inflamed (affects about 5% of the population, UK, 2016). MASH is histologically defined by the predominance of zone 3 macrovesicular steatosis, hepatocyte ballooning grade of more than 1, (poorly defined, but encompasses the enlargement and swelling of hepatocytes), and lobular inflammation grade more than or equal to 1 (presence of at least 1 foci per $\times$200 field) (Kleiner et al. 2005; Younossi et al. 2016b); iii) MASH with fibrosis, experienced by 41% of patients who present with MASH (Younossi et al. 2016b), where there is persistent inflammation and scar tissue. This is associated with the histological features of steatosis, lobular and portal inflammation, hepatocyte damage from hepatocyte ballooning as well as mallory-denk body formation (cytoplasmic hyaline inclusions of hepatocytes) and pericellular fibrosis. The hepatocytes also present with endoplasmic reticulum (ER) stress, apoptosis and/or necrosis (Lindenmeyer et al. 2018; Neuschwander-Tetri 2010); iv) cirrhosis following years of liver inflammation and scaring often resulting in liver failure, with the histological features of increased fibrosis and reduced fat content. Cirrhosis is experienced by 25% of patients who present with MASH (Younossi et al.

2016b) and may progress to hepatocellular carcinoma (HCC) (Mundi et al. 2020; Friedman et al. 2018; Michelotti et al. 2013). Once patients have been diagnosed with MASH, they have to be regularly monitored for secondary complications, including those associated with portal hypertension (ascites, variceal bleeding) as well as end-stage MASLD and HCC (Mundi et al. 2020).

MASLD is typically diagnosed through non-invasive imaging. Ultrasound and computed tomography reliably detect steatosis when more than 20% of the liver volume constitutes fat (Papatheodoridi et al. 2018). MRI can be used to detect MASLD when the volume of hepatic fat is over 5% however, this is more expensive and therefore not part of routine medical care (Friedman et al. 2018). There are no reliable plasma markers for MASLD, and plasma aminotransferase levels, a common marker of MASLD, may only be mildly increased, with 78% of patients having no detectable changes in this liver enzyme function (Younossi et al. 2016b). Although MASH is often suspected when patients present with both steatosis and abnormal aminotransferases, diagnosis can only occur with a biopsy for assessment of histological markers (Mundi et al. 2020). Indeed, the US population based study; the Third National Health and Nutrition Examination Survey (NHANES III), investigated the use of aminotransferases as a surrogate marker for MASH, and showed that only 25% of all patients with MASLD had elevated levels of aminotransferases compared to 6-8% of the general population (Clark et al. 2003).

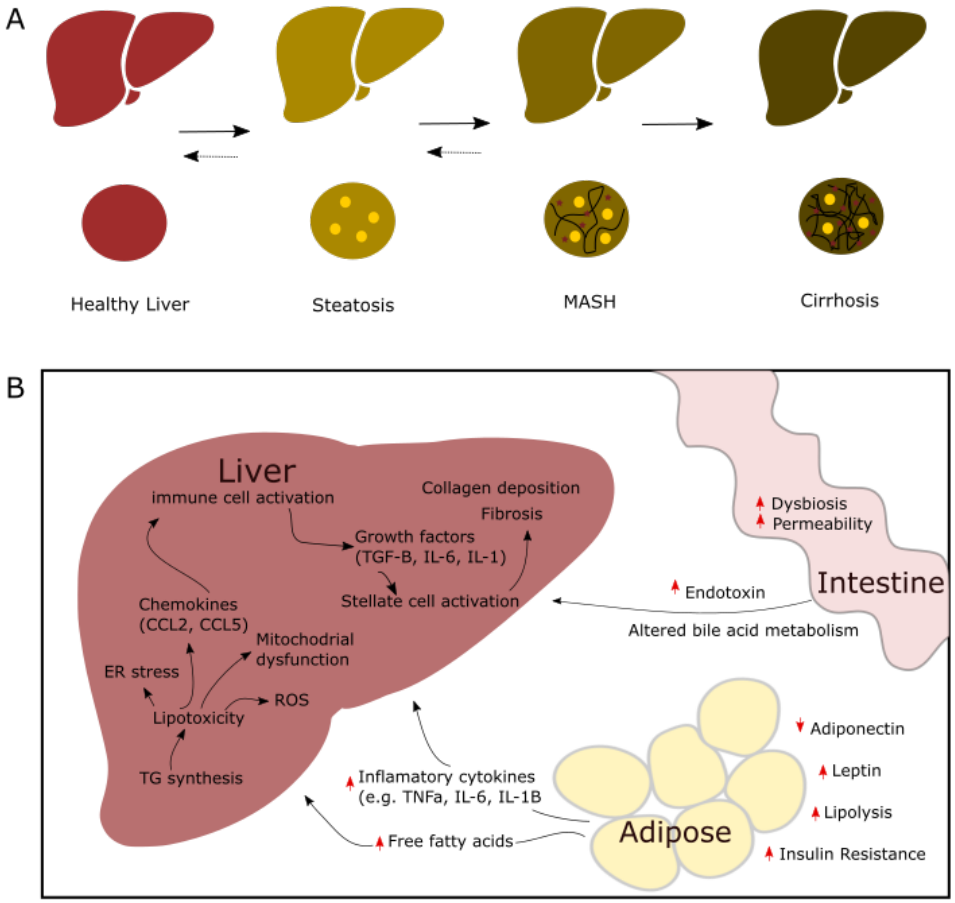


Figure 1.2: Development of MASLD. Figure adapted from Adolph et al. 2017. A) MASLD describes a continuum of disease states. When a healthy liver accumulates more than 5% of it's total volume in fat, steatosis is diagnosed. Following steatosis, non-alcoholic steatohepatisis (MASH), is defined by the infiltration of immune cells. MASH can be described either without fibrosis, or with fibrosis, the next stage of disease progression. Individuals presenting with both simple steatosis and MASH can return to a healthy liver, following the reduction of hepatic fat. From MASH, MASLD can progress to develop cirrhosis, where the fibrosis present increases to become a histological hallmark, and fat content reduces. Advanced MASH and cirrhosis may result in hepatocellular carcinoma and liver. B) The pathophysiology of MASLD is a multi-organ process with inflammatory changes in the liver, gut and adipose tissues. An increase in hepatic fat, either through increased dietary intake, *de novo* lipogenesis, insulin-resistance driven adipose release of free fatty acids result in increased hepatic triacylglycerol (TAG), synthesis and accumulation: Steatosis. Persistent hepatic steatosis may induce metabolic stress including: lipotoxicity, mitochondrial dysfunction, increased production of reactive oxygen species (ROS), ER stress resulting in the release of chemokines (e.g. CCL2 and CCL5). These pro-inflammatory signals activate hepatic immune cells and begin the progression of MASLD to MASH. MASH progression can also be progressed by further pro-inflammatory signals originating from both inflamed adipose tissue (in the case of metabolic syndrome) and from the gut, where metabolic disease can result in dysbiosis, and bacterial products such as endotoxin enter the circulation through a leaky gut wall. These metabolic changes may lead to hepatocyte apoptosis or necrosis, with resulting tissue damage and subsequent fibrosis, caused by the activated stellate cells. Abbreviations: CCL, C-C motif chemokine ligand; ER, endoplasmic reticulum, IL, interleukin; PDGF, platelet-derived growth factor; TGF, transforming growth factor; TNF, tumour necrosis factor.

Risk factors for MASLD can be classified as non-modifiable or modifiable, with the former including: i) age, with risk increasing with age (Lin et al. 2022); ii) sex, there is a greater prevalence in males compared to females (Teng et al. 2023); iii) ethnicity, variation across different populations, with MASLD most frequent in East Asian Indians, followed by Hispanics, Asians, Caucasians and less prevalent in African Americans (Rich et al. 2018; Weston et al. 2005; Machado et al. 2014); and iv) genotype, with identified risk alleles including PNPLA3, TM6SF2, GCKR, MBOAT, MTARC1, APOH, GUSB and HSD17B13 (Sookoian et al. 2017; Sookoian et al. 2023; Sveinbjornsson et al. 2022). Modifiable risk factors include: i) adiposity, with visceral obesity correlating strongly with IHTAG content (Fabbrini et al. 2010); ii) sedentary behaviour, with increasing physical activity (with or without weight loss) associated with a decrease in IHTAG (Semmler et al. 2021); iii) smoking, is an established independent risk factor for the development of MASLD (Hamabe et al. 2011); and iv) diet, with dietary intervention studies demonstrating IHTAG content is altered by both macronutrient quantity (hypercaloric diets increase IHTAG content, and hypocaloric diets decrease IHTAG content) and composition, specifically the type of fat consumed may influence IHTAG content (Parry et al. 2020a; Townsend et al. 2019; Worm 2020). However, the optimal macronutrient balance for decreasing the risk of IHTAG accumulation (and subsequent risk of CVD and T2DM) remains debated and is discussed below.

Of the above risk factors, increased adiposity, which is often associated with the presence of metabolic syndrome (defined by central adiposity, hyperglycemia, dyslipidemia, the imbalance of lipids, and hypertension, is the largest risk factor for MASLD, with MASLD often considered the hepatic manifestation of metabolic syndrome. Indeed, Younossi et al, carried out a meta-analysis of 86 studies reporting high prevalence of metabolic comorbidities globally in patients with MASLD: 51.3% presented with obesity, 22.5% with type 2 diabetes, 69.2% with hyperlipidemia, 39.3% with hypertension, and 42.5% with metabolic syndrome (Younossi et al. 2016b). Additionally, MASH has been observed to be more prevalent and progressive in patients who also present with insulin resistance and T2DM, with the latter being

independent predictor of moderate to severe fibrosis (Younossi et al. 2016a; Hossain et al. 2009; Younossi et al. 2004). Insulin resistance is associated with poor glycemic control, with a corresponding increase in hepatic delivery of non-esterified FA (NEFA), resulting from increased adipose NEFA release, a process down regulated by insulin in healthy individuals (Donnelly et al. 2005; Lewis et al. 2002).

The therapeutic, Resmetirom (Rezdiffra), is the only FDA approved therapeutic to date which is specifically for non-cirrhotic MASH and is currently only licensed in the US. Resmetirom acts on the thyroid as an agonist to thyroid hormone receptor-β, which has been associated with reduced liver fat content (Karim et al. 2023). However, the primary treatment strategies aim to increase weight loss and reduce insulin resistance through lifestyle, medications or surgical interventions (including gastroectomy, Roux en Y bypasses and intra-gastric balloons) (Mundi et al. 2020). Multiple randomised control trials have looked at the effect of weight loss on MASLD through lifestyle modifications, including weight loss through caloric deficit either by increasing activity (energy expenditure), or reducing food intake (energy consumption), or both. Kuotoukidis et at carried out a meta-analysis of 22 clinical studies investigating lifestyle change on MASLD (containing 2588 participants, 66% male), and confirmed that despite heterogeneity in trial set-up, there was a consistent association between weight loss interventions and improved biomarkers of MASLD in the short to medium term, limited evidence was provided on long term outcomes (Koutoukidis et al. 2019). Moreover, this association continued with later stage MASLD as confirmed by Vilar-Gomez et al who demonstrated that the degree of weight loss was independently associated with improvement in MASH related histological features. 58% of individuals who lost more than 5% body fat had resolution of MASH whereas 90% of those who lost more than 10% body weight had resolution of MASH (Vilar-Gomez et al. 2015). Further research is required to understand the metabolic mechanisms underlying these weight loss induced hepatic changes in individuals presenting with MASLD.

1.3 Fat metabolism

The liver receives FAs derived from: adipose tissue lipolysis, dietary FA and circulating lipoproteins. The liver also produces FA from non-lipid precursors (i.e. glucose and amino acids), through the process of *de novo* lipogenesis (DNL) (Alves-Bezerra et al. 2018). The availability and metabolism of FA is dependent on the metabolic and nutritional state of the individual with insulin acting as the key regulator (Titchenell et al. 2017). Additionally, although FAs primarily function as an energy source, they are required for cellular health and function; specifically they are involved in numerous signaling roles, and form a structural component of the cell as well as assisting with the absorption of some essential vitamins (A, D, E and K) (Berg et al. 2011).

1.3.1 Biochemistry of fatty acids

FAs comprise hydrocarbon chains and come as a variety of species, with different properties and consequently functions. Between 1 and 3 FA chains may be esterified to a glycerol backbone yielding monoacylglyceride (MAG), diacylglyceride (DAG) or TAG respectively. TAG is the most inert of these species and is the primary storage form of FAs in all tissues (Berg et al. 2011; Zechner et al. 2017). TAGs are classified according to their chain length and the glycerol head group may also have a phosphate group instead of the third FA to form phospholipids (PL), which are important for cellular function and membranes (Berg et al. 2011). FAs vary by degree of saturation and are classified as saturated where no double bonds are present, either mono-unsaturated FAs (MUFAs) with only one double bond present or, poly-unsaturated FAs (PUFAs), with more than one double bond present. The omega-3 and -6 acids, are classified as essential FA i.e. they cannot be synthesised *de novo*, these therefore must be consumed as part of the diet (Berg et al. 2011; Sokoła-Wysoczańska et al. 2018).

1.3.2 Dietary fat metabolism

In a healthy individual, the body is capable of metabolising in excess of 100g of fat per day without a marked increase in plasma TAG (Feingold 2000), with some individuals demonstrated to be able to consume up to 500g of dietary fat in a day and absorb 95% of it (Kasper 1970). The typical American diet contains 100-150g of fat per day (Wang et al. 2013). The contribution of dietary fat to the liver depends on the quantity and frequency of consumption. Stable isotope labelling has found that dietary fat can contribute up to 15% of hepatic fat in individuals with MASLD, although this will be considerably lower in a healthy individual (Donnelly et al. 2005).

Dietary fat digestion begins in the mouth and continues throughout the digestive tract to the small intestine where the majority is absorbed within the first 60cm of the small intestine (Newton et al. 1978). 95% of dietary fat is in the form of TAG and must be broken down due to its hydrophobic nature in order to leave the gut. TAG is acted upon by lingual lipase within the mouth joined by gastric lipase in the stomach, and then pancreatic lipase in the small intestine (Xiao et al. 2019). TAG lipolysis primarily occurs in the proximal intestine liberating two FAs and a MAG molecule. Bile acids act to emulsify these intestinal lipids to form micelles in order to prevent the formation of aggregates of lipid globules (Sarkar et al. 2016). The FA/MAG within these micelles are taken up across the brush border of the apical membrane of enterocytes either via diffusion when there is a high concentration of fat or via active transport when there is a low concentration of fat (Iqbal et al. 2009).

In humans, NEFAs may additionally enter enterocytes from the circulation via the enterocytes basolateral membrane, although this is a minor pathway and the size of the contribution needs further assessment. Fat is predominantly taken up via the enterocytes apical membrane, from within the intestinal lumen. The side of entry of a fat determines the metabolic fate. Fat entering from the apical side, the intestinal side, are more likely to enter a TAG synthetic pathway whereas those entering from the basolateral (circulatory) side are more likely to either be oxidised or used for PL synthesis (Gangl et al. 1975).

Dietary fats are absorbed via passive diffusion or by transport proteins such as CD36 and fatty acid transport proteins (FATPs). FATPs consist of six evolutionary conserved FA binding proteins, which exhibit different tissue distributions. In the small intestine, FATP4 is predominantly expressed and is associated with the enterocyte plasma membrane (PM) as well as the endoplasmic reticulum (ER). It is estimated to account for 60% of fat uptake from the intestinal lumen. FATP4 has acyl-CoA ligase activity, adding a Coenzyme A (CoA) group to incoming FAs, preventing their loss from the enterocyte through a process called vectoral acetylation. Inside the enterocyte, FA-CoAs re-form micelles before further trafficking (Milger et al. 2006; Stahl et al. 1999). When vectoral acetylation hasn't occurred, FA binding proteins (FABP) prevent FA loss by diffusion. FABPs (1 and 2) attach to FAs, aiding intracellular transport. In enterocytes and the liver, FABPs constitute 5-6% of cytosolic proteins (Pelsers et al. 2003; Sinha et al. 2017).

CD36, a glycoprotein highly expressed on the apical luminal side of the enterocyte, binds long-chain FAs for uptake, although its quantitative contribution remains debated (Tran et al. 2011). It is suggested that the binding of long-chain unsaturated FAs to CD36 signals the beginning of fat digestion via afferent nerves. Polymorphisms in CD36 are associated with variations in preferences and perceptions of dietary fat (Keller et al. 2012). These differences may influence health, as dietary fat quantity and composition impact health (Herpen et al. 2011; Townsend et al. 2019; Meer et al. 2008). Additionally, CD36 is suggested to regulate downstream chylomicron (CM) release (Tran et al. 2011).

The roles of CD36 and FATPs in FA uptake are complex and multi-faceted. While traditionally considered cell surface FA transporters, the membrane topology and pleiotropic functions of CD36 do not support a singular function in FA uptake. Similarly, FATPs are not exclusively found in the plasma membrane, and their primary activity is that of CoA-synthetases that activate FAs with a leader group. Their role in FA uptake may be more accurately linked to metabolic trapping rather than direct cell surface transport. It is plausible that CD36 and FATPs function in a coordinated complex to facilitate FA uptake and subsequent intracellular processing.

Further research is required to delineate the specific contributions and interactions of these proteins in enterocyte FA metabolism.

The conversion of FA to TAG within the enterocyte acts to mitigate adverse effects caused by FA induced lipotoxicity (Mansbach et al. 2010) within the ER membrane. About 80% of FA is converted to TAG through sequential action from MAG acyltransferase (MGAT) and DAG transferase (DGAT), with each enzyme adding a FA group (Feingold 2000). A small proportion (∼20%) is recombined via the glycerol-3-phosphate pathway using glycerol-phosphate acyltransferase to TAG (Lennon et al. 2016; Khatun et al. 2016). Synthesised TAG forms LDs which either bud off to form cytoplasmic LDs or are secreted into the ER lumen for CM synthesis (Kohan et al. 2015).

The production of CMs allows for the targeted delivery of FA to the body (e.g. adipose liver, and muscle tissue). Formation of CMs begins within the ER membrane, where apolipoprotein (ApoB-48) is lipidated, facilitated by microsomal TAG transfer protein (MTTP). ApoAIV is added to pre-CMs in the ER and plays an important role in determining CM size as well as being an acute satiety factor, implicated in regulating both gastric function and blood glucose homeostasis and has been investigated as a therapeutic target for obesity-related disease (Kohan et al. 2015). Pre-CMs are processed into mature CMs within the Golgi and are delivered to the Golgi within pre-CM transport vesicles. These are generated when FABP1 binds to the pre-CMs with CD36, CAMP7, and ApoB48 facilitating the budding of these transport vesicles. Maturation occurs with the addition of other apolipoproteins (ApoA1 and ApoAIV) and apoB48 glycosylation (Figure 1.3)(Giammanco et al. 2015).

CMs are secreted through the basolateral membrane. It is thought that the basement membrane below the enterocytes may become leaky to allow for the movement of CM across (Tso et al. 1986). From here, CMs enter the lamina propria, a layer of loose connective tissue under the basolateral side of enterocytes below the basement membrane. Together with the epithelium they form the intestinal mucosa, which

is highly vascularised by both the circulatory system and the lymphatic system. Control of CM transport through the lamina propria has not been extensively studied but may play a regulatory role with movement of CM typically occurring by diffusion, facilitated by convective fluid movement resulting from interstitial hydration (Tso et al. 1986). Intestinal blood flow is increased postprandially, which is speculated to modulate CM release with vasodilation thought to help mobilise the CM pools (Xiao et al. 2019). From the lamina propria, the CMs are taken up into lacteals, where they move through and leave through intercellular junctions (Dixon 2010). It is believed that lacteals are able to discriminate CMs size and composition with lacteals speculated to be involved in protecting against diet induced obesity (Zhang et al. 2018; Dixon 2010). From the lacteals, the CMs go to the meseneric lymphatic ducts, which are thought to play an active role in CM mobilisation, then to the thoracic duct before being released into the circulation, specifically the subclavin vein and on to the rest of the body (Kassis et al. 2016).

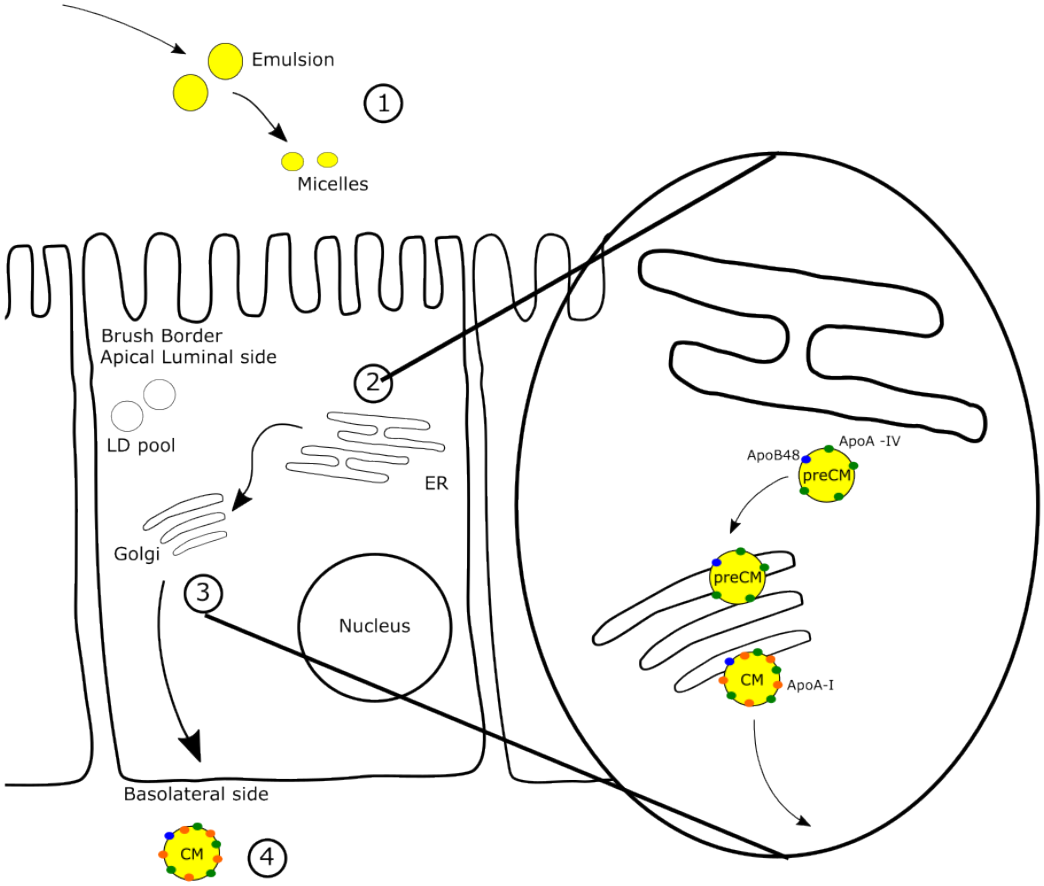


Figure 1.3: Overview of dietary lipid absorption in the intestine: After the ingestion of a meal, dietary fats, are emulsified in the small intestine by bile salts and pancreatic lipases. 1. **Micelle formation**: The emulsified triglycerides and other dietary lipids are then incorporated into mixed micelles, which are small aggregates of bile salts, phospholipids, cholesterol, and fatty acids. This aids in the absorption of these lipids across the intestinal epithelium. 2. **Intracellular lipid assembly**: Within the intestinal epithelial cells, the absorbed triglycerides and other dietary lipids are re-esterified and packaged with apolipoproteins and phospholipids to form pre-chylomicrons within the ER. 3. **Maturation**: Pre-chylomicrons are then transported to the Golgi apparatus, where they undergo further modifications, including the addition of apolipoprotein B-48. 4. **Secretion**: The mature chylomicrons are then released into the lymphatic system through the lacteals, eventually entering the bloodstream. Once in the bloodstream, chylomicrons deliver TAG to various tissues, including adipose tissue and muscle, where they are either stored or utilized for energy. The remnants of chylomicrons are eventually cleared from the bloodstream by the liver. This process is needed for the efficient absorption and utilization of dietary lipids in the body. Figure adapted from Hesse et al. 2013

Lipid retention within the intestines extends beyond both the prandial and postprandial period. In a healthy individual, enterocyte lipid concentration peaks around 3-5 hours postprandially and returns to baseline 6-8 hours postprandially (Evans et al. 1998). There is an additional 'flushing' effect observed. Stable-isotope studies have shown that following a second meal, 10-20% of a previous meal can contribute to CM content for the initial 20 minutes of the second meal consumption. TAG from a meal can continue contributing to CM lipid content for about 18 hours following ingestion (Evans et al. 1998). Indeed, when comparing sequential meals of identical macronutrient composition, postprandial CM-TAG concentrations increased in sequential meals when compared to those of the earlier meal (Mattes 2009a). This lipid pool mobilised to provide this secondary meal effect has been histologically shown to be from the jejunal tissue (Robertson et al. 2003) but the mechanisms involved remain unknown (Xiao et al. 2019). This effect could also be considered part of the, the cephalic phase which is a response to seeing, thinking and tasting food resulting in the body secreting insulin, ghrelin (a gastric signal of satiety) and other pancreatic polypeptides (Ahrén et al. 2001; Simonian et al. 2005). This cephalic phase is believed to be initiated by oral taste receptors sensing FA (Mattes 2009b).

Ingestion of glucose has also been shown to mobilise intestinal lipid stores. Investigation of human jejunal tissue by Jonchere et al and duodenal tissue by Xiao et al, showed that following initial accumulation of LDs in enterocytes, ingestion of a subsequent glucose solution resulted in secretion of the remaining lipid stores (Jonchere et al. 2018; Xiao et al. 2019). However, this is dependent on sufficient lipid stores, and following a 10 hour fast, glucose consumption did not result in secretion of enterocyte lipid (Xiao et al. 2019). Glucose is also proposed to have an effect through PL composition remodelling of LDs, CMs and the ER which will impact lipid storage and secretion (Hashidate-Yoshida et al. 2015; Böhn et al. 2015; Rong et al. 2015).

Understanding the factors effecting release of dietary FA into the circulation remains important for understanding MASLD, as these factors will alter the frequency and concentration of FA that the liver receives and consequently impacts on the progression of IHTAG. Other factors which have been implicated in the development

and progression of MASLD include hormones GLP-2 (Xiao et al. 2019) and oestrogen (Botham et al. 1999). Additionally, dietary fiber, along with other intestinal factors such as intestine transit time and gastric emptying time have been implicated, although further questions remain (Ponz de Leon et al. 1982; Wang et al. 2013).

In the circulation, CMs pass through adipose depots where, in an insulin stimulated manner, they are acted upon by lipoprotein lipase (LPL). Secreted by adipocytes, LPL attaches to the luminal side of the endothelium of the adjacent capillaries within the adipose depot to intercept passing CMs. LPL is stabilised by lipase maturation factor-1. LPL acts to catabolise TAG to release FA which are taken up by FATPs on adipocytes for either energy production or storage. Some FA however, are not taken up and instead bind to albumin as NEFA to be transported throughout the circulatory system to other tissues, these are often referred to as CM derived spillover NEFA (Feingold 2000).

Following the action of LPL, CM particles undergo a substantial reduction in size and become chylomicron remnants (CMR), which are enriched in cholesterol esters. This change in composition results in the transfer of apolipoproteins (Apo A and C) to other lipoproteins (primarily high density lipoprotein (HDL) and the acquisition of an ApoE molecule. The loss of ApoC-II, prevents the activation of LPL halting further hydrolysis of TAG (Feingold 2000; Li et al. 2014). The liver clears CMR from the circulation as the hepatocytes express low density lipoprotein (LDL) receptors (alongside LDL related protein (LRP) and syndecan-4) which bind to the ApoE on the CMR for endocytosis (Feingold 2000; Cooper 1997).

Within the hepatocyte, CMR derived TAG is used for multiple process as discussed in the following sections. The cholesterol esters are used for VLDL formation, bile production or are secreted with bile to the intestine (Kang et al. 2000). The cholesterol content regulates plasma TAG concentrations, and an increased cellular cholesterol content results in reduced hepatic expression of the LDL receptor. This regulation occurs at a transcriptional level via sterol regulatory element binding proteins (SREBP), and the LDL protein is retained inactive in the ER in conditions

with higher cholesterol and released when cellular cholesterol drops (Feingold 2000; Côté et al. 2014; Kang et al. 2000).

The phenotype of an individual may impact on CM metabolism. CM-derived spillover NEFA occurs to a greater extent in lean compared to obese individuals and in females compared to males (Piché et al. 2018). In obesity, adipose tissue metabolism is down-regulated, so clearance of CM-TAG may be reduced, resulting in greater amounts of TAG derived from CMRs potentially entering the liver (Xiao et al. 2020). Tollin et al, investigated the influence of age and sex on TAG clearance, by using an infused lipid emulsion (intralipid) where they measured the removal of intralipid particles from plasma in Swedish adults aged between 20 and 70 years. They found clearance of TAG rich particles was faster in women compared to men across all age groups and, in the male population, clearance did not change with age while the clearance rate decreased in women with increasing age. For both genders there was a negative correlation between particle clearance and obesity (Tollin et al. 1985). However, whether decreased clearance or increased secretion is more atherogenic remains to be elucidated.

The potential impact of dietary composition and concentration on the different aspects of transporting dietary fat around the body requires further investigation. This includes considerations such as; impact of dietary composition on the size of CMs, TAG content (quantity and quality) remaining in CMRs following action of adipose lipolysis, NEFA spillover quantity and contribution to ectopic fat accumulation, rate of clearance from the circulation and the interaction with phenotype for all of these. Understanding these, would allow for more targeted lifestyle advice to be given to patients presenting with MASLD or at risk of MASLD.

1.3.3 Adipose tissue

Adipose tissue serves as a dynamic endocrine organ, primarily functioning to serve nutrients in the form of TAG but also serves to orchestrate various hormones and signaling molecules to influence whole-body lipid metabolism and energy homeostasis. Leptin, a well-studied adipokine primarily produced by adipocytes,

plays a pivotal role in regulating appetite and energy expenditure by signaling the state of energy storage to the brain, particularly the hypothalamus. Leptin deficiency or resistance is associated with increased food intake and obesity (Obradovic et al. 2021). Adiponectin, another adipokine secreted by adipose tissue, exerts beneficial effects on lipid metabolism and insulin sensitivity. It enhances FA oxidation in skeletal muscle, reduces hepatic glucose production, and possesses anti-inflammatory properties. Low levels of adiponectin are observed in obesity and are associated with insulin resistance and cardiovascular risk (Yamauchi et al. 2013). Conversely, pro-inflammatory cytokines like tumor necrosis factor-alpha (TNF-α) and interleukin-6 (IL-6) are released by macrophages within adipose tissue in obesity. These cytokines contribute to the development of insulin resistance and systemic inflammation and their functioning may impinge on the development of MASLD (Hotamisligil 2006).

Within adipose tissue, fat is stored as TAG in LDs, when required it is liberated as NEFA. Insulin acts as a molecular switch between the nutritional status, of fasted and fed (Figure 1.4):

1.3.3.1 Adipose tissue metabolism in the fasted state

In the fasted state, FAs are released from adipocytes to be received by the liver with this release initiated by the catabolic process of lipolysis where TAG is hydrolysed sequentially: TAG to DAG to MAG to its constituent FAs and glycerol group catalysed by patatin-like phospholipase domain containing- 2 (PNPLA2) (also known as adipocyte triglyceride lipase (ATGL), hormone sensitive lipase (HSL) and monoacylglycerol lipase (MGL), respectively. The action, inhibition and trafficking of these lipases is tightly controlled, predominantly by insulin, with PNPLA2 being the rate limiting enzyme (Luo et al. 2016). Lipolytic activation is mediated by a reduction in plasma insulin and the systemic release of adrenaline and noradrenaline (catecholamines). The catecholamines are the primary mediators, and they act to activate and inhibit adipose tissue lipolysis depending on the adrenergic receptor (AR) expressed by the adipocytes. Activation results in phosphorylation of PLIN1 and HSL to initiate lipolysis. Alterations in receptor sensitivity have been reported

in the fasted state, with a reduction in insulin sensitivity and an increase in β-AR sensitivity corresponding with the promotion of lipolysis (Lafontan et al. 2009; Nielsen et al. 2014). An alternative pro-lypolytic signalling pathway has been described with cardiac hormones atrial natriuretic peptide and B-type natriuretic peptide. This pathway acts in a similar way with GPCRs activated to coordinate cGMP mediated phosphorylation of PLIN1 and HSL. Further work is needed to form a more precise picture of the switching on and off of these pathways and the quantities of their FA output, which will aid in understanding the flux of adipose derived fat to the liver and the role it may play in MASLD progression (Nielsen et al. 2014).

In obesity, there are associated alterations in adipocyte biology; increased adipocyte size and inflammation (Koh et al. 2021). The effect of obesity on adipose tissue FA release is an area of active research, with recent work demonstrating that FA release does not rise proportionally with fat mass (Karpe et al. 2011). Rather, inflammation of the adipose tissue, is associated with obesity which in turn has been linked with adverse hepatic outcomes including the development of MASLD and progression to MASH (Fuchs et al. 2021; Setyaningsih et al. 2021).

1.3.3.2 Adipose tissue FA metabolism in the post-prandial state

In the post-prandial state, in an insulin coordinated manner adipose lipolysis is inhibited through a signalling cascade from the insulin receptor in a cAMP mediated pathway to suppress the lipolytic cascade. Insulin additionally acts to promote TAG storage, synthesis and uptake (Chakrabarti et al. 2013; Nielsen et al. 2014). This results in a decrease in adipose derived FA entering the circulation and therefore potentially decreases the contribution of adipose derived fat to hepatic FA uptake whilst in the post prandial state.

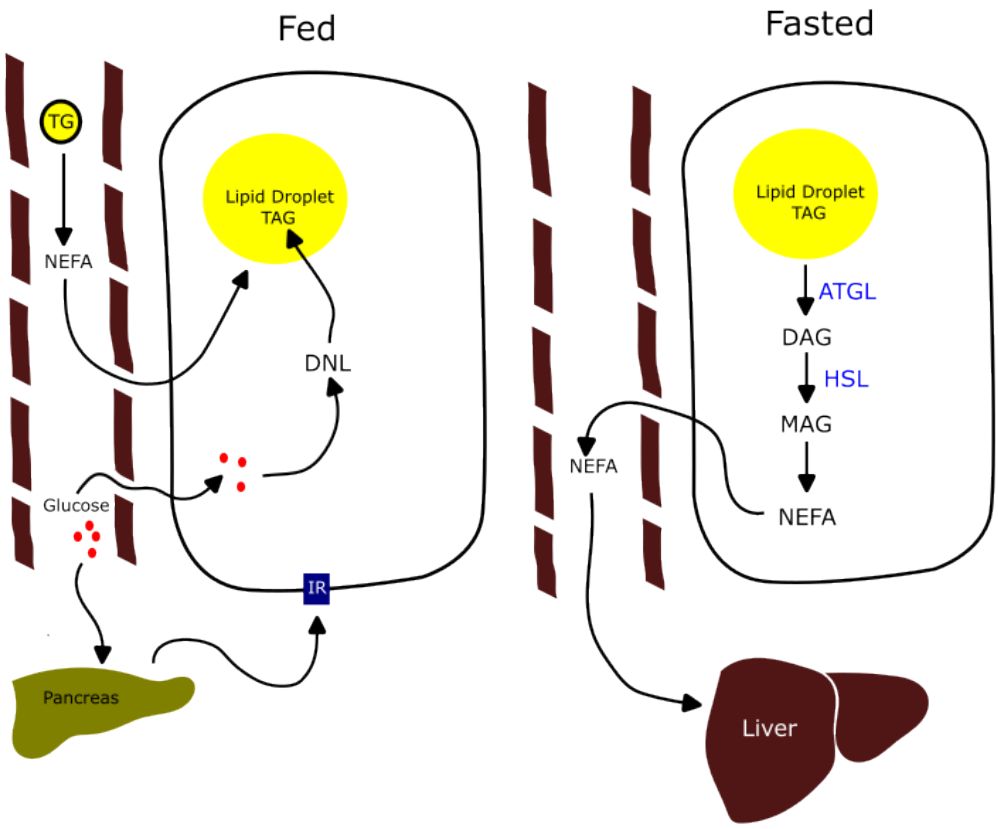


Figure 1.4: Fatty acid uptake and release in adpiocytes. In the fed state, triacylglycerol (TAG) in lipoproteins (chylomicrons (CM) or very-low-density lipoproteins (VLDL)) travel through the circulation to the adipose depots. Here, lipoprotein lipase(LPL) acts upon the lipoproteins to liberate NEFA which is taken up into the adipocyte and esterified to TAG and stored in a LD. In the fed state, there are also higher concentrations of plasma glucose, which is taken up into the adipocyte. Excess glucose is fed into the *de novo* lipogenesis pathway to form a fatty acids (FAs), which is esterified to TAG and stored within the lipid droplet. The plasma glucose also activates the β cells within the pancreas resulting in insulin being secreted. Insulin acts as a molecular switch in the hepatocytes and works to enhance TAG generation and storage pathways. In the fasted state, the TAG in the adipocyte is liberated and hydrolysed sequentially by enzymes AGTL, and HSL to yield non-esterified FA (NEFA). The NEFA is then secreted and travels through the circulation until it reaches the liver. Figure redrawn and adapted from Luo et al. 2016

1.4 Intrahepatic fatty acid uptake, synthesis and metabolism

1.4.1 Hepatic fat uptake

The liver receives fat both as TAG within lipoprotein remnants, and also as NEFA; both circulate systemically and upon reaching the hepatic portal vein they are taken up by hepatocytes (Mashek et al. 2015). The amount of FAs taken up into the liver is proportional to the plasma concentration which is in turn established from phenotypic factors (i.e. age, gender, BMI) and dietary consumption (Hagenfeldt et al. 1972). In the liver, FA are taken up both through passive diffusion and also facilitated transport mechanisms. CD36, expressed on the sinusoidal membrane of the hepatocytes has been implicated to facilitate the uptake of long chain FA from the blood stream. This process is regulated by nutritional status and insulin, with higher expression levels of CD36 observed in conditions such as insulin resistance and MASLD (Wilson et al. 2016).

Additionally, the liver expresses fatty acid transport proteins (FATPs), particularly FATP2 and FATP5. FATP2 is localized in the peroxisomal membrane, whereas FATP5 is found in the plasma membrane of hepatocytes. Both proteins exhibit acyl-CoA ligase activity, converting FAs into FA-CoAs, thereby trapping them within the hepatocyte and preventing their efflux (Hirsch et al. 1998). This metabolic trapping is essential for directing FAs towards specific intracellular pathways, such as TAG synthesis or β-oxidation. FABPs, including liver-type FABP (L-FABP), further facilitate intracellular FA trafficking by binding to FAs and enhancing their solubility and transport within the cytoplasm (Richieri et al. 1994).

Both human and murine models have implicated CD36 and FAT as having potential to have a detrimental influence of health promoting the progression of MASLD with alterations in the quantity expressed on the hepatocyte surface influencing the quantity of NEFA taken up. In a murine model, when CD36 was over-expressed, the mice presented with a fatty liver, and when CD36 was knocked down the IHTAG was reduced (Wilson et al. 2016). In both murine primary hepatocytes and the

hepatoma cell line, HepG2, CD36 has been demonstrated to regulate DNL as it is activated by insulin to form a complex which results in the disruption of SREBP cleavage activating protein (SCAP) and insulin-induced-gene 2 (INSIG2), resulting in the translocation of SREBP1 to the Golgi for processing. Down-regulation of SREBP1 in high fat fed CD36 knockout mice resulted in reduced DNL and over-expression of CD36 resulting in higher insulin-mediated DNL and increased LD formation *in vitro* (Zeng et al. 2022).

Lipoprotein particles are taken up by the LDLR which takes up both LDL and VLDL by binding and internalising lipoproteins in clathrin coated pits, before releasing them into endocytic compartments. The receptor is then recycled back to the surface to internalise more lipoproteins. The nascent endocytic vesicles recruit the early endosome antigen (EEA1) protein which acts as a membrane tether upstream of SNAREs (SNAP Receptors), to initiate the process of fusing endocytic vesicles together and with the early endosome (Mills et al. 1999). A V-pump then acidifies the endocytic vesicles and the endosome while calcium is lost through the action of the TRPV2 calcium channel. This acidification and loss of calcium accelerates the lipoprotein dissociation from the receptor (Davis et al. 1987; Saito et al. 2007; Zhao et al. 2009). Pompey et al, used quantitative fluorescence imaging to look at the spaciotemporal resolution of lipoprotein release during LDLR dependent uptake. To carry out these experiments, fibroblasts expressing LDLR were used and by visualizing uptake it was found that most dissociation occurred before the entry of the lipoprotein to the early endosome (Pompey et al. 2013). There are two mechanisms in action here: the first, utilizes the β-propeller (a repeating protein motif) and the second is independent of the β-propeller subunit. The mechanism which does not use the β-propeller motif is sufficient for the release of both LDL and VLDL but the mechanism which involves the β-propeller motif accelerates the release of both lipoprotein particles into the endocytic pathways (Pompey et al. 2013; Innerarity 2002)

LDL and VLDL bind to the LDLR receptor via different mechanisms: LDL binds through ApoB100 and VLDL binds through and interaction with ApoE, binding to different regions of the receptor (Guo et al. 2004). Both these binding sites however, are calcium sensitive, and loss of calcium results in a conformational change allowing the particle to interact with the β-propeller subunit initiating release (Pompey et al. 2013; Guo et al. 2004). This cycle takes about 6-7 minutes, however questions remain regarding the kinetics of this process because it is about 20 minutes before the changes in calcium and pH occur which would allow for the conformational change; thus there are likely to be other factors involved. Pompey et al have suggested that the rapidity of this process may be as a result of the proximity of the pumps to the LDLR-lipoprotein complex, with changes in local environment being sufficient to initiate the required conformational changes without the whole endocytic vesicle changing (Pompey et al. 2013). Receptor - lipoprotein release kinetics will impact the rate of accumulation of lipoprotein remnant derived TAG within the hepatocyte, as the receptor must be recycled back to the PM to receive more lipoprotein particles.

1.4.2 Esterification pathways

1.4.2.1 VLDL synthesis

If TAG is not stored in LDs, then it may be secreted in VLDLs. The synthesis of VLDL begins within the ER; where TAG associates with ApoB100 as it is translated and this complex then moves through the secretory organelles with more TAG added en route (Alves-Bezerra et al. 2018). Adipose-derived FAs have been demonstrated with stable-isotope tracer studies to be the greatest contributor to IHTAG and VLDL-TAG compared to dietary FA in individuals with MASLD (Donnelly et al. 2005). In healthy individuals, the contribution of NEFA to IHTAG and VLDL-TAG varies in an insulin dependent manner with both DNL and remnant derived lipoproteins thought to have a considerable effect (Nielsen et al. 2012). Indeed, in lean insulin sensitive (IS) individuals 75-84% of VLDL-TAG is derived from systemic NEFA. VLDL is the initial endogenous carrier of TAG delivering to other

tissues, like skeletal muscle and adipose tissue with LPL hydrolysing the VLDL particles to release NEFA,and generate IDL which are further metabolised to form LDL. The LDL is taken up by numerous tissues, but primarily the liver (via the LDL receptor). HDLs serve to do the opposite of the VLDL and LDL particles and nascent HDL molecules are secreted by the liver and the intestine and acquire PL and cholesterol (mediated by ABC1A) resulting in mature HDL which can then deliver cholesterol and TAG back to the liver (Feingold 2000).

Nutritional state can effect VLDL release and in the postprandial state, VLDL synthesis and release is upregulated, allowing FA to be moved to the adipose tissue for storage and preventing the build up of LD within hepatocytes. Under fasting conditions, VLDL secretion decreases (Nakajima et al. 2011). Understanding the impact of phenotype on VLDL secretion provides insight into the complex regulation of lipid metabolism and its implications for individual health with both gender and age changing VLDL secretion (Palmisano et al. 2017). Genetic predisposition plays a significant role in determining an individual's VLDL secretion pattern for example, polymorphisms in genes involved in lipid metabolism, such as those encoding ApoB and MTTP, can affect VLDL assembly and secretion rates. These genetic variations contribute to inter-individual differences in VLDL particle size, composition, and turnover, thereby influencing an individual's susceptibility to dyslipidemia and CVDs (Kathiresan et al. 2008; Zeissig et al. 2010). Phenotypic traits related to obesity and insulin resistance also impact VLDL secretion with obesity often associated with elevated VLDL production due to the enhanced availability of TAG for hepatic VLDL synthesis (Adiels et al. 2008). Additionally, insulin resistance disrupts the suppression of VLDL secretion by insulin, leading to increased VLDL secretion from the liver, which has consequences for other tissues and increases the risk for progression of diseases such as atherosclerosis (Bjornstad et al. 2018). Dietary choices, physical activity levels, and nutrient impact on VLDL secretion, for example, a high-carbohydrate, low-fat diet may lead to increased VLDL synthesis and secretion, while a diet rich in UNSFA can have the opposite effect (Lewis et al. 1991; Parks et al. 1999).

1.4.2.2 Lipid droplets

Hepatic LD are a dynamic store of both lipid and protein. They consist of a core of TAG and sterol esters with a PL monolayer. The understanding of LD formation is an active area of interest. Biogenesis begins within the lipid bilayer of the ER and the PL monolayer composition is believed to be important in LD expansion, with phosphatidylcholine, the principal PL, acting as a surfactant (Krahmer et al. 2011). TAG synthesis protein GPAT4 has been found to co-localize on larger LDs (moving from the ER), suggesting that there are distinct populations with differing capacity for localised TAG synthesis and consequent expansion (Wilfling et al. 2013). However, proteomic analysis of LDs has revealed that the majority of the proteins on LDs are not involved in lipid metabolism pathways but rather function in processes such as cell signalling, membrane trafficking and steroid metabolic (Su et al. 2014).

In healthy individuals, LDs do not accumulate to a substantial level, as FA are kept in constant flux (Alves-Bezerra et al. 2018). In individuals with MASLD, the flux of FAs is disrupted, resulting in an accumulation of LDs with the secretion of TAG in VLDL unable to compensate for the increased presence of TAG (Perla et al. 2017). GWAS investigations by Mann et al, showed that the majority of genes altered in all stages of MASLD were related to the formation and turnover of LDs. Within this study, no genes were involved in either the global inflammatory system nor those implicated in T2DM (aside from GCKR which is pleiotropic and also regulates DNL) which further implicates that it is principally the presence of LDs and management of the FAs that initiates and progresses MASLD. Of the genes implicated in this GWAS by Mann et al, the top 10 included PNPLA3 and TM6SF2, which suggests a pathological mechanism directly relating to the size of the LD rather than the absolute amount of lipid accumulation. CIDEB, also implicated, is suggested to have three functions; i) promoting LD fusion, ii) regulating SREBP1/2 activity and iii) promoting the packaging of TAG in VLDL. Humans and mice with mutations in CIDEC (expressed in white adipose), develop small multilocular LDs with the same mechanisms speculated to occur *in vivo* in humans in the liver with CIDEB (Mann et al. 2022). Indeed, Verwij et al, generated an *in vitro* knockdown

model of CIDEB which prevented the accumulation of large LDs, irrespective of total FA content, and this reduction in large LDs demonstrated to be protective of MASLD in mice (Verweij et al. 2022). High fructose-fed CIDEB knock-down rodent model, also presented with less hepatic steatosis and smaller LDs after 2 months and these changes were associated with a reduction in SREBP1/2 activity with smaller VLDLs. However, CIDEB has been identified as causative in MASLD progression where there is a somatic mutation in patients with advance forms of MASLD (Mann et al. 2022). Further research is required to determine the consequences of LD size and the specific mechanisms driving these size changes for MASLD.

1.4.2.3 DNL

DNL predominantly occurs within the liver in humans and is the conversion of non-lipid precursors to FA that can either be esterified to TAG for secretion in VLDL or stored, or undergo oxidation although the latter is debated (Timlin et al. 2005). Glucose, is stored as glycogen or alternatively, converted into FA by the DNL pathway where, as a principle precursor, glucose is converted to pyruvate, which is metabolised to citrate in the tricarboxylic acid cycle (TCA cycle) within the mitochondria. Citrate can then be hydrolysed to form the acetyl-CoA for DNL by acetyl citrate lyase (Zhang et al. 2015). DNL takes place in the cytosol and begins with the carboxylation of acetyl-CoA to malonyl-CoA by acetyl-CoA carboxylase (ACC), the first committed step in the pathway, which is then acted upon by FA synthase (FASN) to primarily yield the end product palmitate (a 16 carbon SFA) (Zhang et al. 2015; Kim et al. 2017). There are two isozymes of ACC in mammals: ACC1 and ACC2 (Thampy et al. 1988). These are thought to have distinct roles with ACC1 being a cytosolic enzyme which is committed to the rate-limiting step in DNL and ACC2 being mitochondrial membrane associated, generating malonyl-CoA primarily to inhibit carnitine palmitoyltransferase (CPT-1), which is responsible for long-chain FA transport into the mitochondria, required for mitochondrial β-oxidation (Ruderman et al. 2003; Kim et al. 2017).

Flux through the DNL pathway occurs to a greater extent in the postprandial state when there are excess substrates (glucose and amino acids). DNL is activated via the insulin receptor which signals via AKT through mTORC1 and FOXO transcriptional factors. An increased insulin to glucagon ratio, in the fasted state results in the suppression of DNL and in the fed state, with increased insulin and substrate precursors, DNL is increased (Titchenell et al. 2016). In healthy individuals, the contribution of DNL derived FA to IHTAG and VLDL-TAG is minor: 5-10% between the fed and fasted state of IHTAG and VLDL-TAG palmitate. The contribution of DNL derived FA to IHTAG and VLDL-TAG has been observed to increase significantly in subjects with MASLD and can account nearly 30% of IHTAG and VLDL-TAG palmitate, particularly in the post prandial state (Parks et al. 1999; Timlin et al. 2005). The role of DNL in the development and progression of MASLD requires further consideration as although it has commonly been considered a detrimental pathway towards the progression of MASLD, this remains debated (Mashek et al. 2020).

Whilst DNL had been of recent focus, the precise control and interaction with dietary nutrients is not yet understood. Inhibition of DNL enzyme, ACC (ACC1 or ACC2) in both humans and mice, and thus DNL was investigated by Horton et al. and was shown to reduce hepatic steatosis, but increase plasma TAG (Kim et al. 2017). In mice, the presence of hyperinsulinema increased SREBP1-C which is a transcription factor which activates enzymes for DNL synthesis. Genetic ablation of SCAP, a protein required for SREBP activation and subsequent DNL activation ameliorated steatosis and reduced plasma TAG in rodents. ACC1 knockout in mice is embryonic lethal, however, a liver specific knockout in mice treated with a high sucrose diet showed a reduced DNL rate compared to control. Knocking down ACC2 had conflicting results, with higher FA oxidation in a germline knockout in the muscle and heart tissue but a lower body fat, but another germline knockout had no alteration in FA metabolism. However, it is worth noting that the relevant importance of these finding are debated as rodents have a higher DNL compared to humans (Aarsland et al. 1997; Shimomura et al. 1999; Wolfe 1998).

To further progress understanding of DNL and interrogate therapeutic avenues, Kim et al, utilized MK4074, a pharmacological inhibitor of ACC1 and ACC2 and, after one month saw lower hepatic steatosis but an increase in plasma TAG in mice and humans. In the fed state, there was an increase in acetoacetate and β-hydrocybuterate, ketones, with the same seen in the fasted state to a greater extent. ACC inhibition was also associated with increased VLDL production, with GPAT1, the first committed step in TAG synthesis having increased activity likely due to increase SREBP1c activation. DNL can also be knocked down by inhibition of FASN which deletes endogenous PPARα ligand reducing its activity and the expression of the PPAR genes involved in FA oxidation. The ACC liver knock out mouse had reduced flux through FASN and reduced PPARα genes and other genes (HMGcoa synthase, CPT1a). FASN knockout liver accumulated malonyl CoA blocking mitochondrial oxidation, whereas the ACC knockdown liver has reduced malonyl CoA and therefore enhanced FA oxidation (Kim et al. 2017).

Although DNL is understood to contribute to the accumulation of IHTAG, the extent to which it is adverse for the progression of MASLD remains to be elucidated. Figure 1.5 shows the role of DNL in the post-parandial state state.

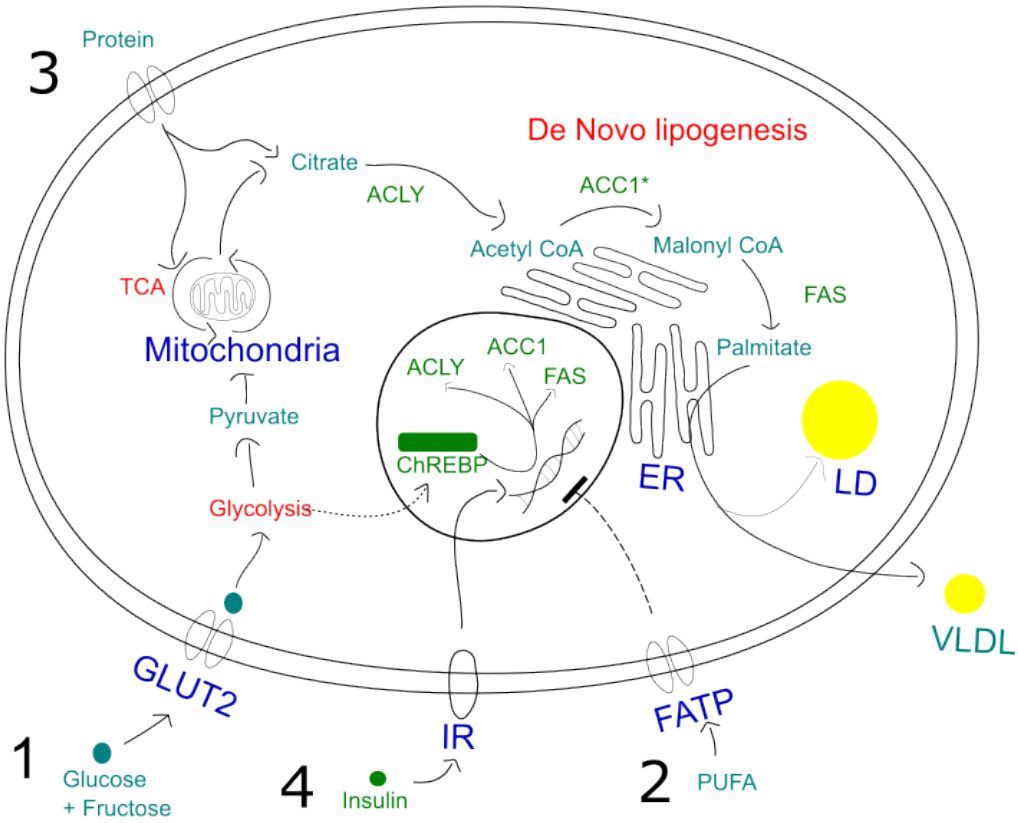


Figure 1.5: Hepatic *de novo* lipogenesis. In the post-prandial state, DNL acts to maintain energy homeostasis by metabolizing extra macronutrients into FA for either storage as TAG in LD or for secretion in VLDLs. 1) **Glucose:** Glucose is taken up into the cell via GLUT2 receptor and metabolized via glycolysis. Fructose is also metabolized by glycolysis but skips the initial rate limiting steps. Glycolysis produces pyruvate which feeds into the citric acid (TCA) cycle within the mitochondria, to produce citrate. Which is then metabolized by ACLY (ATP citrate lyase), ACC1 (acetyl CoA carboxylase) and FAS sequentially to yield palmitate. Palmitate is then esterified to TAG and either stored in LDs or secreted in VLDLs. 2) **Fats:** Fats, specifically PUFA, inhibit the transcription of DNL associated genes. 3) **Protein:** Proteins feed into these pathways at various points depending on the amino acids. 4) **Insulin:** Insulin upregulates DNL by upregulating the transcription of DNL associated genes. Glycolysis metabolites also upregulate DNL associated genes. Abbreviations: DNL, *de novo* lipogenesis; LD, liver disease; TAG, triacylglyceride; VLDL, very low-density lipoprotein. Figure adapted from review published during this thesis (Cross et al. 2023)

1.4.3 Oxidation pathways

In health, FA within the liver enter oxidation pathways within the cells to provide energy in the form of ATP via β-oxidation in the mitochondria and peroxisomes. Mitochondrial oxidation is the major oxidation pathway for short, medium and long chain FA, with all being oxidised to acetyl-CoA, which then either enters the TCA cycle to undergo complete oxidation to CO_2 or undergo ketogenesis where the ketone bodies acetoacetate, acetone, and β-hydroxybutyrate may be formed. β-hydroxybutyrate is often used as a marker of hepatic FA oxidation (Zhang et al. 2015; Alves-Bezerra et al. 2018).

In MASLD patients, although some demonstrate enhanced FA oxidation, it is insufficient to normalise lipid levels and is not seen in all patients. Additionally, enhanced cellular damage including oxidative stress and consequential disease progression have been proposed (Ipsen et al. 2018). However, understanding of the role of oxidative stress in MASLD patients remains inconclusive, with speculated adaptive mechanisms resulting in the uncoupling of the oxidation processes from ATP production to prevent excess ATP production (Perla et al. 2017). Additionally the role of the peroxisomal oxidation in contributing to oxidative stress remains unclear.

Peroxisomes, are membrane bound organelles which carry out FA oxidation that cannot be done by the mitochondria (LCFA (>22 carbons), branched chain FA, d-amino acids and polyamines, ether lipids and bile acids). Peroxisomes act as important regulators and interact with the ER (for anabolic processes), mitochondria (for catabolic processes), LDs and lysosomes. Peroxisomes are implicated in energy homeostasis, with disruption increasing the risk of obesity, dyslipidemia and dysregulated glucose homeostasis (Wanders et al. 2023). Additionally, peroxisomes function to coordinate H_2O_2 synthesis and degradation. Products are shuttled to the mitochondria for complete oxidation, as peroxisomes lack an electron transport chain. Peroxisomes also carry out α-oxidation which is oxidative decarboxylation to remove the terminal carboxyl group, which is important in the multi methyl branched FAs (Kleiboeker et al. 2022). High levels of malonyl-CoA inhibit transfer

of LCFA to the mitochondria and therefore block the β-oxidation of these LCFA from the peroxisome. Peroxisomal and mitochondrial oxidation are consequently inversely associated, when mitochondrial oxidation is high, peroxisomal oxidation is low (Kleiboeker et al. 2022; Fransen et al. 2017).

Peroxisomal regulation of LD is enabled by a spatial association between LDs and peroxisomes as they are generated from the same ER subdomains with similar enzymes. In hepatocytes, fasting induces peroxisome and LD contact which in turn regulates lipolysis as peroxisomal β-oxidation is a regulator of cellular lipid homeostasis and inhibits the autophagic degradation of LDs (Kleiboeker et al. 2022). A detailed study by Ding et al probed the peroxisome - LD relationship in hepatocytes and found a mechanism whereby increased reactive oxygen species (ROS) level resulted from higher levels of peroxisomal oxidation which were sensed by PEX2, an E3 ubiquitinase which in turn downregulated ATGL through ubiquitination. These interactions also generate bridging events to physically locate the peroxisomes and LDs together, and thus enable peroxisomal regulation of LD access (Ding et al. 2021)

1.5 Influence of dietary composition on hepatic metabolism

Adult humans require the dietary macronutrients of carbohydrate, fat and protein for health, which are typically consumed in a ratio of 45-65%, 20-35% and 10-35% of total energy consumption respectively (Manore 2005; Espinosa-Salas et al. 2024). Macronutrients are metabolised differently and consequently their propensity for obesity development varies with protein accepted to elicit a greater satiating effect and therefore high consumption is associated with weight-loss as energy intake is reduced (Paddon-Jones et al. 2008). Contrary, both high carbohydrate and fat consumption have been readily associated with an increased risk of developing obesity (Schutz 1995). The impact of macronutrient composition, specifically FA on the accumulation of IHTAG remains to be determined. Research is often confounded by differences in calorie intake, limited control of other dietary aspects and a lack of sex matching (Hodson et al. 2019). An overview of the varying study designs and protocols and their respective advantages and disadvantages for answering questions regarding the impact of dietary changes has historically been succinctly highlighted by Jo L Freudenheim and to-date remain unchanged (Freudenheim 1993). Further understanding of the interaction between diet, and IHTAG accumulation will aid in the development of dietary recommendations which may contribute towards reducing the prevalence and improving the management of MASLD.

Evidence from human studies has demonstrated that the quantity and quality of dietary fats and sugars is important health and reducing the risk of developing disease such as MASLD. Diets enriched in SFA have been shown to result in increased IHTAG relative to diets enriched in UNSFA (Luukkonen et al. 2018; Parry et al. 2020a). The UNSFA, PUFA is typically consumed as part of dietary plant seeds, nuts and fish, and MUFA is additionally found in diary and meat. The two most studies are the omega fats (3 and 6), which have different effects on the body and are an active research area although this is outside the scope of this thesis (Gómez Candela et al. 2011). Briefly, they both suppress lipogenesis and stimulate FA oxidation and promote autophagy (Girard et al. 1994; Gómez Candela

et al. 2011; Parker et al. 2012). Within the hepatocyte PUFAs have been shown to tonically suppress SREBP1 which results in the reduced expression of many FA processing enzymes including ACLYL, FAS, ELOVL SCD1, GPAT1, G6PD, PLTP and PNPLA3 (Kim et al. 2017).

Mediterranean diets (MDs), typically enriched in MUFA are associated with positive health outcomes with lower levels of CVD and decreased mortality (Davis et al. 2015). Ryan et al compared the MD with a low fat- high carbohydrate diet where twelve individuals, with biopsy proven MASLD (50:50 M/F) were recruited and took part in a 6 week cross over diet, with a 6 week washout period. The MD was high in both MUFA and omega-3 PUFA, and the overall dietary composition was 40% derived from FA, 40% carbohydrate and 20% protein of total energy expenditure. Although mean weight-loss was not significantly different between the two diets, the MD diet resulted in a significant reduction in hepatic steatosis when compared to the control diet, as well as an increased insulin sensitivity in those individuals who were on the MD diet (Ryan et al. 2013). Suggesting that MUFA enriched diets are healthier for livers when compared to diets lower in fat but higher in carbohydrate.

Human dietary intervention studies have shown that consumption of SFA compared to either UNSFA or carbohydrate, in the context of a hypercaloric diet resulted in greater IHTAG accumulation despite similar weight gain between groups (Luukkonen et al. 2018). SFA rich diets are considered to be associated with more adverse health outcomes than UNSFA including an increased risk of CVD and MASLD (Luukkonen et al. 2018; Koutoukidis et al. 2019). The main dietary source of SFA is from animal products; meat and dairy as well as palm oil, which is added to a large number of foods. Human studies have reported greater insulin resistance, steatosis and a proinflammatory state when measured with serum TNF-α and interleukin-1 (IL1) in SFA enriched diets (Koska et al. 2016). Diets enriched in SFA have also been shown to increase plasma VLDL concentration, contributing to dyslipidemia (Mensink et al. 1992). In animals, SFA has been associated with increased ER stress, death receptor signalling, mitochondrial apoptosis, TLR stimulation, inflammasomes, and autophagic impairment (Townsend et al. 2019;

Egnatchik et al. 2014). Dietary SFA are also associated with increased total plasma cholesterol (Parry et al. 2020b; Katan et al. 2010).

Parry et al demonstrated that consumption of a eucaloric diet, enriched with SFA increased IHTAG compared to consumption of a eucaloric diet enriched in free sugars (Parry et al. 2020a). The underlying mechanisms for why SFA increases IHTAG to a greater extent remains unclear but it has been suggested that increased FA flux, altered metabolic processes and ER stress may play a role (Wang et al. 2006; Townsend et al. 2019). *In vitro* data, using Chinese Hamster Ovary cells (CHOs) by Borradaile et al linked to palmitic acid, in CHOs to increased ER stress, when palmitate was incorporated into the ER PL membrane (Borradaile et al. 2006) and similar mechanisms may occur within human hepatocytes.

Whether SFA, with varying chain length have the same contribution to adverse health outcomes is debated. It has been suggested that there is insufficient evidence to attribute all SFA sources as having a deleterious effect on metabolic health, with advocates suggesting SFA derived from dairy products may not be as harmful regarding the risks of MASLD, although of note, this study was funded by the diary industry (Unger et al. 2019). However, evidence against dairy derived SFA being less harmful has been described by Menzel who looked at the dietary FA profile in vegans, who consume no dairy products, with omnivores (n=36, average duration of 4.8 years) with no difference in total energy intake, but significant differences in the plasma FA compositions to favour PUFA with lower total FA, and SFA and MUFA proportions in vegans, with these compositions favouring improved health outcomes (Menzel et al. 2022). Further studies are required to understand the exact influence of SFA of different lengths and how differing combinations of them will impact on human health.

1.5.1 Carbohydrates

Carbohydrates, classified as either simple or complex (monosaccharides or polysaccharides respectively) move through the body differently, with simple carbohydrates absorbed in the small intestine to the blood where they are circulated throughout

the body to be either used as fuel or stored for later. Complex carbohydrates e.g. grains and oats are broken down to produce simple sugars, however, depending on the nutrient structure, they have a slower rate of digestion (the glycaemic index). Consequently absorption of complex carbohydrate derived sugars occurs within different regions of the gastrointestinal tract with differing glycaemic load (a measure that accounts for the blood sugar changes elicited by the carbohydrate) (Vlachos et al. 2020). Direct relationships between the glycaemic load on body weight, T2DM and CVD have been extensively reviewed by Vega-López et al who concluded that the glycaemic load is unlikely to be indicative of the disease risk or health outcomes and instead other dietary quality measures are more important e.g. total intake and dietary fibre (Vega-López et al. 2018).

A large proportion of studies investigating the role of dietary carbohydrate in MASLD have focused on sugar sweetened beverages (SSB) which are the largest contributor of added sugar to the diet in the US (Malik et al. 2022). A significant relationship has been observed with consumption of SSB and an increase in weight, T2DM and CVD (Anderson et al. 2020; Li et al. 2020; Pietrantoni et al. 2022; Li et al. 2023). Maersk et al. compared consumption of sucrose sweetened beverages, with both non-calorific and iso-calorific beverages and observed an increase in ectopic fat, including the liver, specifically with the SSB despite no difference in body weight and total calorie intake compared to the other control groups (Maersk et al. 2012). Some of the effects of SSBs are believed to be due to the body incorrectly adjusting energy requirements in subsequent meals following liquid calorie consumption, as liquid calories are proposed to be less satiating than solid food therefore an individual is more likely to consume excess food (Drewnowski et al. 2007). Additionally, the proportion of fructose within these beverages may have additional negative impacts for IHTAG accumulation (Pepin et al. 2019). This correlation has been seen to such a degree that a number of countries have imposed a sugar tax on drinks as a means to tackle the obesity epidemic (White et al. 2023; Eykelenboom et al. 2021; Essman et al. 2022).

1.5.1.1 Dietary fructose

The two major monosaccharides are glucose and fructose and the debate on their respective contribution to metabolic disease continues (Choo et al. 2018). Fructose has been associated with obesity, and specifically increased IHTAG accumulation (Perez-Pozo et al. 2010; Cai et al. 2018), however, mechanistic understanding of fructose metabolism and consequential increases in IHTAG is still an active research area (Herman et al. 2021). Using labelled isotopes Jang et al. demonstrated that in mice, with a low dose of fructose the small intestine is able to metabolise the majority of fructose by the action of a fructose phosphorylating enzyme ketohexokinase within the gut. When a high dose of fructose was administered, fructose was released into circulation and consequently the liver where it is metabolised for ATP generation and IHTAG storage (Jang et al. 2018). Fructose is proposed to promote visceral adiposity, hepatic DNL and hypertension (from hyperuricemia, resulting from the production of uric acid as a fructose metabolite) (Perez-Pozo et al. 2010). Both glucose and fructose stimulate DNL which may lead to an increase in palmitate production, which is consequently stored as TAG or secreted in VLDLs. Fructose lacks a negative feedback step so is a potent inducer of DNL; It stimulates more lipid production than glucose whilst utilizing more ATP (Geidl-Flueck et al. 2023). However, the role of fructose towards MASLD requires further elucidation with conflicting results from different animal models (Yu et al. 2021; Schmidt et al. 2021).

1.5.1.2 Dietary glucose

Whole-body and liver glucose metabolism exhibit regulatory mechanisms to ensure glucose homeostasis in the fed and fasted states. In the fed state, after a meal, an increase in blood glucose levels triggers the release of insulin from pancreatic beta cells. Insulin orchestrates a cascade of events, facilitating glucose uptake into insulin-sensitive tissues such as skeletal muscle and adipose tissue. In muscle, glucose is utilized for energy production through glycolysis or stored as glycogen, while adipose tissue stores glucose as triglycerides (DeFronzo et al. 2009). In the liver, insulin effectively suppresses gluconeogenesis and glycogenolysis, minimizing hepatic glucose output (Saltiel et al. 2001).

In the fasted state, the liver provides a systemic source of glucose through two metabolic processes: i) glycogenolysis, the breakdown of stored glycogen and the initial source of secreted glucose; and ii) gluconeogenesis, a process by which glucose is produce from non-carbohydrate precursor molecules (lactate, pyruvate, most amino acids, glycerol and propionate), an important source following the depletion of hepatic glycogen stores (Hanson et al. 2013). Glucose release is triggered by the decrease of insulin secretion and increase of glucagon secretion from the pancreatic β- and α-cells respectively (Cooperberg et al. 2010). The liver releases glucose into the circulatory system to help maintain glucose homeostasis, ensuring an adequate supply for energy-requiring tissues, particularly the brain. The fasted state prompts a shift in peripheral tissue fuel utilization where skeletal muscle and other tissues transition from glucose to alternative energy sources, primarily FA and ketone bodies, which are critical adaptations to spare glucose for essential processes and to meet the energy needs of vital organs (Cahill 2006).

1.6 Implicated cellular mechanisms in development of hepatic steatosis

Despite the substantial research to-date, it is still not entirely clear what the cellular mechanisms, and their interaction with dietary factors, are that contribute to the development of MASLD. However, alongside variations with the glucose and fat metabolic pathways, implicated are: ER stress, extracellular vesicles (EVs), mechanical stress and circadian rhythms have been suggested to be involved:

ER Stress: Although the majority of TAG within the liver are stored in cytoplasmic LDs, it may be aberrantly stored within the ER potentially resulting in ER stress, which is a multi-path defensive system to protect the cell from further damage and culminates in inhibited protein translation and folding, alongside an expansion of ER membrane (Baiceanu et al. 2016). Hepatic TAG accumulation has been associated with chronic ER stress in *in vitro* and *in vivo* mouse models (Alves-Bezerra et al. 2018). Moreover, ER stress has been shown to enhance TAG accumulation through activation of lipogenic genes, thus potentially self-propagating the pathogenic

process (Borradaile et al. 2006). ER stress has been shown to increase degradation of ApoB100 by both proteasomal and nonproteasomal mechanisms, which may result in reduced VLDL secretion (Alves-Bezerra et al. 2018). Fu et al. analysed the proteomic and lipidomic characteristics of hepatocytes from lean and obese mice, with alterations in ER, FA and PL composition resulting in inhibition of sarco/ER ATPase (SERCA) activity (a regulator of calcium homeostasis) and associated ER stress. Correction of the altered PL composition *in vivo* was shown to both reduce chronic ER stress and improve glucose homeostasis, although these findings have yet to be replicated in humans (Fu et al. 2011). A comprehensive review by Flessa et al, have described current knowledge of the interactions between liver metabolism and specific arms of the ER stress pathway. The authors describe how each of the three branches has been implicated in being involved in the development of hepatic steatosis, where each arm interacts differently with other hepatic processes such as autophagy, apoptosis, lipotoxicity, with the nature and contribution of these interactions, at the different stages of MASLD needing further examination (Flessa et al. 2022).

Extracellular vesicles (EVs): EVs are are nanometric membrane surrounded particles, packaging molecular cargo and transporting it from donor to recipient cells. They are released by exosomes, from the late endosomes which are full of intraluminal vesicles named multivesicular bodies and microvesicles from the outward budding of the PM. Burrata et al investigated the relationship between lipotoxic stress and the membrane lipid profiles of EVS released from Huh7 cells; EVS are important in cellular communication and there is an increase in EV release in MASH. Treatment with high amounts of palmitate resulted in ceremide enriched EVS which are understood to activate stellate cells and instigate further fibrosis. Data showed that it was either membrane saturation and or the ER stress which were crucial for determining which lipids were discarded. As this study utilized a single FA: palmitate, already understood to cause ER stress it is not possible to disentangle these two. However, EVs may be a potential route for discarding excess SFA. When ER stress was induced through other means, there was a change in the composition

of the EVs but not in the quantity generated (Buratta et al. 0123). Using mouse primary hepatocytes as a model and applying culturing media obtained from kupffer cell/macrophage cells treated with SFA enriched EVs mouse hepatocyte insulin signalling was observed to be impaired. This was thought to have occurred following a SFA-EVs mediated activation of a toll-like receptor 4 (TLR4) proinflammatory response initiated by the macrophages (Garcia-Martinez et al. 2023).

Circadian rhythms: These are 24 hours cycles, essential for adapting the internal environment to the external environment. Disruption in these processes has been shown to have implications for whole body metabolism. This is a two way process, with the metabolism helping to entrain the body clock but also is affected by the body clock. The suprachiasmatic nucleus (SCN) sets the rhythm, with the peripheral clock helping to add extra regulation. The SCN helps to regulate glucose and FA homeostasis by regulating glucose uptake and insulin release. Disruption has been strongly associated with obesity, by altering both hormone concentrations and metabolic gene expression (Dibner et al. 2010; Maury et al. 2010). Eckel-mahnan et al. have described how both the quality and timing of meals alters circadian metabolism, with a high fat diet (where there is more than 40% fat) disrupting normally oscillating genes (Eckel-Mahan et al. 2013). These changes may influence the development and progression of MASLD.

Several lipid species, including PL and NEFA, contribute to circadian rhythmicity. PPARγ may be regulated by the circadian clock component (Goto et al. 2011), while the potential effects on other PPARs need elucidating; PPARs are activated by dietary FA and their metabolic derivatives, thus serving as lipid sensors that activate lipid metabolism, including lipogenesis and lipolysis. Liu et al, reported that plasma levels of phosphatidylcholine (PC) 36:1 fluctuate diurnally and that PC production is regulated by hepatic PPARδ. Tandem mass spectrometry scanning identified PC 36:1 as PC (18:0/18:1), which acts as a ligand for PPARα in muscle, producing a rhythm of FA uptake (Liu et al. 2013); this finding suggests that rhythmic oscillations of lipid metabolites derived from hepatic lipogenesis can integrate metabolic functions between the liver and muscle. PPARs are associated

with SREBP-1c, a master regulator that controls hepatic DNL. Recent studies have shown that a sn-glycero-3-phosphocholine (GPC) (16:0/18:1), presumed to be a ligand of PPARα, is produced in an SREBP-1c-dependent manner, establishing a circadian rhythm for lipid oxidation in the liver (Guan et al. 2018). Further work is needed to understand the potential variation throughout a 24 hour period of the different hepatic metabolic pathways.

Mechanobiology: Potentially associated with MASLD progression is mechanobiology, which has shown that tissue stiffness contributes to malignancy, with matrix stiffness associated with double stranded DNA breaks and a depletion of DNA repair factors with associated chromosomal damage. Hepatocytes are known to be sensitive to stiffness, with increasing stiffness having been previously associated with the loss of hepatocyte specific functional markers (Natarajan et al. 2020). However, between 20 - 63% of MASLD related HCC is non cirrhotic with relatively soft tissue. A proposed mechanism for this damage is from LDs deforming and distorting the nucleus, serving as an internal mechanical stressor, despite the overall 'soft' environment. The nucleus is a known central integration site for mechanical stress as many cell types sense deformation through the nuclear membrane tension, and adapt to the resulting environment through alterations in epigenetics and 3D chromatin structure, with potential resulting changes in gene expression (Loneker et al. 2023). Loneker et al carried out an investigation into the effects of stiffness and the interaction with LDs. Seeding primary human hepatocytes (PHH) onto polyacrylamide gels replicating either the stiffness of a normal liver, or a chirrotic liver; a looser or stiff gel respectively. These cells were then treated with 400µM oleic acid, or a control group treated with Bovine Serum Albumin (BSA). The addition of oleate, decreased cell area but did not change overall cell volume. The nuclear cross sectional area and volume increased in response to increasing stiffness, both with and without oleic acid, but there was a reduced ability or nuclear spread in cells treated with oleic acid compared to control at any gel stiffness. All of these changes could impact on molecular crowding, osmotic pressure and consequently, reaction rates. Additionally, at all gel stiffness, the LDs deformed the nuclear membranes.

Lonker et al exploited the circularity of the hepatocyte nuclei to quantify the areas of local deformation, and showed that control cells had a lower amount of irregularity compared to those treated with controls at all gel stiffness's (Loneker et al. 2023). This implicates LD shape and size and therefore any lipid composition changes which impinge on this, with mechanical stressors on the cell, which may, in an *in vivo* environment alter the progression of MASLD. Whether this influences on MASLD generally or just the propensity for developing HCC remains to be elucidated.

1.7 Current models of hepatic steatosis

A major challenge in trying to understand the interaction between dietary composition and hepatic metabolism is the limited availability and accessibility of human liver models. Whole-body *in vivo* studies in humans, while preferred, do not allow for the direct measurement of cellular factors (with typically only total fat measured by MRS reported) and although whole-organ (*ex situ*) livers are advantageous for direct experimentation within a physiological setting, livers are hard to obtain and require specialized equipment and expertise.

Of the available models for MASLD, large animal models e.g. monkeys or pigs, offer the greatest proximity to human models, however, the use of large animal models pose potential ethical issues. Rodent models are commonly used for MASLD but are of varied relevance, with species specific differences in hepatic metabolism as shown by Teufel et al who carried out a GWAS comparing mRNA expression in mice with humans presenting MASLD and showed only about ∼10% of the genes differentially expressed in humans were also differentially expressed in the murine models tested (Teufel et al. 2016). There was an additional added potential divergence in relevance as animals are kept under laboratory conditions, which resulted in an altered microbiome, and given the noted link between the microbiome and MASLD this could impact results (Bowerman et al. 2021). As proposed by Jahn et al, the field would significantly benefit from greater consensus of what the minimal requirements of an appropriate animal model should be (Jahn et al. 2019).

In vitro studies, using either PHH or immortalised cells remain the work-horse model for understanding MASLD. PHH are considered the gold-standard, however, they come with considerable limitations including high costs, variability between batches, challenging isolation protocols, no profileration and they lose differentiated phenotypes (Zeilinger et al. 2016; Kegel et al. 2016). In contrast, immortalised cell lines are easily accessible and robust, however common culturing protocols, often include supraphysiological concentrations of nutrients, have been reported to poorly mimic PHHs or exhibit an exaggerated hepatoma-like metabolism, making it difficult to ascertain physiological relevance (Gunn et al. 2017; Gunn et al. 2020).

Huh7 cells represent a well-known human hepatoma cell line derived from a hepatocellular carcinoma of a 57-year-old Japanese male patient (Kawamoto et al. 2020). These cells have served as a critical tool in various fields of biomedical research, particularly in liver-related studies. One of the key advantages of Huh7 cells lies in their ability to exhibit several characteristics akin to PHH, such as the expression of liver-specific functions and the retention of metabolic activities, making them a valuable model for *in vitro* liver research. Additionally, their relative ease of culturing and propagation, as well as their capability for genetic manipulation, have facilitated extensive experimentation, allowing for a deeper understanding of various liver pathologies and the mechanisms involved (Nakabayashi et al. 1984). Huh7 also have been demonstrated to have effective lipid metabolism when confluent (Green et al. 2020; Ramos et al. 2022). Our group has previously described the impact of culturing media on Huh7 cellular metabolism, with the use of human serum (HS), rather than FBS, altering the phenotype to be similar to that which is seen *in vivo*. HepG2 cells are also often used to investigate IHTAG, however, these are characterised by a mutation in PNPLA2, which may affect metabolic functions (Gunn et al. 2017).

Advantages are likely to be gained from 3D models of hepatic metabolism, and a number of groups are working on developing these. As surmised in detail by Ramos et al, many 3D models are under development for MASLD. Organoids provide a way of trying to generate a more physiological model where cells are embedded within an

organotypic structure, with the benefits of better differentiation, migration, cell-cell interactions as well as the cells maintaining better genomic stability, making them more suitable for long term storage and high throughout screen for drugs. Further developments, including systems using 3D bioprinting (liver on a chip systems), which are designed to overcome spatial heterogeneity and aim to replicate the ECM environment are under development. 3D models enable control over fluid sheer stress, nutrient/gas exchange and waste removal. Work is being undertaken to make these an automated environment, although these models are being developed are utilising HepG2 cells (Ramos et al. 2022).

The difficulty of *in vivo* studies, with the significant caveats faced by all *ex vivo* or *in vitro* models, emphasizes the importance of complementing research findings from one model with data from another to ensure comprehensive and reliable insights into liver biology and pathology until the differences between these models are better defined.

1.8 Summary

The liver is a key organ in the metabolism of glucose and lipids (FA and cholesterol) and plays a role in the regulation of their systemic levels; maintaining function is important for metabolic homeostasis. Thus, further understanding the interaction with diet and the other aforementioned risk factors is important in lowering the risk of metabolic diseases. Understanding how the different fat inputs, either NEFA or TAG-rich lipoprotein remnants contribute to the accumulation of IHTAG will aid the understanding of the progression of MASLD and consequently, what actions or pharmaceutical agents will be most suitable for alleviating the disease.

1.9 Thesis aims

This thesis aimed to investigate the influence of dietary nutrients on intrahepatocellular lipid metabolism, specifically the effect of both quantity and quality of FA on IHTAG. This will be achieved using a combination of *in vitro* with the following aims:

- Determine the *in vitro* impact of treatment NEFA composition, specifically enriching for either SFA or UNSFA, on the accumulation of IHTAG. Determine potential differences in IHTAG storage and cellular metabolic function using a combination of human cell-line and primary cell models.
- Determine, the effect of IHTAG composition on the turnover of IHTAG and metabolic changes that may arise from shifting treatment FA composition in an *in vitro* model of hepatic steatosis.
- Investigate the effect of FA delivery, either as NEFA or diet derived TAG-rich lipoprotein remnant particles and the effect of CMR FA composition on IHTAG using *in vitro* cellular models.

1.10 Scientific contributions

The work of this thesis has contributed to a number of academic papers including two reviews and one methodological paper:

Title Dysregulation of hepatic metabolism with obesity factors influencing glucose and lipid metabolism

Journal Proceedings of the Nutrition Society

Authors Shilpa Nagarajan, Eloise Cross, Fabio Sanna, Leanne Hodson

---

Title Nutritional regulation of hepatic *de novo* lipogenesis in humans

Journal Current Opinion in Clinical Nutrition and Metabolic Care

Authors Eloise Cross, David Dearlove, Leanne Hodson

Title Determining the temporal, dose, and composition effects of nutritional substrates in an *in vitro* model of intrahepatocellular triglyceride accumulation

Journal Physiological Reports

Authors Shilpa Nagarajan, Eloise Cross, Elspeth Johnson, Fabio Sanna, Lorna Daniels, David Ray, Leanne Hodson

2

Characterisation of an *in vitro* model of IHTAG accumulation with FA treatments enriched in UNSFA or SFA

2.1 Introduction

The liver is a key organ in the metabolism of lipids and carbohydrates. Within the liver, hepatocytes are constantly transitioning between states of energy storage and release in response to nutritional state (i.e. fasted and post-prandial states). Perturbations which influence the balance of substrate flux may lead to IHTAG accumulation. Obesity, metabolic syndrome, and other lifestyle factors, such as dietary habits and physical inactivity, have emerged as contributors to the accumulation of IHTAG (Mundi et al. 2020; Ahadi et al. 2021). Recognising the roles these risk factors play, could potentially improve our approach to both preventing and managing the prevalence and prognosis of MASLD.

Recent research has focused on dietary factors encompassing both composition and concentration of nutrition; irrespective of macronutrient composition, hypercaloric diets augment Rosqvist et al. 2014) whilst hypocaloric diets reduce IHTAG (Houttu et al. 2021). What remains unclear, is how macronutrient composition influences IHTAG accrual, specifically the impact of fat composition on the dynamics of IHTAG accumulation and mobilisation. Evidence from human studies both in the

context of hypercaloric and isocaloric diets has shown that diets enriched in SFA result in greater IHTAG accumulation in contrast to diets enriched in UNSFA (e.g. MUFA/PUFAs) (Luukkonen et al. 2018; Rosqvist et al. 2014; Houttu et al. 2021). Furthermore, switching to a hypocaloric diet, specifically one enriched in UNSFA promotes greater hepatic fat loss among MASLD patients and (Arslanow et al. 2016). These findings have sparked discussions surrounding the underlying mechanisms responsible for this dichotomy, with insulin resistance and increased FA flux proposed as potential drivers for this divergence (Luukkonen et al. 2018). However, the mechanisms have remained elusive, primarily due to the inaccessibility of human liver hepatocytes. Consequently, to understand the influence of fat quality at a cellular level, the development of physiologically-relevant *in vitro* models is required.

Previous *in vitro* models aimed at simulating MASLD have been developed, however, they have a number of limitations including: i) short culturing time (typically 24 hours), which may capture only an acute response to nutritional substance changes rather than a sustained physiological response (Long et al. 2019; Ren et al. 2021; Moravcová et al. 2015); ii) use of only a single FA in the culture medium which is not representative of the complexity *in vivo* (Carotti et al. 2020; Ren et al. 2021); iii) use of FA concentrations at supraphysiological levels with no report on the glucose concentration used to culture the cells (Gomaraschi et al. 2019; Long et al. 2019). An *in vitro* cellular model with the ability to better replicate nutritional inputs would provide a better platform for investigating the interactions between dietary macronutrients and hepatic metabolism, specifically the accrual of IHTAG. Previously, our research group developed a cellular model of IHTAG accumulation which resulted in macrovesicular LD formation and profiled the metabolic function. This was achieved through culturing Huh7 cells with a high-fat, high-sugar containing treatment medium (11mM glucose, 5.5mM fructose and 800µM FA) (Gunn et al. 2020). Notably, this model predominantly utilized the UNSFA oleic acid and given the observations from human *in vivo* studies, where consumption of SFA resulted in a greater accumulation of IHTAG when compared to UNSFA (Luukkonen et al. 2018; Rosqvist et al. 2014; Houttu et al. 2021), we

sought to expand on this initial cellular model to investigate the impact of increasing the proportional concentration of SFA the hepatocytes received.

The aim of this chapter was to describe the effects of manipulating the FA composition within the culture medium. As such, two treatment media were generated: i) enriched in UNSFA and ii) enriched in SFA. Cell viability, metabolism and function were assessed in both Huh7 and PHH cells.

2.2 Methods

2.2.1 Cell culture

Two cell types were used for the work completed in this thesis; Human hepatocellular carcinoma cells (Huh7) (gifted from Dr Camilla Pramfalk (Karolinska Institutet), Primary human hepatocytes (PHH) (see Appendix Table A.1.1) for cell origin and phenotype). 5 human donors were used for this thesis. Huh7 cells were maintained at 37 °C in 5% carbon dioxide with 5.5mM glucose in Dulbecco's modified Eagle's medium (DMEM) + Glutamax™ (Gibco™, 21885025) with 10% foetal bovine serum (FBS) (Seralab, EU-000-F), 1% L-glutamine (Gibco™, 11539876), and 10,000 U/ml penicillin-streptomycin (Sigma-Aldrich, P4333). PHH cells, were stored within liquid nitrogen and only thawed for experiments.

2.2.1.1 Freezing and thawing

Cells were frozen and thawed as required. To initiate the thawing processes, cryovials containing cells were placed in a waterbath at 37°C for 2 minutes. 1mL of appropriate media was added and the cells were gently pipetted before being transferred to 5mL of pre-warmed media. Huh7 cells were thawed and transferred to a T75 (Sigma-Aldrich, Z707503) flask together with an additional 10ml of culturing media. 24 hours later, media was changed and cells were then cultured as described and passaged at least once before being used for any experiments. When not in use, cells were resuspended in the appropriate media with 10% DMSO (Sigma-Aldrich, D2650-5X5ML) and stored in liquid nitrogen.

2.2.1.2 Passaging and seeding of Huh7 cells

Cells were passaged upon reaching 80% confluency and dissociated from the culturing plate by incubation with TrypLE™ (Gibco™, 12604021)(5mL for a T75 flask, 10mL for a T175 flask (Sigma-Aldrich, CLS431080)) for 5 minutes at 37°C in 5% carbon dioxide. When cells were observed to detach from the culturing plate, the dissociation enzyme TrypLE was then neutralised by dilution with an equal volume of culturing media. Cell suspensions were centrifuged at 240xg for 5 minutes at

room temperature. Supernatant removed and cells resuspended in 5mL of complete media. Cells were counted using Cellometer SD100 counting chambers (Nexcelom Bioscience, CHT4-SD100-314) and appropriate densities were seeded into a new flask and experimental plates if required. Cells were seeded at an appropriate density (for a 96 well plate, 10,000 cells per plate, for a 24 well plate, 40,000 cells per well (Corning® CellBIND® multiple well plates, various), and cultured for 24 hours in maintenance media before being transferred to experimental media.

2.2.1.3 Culturing of PHH cells

For culturing PHH cells, plates were coated 24 hours before experiment with collagen type 1 (rats tail, ThermoFisher, A1048301). Plates were coated until the bottom was covered (200µL for 24 well and 50µL for 96 well plate). Plates were then washed with PBS. PHH cells were thawed as described. Once thawed, cells were counted to assess viability and number. A Cellometer SD100 counting chambers was used with the cell solution mixed 1:1 with 0.4% Trypan blue (ThermoFisher, 15250061) used to detect non-viable cells (those that take up the dye). Cells were transferred into plating medium (500mL of Williams E media (Sigma-Aldrich, W4125) with PHH thawing and plating supplements kit (ThermoFisher, CM3000), comprising of FBS (5%), dexamathasone (1µM), and a cocktail B solution of: penicillin-streptomycin (1%), human recombinant insulin (4µg/mL), GlutaMAX^{TM} (2mM) and HEPES (15mM) for 24 hours, before being transferred to experimental medium.

2.2.1.4 Treatment media

Previously, our group developed a cellular model of hepatic TAG accumulation (Gunn et al. 2020), by modifying nutritional substrates to induce macrovesicular LD accumulation. To probe the mechanisms underlying the greater IHTAG accumulation observed in human studies when SFA-enriched diets are consumed, we developed a FA mix that was characterised by a higher proportion of SFA (Table 2.1). These ratios were established based on an analysis of total FA in human blood samples by Hodson et al (Hodson et al. 2009).

2.2.1.5 Experimental FA stock production

FA stock solutions were produced by combining appropriate amounts of individual FA: α-linolenic acid (Cayman, 90210), linoleic acid (Cayman, 90150), palmitic acid (Sigma-Aldrich, P0500) and oleic acid (Cayman, 90260) to create a stock solution of 10mM (Table 2.1). To facilitate the dissolving of the FA into media, they were first combined in 1mL of ethanol, which later evaporates off (599.9µL and 634µL for OPLA and POLA respectively) before being incubated on a heat block at 40°C. Once liquid, the FAs were added drop-wise to a solution of 10% g/v BSA in DMEM F12 (ThermoFisher, 11320033), (95mL DMEM F12 and 9.5g BSA) and heated gently until visibly dissolved. Caution was taken to not overheat the solution in order to prevent aggregation. Stock was then sterile filtered with a 0.2µm filter. The final stock solution concentration was measured (see Section 2.2.5.7) before being used in experimental procedures.

Table 2.1: FA proportion for different FA treatment conditions and physiological ranges

	OPLA (%)	**POLA (%)**	**Observed Physiological (%)**
Oleic Acid	45	44	43-48
Palmitic Acid	30	45	27-43
Linoleic Acid	24	10	13-33
α-Linolenic Acid	1	1	N/A

For simplicity, these two different culture media shall be referred to as OPLA and POLA respectively, acknowledging their dominant FA composition with each letter a reference to the constituent FAs used.

2.2.1.6 Treatment protocol

For Huh7 cells, the standard treatment media, in addition to the FA (given at either high concentrations 800µM, low concentration 200µM, or no-fat control 0µM), was composed of DMEM 5.5mM glucose, with an additional 1% L-glut, and 10,000U/ml penicillin-streptomycin. Instead of FBS as used in the maintenance media, treatment media contained 2% Human male AB serum (HS)(Lot BRH1108782, Seralab, SM-412-HS), as it has been demonstrated to establish a more physiological cellular phenotype (Gunn et al. 2017; Pramfalk et al. 2020;

Green et al. 2015). PHH treatment media was made by adding PHH Maintenance Supplements (Thermofisher, CM4000), which contained dexamethasone, penicillin-streptomycin, insulin, tranferrin, selenium complex, BSA, linoleic acid, glutMAX^{TM}, and HEPES to 500mL of William's Medium E without phenol red. To this base media, the experimental FA compositions were added. Although the treatment conditions contain BSA, it was not included in the no-fat control as albumin has been documented to behave different depending on the ratio of FA it is bound to and has been shown to have biological effects itself and there will be albumin inherently present within the serums used (Vusse 2009). Cellular treatment media also contained 5mM of glucose.

Cellular media was changed every other day throughout the treatment. Huh7 cells were typically treated for 7 days total, with three changes of media unless otherwise stated (Figure 2.1). PHH cells were treated for 5 days, with two media changes, as viability started to decline after this time.

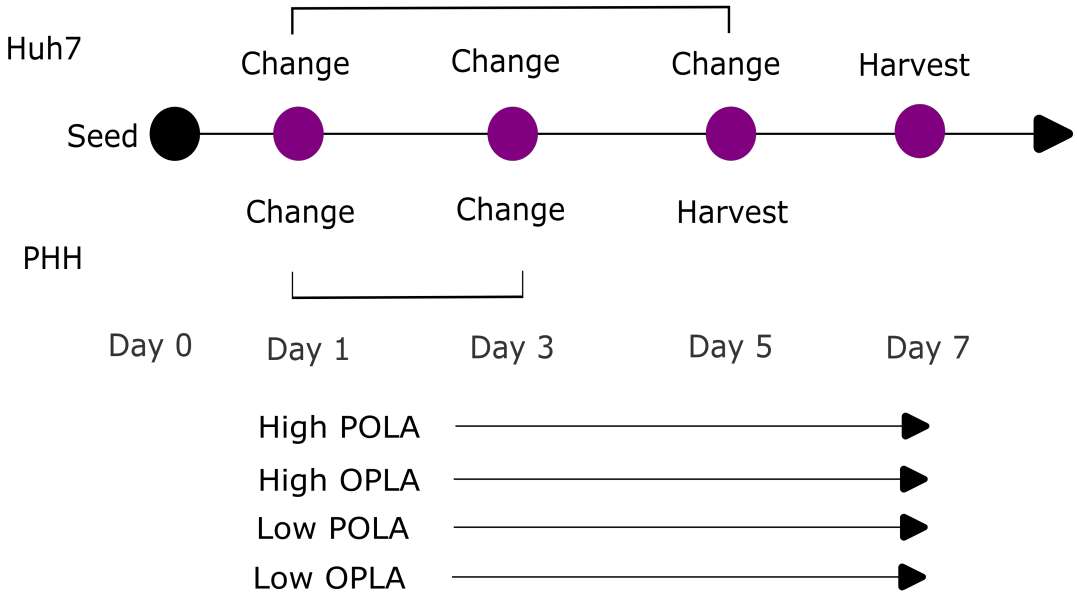


Figure 2.1: Cell culturing timeline for both Huh7 and PHH cells. Cells were seeded on day 0. From day 1, both Huh7 and PHH cells were cultured with experimental media. Experimental media was changed on days 3 and 5 for Huh7 cells before they were harvested for experimentation on day 7. For PHH cells, their media was changed again on day 3 and then the cells were harvested for experimentation on Day 7.

2.2.1.7 Reagent preparation

Depending on the experiment planned, cells were collected in different buffers. For lipid extraction experiments, cells were harvested in NP40% buffer and for Western blot experiments a RIPA buffer was used:

- NP40% (1% IGEPAL® CA-630 (Nonidet, P-40), 50 mM Trizma® hydrochloride (Sigma-Aldrich, 1185-53-1), and 150 mM sodium chloride)
- RIPA (10mM Tris-HCl, pH 8.0, 1mM EDTA , 0.5mM EGTA , 1% Triton X-100, 0.1% Sodium Deoxycholate , 0.1% SDS , 140mM NaCl , Dilute with dH_2O)

2.2.2 Cellular analysis

2.2.2.1 Protein analysis

Total protein content was assessed using the Bio-Rad DC^{TM} kit (Bio-Rad, 5000116). This is based on the Lowry method (Lowry et al. 1951). Protein first reacts with copper in an alkaline solution before Folin reagent is reduced by the protein-copper complex. This results in a colour change (the appearance of blue) which can be detected on a automatic plate reader (Versamax) at 650nm. For quantification, a standard curve was generated using BSA (Sigma, A7030) dissolved in PBS. This BSA was serial diluted to generate the concentrations 4-0.25 mg/mL, diluted in the same lysis buffer as the samples (either 1% NP-40 or RIPA). 5µL of sample was pipetted into a 96-well plate in duplicate. To each well, 25µL of the provided A + S solution (made of 24.5µL of Reagent A and 0.5µL of Reagent S) was added. 200µL of Reagent B was added before the plate was incubated for 15 minutes at room temperature before quantification. A standard curve and its corresponding equation were generated to allow calculation of protein concentration from the absorbance values.

2.2.2.2 Viability assay

Cellular viability was assessed using the Nano-Glo® Live Cell Assay System (Promega, N2011), which generates a luminescent signal proportional to the quantity of live cells. For this experiment, cells were cultured as outlined in Section 2.2.1.6

at either 0µM, 200µM or 800µM of OPLA or POLA in 96-well plates. The assay was carried out according to the manufactures instructions. Briefly the provided Nano-Glo® live cell substrate was diluted 20-fold in Nano-Glo® LCS dilution buffer, and 25µL added to the media in the plate (100µL). Plates were gently shaken for 15 seconds before a single-time point luminescence reading was taken. The Nano-Glo® live cell assay system was utilised every other day throughout 7-days of treatment. Data were normalised relative to control and adjusted to account for the number of days in between data collection (see Section 2.2.1).

2.2.2.3 ATP concentration

ATP concentration was quantified using the CellTiter-Glo® Luminescent Cell Viability Assay (Promega, G7570). Cells were cultured as described in Section 2.2.1.6 and Section 2.2.1) at concentrations of either 0µM, 200µM, 400µM or 800µM in a 96-well plate. A standard curve was generated in same plate from a 1mM ATP salt solution (15000nM, 11250nM, 7500nM, 5625nM, 3750nM, 1875nM, 937.5nM, 0M) in culturing media. The provided assay reagents were mixed together (substrate buffer and substrate powder) until homogeneous and added 1:1 v/v to the experimental wells, then incubated for 10 minutes in the dark, with the first two minutes on an orbital shaker (300rpm). Luminescence was measured and the standard curve utilised to establish ATP concentration.

2.2.2.4 Single cell gel electrophoresis (comet assay)

An assessment of DNA damage by single cell gel electrophoresis (SCGE), also known as the comet assay, was carried out using the Comet SCGE assay kit (Enzo, ADI-900-166). Cells were cultured as previously described in 200µM and 800µM OPLA, POLA and no-fat control before being detached from the plate with TrypLE. Cells were centrifuged at 240xg for 5 minutes, the pellet washed with PBS then diluted to a density of 100,000 cells/mL. Diluted cells were mixed with low melting agarose at 1 to 10 v/v ratio, 75µL of this cells/agarose mix was layered on the provided comet slide and incubated at 4°C for 15 minutes. Next, slides were incubated in the provided lysis solution at 4°C for 30 minutes, before being immersed in

freshly prepared alkaline solution (pH >13, 300mM NaOH, 1mM EDTA) for 30 minutes at room temperature in the dark. For the electrophoresis, slides were placed equidistant from electrodes in an alkaline solution (pH >13, 300mM NaOH, 1mM EDTA), a voltage of 1 volt/cm was run at a current of 300mA for 30 minutes. After, slides were incubated with the provided CYGREEN® Nucleic Acid Dye, 100µL per sample (30 minutes, room temperature, dark), then rinsed in water and allowed to dry at 37°C before being imaged. Ten images per slide were taken and analysed by OpenComet software on ImageJ (Schneider et al. 2012; Gyori et al. 2014). Damaged DNA was pulled along with the electrical current, whereas intact DNA remained in place. The resulting effect, following fluorescent staining is an image akin to a comet. Quantification of the 'head region', the stained and intact DNA which remained where the nucleus was, and the 'tail region', the damaged DNA allows quantification of any DNA damage caused by the treatment (Figure 2.2).

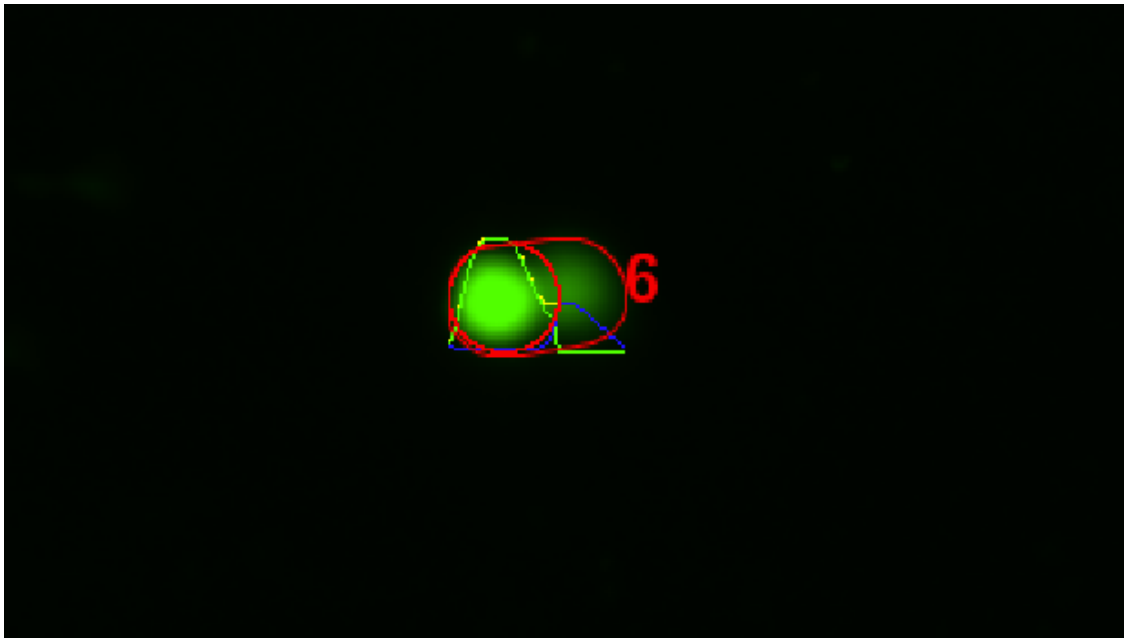


Figure 2.2: Quantification of DNA damage using single cell gel electrophoresis (comet assay). Quantification was carried out using OpenComet software in ImageJ. The resulting pattern of fluorescently labelled DNA resembled a comet:the head-region of the comet was the DNA which remaind intact within the space of the nucleus, and the fainter tail-region being the damaged DNA which had been pulled out of the nucleus by gel electrophoresis.

2.2.3 Glucose methods

2.2.3.1 Glycogen

Assessment of cellular glycogen was carried out with the Biovision glycogen kit (Biovision, k646-100). For work in this thesis, the flourometric version of the assay was performed. Cells were harvested in deionised water (200µL for a 24-well plate) and homogenates were immediately boiled for 10 minutes on a heatblock at 90°C to inactivate enzymes. Samples were then sonicated. At this point a protein assay (Section 2.2.2.1) was performed. Samples were then centrifuged at 18,000xg for 10 minutes to remove insoluble material. 5µL of sample was pipetted into a white 96-well plate in duplicate and the assay volume made up to 50µL with hydrolysis buffer (provided with the kit). A standard curve was generated from a glycogen stock of 0.2mg/mL by adding 10µL of standard to 90µL distilled water. Of this mixture, a curve was generated by adding 0, 2, 4, 6, 8 and 10µL of glycogen plus hydrolysis buffer to a final volume of 50µL per well resulting in 0, 0.04, 0.08, 0.12, 0.16 and 0.2µg per well. The provided hydrolysis enzyme mix was then added in a volume of 1µL for the fluorometric assay. This was then incubated for 30 minutes at room temperature. The reaction mixture was then added. For the fluorometric assay, this comprised of 48.7µL development buffer, 1µL development enzyme mix and 0.3µL per well. The reaction mixture was incubated for 30 minutes at room temperature, protected from the light. Fluorescence was then measure (Ex/Em = 535/587nm).

The following calculation was then carried out as described by the manufacturers.

$$C = B/V \times D(\mu g/\mu L)$$

Where:

- C is sample glycogen concentration
- B is the amount of glycogen from the standard curve (µg)
- V is the sample volume added to the reaction well (µL)
- D is the sample dilution factor

2.2.3.2 Glucose production

To measure cellular glucose production, Huh7 cells were serum starved for 24 hours and then transferred to Krebs Ringer Hepes (KRH) buffer for one hour before the media was collected and glucose measured. The serum starvation media comprised: 0.2% BSA, 1% P/S, 1% GlutaMax^{TM} (Gibco^{TM}, 35050038) , 1% Sodium Pyruvate (Gibco^{TM}, 11360070) in Phenol-Free Media (Thermofisher, A1443001). To this base media, the appropriate amount of FA was added to match that of the treatment media and glucose (Gibco^{TM}, A2494001) was added to the base media to constitute 5.5 mM of Glucose. The KRH media comprised of: NaCl (120mM), KCl (4.8 mM), $CaCl_2H_2O$ (2.5 mM), KH_2PO_4 (1.2 mM), $MgSO_4 \cdot 7H_2O$ (1.2 mM), $NaHCO_3$ (15 mM), HEPES buffer (10 mM) (Sigma, H0887) and was supplemented with 0.2% BSA, 1% P/S, 1% GlutaMax^{TM}, 2mM Sodium Pyruvate, 20 mM Lactate. To this, half the samples were treated with 10% deuterated water (^2H_2O) (CK Isotopes, DOLM-242-1) and then these were subdivided to be either control (stimulated with nothing) or stimulated with insulin (Merck, I9278) (100nM), or glucagon (Merck, 9007-92-5)(100µM).

Media glucose production was measured using the Glucose-Glo^{TM} Assay (Promega, J6021). Methods were carried out as per the manufacturers instructions. The assay was based on the production of a bioluminescent signal, generated by the coupling of glucose oxidation, which generated NADH, with a bioluminescent NADH detection system. This relies on the conversion of pro-luciferin reductase substrate (provided with the kit), to luciferin, which is then used by the provided ultra-Glo^{TM} recombinant luciferase to produce a light signal. 96-well plate (Corning, 353296) were used to enable the light signal generated to be easily observed. Standard curves were generated with a serial dilution of glucose, in PBS, starting at 50µM. Each sample and standard was measured in duplicate. To begin, 50µL of sample (KRH media from the cells), or control was added, followed by 25µL, of the glucose detection agent. Glucose detection agent mixture was constituted by solutions provided in the kit, and comprised, 25µL luciferine buffer, 0.125µL Reductase, 0.125µL Reductase substrate, 2µL glucose dehydrogenase, 0.125µL NAD. Plates

were shaken for 60s, then incubated at room temperature for 60 minutes. The luminescent signal was then recorded (BMG FLUOstar Omega Microplate, 48638). A standard curve and its equation were generated to allow calculation of glucose concentration from the luminescence values.

2.2.4 FA methods

To extract cellular or media FA for gas chromatography (GC) and GC-mass spectrometry (GCMS) cells were lysed in a 1% NP-40 TAG Buffer and sonicated to lyse the cells. The Folch method (Folch et al. 1957) was used to isolate total lipids from the sample. TAG and phospholipid fractions were separated using solid-phase extraction (SPE) (Burdge et al. 2000).

2.2.4.1 Folch method

The Folch extraction method is based on on the polarity between chloroform and methanol (Folch et al. 1957). To begin, 10µL of internal standard (containing known concentrations of glyceryl triheptadecanoate (15:0) (Sigma-Aldrich, T2151-100MG), heptade-canoic acid (17:0) (Sigma-Aldrich, H3500-1G) and 1,2-diheptanoyl-sn-glycero-3-phosphocholine (17:0) (Sigma-Aldrich, P4148-100MG)) was added to 500µL of sample (made to volume with 0.9% saline solution if required), including a blank, were combined and 5mL of chloroform:methanol (2:1 v/v) was added. Samples were then mixed on a rotary mixer for 15 minutes, then 1mL of 1M NaCl was added which sequesters salts and hydrophilic cell components in the aqueous phase, leaving lipids in the largely non-polar solvent phase. Following a further 15 minutes of mixing followed by 10 minutes of centrifugation at 800xg, 14°C, the top aqueous phase was removed and discarded. The solvent phase was evaporated to dryness at 50°C under nitrogen in a TurboVap LV (Biotage).

2.2.4.2 SPE column isolation and methylation

Solid phase extraction (SPE) columns, ISOLUTE SPE columns (Biotage, 470-0010-A) contain aminopropyl silica, which forms hydrogen bonds with lipids. In combination with specific solvents, different lipid classes can be isolated using selective extraction and elution. First, columns were pre-washed with acetone and chloroform (2x 1mL of each sequentially). Meanwhile, the lipid resulting from the Folch extraction was first resuspended in 1mL of chloroform before being added to the ISOLUTE SPE column. Any TAG and CE present, would have bond weakly to the silica, and consequently were eluted by a wash with chloroform and collected.

PLs were eluted with chloroform and methanol (2mL of 3:2 v/v). Both the eluted TAG/CE and PL fractions were evaporated to dryness in the TurboVap LV. The non-polar lipid fraction (TAG and CE) was then reconstituted in 1 mL hexane and fresh ISOLUTE SPE columns were prewashed with hexane before the samples were added. Hexane was used to elute CE and discarded before TAG was eluted with a solution of chloroform and ethyl acetate (2mL of 100:5:5 v/v/v), which was then evaporated to dryness in the TurboVap LV.

Samples were methylated to generate FA methyl esters (FAMES) in order to reduce the polarity of FAs and allow separation and measurement of FA species via GC. Transesterification was achieved by adding 400µL toluene (containing 0.01% butylated hydroxytoluene (Sigma-Aldrich, B1378)), 800 µL sulphuric acid in methanol (1.5% v/v for TAG and 6% v/v for PLs) to samples and incubating them in a water bath at 80°C (1 hour for TAG and NEFA and 2 hours for PLs). After cooling to room temperature, 2 mL of neutralising solution (25 mM $KHCO_3$ and 25 mM K_2CO_3 in H_2O) and 2 mL cyclohexane were added to extract the FAMEs. Samples were mixed and centrifuged at 800 xg for 10 minutes before the solvent phase was removed and evaporated to dryness under nitrogen in the TurboVap LV. Fractions were finally reconstituted in either 150µL or 500µL chloroform depending on the amount of FAs present and had 10µL external standard (methyl tricosonate; 23:0 (Sigma-Aldrich, T9900-1G) added.

2.2.4.3 Gas chromatography

GC allows the separation of compounds based on the time it takes for them to travel through a column. The time taken for the FA to pass through the column depends on the affinity of the FA towards the column. For this thesis, two GC machines have been utilised. Samples using the naturally abundant isotopes of the FA were analysed on a GC (Agilent, 7890) and samples where different FA isoforms were used were analysed on a GC model (Agilent, 6890N). All samples were run using a 30 m, 0.53 mm ID column uses a DB-WAX stationary phase (Agilent, 125-7032) with a helium gas phase. For samples where different stable-isotope FAs have not

been used the following setting were used for GC analysis: Starting at 60°C, the over temperature ramp (increase) rate was 20°C per minute to 200°C, then after a 12 minute hold phase (where the temperature is kept constant), a further ramp of 2°C per minute until 220°C, then a 2 minute hold, another tamp of 1°C a minute until 230°C with a final hold of 25 minutes. For experiment using different stable isotopes of FA, a longer experimental period was used to establish more separation between the compounds travelling through the GC. The following GC settings were used: Starting at 60°C, the oven temperature ramp rate was 20°C per minute to 200°C, then after a 24 minute hold phase, a further ramp of 1°C per minute until 210°C, then a 5 minute hold, another ramp of 10°C a minute until 230°C with a final hold of 42 minutes. An injection volume of 0.2-5µL was used depending on the sample. Peaks for individual FAs were identified by comparison with the retention times of a set of external standards of known composition of FAMEs (RM6 (Restek, RE35027) and STDB (Sigma-Aldrich, 18919-1AMP)).

Internal standards were incorporated at a known concentration, therefore, in the resulting chromatograph it was possible to compare the size of the peak of the FA of interest with that of the known internal standers and thus estimate the concentration of the FA of interest. Initial analysis of the relative sizes of the peaks on the chromatogram was carried out using the OpenLab software (Agilent). Final data was expressed relative to protein content of the sample. Each TAG was expressed as a percentage of the total amount of TAG present in the sample (molar percentage; mol%). As a marker of enzyme activity, product to precursor ratios were calculated from molar percentage values. Stearoyl-CoA desaturase activity can be estimated by the ratio of its products, palmitoleate and oleate (C16:1n-7 and 18:1n-7), to their precursors, palmitate and stearate (C16:0 and C18:0) respectively. Likewise, activity of FA elongase 6 (ELOVL6) was estimated by the ratio of stearate (C18:0) to palmitate (C16:0). Index of enzyme activities were estimated according to previous studies (Peter et al. 2011; Walle et al. 2016; Papandreou et al. 2017).

2.2.4.4 Gas chromatography - mass spectrometry

Gas chromatography - mass spectrometry (GCMS) (Agilent, 5973) was used to determine stable-isotope enrichment in samples with a 30 m, 0.32 mm ID column which uses a fused silica stationary phase (RE10224 Rtx-5, Agilent) with helium as the carrier gas. GCMS works by first ionising the samples, then accelerating them through the column before they are deflected by a magnetic field. The amount of deflection varies depending on the compounds size and therefore allows the mass to be determined and the particle identified based on output values of known masses. Since mass is also affected by the charge of the particle, mass is corrected to charge and expressed as mass to charge ratio (m/z). For this thesis, the GCMS was run in negative ion mode, with a collision voltage of 10kV, a scan time of 500ms, and a gas flow rate of 850L/min. Starting at 50°C, the oven temperature ramp rate was 25°C/ min to200°C, then 10°C/min 230 °C, with a final hold for 10 min. The ionisation voltage was 70eV with the source at 230°C. The injection volume was initially 0.2µL, however this was varied to obtain values for samples samples to have a similar mass size for the parent ion. Selected ion monitoring was used to quantify the number of ions at the mass-to-charge ratios of the FA of interest. A chromatograph was generated by the GCMS machine and the ratio of the area of the isotope of interest was compared to that of the predominant isotope.

2.2.4.5 *De novo* lipogenesis quantification

Intracellular DNL was measured by tracing the deuterium (^{2}H), from the culture media, into palmitate in both intracellular TAG, PL, and media TAG. ^{2}H-palmitate enrichment was determined by GC-MS.

Following the reasoning of Cobelli et al., the tracer to tracee ratio (TTR) can be used to indicate DNL (Cobelli et al. 1982). This can be calculated as per Equation 1.

Equation 1: Tracer to tracee ratio

$$TTR = \frac{m_1}{m_0}$$

Following the reasoning of Diraison et al., the fraction of FAs derived from DNL, F, was determined by examining the measured ratio of deuterium atoms to the total number of molecules and the expected ratio of deuterium atoms to the total number of molecules (Diraison et al. 2003). Calculations of DNL were based on the maximum number of deuterium molecules that can be donated to newly synthesised palmitate (17 *in vitro*, 22 *in vivo*) and the amount of deuterium enrichment present (Lee et al. 1994). The expected number is given by the product of the media deuterated water enrichment and the maximum number of hydrogen atoms which could be incorporated in the FA of interest.

Equation 2: Fraction of FA derived from DNL after culturing cells with heavy water.

$$F = \frac{\frac{(m_1+m_2...)}{(m_0+m_1+m_2...)}}{\%Enrichment \times max.duteria}$$

Historically, the amount of DNL has been measured by the TTR ratio - the tracer to tracee ratio. The unlabeled molecular mass of palmitic acid is 270 and the mass with one additional labelled hydrogen is 271. Therefore, this ratio looks at ions 271/270 to determine the proportion of the FA pool contributed to by DNL. For this thesis, to establish which analytical technique was most appropriate, the relative contribution of each of the ion labelled FA present was assessed within the samples generated (Figure 2.3a). This showed that there is an exponential decrease in deuterium incorporation. For this thesis, based on those ions that made a significant contribution to abundance from preliminary experiments, it was determined that only the first 5 ions should be incorporated into the calculation of the amount of (^{2}H) palmitate measured as the prevalence of the other ions was not a significant contribution.

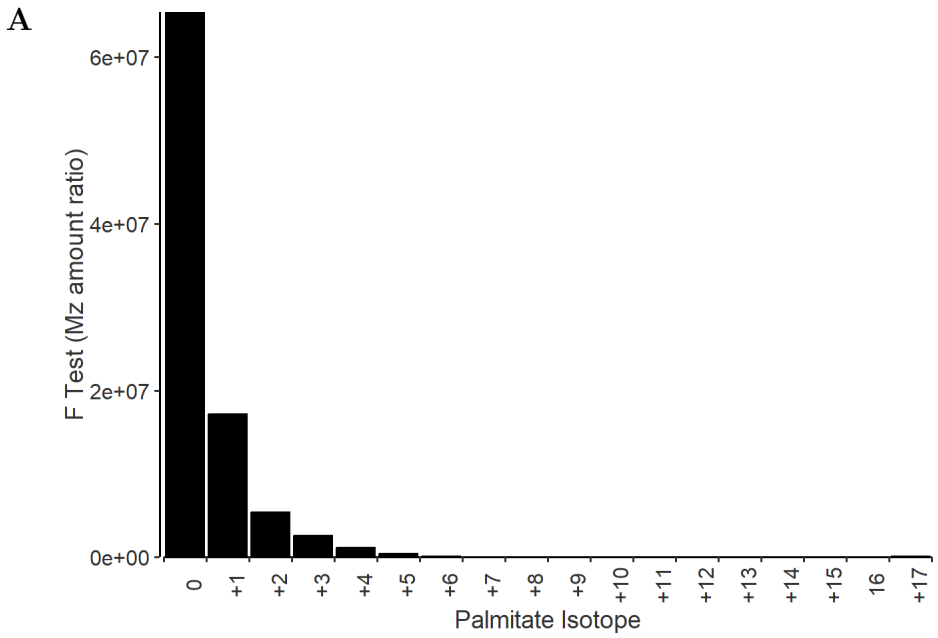


Figure 2.3: Inclusion of duterium into *de novo* lipogeneiss (DNL) derived palmiate in Huh7 cells. Prior to analysis, Huh7 cells were treatd with deuterated water and cultured for 7 days. Data show the typical number of deuteriums incorporated into palmitate for all condition types as measured by mass spectrometry. Data show the sum of the mean absolute values for the mass spectrometry ratio between the different isotopes.

2.2.4.6 Analysis of cellular oxidation

Labelled FA, specifically D31 palmitic acid and D33 oleic acid, when incorporated into the treatment medium are oxidised to yield deuterated water. This was analysed by gas chromatography-combustion-isotope ratio mass spectrometry (GC-IRMS) as per the manufacturer's instruction. Platinum catalysts were used with a helium gas carrier.

2.2.5 Biochemical Analysis

Biochemical analysis was carried out using automatic clinical biochemistry analysers to measure: TAG, cholesterol, glucose, urea, lactate, ApoB, and β-hydroxybutyrate (3-OHB). Assays were carried out according to manufacturer's instructions and used an appropriate calibrator or standard curve for quantification, as well as quality control samples (IL Test™ Control Level 1 and 2 or Human Assayed Multi-sera Level 2 and 3). Assays were previously optimised for low concentrations found

in vitro (Green et al. 2015). The relevant lysis buffer was used as a background control for intracellular cholesterol/TAG measurements and complete media used as a background for media analysis (NEFA, TAG, glucose, 3-OHB, Urea, ApoB, Lactate). Assays were carried out using either a iLab 600/650 (Instrumentation Laboratory) or a AU480 Chemistry Analyzer (Beckmancoulter, A91961) .

2.2.5.1 3-hydroxybutyrate concentration

The RANBUT D-3-Hydroxybutyrate (3-OHB) assay (Randox, RB1007) was used to measure 3-OHB concentrations in both cell media and plasma. This kit provided the reagents necessary for the oxidation of 3-OHB with 3-OHB dehydrogenase; the concomitant reduction of NAD+ to NADH changes absorbance of the sample, which directly correlates to the amount of 3-OHB present. The enzyme and co-enzyme mix was reconstituted in the supplied buffer before each experiment, and standards of 500, 125 and 62.5µM were used as calibrator samples.

2.2.5.2 Cholesterol concentration

Cholesterol assays (QuantILab, 0018250540) were performed to measure intracellular and plasma cholesterol. The cholesterol assay was based on an established method by Allain et al (Allain et al. 1974); cholesterol esters contained within the sample are first hydrolysed into cholesterol and NEFA via cholesterol esterase. The cholesterol can then be oxidised to cholest-4-en-3-one + H_2O_2 by cholesterol oxidase. $2H_2O_2$ are combined with 4-aminoantipyrine and pheno, peroxidation occurs, producing quinoneimine. The absorbance of quinoneimine is then measured at 510nm. This assay was carried out according to the manufacturers instruction.

2.2.5.3 Glucose concentration

Glucose in plasma and neat cell media was measured using the quantILab® Glucose (Oxidase) assay (quantILab®, 0018250850). The Glucose (Oxidase) reagent contained the enzymes and substrates for the following reactions: Glucose oxidase converts D-glucose to gluconic acid and H_2O_2, before H_2O_2 reacts with phenol and 4-aminoantipyrine via peroxidase to produce red quinoneimine. The absorbance

of the red dye measured is directly proportional to the amount of glucose in the sample. This assay was carried out according to the manufacturers instruction.

2.2.5.4 Lactate concentration

The L-lactate (LAC) assay (Randox LC3980), was used to determine the lactate concentration in cell media. The method used was based on the conversion of lactate to pyruvate and H_2O_2 via oxidation by lactate oxidase. The reaction of H_2O_2 with 4-aminoantipyrine and N-ethyl-N-(2,hydroxyl-3-sulphpropyl)-m-toluidine generates a purple colour, which can be measured by spectrophotometry. Lactate in cell media was measured after calibration with Calibration Serum level 3 and dilution of the sample 1:10 in distilled water. This assay was carried out according to the manufacturers instruction.

2.2.5.5 TAG concentration

TAG concentrations were determined using the quantILab® Triacylglycerides assay (quantILab®,0018255640). Media TAG and plasma were measured neat. Glycerol standards of 50, 100, 200 and 1000µM were used as calibrator samples before each assay was run. First, the sample was combined with the Triglycerides reagent, which contains the enzymes and substrates for the following set of reactions. TAG was first hydrolysed to glycerol and NEFAs by lipoprotein lipase, before the glycerol was phosphorylated to glycerol-3-phosphate. Oxidation by glycerophosphate oxidise produces dihydroxyacetone phosphate and H_2O_2 which further reacted with 4-aminoantipyrine and 4-chlorophenol to produce red quinoneimine; this was measured by absorbance at 540nm.

2.2.5.6 Urea concentration

Urea measurements in neat media were performed using the Urea Nitrogen Assay (quantILab®, 0018255450). Urea was first converted to $2NH_4^+$ and $2HCO_3^-$ via urease. NH_4 was then combined with α-oxoglutarate and NADH to form L-glutamine, NAD^+ and H_2O by the action of glutamate dehydrogenase; depletion of NADH decreased absorbance, which was used to determine urea concentration (Sampson et al. 1980).

2.2.5.7 NEFA concentration

Media NEFA was quantified on using the NEFA assay kit (Randox, FA115). This was a colourmetric assay and was carried out according to the manufacturers instructions.

2.2.5.8 Ubiquitin enrichment

Analysis of ubiquitination was carried out using the Ubiquitin Enrichment Kit (Thermofisher, 89899). Cells were harvested in RIPA buffer (see Section 2.2.1.7) and added 1:1 with TBS in the provided spin column to make a total volume of 500µL. The provided polyubiquitin positive control was also included in the experiment and analysis. 20µL of the poly-ubiquitin affinity resin was added to each sample and samples were incubated overnight at 4°C on an end-over-end rotator. Next, the stop-cap was removed on the column and the columns placed into 1.5mL eppendorf tubes and centrifuged at 5000xg for 15 seconds. The tubes were then re-caped and 300µL of wash buffer was added (one part RIPA buffer, with 9 parts TBS, 1mL made up for each sample being prepared). The column cap was then removed and the column placed into a new 1.5mL eppendorf tube before being centrifuged for 15 seconds at 5000xg. This step was repeated two more times. Sample was released from the columns in 50µL SDS-PAGE sample loading buffer. Columns were vortexed for 2-3 seconds and columns incubated in a heat block at 90°C for 10 minutes. Samples were then released from the column by centrifuging at 5000xg for 30 seconds. These ubiquitin enriched samples were then analysed by western blot.

2.2.6 Western blot

Before the assay was performed, the protein content of the samples was established as described in Section 2.2.2.1. 20µg of protein for each sample was heated to 90°C for 10 minutes. Biorad Criterion stain-free, precast gels with 7.5 % acrylamide (Biorad, 4561023) were loaded with a protein ladder (JenaBioscience, Blue-Eye, PS-104), one at either side of the sample wells. Samples were loaded into the gel and run at 230V in a tris-glycine-SDS running buffer (Biorad, 1610732) in a transfer tank (Biorad) for approximately 45 minutes. Gels were imaged to verify protein migration using a Biorad Chemidoc visualiser. Wet transfers with a tris/

glycine buffer (Biorad, 1610734) were used to transfer the separated proteins to a 0.45µm polyvinylidene-fluoride (PVDF) membrane (Immobilon, IPVH00010), pre-activated in methanol for 2 minutes. The transfers were carried out at 80V for 45 to 60 minutes and the membranes imaged on the visualiser to verify protein transfer. Membranes were blocked in blocking buffer (5% milk powder in TBS-T (1% tween-20 in tris-buffered saline)) for 60 minutes at room temperature with rocking. The blocking buffer was replaced with the primary antibody (anti ATGL, ab207799, Abcam) 1/500 dilution for the protein of interest, diluted in the same milk solution. Membranes were incubated overnight at 4°C with rocking. After removing the primary antibody buffer, the membranes were washed in TBS-T (four times ∼5 minutes) and then incubated for 60 minutes at room temperature with the appropriate secondary antibody (goat anti rabbit IgG, ab6721, 1/1000, abcam) in the milk. After washing in TBS-T, the membrane was incubated for 60 seconds in ECL substrate (Biorad, 1705060) and the protein bands imaged on the visualiser. The imaged band intensities for the protein of interest were measured using FIJI (Schindelin et al. 2012; Schneider et al. 2012) and normalised to those of a loading control protein.

2.2.7 Size exclusion chromatography

Cells were prepared using the 7-day protocol in T75 flasks. After 7- days in experimental medium, samples were washed twice with PBS and once with serum-free DMEM, which was collected for analysis of background. Cells were then incubated with 11mL of serum-free DMEM, before 10.5mL was removed and concentrated in Amicon Ultra-15 centrifugal filter devices (Merck, C7715) and centrifuged at 4500xg until approximately 200µL concentrated media remained (∼20 minutes). Concentrate was weighted to account for column efficiency and establish a contraction factor. The following analysis was done by Professor Camilla Pramfalk at Karolinska Insitutet, Sweden as described by Parini et al to determine media lipid content (Parini et al. 2006).

Size exclusion chromatography (SEC) was used to separate the lipoproteins in the cell media. This technique is similar to other chromatographic techniques and allows large, macromolecular particles contained within a solution to be separated based on their size, with the largest particles eluting first. Samples were automatically injected at a volume of 30µL and were carried over the column using an elution buffer (150 mM NaCl, 10 mM Tris-HCl and 0.02% sodium azide, pH7.4); this is delivered by the first pump at a flow-rate of 40 µL/min. Next, the separated lipoprotein fractions were continuously mixed with either cholesterol or TAG reagents. The reagents were kept on ice and delivered by the second pump at 40 µL/min flow rate. After this, the mixture passed through a 500 µL reaction-coil, PEEK tubing of internal-diameter 0.75 mm (Scantec Laboratory) immersed in a water bath at 37°C. Finally, the absorption was monitored with an UV-VIS detector at 500 nm and data were collected every 20 seconds. Total run-time for each sample was 75 min and 90 min for cholesterol and TAG analyses, respectively. Chromatograms were integrated by the D-7000 HPLC system manager software. The lipid content in the respective lipoprotein fraction was calculated as the product of the area percent and the lipid content determined from the injected sample.

2.2.8 Confocal imaging

Cells were fixed on coverslips in 4% PFA (w/v) and stored at 4°C until imaging. Coverslips were washed twice with PBS before cells were stained for imaging. The cellular model described in both chapter 3 and chapter 5 were stained with lipid, actin filaments and nuclear markers for imaging. Prior to staining, cover slips were incubated with 300µL of 0.01% Triton-X100 (Sigma-Aldrich, T8787) for 3 minutes. To stain the LDs, LipidTox™ (1:200 in PBS) (ThermoFisher, H34477) was applied for 30 minutes before the cover slips were washed twice with PBS. Alexa Fluor™ 488 Phalloidin (1:40 in PBS) (ThermoFisher, A12379) was used to stain the actin cytoskeleton and again coverslips were incubated for 30 minutes before being washed with PBS. To stain the nucleus, DAPI stain containing mounting media was used (Fluoromount-G™ Mounting Medium, with DAPI, ThermoFisher, 00-4959-52). Coverslips were then sealed and images were taken on a confocal microscope

using wavelengths: excitation/emission: 635/652nm for Lipid, excitation/emission: 495/518nm for the phallodin stain and excitation/emission: 358/461nm for DAPI.

2.2.9 Statistical analysis

Statistical analysis were computed with R studio (R version 4.3.1 (2023-06-16 ucrt) – "Beagle Scouts"). Data shown is reported as mean +/- SD with statistics reported as Bonferroni multiple comparisons. Statistical significance is as follows: P<0.001, P<0.01, P<0.5. When comparing treatments to control, '*' is used, when comparing different concentrations of the same treatments, '¤' is used and when comparing between the same concentrations but different treatments, then 'θ ' is used. All experiments consisted of a minimum of three biological replicates unless otherwise stated. All statistics throughout this thesis were computed with Excel and R Studio with figures prepared using the ggplot2() and ggpubr() R packages. Unless stated otherwise, data were analysed with one- or two-way ANOVAs with Bonferroni's *post-hoc* multiple comparisons were used to determine significant differences ($p < 0.05$).

2.2.9.1 General R packages used

Data was presented following adjustment with the following packages:

- ggplot2 (version 3.4.2)
- ggprism (1.0.4)
- dplyr (version 1.1.2)
- DT (version 0.28)
- tidyverse (2.0.0)
- gridExtra (2.3)

2.3 Results

2.3.1 Cell viability and vitality

Initial work was undertaken to ensure that our differing FA treatments did not result in cytotoxicity as is seen by treatment with only palmitic acid (Nissar et al. 2015). This was done through determining both the viability, a measure of the Huh7 cells ability to survive under the given experimental conditions, and through determining the vitality of the cells, a measure of how metabolically active they are through ATP generation. The influence of the two different FA concentrations on Huh7 viability was carried out; OPLA composition defined by the group prior to this thesis (Gunn et al. 2020) or by POLA, a FA mix that contained a greater proportion of palmitic acid that was developed to investigate the effects of a more SFA media on hepatocellular metabolism and function.

Our group previously established that OPLA did not influence ATP generation (Gunn et al. 2020). Two experiments were therefore undertaken; one to compare the metabolic activity by looking at ATP generation of OPLA and POLA at the end of a 7-day treatment, and another to compare the ATP generation of cells treated with single FA alone compared to OPLA and POLA conditions. For single FA treatments, cells were treated with either palmitic acid or oleic acid and cultured with the same concentration of FA (400µM). Pilot data shown in Figure 2.4a demonstrated that cells produce very little ATP when cultured with a single FA compared to those cultured with a mixture of FAs, suggesting the cytotoxic nature of culturing with a single FA with results replicated by others in the group (data not shown). Investigating the ATP concentration at the end of a 7-day period, comparing OPLA and POLA at both a high and low concentration showed that the new POLA composition did not significantly alter the ATP concentration in the cells when compared with cells treated with OPLA. Additionally, there were no significant differences in ATP between the high and low concentration of FA (Figure 2.4b). Further viability experiments carried out on day 7 of treatment revealed no significant difference between OPLA and POLA compositions at either a high or a low concentration (Figure 2.4c).

Huh7 cells proliferate *in vitro*, and as the number of cells increases, so does the corresponding luminescent signal produced in a viability assay. The viability assays carried out therefore assumed that the different cellular treatment medias did not alter proliferation rates in the Huh7 cells. However, to validate this assumption, protein concentration was quantified following 7 days of culturing with OPLA and POLA at both and low concentrations and no-fat control treatment media (Figure 2.4d). There were no significant differences observed in total protein content regardless of treatment composition suggesting neither FA concentration nor composition had an effect on proliferation.

DNA damage was assessed using a comet assay and no significant differences in the proportion of DNA damage were observed with OPLA and POLA at either low or high treatment concentrations (Figure 2.4e). This suggests that the palmitic acid in POLA does not manifest cytotoxic effects on DNA integrity.

For PHH, the reduced quantity of viable cells posed limitations on our ability to conduct an exhaustive assessment of cellular vitality as carrid out for Huh7 cells. Nevertheless, as part of the standard cell seeding protocols (see Section 2.2.1.3) the number of live cells was quantified using Trypan blue to ensure appropriate seeding density. This procedure allowed insight into the condition of the cell viability at the time of thawing and seeding. Across the 5 vials of PHH used in this chapter, the average viability was 68+/-8 % which was considerably lower than the 95+/-3% viability of HuH7 cells.

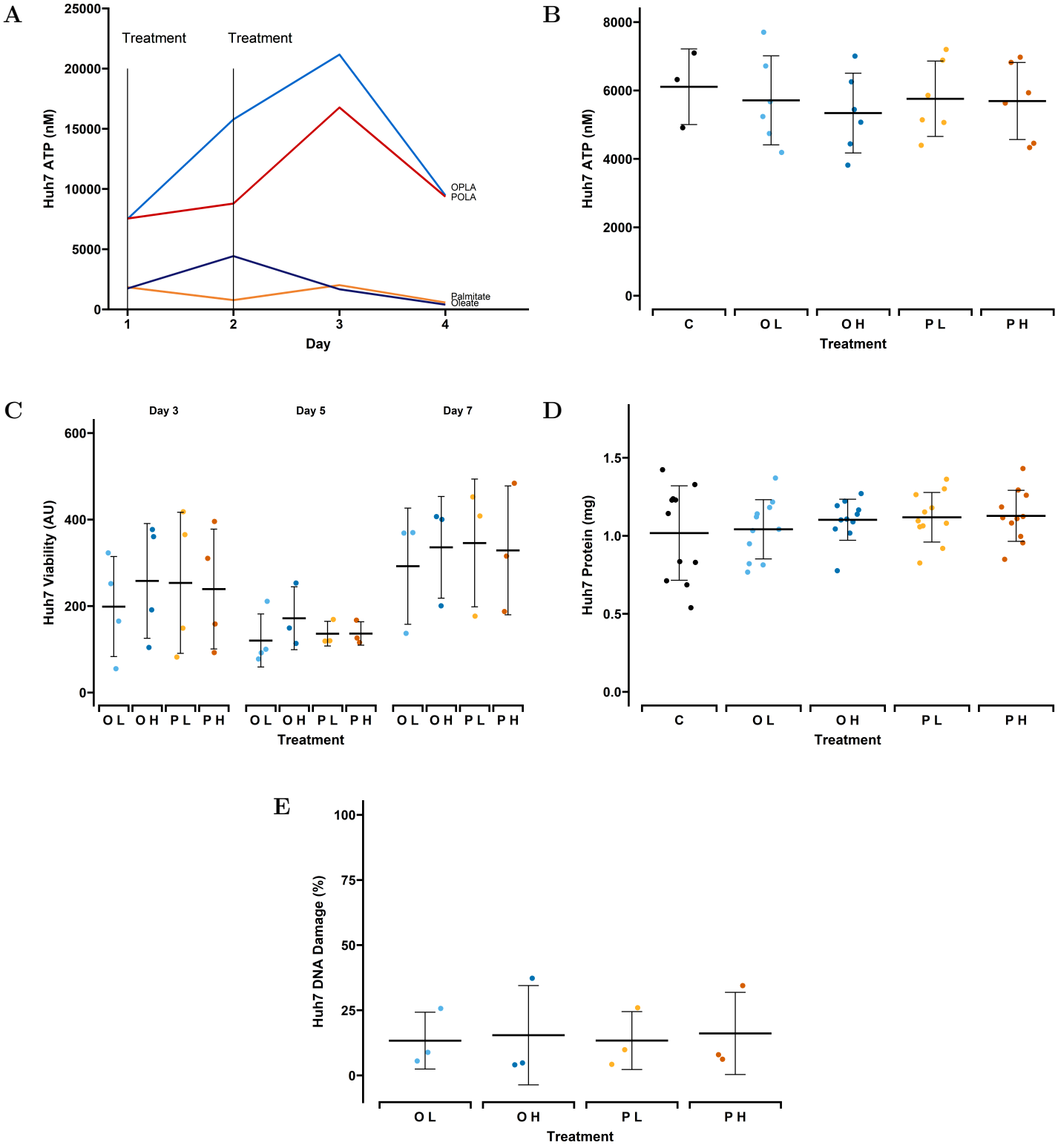


Figure 2.4: Huh7 cell viability following 7 day treatment with fatty acids. A) Initial investigation into ATP production in Huh7 cells treated with 400µM or either: palmitic acid, oleate, OPLA or POLA across 4 days, with media changes on day 0,1 2. n=1. No statistical analysis undertaken; B) ATP concentration at day 7; C) Protein concentration at day 7; D) Cell viability, normalised to the no-fat control,n at day 3, 5 and 7; E) Proportion of DNA damage at day 7. Data presented as mean +/- SD, n = 6 per treatment unless stated otherwise. Abbreviations: C, no fat control; OL, low (200µM) concentration OPLA, OH, high (800µM) concentration OPLA; PL, low (200µM) concentration POLA; PH, high (800µM) concentration POLA.

2.3.2 FA compositions in Huh7 cells

The cellular and media TAG and PL concentration was quantified by GC to assess whether FAs were taken up, stored and/or secreted. The experimental procedure, described in detail in Section 2.2.1, involved a 7 day treatment of the cells.

2.3.2.1 Huh7 TAG FA composition following treatment with FAs

All the treatment conditions had a reduction in media FA concentration at the end of the 7 day treatment period (Figure 2.5a) indicating uptake of FAs into cells. It was observed that cells treated with a higher amount of FA took up a greater amount of media FA. At the lower media FA concentration, there were no significant differences in FA uptake between OPLA and POLA. However, at the higher media FA concentration, POLA treated cells displayed significantly higher FA uptake from the media and IHTAG content increased (Figure 2.5a). Cells treated with low FA concentrations of either composition had a significantly higher IHTAG content when compared to control cells and cells treated with high FA concentrations had a significantly higher IHTAG content than cells treated with low FA and the no-fat treated control (Figure 2.5b).

Within the cellular TAG pool, the three specific FAs (palmitic acid, oleic acid, linoleic acid), provided in OPLA and POLA treatment media, showed a marked increase relative to control, when cell were treated at both high and low concentrations (Figure 2.5c). The relative proportions of these FAs closely mirrored the compositions of OPLA and POLA; the presence of palmitic acid in the cells was significantly higher for cells treated with POLA compared to those cells treated with OPLA, although this difference reached statistical significance only with high FA concentrations. In contrast, the proportion of oleic acid showed no significant differences across the cells resulting from the different treatment. In-line with the increase FA concentration in the media, an augmented proportion of linoleic acid was observed and OPLA treated cells exhibited a significantly higher proportion of linoleic acid content at both high and low concentrations of treatment media when compared to POLA. Furthermore, cells cultured with a high concentration of OPLA showed a significantly

greater proportion of linoleic acid when compared to those treated with a lower concentration of OPLA (Figure 2.5c). The molar concentrations of the IHTAG resulting from the different treatments can be seen in Appendix Figure A.1.2.

By categorising FAs based on their saturation, data showed that despite the increase in palmitic acid in cells treated with POLA compared to those treated with OPLA at a high concentration, the overall proportion of SFA decreased with increasing FA in the treatment medias across all groups, potentially due to an increased relative contribution from DNL (Figure 2.5d). A similar pattern emerges in regard of the contribution of MUFA to total TAG, with a decreased proportion in those cells treated with a higher concentration of treatment FAs, but no differences arose when comparing treatment compositions. The proportion of IHTAG constituted by PUFA was significantly higher in those cells treated with OPLA compared to POLA across both high and low concentrations, with those cells treated with OPLA being significantly higher in PUFA compared to the no-fat control. For either condition, increasing the FA concentration in the treatment media increased the contribution of PUFA to total IHTAG (Figure 2.5d).

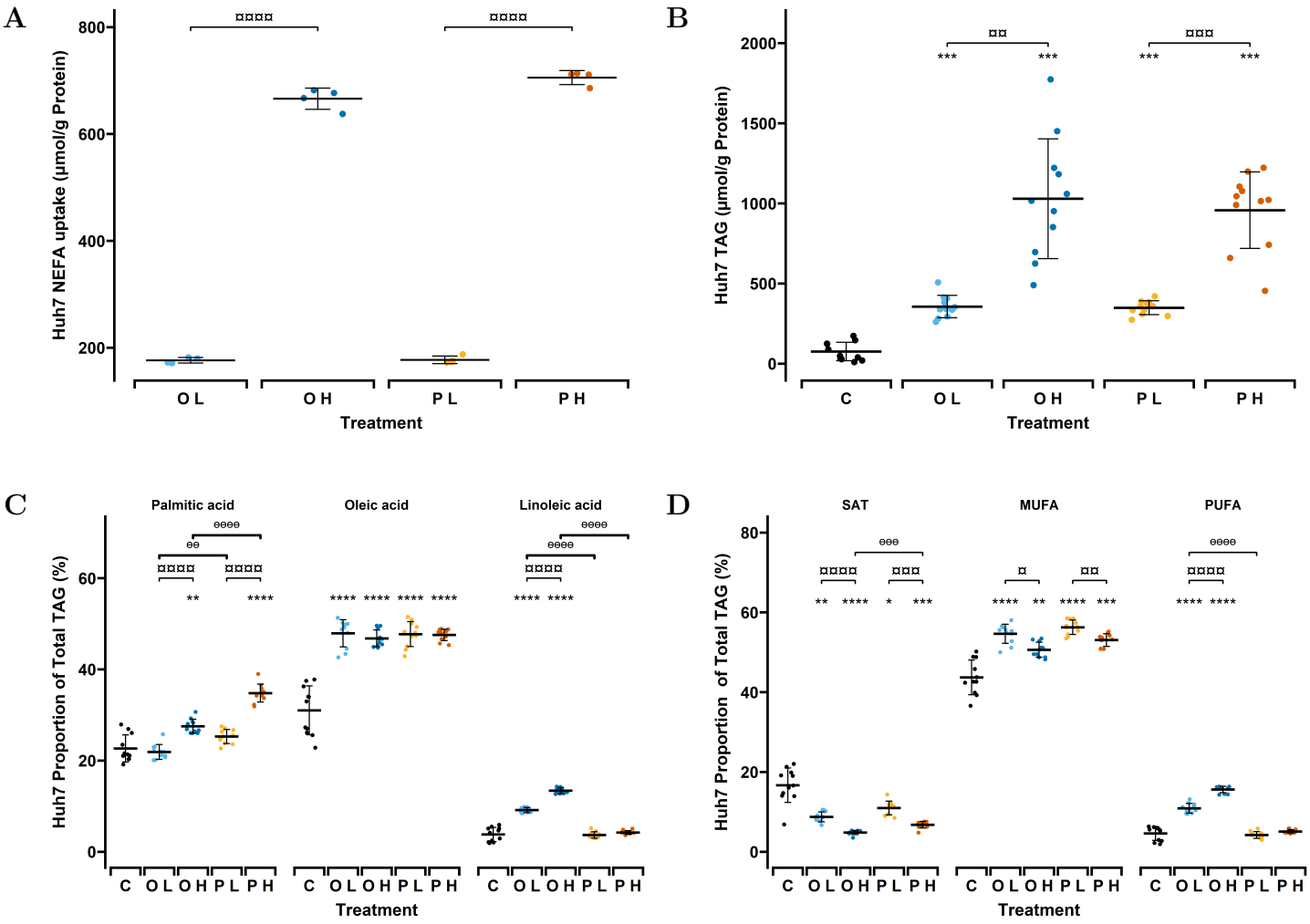


Figure 2.5: Intrahepatocellular triacylglycerol (IHTAG) content and composition in Huh7 cells following treatment with different FA compositions. Data determined by gas chromatography unless otherwise stated. A) NEFA uptake from the media (n=6 per treatment, measured with iLab Clinical Biochemistry Bioanalyzer); B) Total IHTAG content; C) Proportion (%) of the total TAG after culturing with OPLA and POLA, by OPLA and POLA FA (α- linoleic acid not included as represents <1 mol% and did not change with treatment); D) Composition of total IHTAG by degree of saturation. Data presented as mean +/- SD, n = 9 per treatment unless stated otherwise. Abbreviations: C, no fat control; OL, low (200µM) concentration OPLA, OH, high (800µM) concentration OPLA; PL, low (200µM) concentration POLA; PH, high (800µM) concentration POLA. Significance is indicated by '*' for comparison of treatment with control, '¤' for OPLA and POLA between concentrations, and 'θ' for OPLA versus POLA at the same concentration. Significance levels indicated are * $p<0.05$, ** $p<0.01$ and *** $p<0.001$ with the symbol changing appropriately.

Ratios of different fats were examined as described in Section 2.2.4.3. The ratio between palmitoleic acid (16:ln- 7) and palmitic acid (16.0) was assessed as a marker of FA desaturation and the proportion of palmitic acid undergoing desaturation decreased as FA concentration increased, and compared to the no-fat control (Figure 2.6a). The oleic acid (18:1n-9) / stearic acid (18:0) ratio was used as a marker of desaturation, with high FA concentration showing a decrease in the desaturation ratio (Figure 2.6c). Investigating the ratios of palmitic and stearic acid, as a proxy marker for elongation, no significant differences were observed between the treatment compositions (Figure 2.6b). Conversely, the ratio between vaccenic acid (18:1n-7) and palmitoleic acid (16:1n- 7) as a marker of the hydrolysis of the longer FA, showed an increased ratio comparing between those cells treated with a high concentration of FA with those treated with a low concentration of FA (Figure 2.6d). Proportional contribution and molar concentrations of palmitoleic acid and stearic acid can be seen in Appendix FigureA.1.2.

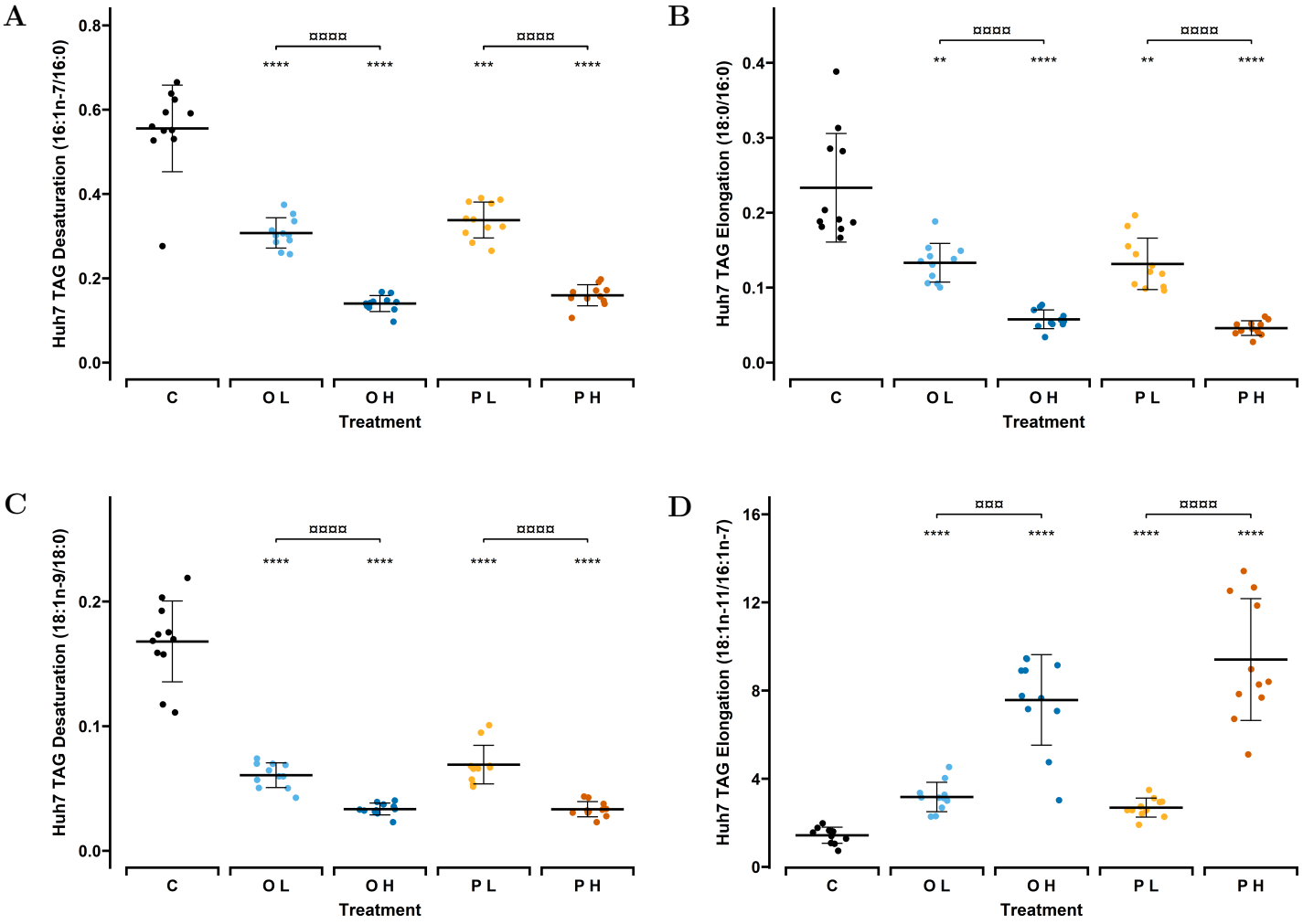


Figure 2.6: Ratio of intrahepatocellular triacylglycerol (IHTAG) derived fatty acids (FA) in Huh7 cells following treatment with FA. Data determined by gas chromatography. A) Ratio of palmitoleic acid to palmitic acid (16:1n-7/16:0); B) Ratio of stearic acid to palmitic acid (18:0/16:0); C) Ratio of oleate to stearic acid (18:1n-9/18:0); D) Ratio of vaccenic acid to palmitoleic acid (18:1n-7/16:1). Data presented as mean +/- SD, n = 9 per treatment. Abbreviations: C, no fat control; OL, low (200µM) concentration OPLA, OH, high (800µM) concentration OPLA; PL, low (200µM) concentration POLA; PH, high (800µM) concentration POLA. Significance is indicated by '*' for comparison of treatment with control, '¤' for OPLA versus POLA between concentrations, and 'θ' for OPLA versus POLA at the same concentration. Significance levels indicated are * $p<0.05$, ** $p<0.01$ and *** $p<0.001$.

2.3.2.2 Huh7 PL composition following FA treatments

Intracellular PL content was also determined using gas chromatography. There were no significant differences between the total amount of PL derived FA across all treatment groups (Figure 2.7a). However, the composition of PL, reflected the OPLA and POLA treatments, as cells treated with either concentration of POLA exhibited a higher proportion of palmitic acid within the PL fraction when compared to the no-fat control, with higher POLA treatment resulting in a greater proportion of palmitic acid in the PL fraction when compared to a low POLA treatment. This difference in treatment FA concentration on palmitic acid PL was not seen with OPLA treatment, although high concentrations of OPLA did result in significantly more palmitic acid in the PL fraction compared to the no-fat control (Figure 2.7b). There were no significant differences in the proportion of oleic acid in the PL fraction. With the exception of the low concentration of POLA, all other treatments resulted in an increase in the proportion of linoleic acid in the PL fraction compared to a no-fat control. A significant increase in the proportion of linoleic PL was also observed for both OPLA and POLA, between their low and high concentrations and between the two compositions, with more linoleic acid in the PL fraction of those cells treated with OPLA compared to POLA at either treatment concentration. For molar concentrations of PL FA refer to Appendix FigureA.1.3.

With treatment with FA, there was a statistical trend for a reduction in the proportion of total SFA within the PL fraction when compared to the no-fat control, as evidenced in the molar concentrations amounts (see Appendix Figure A.1.3). Notably, when cells were cultured with lower concentrations of OPLA, a higher proportion of SFA within the PL fraction was observed compared to cells cultured with a high concentration of OPLA; there were no other differences between treatment groups. The FA treatments did not alter the proportion of MUFA in the PL fraction. There was a significant difference in the proportion of PUFA within PL fraction with the low and high concentrations of OPLA and the high concentration of POLA compared to the no-fat control. Additionally, OPLA resulted in a greater proportion of PUFA within the PL fraction compared to

those cells treated with POLA (Figure 2.7c). These changes may impinge on both membrane fluidity and also the interactions between proteins and these membranes (Desai et al. 2018; Casares et al. 2019).

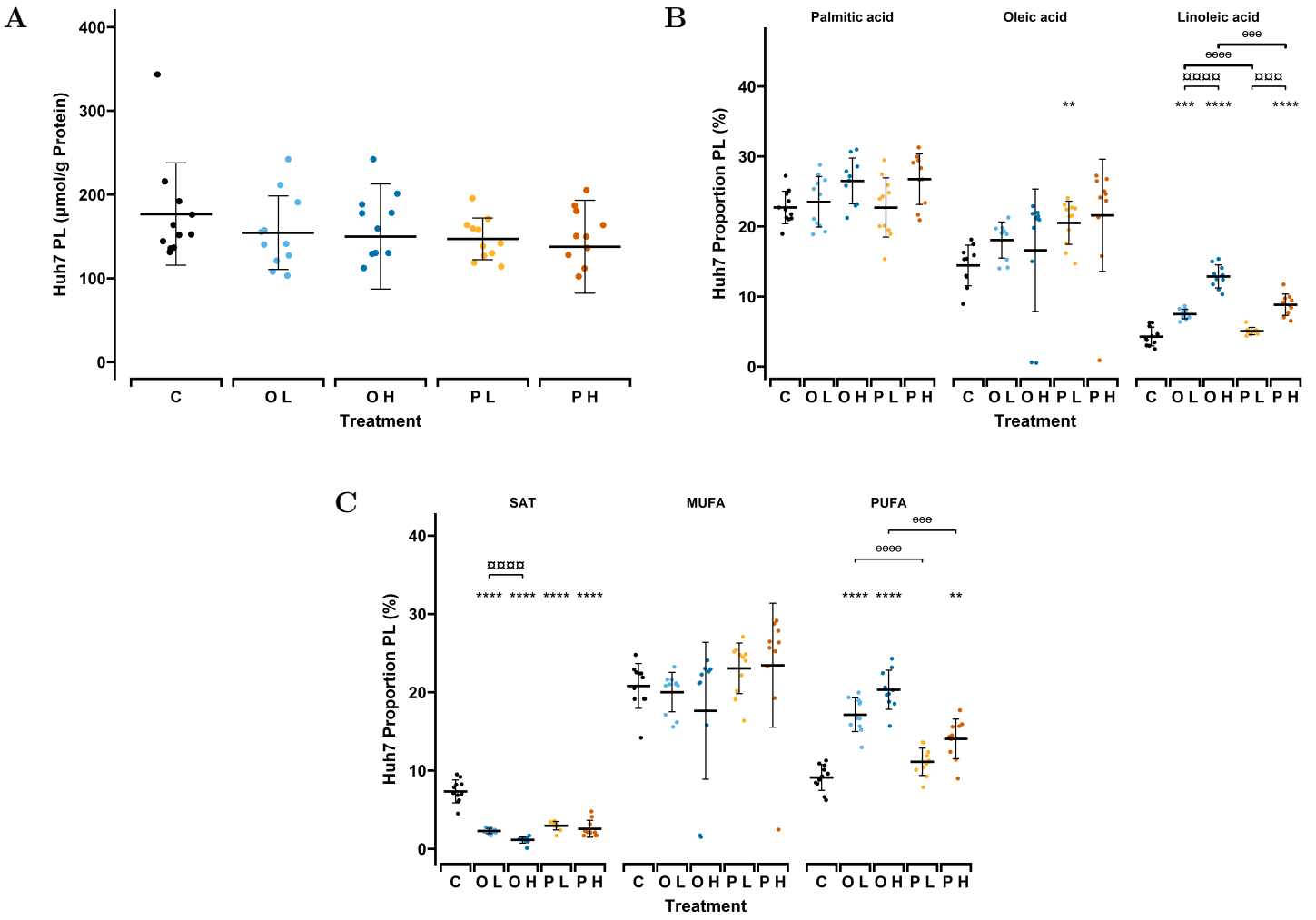


Figure 2.7: Intrahepatocellular phospholipid (PL) content and composition in Huh7 cells following treatment with different FA compositions. Data quantified using gas chromatography. A) Total intracellular PL amount; B) Proportion of total PL constituted by specific FAs in OPLA and POLA (α- linoleic acid not included as it is not in scale with these graphs and does not significantly change) C) FA constituents of the PL fraction sorted by degree of saturation as a proportion of total PL amount. Data presented as mean +/- SD, n = 9 per treatment. Abbreviations: C, no fat control; OL, low (200µM) concentration OPLA, OH, high (800µM) concentration OPLA; PL, low (200µM) concentration POLA; PH, high (800µM) concentration POLA. Significance is indicated by '*' for comparison of treatment with control, '¤' for OPLA versus POLA between concentrations, and 'θ' for OPLA versus POLA at the same concentration. Significance levels indicated are * $p<0.05$, ** $p<0.01$ and *** $p<0.001$.

The ratios of PL palmitic acid (16:0) to palmitoleic acid (16:ln-7), as a marker of desaturation was reduced across all treatments compared to the no-fat control. For OPLA and POLA, the palmitic acid to palmitoleic acid ratio was attenuated with a higher concentration of the treatment FA (Figure 2.8a). The stearic acid (18:0) to palmitic acid (16:0) ratio was reduced in cells treated with a higher concentration of FA compared with the no-fat control and low FA concentration treatments. No differences were seen in the stearic acid to palmitic acid ratio between the two different treatment compositions (Figure 2.8b). Comparing the ratio of oleate (18:ln-9) to stearic acid (18:0) no significant differences emerged (Figure 2.8c). Comparing vaccenic acid (18:ln-7) with palmitoleic acid (16:1n-7), those cells treated with a low FA concentration of either composition had a signficantly lower ratio compared to the no-fat control. No other differences were statistically significant (Figure 2.8d). Molar quantities and proportions of PL palmitoleic acid and stearic acid can be seen in Appendix Figure A.1.3.

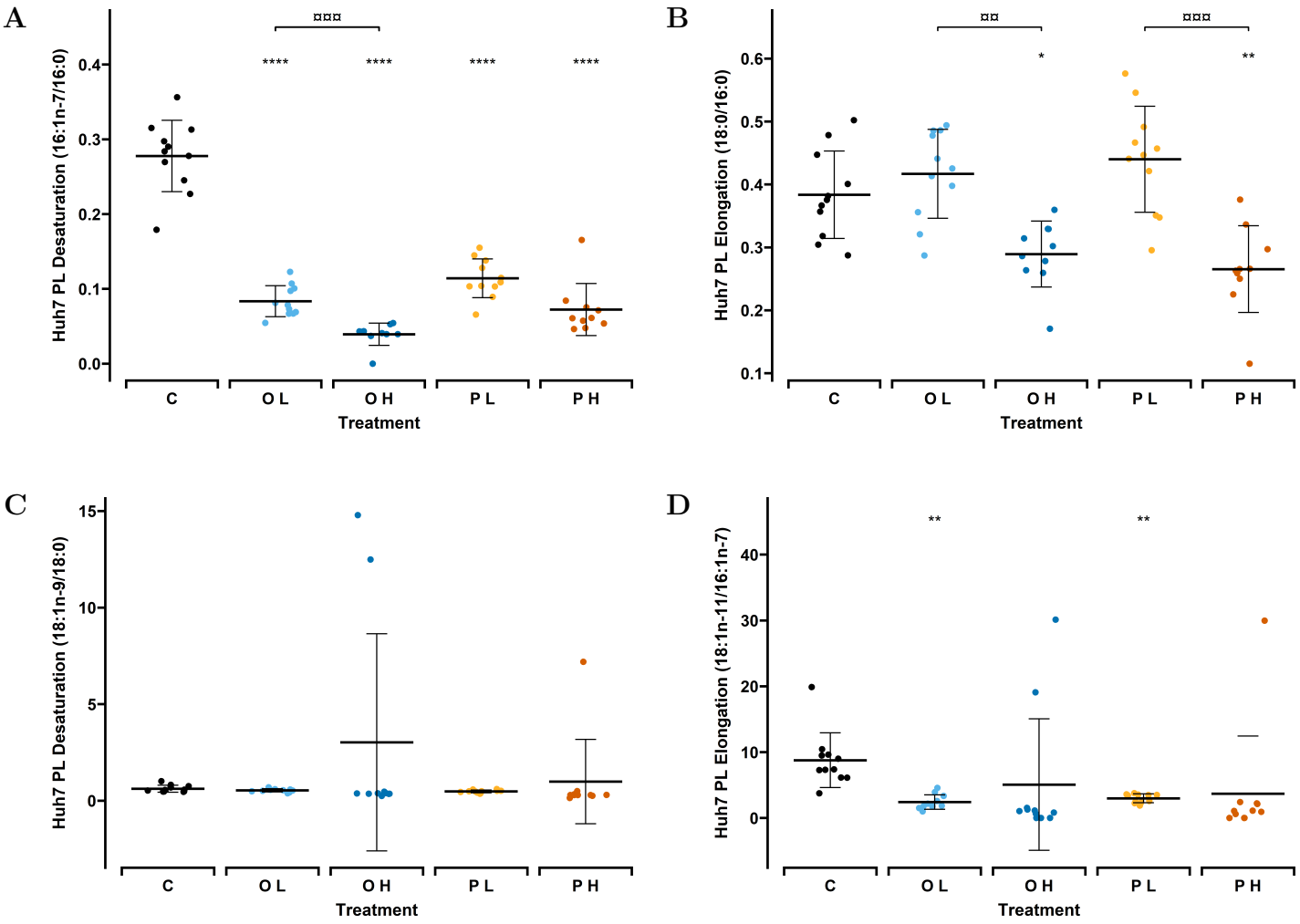


Figure 2.8: Ratios of phospholipid derived fatty acids (FAs) in Huh7 cells following treatment with FA treatments. Quantified by gas chromatography. A) Ratio of palmitoleic acid to palmitic acid (16:1n-7/16:0); B) Ratio of stearic acid to palmitic acid (18:0/16:0); C) Ratio of oleate to stearic acid (18:1n-9/18:0); D) Ratio of vaccenic acid to palmitoleic acid (18:1n-7/16:1). Data presented as mean +/- SD, n = 9 per treatment. Abbreviations: C, no fat control; OL, low (200µM) concentration OPLA, OH, high (800µM) concentration OPLA; PL, low (200µM) concentration POLA; PH, high (800µM) concentration POLA. Significance is indicated by '*' for comparison of treatment with control, '¤' for OPLA versus POLA between concentrations, and 'θ' for OPLA versus POLA at the same concentration. Significance levels indicated are * $p<0.05$, ** $p<0.01$ and *** $p<0.001$.

2.3.3 Primary human hepatocyte TAG composition

2.3.3.1 Primary human hepatocyte phenotype effect

PHH exhibit variation due to their genetic background and the environmental factors they have been exposed to, including medication (prescribed or recreational) and diet. As the PHH used in this study displayed the presence of LDs, the variation between each PHH batch was determined. Given the limited availability of PHH cells, this analysis was conducted using the cells treated with a no-fat control, with measurements taken at the end of the 5-day treatment protocol. We made the assumption that cells would not lose significant amounts of lipid and the proportion of different lipids present would remain constant throughout the treatment period. Figure 2.9a shows the total IHTAG by donor, while Figure 2.10a illustrates the distribution of FA based on degree of saturation within the TAG pool for each batch. Although only one replicate per donor is shown, noticeable variation in IHTAG concentration were evident between donors.

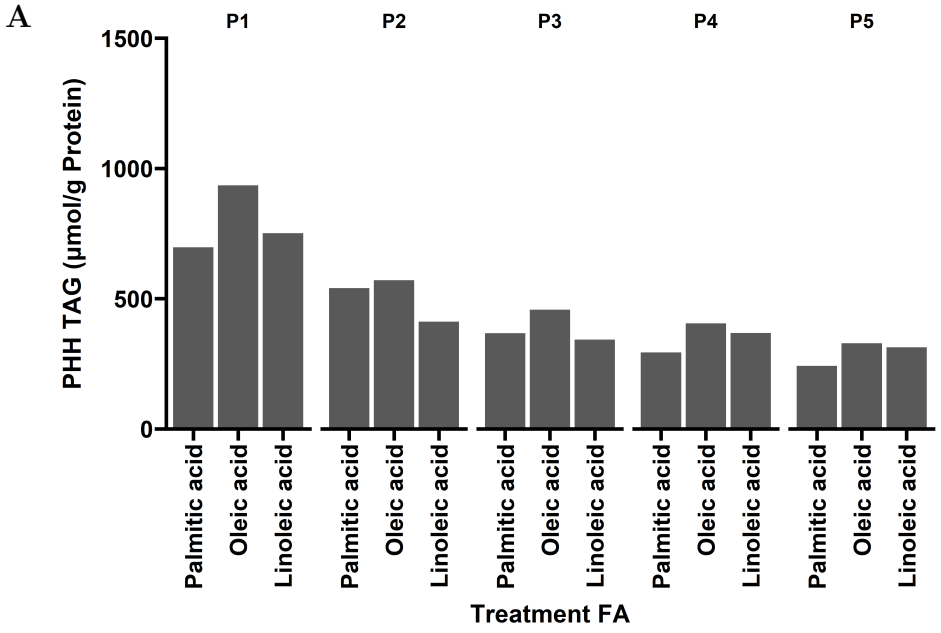


Figure 2.9

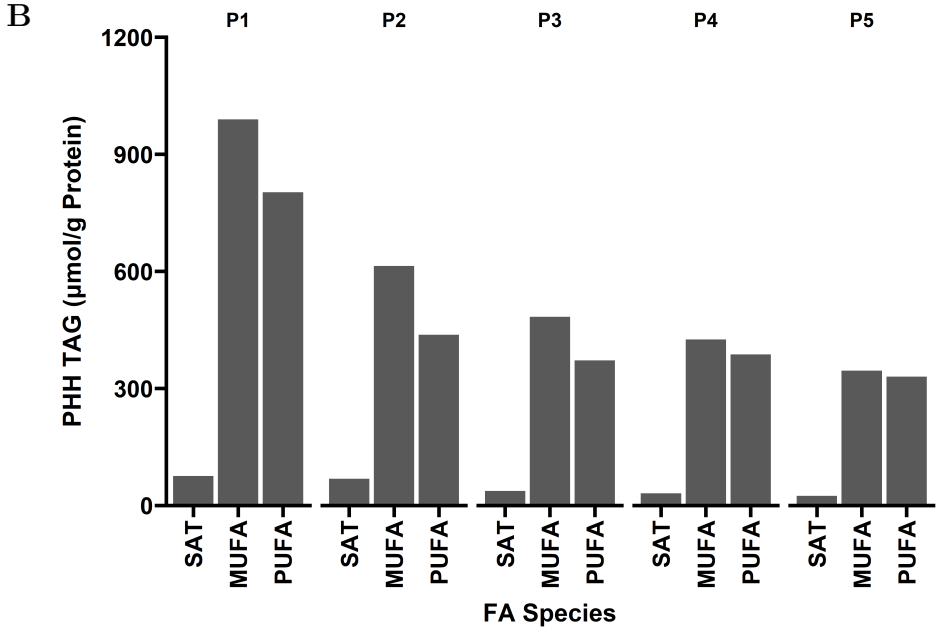


Figure 2.10: Intrahepatocellular Triacylglycerol (IHTAG) by donor. Data determined by gas chromatography. A) Total TAG per donor; B) Proportion of FA species from the TAG pool pre-existing in the PHH cells, visually separated per donor. Data are n=1 for each donor.

2.3.3.2 PHH TAG composition

There was large variability observed in the NEFA uptake across the PHH experiments. At the higher concentration of treatment OPLA and POLA there was a trend towards increased FA uptake. However, this was not statistically significant (Figure 2.11a). For all treatments conditions there was an increase in IHTAG compared to the no-fat control treated cells. With the high concentration of OPLA, there was a significant increase in IHTAG content compared to low OPLA condition; there was no difference in IHTAG concentration with POLA treatment (Figure 2.11b).

The overall PHH IHTAG composition was similar to the given treatment medias, and also that of the Huh7 hepatocytes treated with the same conditions. In PHH, oleic acid was higher in cells treated with OPLA or POLA compared to the no-fat control (Figure 2.11c) and MUFA demonstrated a statistical significant increase in all conditions compared to the no-fat control. There was a significant decrease in cellular TAG derived PUFA between PHH cells treated with high concentration compared to low concentration of POLA (Figure 2.11d). Molar concentrations of the PHH TAG FAs can be seen in Appendix Figure A.1.4.

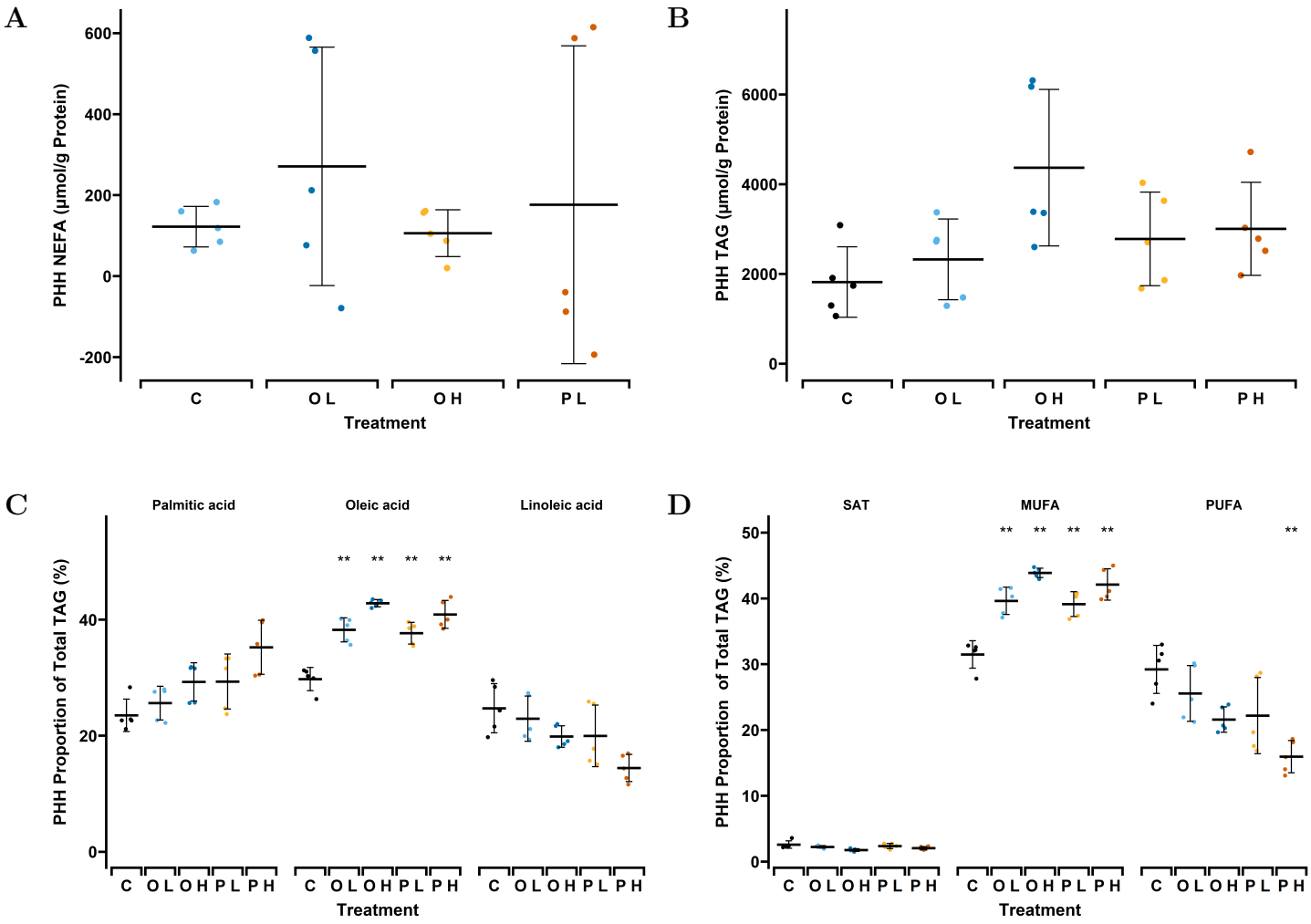


Figure 2.11: Intrahepatocellular Triacylglycerol (IHTAG) in primary human hepatocytes (PHH) cells following fatty acid (FA) treatment. A) NEFA uptake from the media, measured with iLab Clinical Biochemistry Bioanalyzer); B) Total IHTAG content; C) Proportion of total TAG fatty acid treatment (OPLA and POLA fatty acids). α-linoleic acid not included as it is not in scale with these graphs and does not significantly change D) Composition of total TAG described by degree of saturation as a proportion of total IHTAG amount). Data presented as mean +/- SD, n = 5 per treatment. Abbreviations: C, no-fat control; OL, low (200µM) concentration OPLA, OH, high (800µM) concentration OPLA; PL, low (200µM) concentration POLA; PH, high (800µM) concentration POLA. Significance is indicated by '*' for comparison of treatment with control, '¤' for OPLA versus POLA between concentrations, and 'θ' for OPLA versus POLA at the same concentration. Significance levels indicated are * $p<0.05$, ** $p<0.01$ and *** $p<0.001$ with the symbol changing appropriately.

The product to precursor ratios in PHH IHTAG were assessed. No significant differences were seen comparing palmitoleic acid (16:ln-7) with palmitic acid (16:0) (Figure 2.12a). Comparing oleic acid (18:ln- 9)/ stearic acid (18:0), a significant reduction in cells treated with higher FA, compared with no-fat control was seen (Figure 2.12c). The ratio of vaccenic acid (18:ln-llv) to palmitoleic acid (16:ln-7) was significantly higher in cells treated with high OPLA compared to the non-fat control and lower OPLA treatment; a similar trend in cells treated with POLA, although not statistically significant (Figure 2.12d). Molar concentration and the proportions of total IHTAG of palmitoleic acid and stearic acid can be seen in Appendix Figure A.1.4.

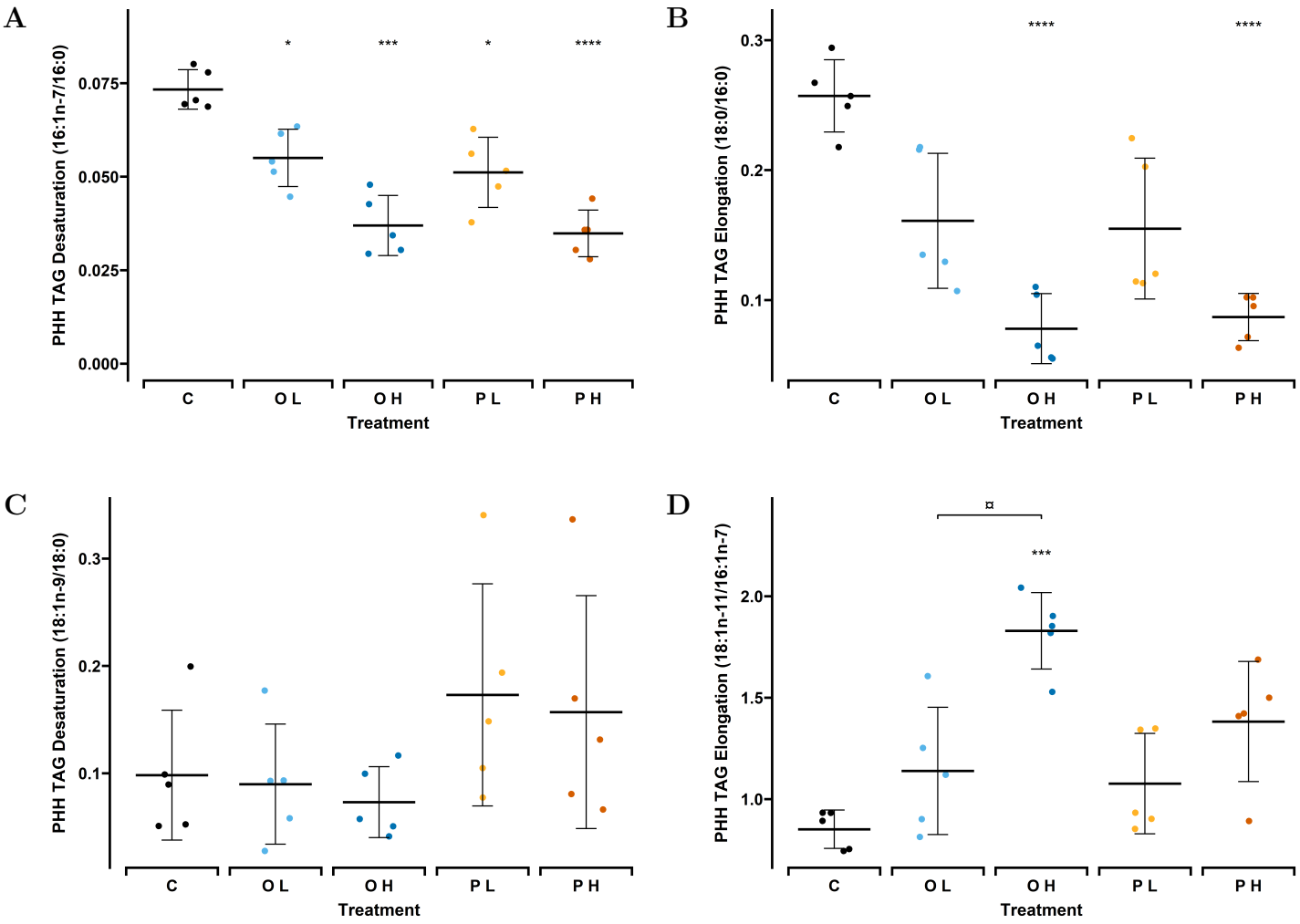


Figure 2.12: Ratio of intrahepatocellular triacylglycerol (IHTAG) derived fatty acids (FA) in Huh7 cells following treatment with FA. Quantified by gas chromatography. A) Ratio of palmitoleic acid to palmitic acid (16:1n-7/16:0); B) Ratio of stearic acid to palmitic acid (18:0/16:0); C) Ratio of oleate to stearic acid (18:1n-9/18:0); D) Ratio of vaccenic acid to palmitoleic acid (18:1n-7/16:11n-7). Data presented as mean +/- SD, n = 5 per treatment. Abbreviations: C, no fat control; OL, low (200µM) concentration OPLA, OH, high (800µM) concentration OPLA; PL, low (200µM) concentration POLA; PH, high (800µM) concentration POLA. Significance is indicated by '*' for comparison of treatment with control, '¤' for OPLA versus POLA between concentrations, and 'θ' for OPLA versus POLA at the same concentration. Significance levels indicated are * $p<0.05$, ** $p<0.01$ and *** $p<0.001$.

2.3.3.3 Primary human hepatocyte PL profile

Within the PHH PL faction no differences were found in the quantity of PLs with the respective FA treatments. Additionally, there were no significant differences in proportion of the treatment derived FAs in OPLA and POLA between the respective FA treatments (Figure 2.13). Molar Concentrations can be seen in Appendix Figure A.1.5.

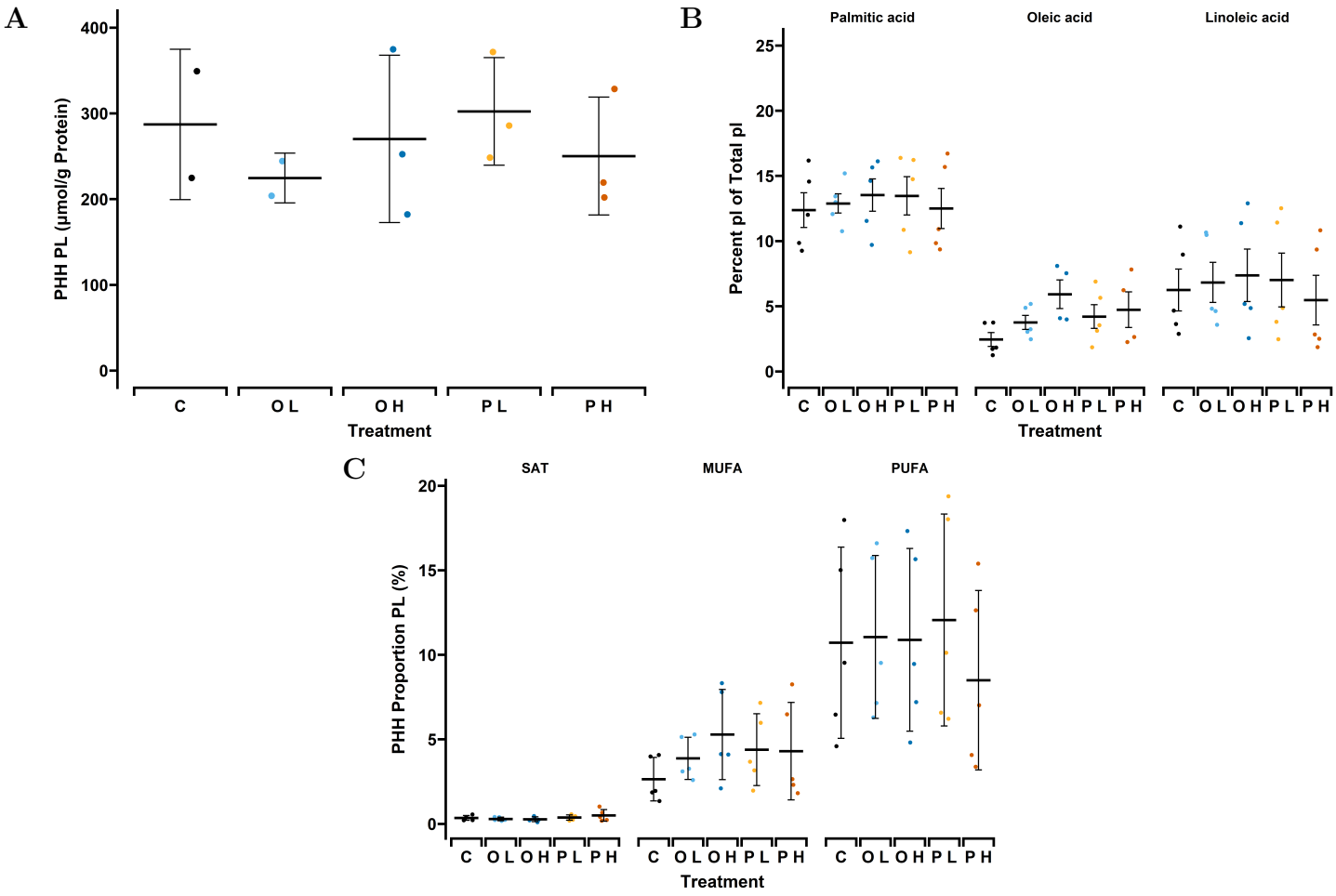


Figure 2.13: Phospholipid (PL) profile of primary human hepatocytes (PHH) following treatment with FA. A) Total intracellular PL amount; B) Proportion of total PL constituted by OPLA and POLA constituents (α- linoleic acid not included as it is not in scale with these graphs and does not significantly change); C) FA constituents of the PL fraction sorted by degree of saturation as a proportion of total PL amount. Data presented as mean +/- SD, n = 5 per treatment. Abbreviations: C, no fat control; OL, low (200µM) concentration OPLA, OH, high (800µM) concentration OPLA; PL, low (200µM) concentration POLA; PH, high (800µM) concentration POLA.

Within the PHH PL pool, the ratios for FA desaturation and elongation, were not affected by the different FA treatment compositions or concentrations (Figure 2.14). For a more detailed breakdown of the molar concentrations and proportions of palmitoleic acid and stearic acid, refer to the Appendix Figure A.1.5.

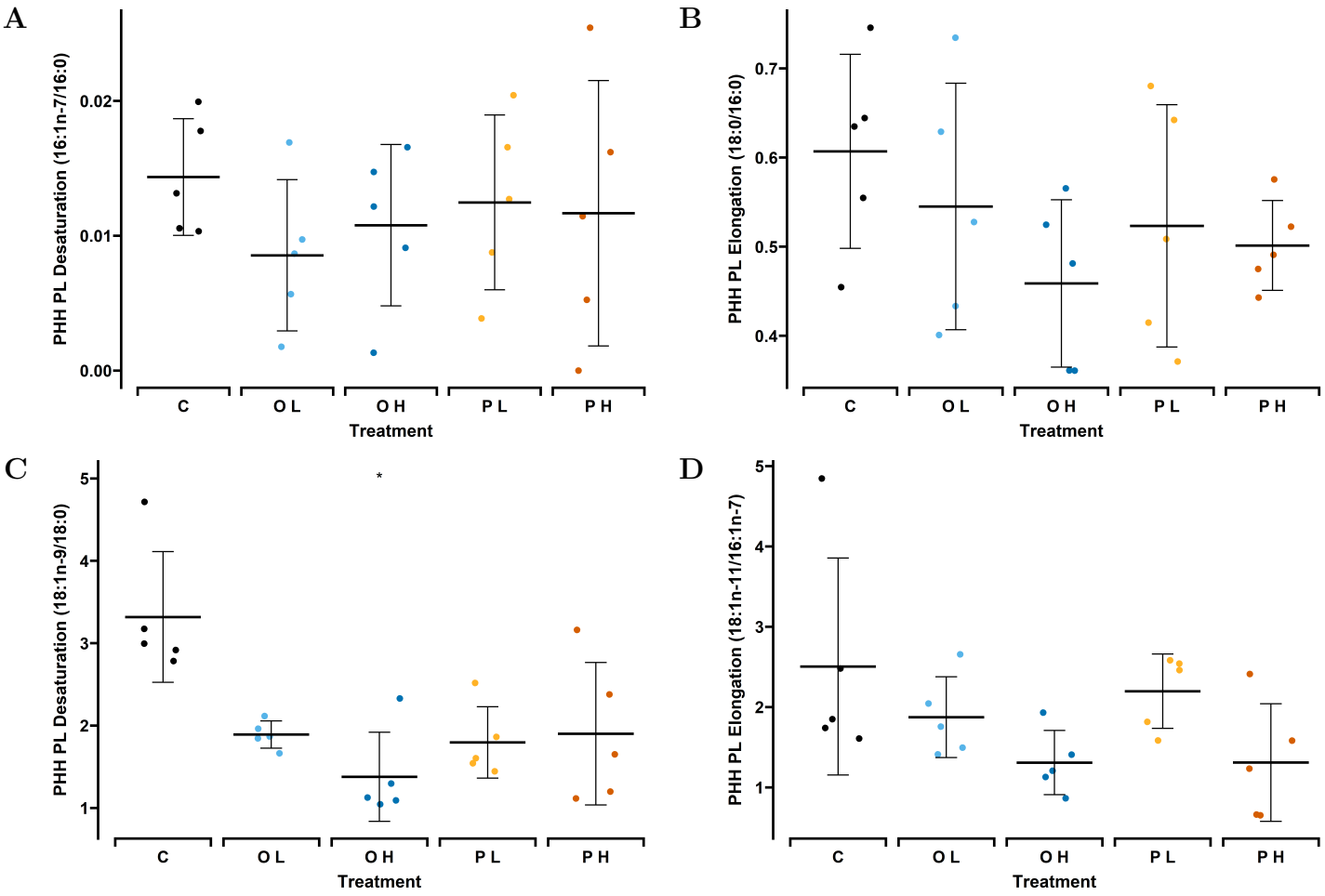


Figure 2.14: Ratio of intrahepatocellular phospholipid (PL) derived fatty acids (FAs) in Huh7 cells following treatment with FAs. Quantified with gas chromatography. A) Ratio of palmitoleic acid to palmitic acid (16:1/16:0); B) Ratio of stearic acid to palmitic acid (18:0/16:0); C) Ratio of oleate to stearic acid (18:1n-9/18:0); D) Ratio of vaccenic acid to palmitoleic acid (18:1n-7/16:1n-7). Data presented as mean +/- SD, n = 5 per treatment. Abbreviations: C, no fat control; OL, low (200µM) concentration OPLA, OH, high (800µM) concentration OPLA; PL, low (200µM) concentration POLA; PH, high (800µM) concentration POLA.

2.3.4 Glucose metabolism

The effect of the OPLA and POLA treatments given at both at high and low concentrations on glucose metabolism was investigated. Huh7 cells were treated with 5.5mM of glucose regardless of the FA treatment. No statistically significant differences in glucose uptake were observed among the different treatment groups at the end of the treatment period (Figure 2.15a). For the PHH, cell culture was exposed to 11mM of glucose, there were no significant difference observed in glucose uptake across various treatment groups (Figure 2.15c). Although PHH were exposed to double the glucose concentration of Huh7 cells, they paradoxically took up lower glucose (although there is significant variation here). Low uptake of glucose is typically associated with insulin resistance which is suggestive of lipotoxicity (Lair et al. 2020). Further work will be needed to understand any potential FA derived effects.

Media lactate concentrations tended to decrease with increasing FA concentration, although this observation failed to reach statistical significance, and there were no significant differences between treatment compositions, suggesting the addition of FA diverts glucose away from anaerobic glycolysis (Figure 2.15b). There was no differences in media lactate concentrations from PHH across the respective FA concentrations (Figure 2.15d).

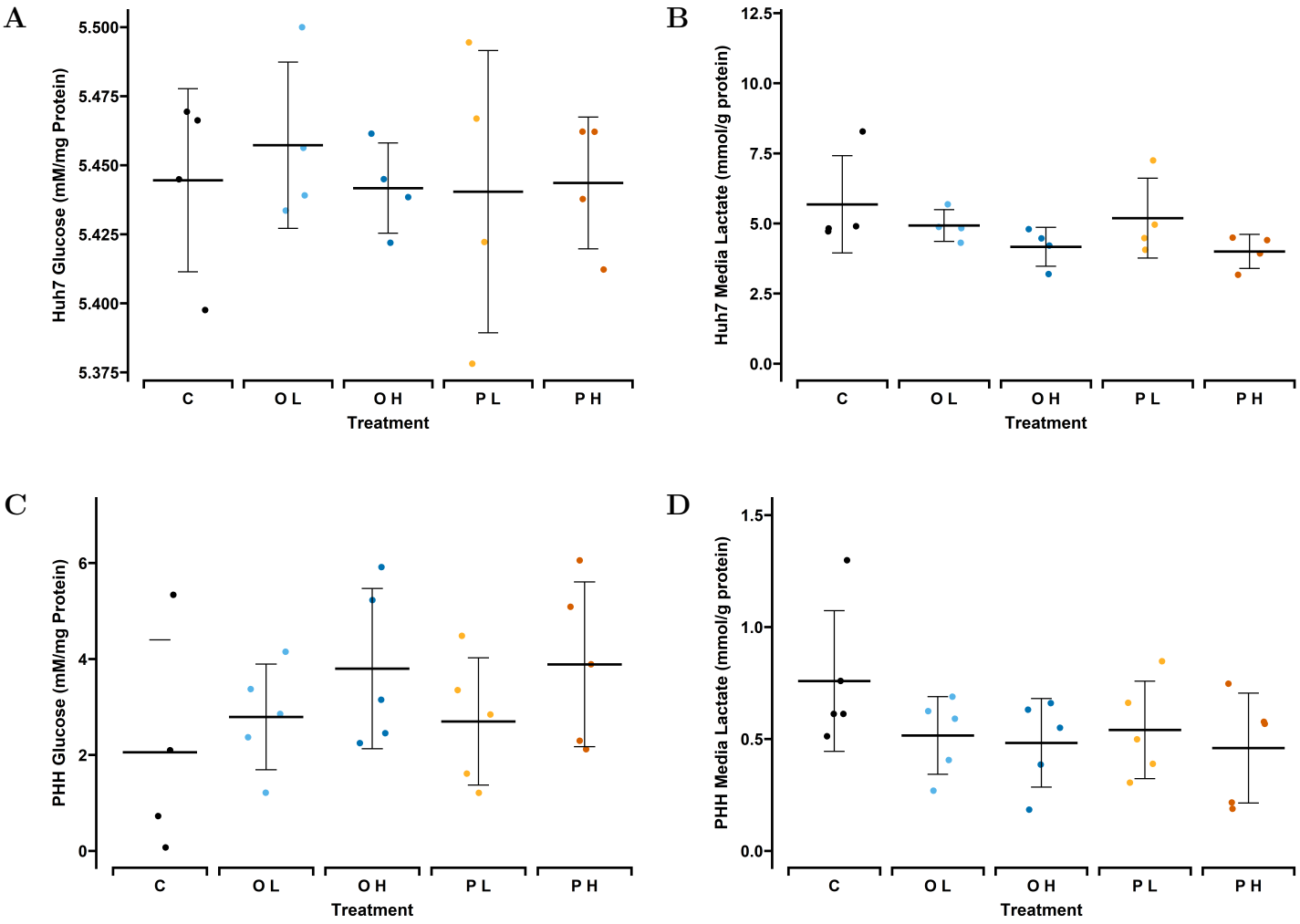


Figure 2.15: Media glucose and lactate in Huh7 cells and primary human hepatoctyes (PHH). Data quantified using a clinical biochemistry analyser. A) Glucose uptake from media in Huh7 cells; B) Media lactate concentrations from Huh7 cells; C) Glucose uptake by human primary hepatocytes (PHH); D) Media lactate concentrations from PHH. Data presented as mean +/- SD, n = 6 per treatment for Huh7 (A+B) and n = for PHH (C+D). Abbreviations: C, no fat control; OL, low (200µM) concentration OPLA, OH, high (800µM) concentration OPLA; PL, low (200µM) concentration POLA; PH, high (800µM) concentration POLA.

In Huh7 cells, a more in-depth analysis of glucose metabolism was carried out. Intracellular glycogen levels were measured and although no statistically significant differences were observed in glycogen content across the respective treatments, there was a trend to suggest increased glycogen content in cells treated with low concentrations of POLA (Figure 2.16a). Glucose production was measured and cells were stimulated with either glucagon or insulin to investigate any effects of the FA treatments on glucose release. The only significant difference was in those cells stimulated with insulin where cells treated with a low concentration of either OPLA or POLA produced a significantly higher amount of glucose in the hour compared to cells treated with a no fat control (Figure 2.16b).

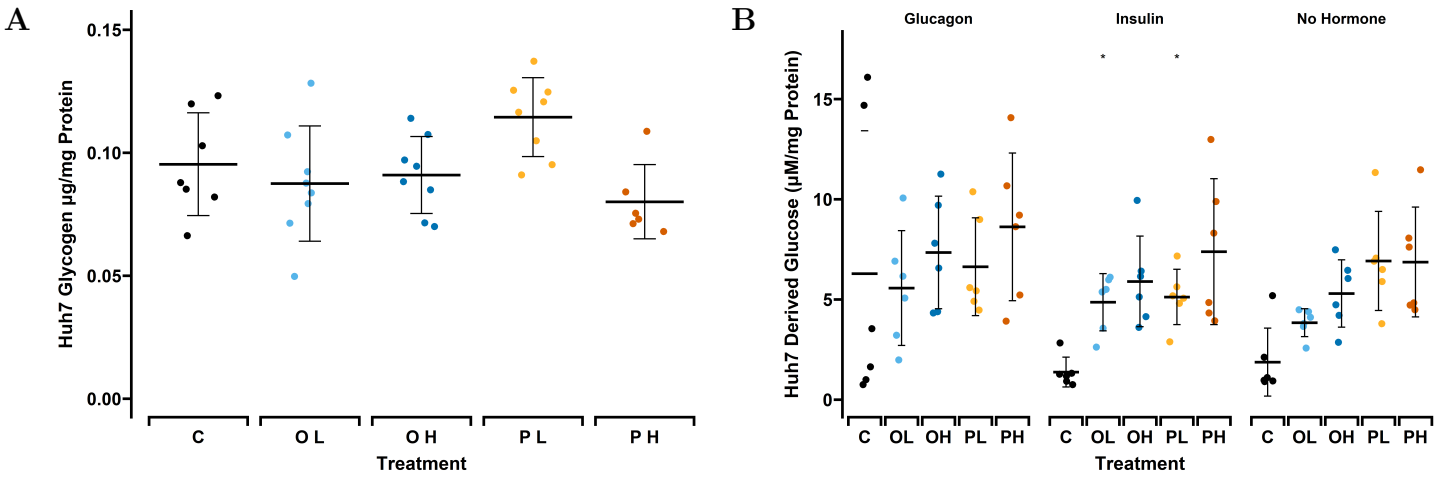


Figure 2.16: Huh7 quantification of glucose production and glycogen storage following treatment with fatty acids (FA) A) Cellular glycogen in Huh7; B) Glucose production. Abbreviations: C, no fat control; OL, low (200µM) concentration OPLA, OH, high (800µM) concentration OPLA; PL, low (200µM) concentration POLA; PH, high (800µM) concentration POLA. Significance is indicated by '*' for comparison of treatment with control, '¤' for OPLA versus POLA between concentrations, and 'θ' for OPLA versus POLA at the same concentration. Significance levels indicated are * $p<0.05$, ** $p<0.01$ and *** $p<0.001$.

2.3.5 *De novo* lipogenesis

De novo lipogenesis (DNL), the process of converting predominantly excess carbohydrates (glucose) to FA was investigated in both Huh7 and PHH using deuterated water, as described in Section 2.2.4.5. For Huh7 hepatocytes, the proportion of DNL derived palmitic acid in TAG, was highest in the cells treated with no-fat control, which may be attributed to the absence of exogenous FAs provided in the media. Cells treated with high concentrations of FA had significantly lower proportions of DNL derived palmitic acid in TAG compared to the no-fat treated controls and there was a significant reduction in proportion of DNL-derived palmitic acid in Huh7 cells treated with high POLA concentrations compared to those exposed to a lower POLA levels (Figure 2.17a). No significant differences were observed in the proportion of DNL derived palmitic acid in PHH cells (Figure 2.18a) .

To determine the total amount of palmitic acid made by DNL, the IHTAG content was adjusted by the proportion of palmitic acid which was DNL derived, as detected by GCMS. Figure 2.17b, shows that the treatment resulting in the greatest amount of DNL derived palmitic acid was the high concentration of POLA, which produced a significantly greater amount of DNL derived palmitate than low POLA. High concentrations of OPLA also resulted in a significant increase in the amount of DNL-derived palmitic acid when comparing to cells treated with low concentrations of OPLA. In the PL fraction, greater FA treatment concentrations resulted in a smaller ratio of DNL derived palmitate to other palmitate and a significant reduction in PL derived-palmitate to palmitate was seen between high concentrations of OPLA and POLA, with this difference being significant comparing between all FA treated cells and the no-fat control (Figure 2.17c). Adjusting for the amount of palmitic acid, higher amounts of DNL derived PL were seen following treatment with high concentrations of FA (Figure 2.17d). Figures 2.18a, 2.18b, 2.18c, 2.18d show the same analysis but for PHH cells. There are no differences between any of the conditions here.

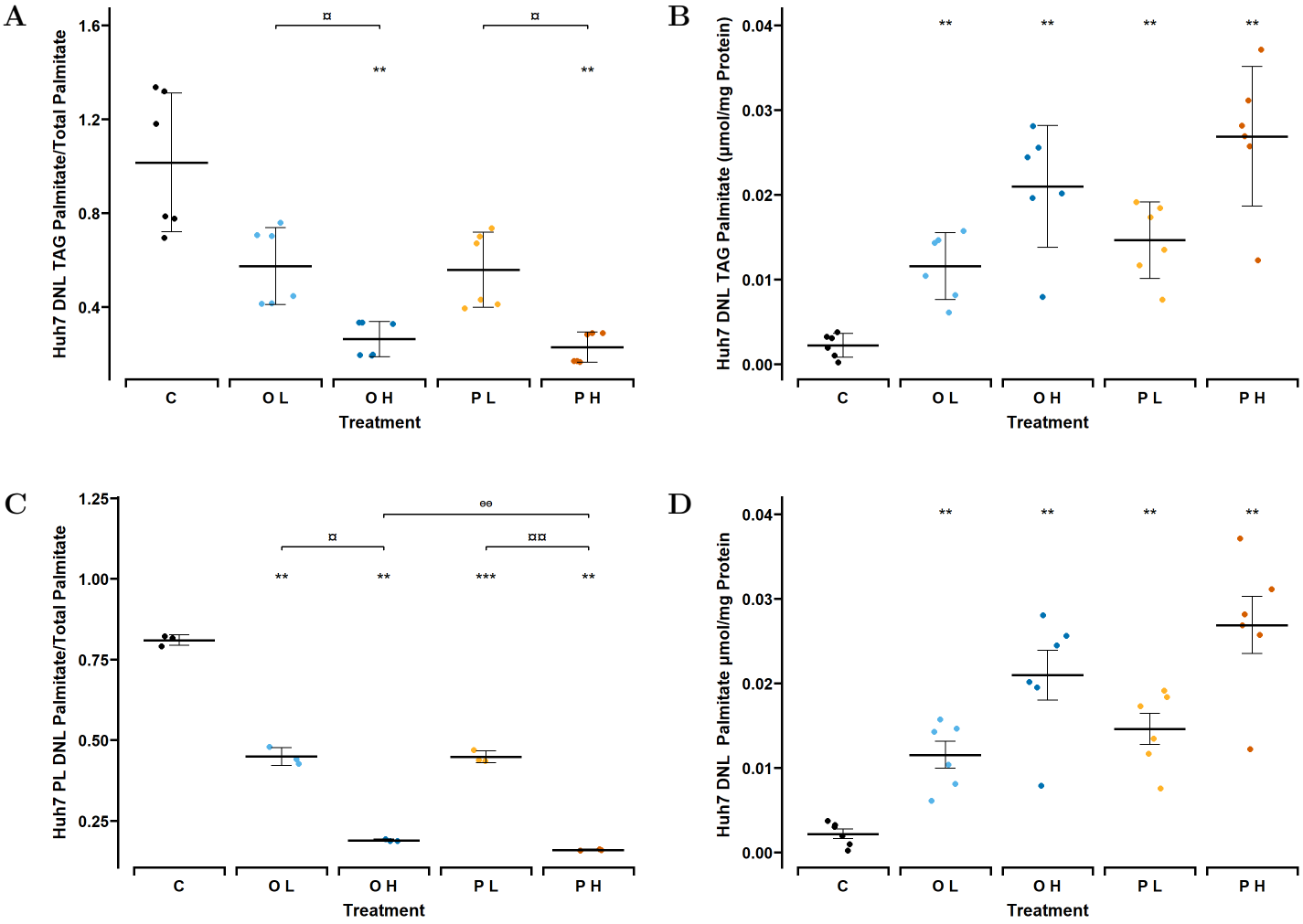


Figure 2.17: *De novo* lipogenesis (DNL) in fatty acid (FA) treated Huh7 hepatocytes. Quantified by gas chromatography mass spectrometry. A) Huh7 DNL derived TAG palmitic acid as a proportion of total palmitic acid; B) Huh7 DNL derived TAG palmitic acid; C) Huh7 DNL derived PL palmitic acid as a proportion of total palmitic acid; D) Huh7 DNL derived PL palmitic acid. Data presented as mean +/- SD, n = 6 per treatment. Abbreviations: C) no fat control; OL, low (200µM) concentration OPLA, OH, high (800µM) concentration OPLA; PL, low (200µM) concentration POLA; PH, high (800µM) concentration POLA. Significance is indicated by '*' for comparison of treatment with control, '¤' for OPLA versus POLA between concentrations, and 'θ' for OPLA versus POLA at the same concentration. Significance levels indicated are * $p<0.05$, ** $p<0.01$ and *** $p<0.001$.

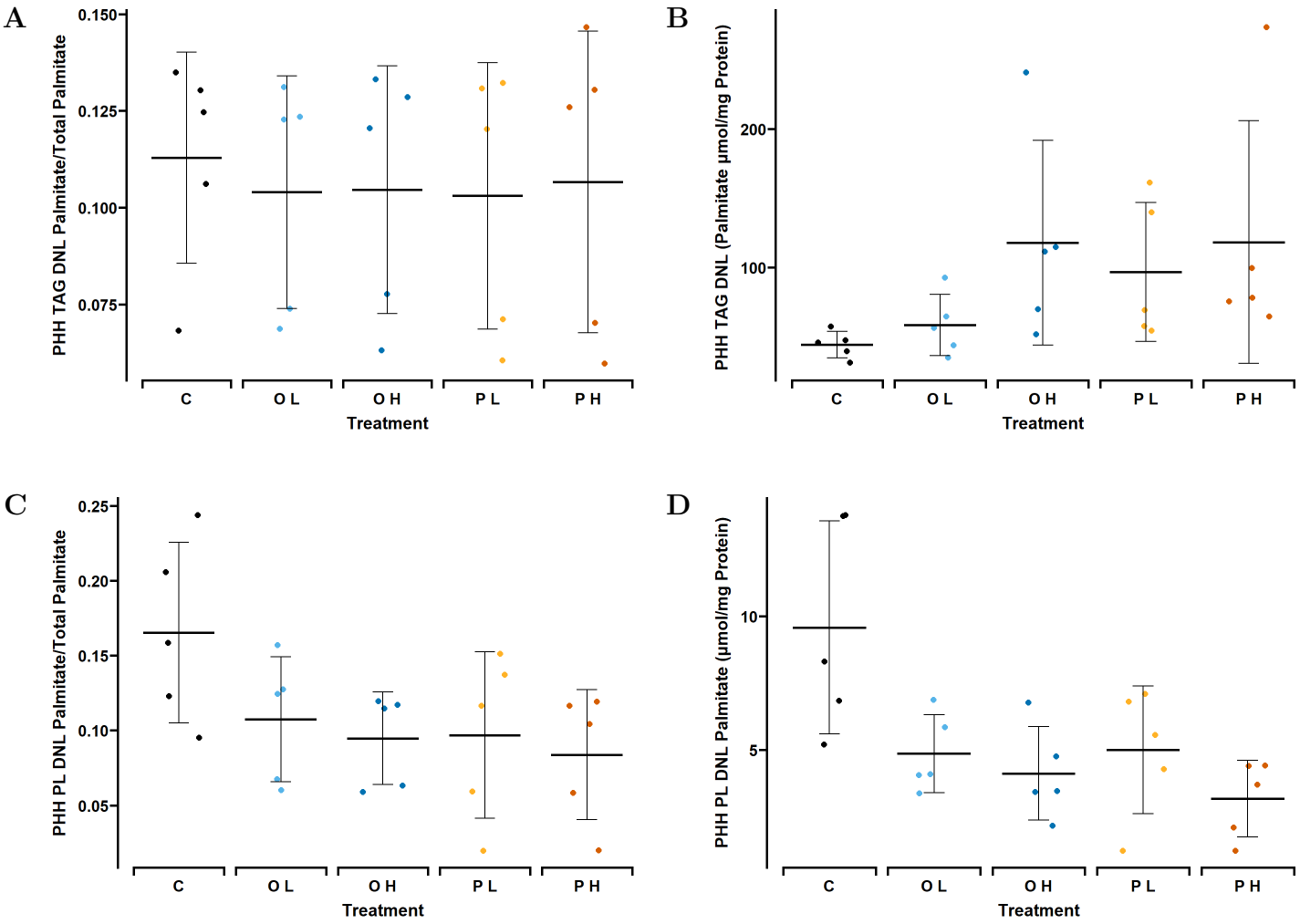


Figure 2.18: *De novo* lipogenesis (DNL) in fatty acid (FA) treated primary human hepatocytes (PHH). Quantified by gas chromatography mass spectrometry. A) PHH DNL derived palmitic acid as a proportion of TAG palmitic acid; B) PHH DNL derived TAG palmitic acid; C) PHH DNL derived palmitic acid as a proportion of PL palmitic acid; D) PHH DNL derived PL palmitic acid. Data presented as mean +/- SD, n = 5 per treatment. Abbreviations: C) no fat control; OL, low (200µM) concentration OPLA, OH, high (800µM) concentration OPLA; PL, low (200µM) concentration POLA; PH, high (800µM) concentration POLA.

2.3.6 Huh7 cellular oxidation

Cellular oxidation was measured in Huh7 cells by culturing cells with labelled oleic acid (D33) and palmitic acid (D31), where deuterated water is produced with complete FA oxidation. To assess if the labelled FA were taken up and incorporated into cellular TAG, the IHTAG was measured and no differences were found between the FA treatment conditions, although data were very variable (Figure 2.19a). Figure 2.19b shows differences in parts per million (PPM) of deuterated water measured following cell culture and no significant differences were observed across treatments, nor when ppm were adjusted for the amount of labelled FA (Figure 2.19c).

Acetate production, a marker of peroxisomal oxidation, was measured in the media and showed Huh7 cells treated with OPLA, regardless of concentration, produced a significantly higher concentration of media acetate when compared to both no-fat control and POLA treated cells irrespective of the concentration. Furthermore, Huh7 cells treated with either concentration of POLA showed no appreciable differences from each other, nor from the control (Figure 2.19d). The media 3-OHB concentration was measured and no statistical significant differences among the different experimental treatments were observed (Figure 2.19e).

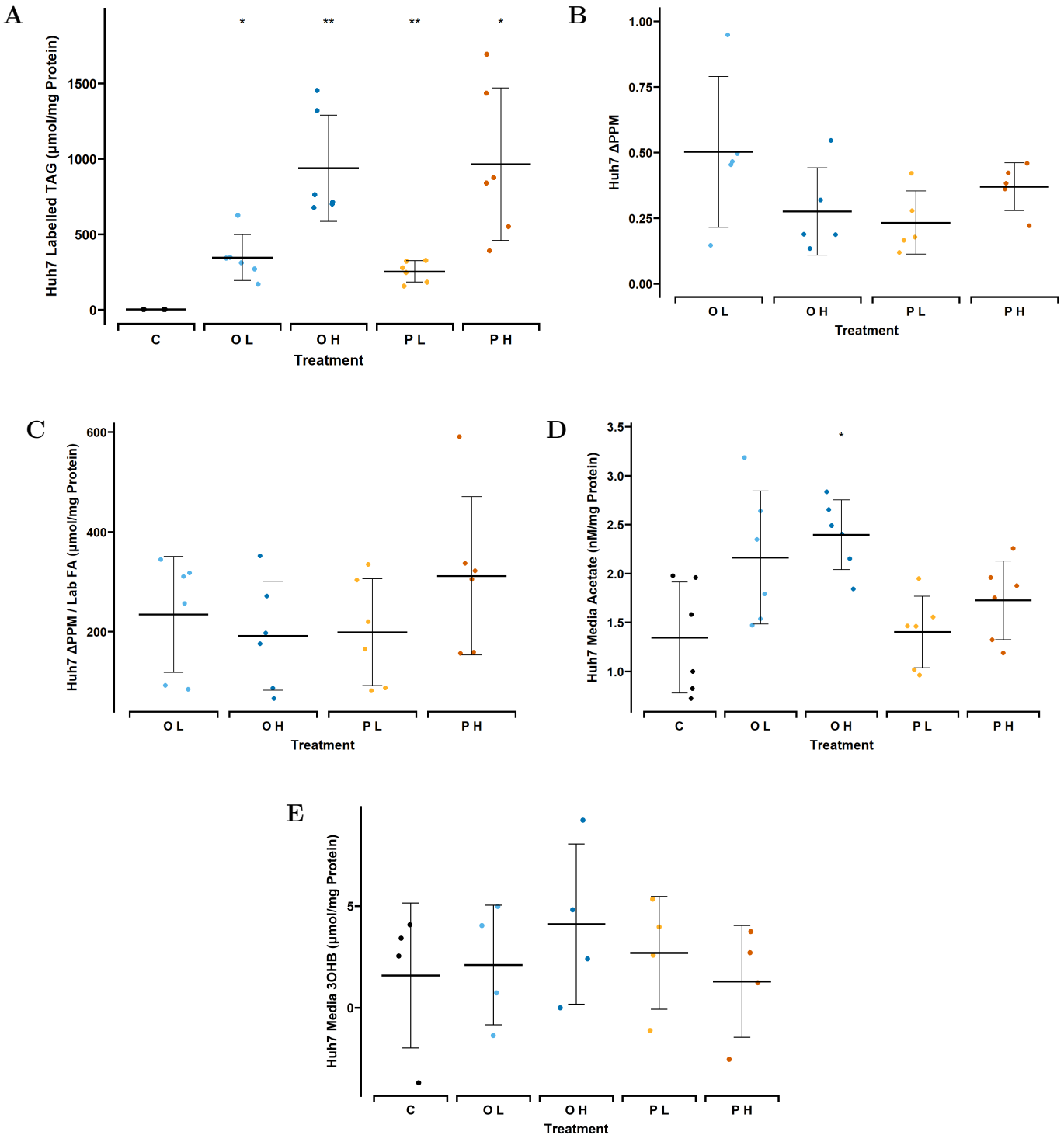


Figure 2.19: Cellular oxidation in fatty acid (FA) treated Huh7 hepatocytes. A) Amount of labelled oleic acid (D33) and palmitic acid (D31) as measured by gas chromatography; B) Parts per million (PPM) of media as measured by isotope ratio mass spectrometry (IRMS); C) Parts per million (PPM) per amount of labelled FA; D) Media acetate concentration; E) Media 3- hydroxybutyrate concentration. Data presented as mean +/- SD, n = 6 per treatment. Abbreviations: C) no fat control; OL, low (200µM) concentration OPLA, OH, high (800µM) concentration OPLA; PL, low (200µM) concentration POLA; PH, high (800µM) concentration POLA. Significance indicated by '*' for comparison of treatment with control, '¤' for OPLA versus POLA between concentrations, and 'θ' for OPLA versus POLA at the same concentration. Significance levels indicated are * $p<0.05$, ** $p<0.01$ and *** $p<0.001$.

2.3.7 Quantification of media lipoproteins from Huh7

Through a collaboration with Professor Camilla Pramfalk, FA exportation was investigated using size exclusion chromatography. Figure 2.20a, shows the concentration of TAG detected from the media of cells treated with either a no-fat control, or OPLA or POLA at either a low or a high concentration. Without adjustments, data showed that cells treated with low concentrations of FA had higher concentrations of TAG in the media compared with those treated with high concentrations. Cells treated with a low concentration of OPLA secreted a greater concentration of TAG when compared with cells treated with a low concentration of POLA. Cells treated with a no-fat control had the lowest quantity of secreted TAG. Figures 2.20b, 2.20c and 2.20d show no significant differnces between treatments when adjusted for total cellular number (using protein concentration).

Figure 2.20e, shows the lipidation of the VLDL particles adjusted for total cellular number. Treatment with high concentrations of FA resulted in greater lipidation of the VLDL lipoproteins measured. There is a trend towards greater lipidation in lipoprotein particles released from cells treated with OPLA compared to POLA at both a high and low concentration, although none of these differences are significant. This same pattern is replicated in the LDL lipoprotein particles when considering the lipidation of these particles, although not significant.

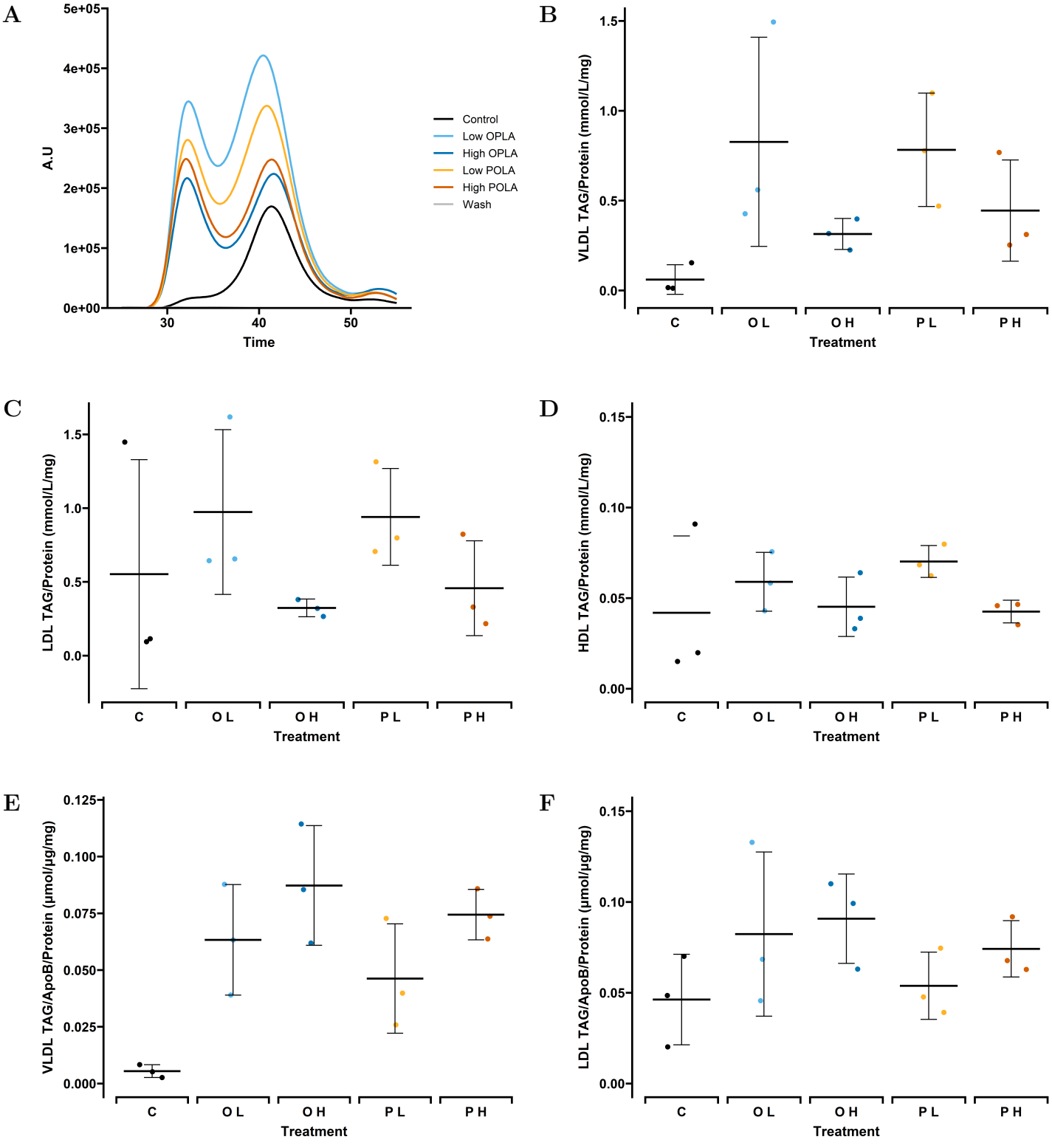


Figure 2.20: Export of triacylglycerol (TAG) by fatty acid (FA) treated Huh7 cells. A) Size Exclusion Chromatography curves for FA treated cells; B) VLDL TAG adjusted for protein; C) LDL TAG adjusted for protein; D) HDL TAG adjusted for protein; E) VLDL-TAG adjusted for protein and ApoB concentration; F) LDL-TAG adjusted for protein and ApoB concentration. Data presented as mean +/- SD, n = 3 per treatment unless stated otherwise. Abbreviations: C, no fat control; OL, low (200µM) concentration OPLA, OH, high (800µM) concentration OPLA; PL, low (200µM) concentration POLA; PH, high (800µM) concentration POLA.

Lipoprotein cholesterol was higher in cells treated with lower concentrations of FA (Figure 2.21a). After adjusting the VLDL, LDL and HDL with protein for the amount of cells, treatment with a lower FA concentration resulted in a higher concentration of media cholesterol in all lipoproteins, although these differences were not significant (Figures 2.21b, 2.21c, and 2.21d respectively). After adjusting lipoprotein cholesterol concentration for ApoB concentration, cells treated with higher FA concentrations resulted in a greater amount of cholesterol per ApoB particle although this difference was not significant for all lipoproteins (Figure 2.21e, 2.21f).

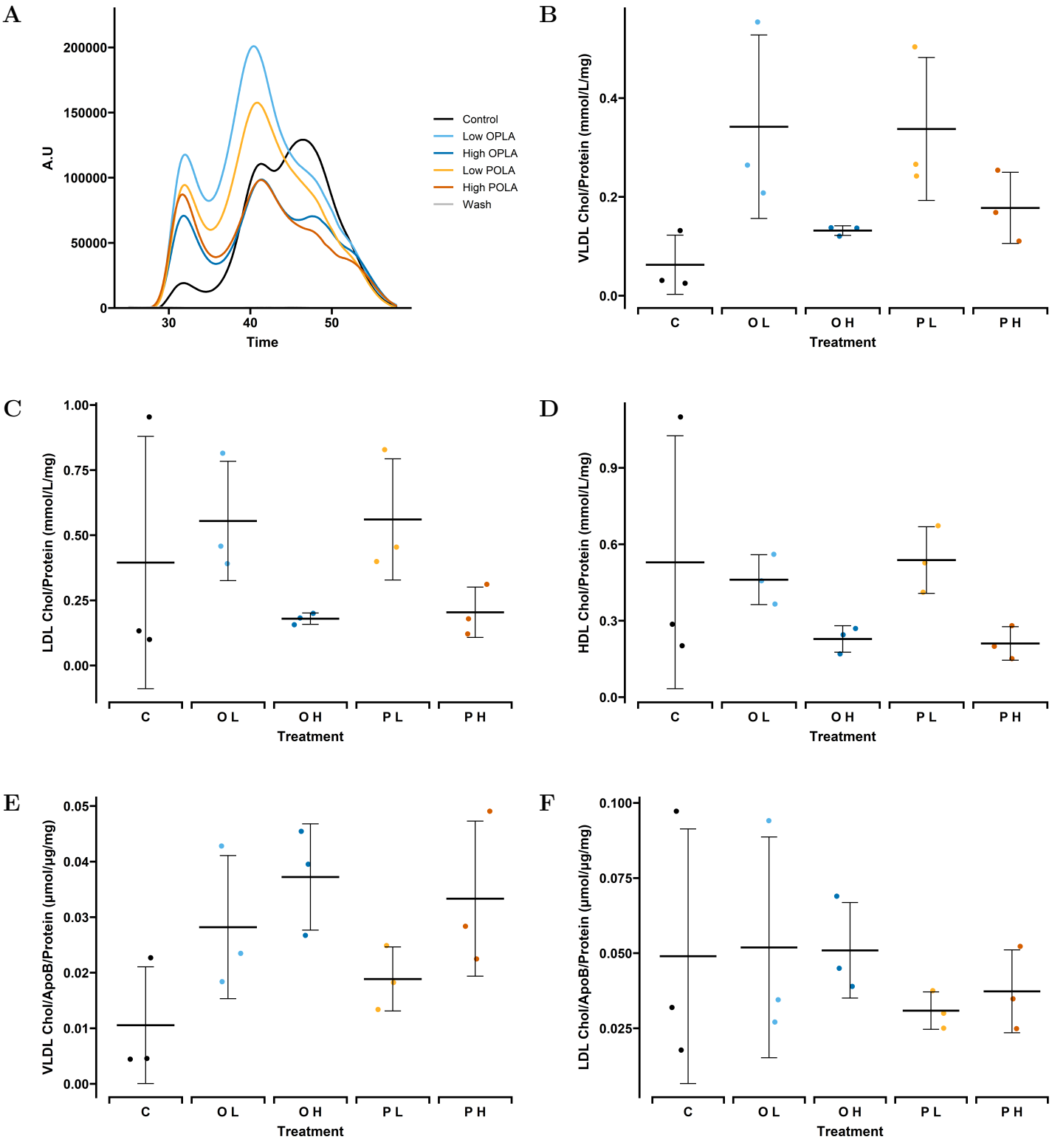


Figure 2.21: Export of cholesterol by fatty acid (FA) treated Huh7 cells. A) Size Exclusion Chromatography curves of cholesterol for FA treated cells; B) VLDL cholesterol adjusted for protein; C) LDL cholesterol adjusted for protein; D) HDL cholesterol adjusted for protein; E) VLDL-cholesterol adjusted for protein and ApoB concentration; F) LDL-cholesterol adjusted for protein and ApoB concentration. Data presented as mean +/- SD, n = 3 per treatment unless stated otherwise. Abbreviations: C, no fat control; OL, low (200µM) concentration OPLA, OH, high (800µM) concentration OPLA; PL, low (200µM) concentration POLA; PH, high (800µM) concentration POLA.

Adjusting the secreted TAG for IHTAG, probing VLDL lipoprotein particles, showed that cells treated with low concentrations of OPLA appear to secreted the greatest proportion of their TAG, although these differences were not significant (Figure 2.22a). Comparing the relative proportion of secreted cholesterol to intracellular cholesterol, there were no significant differences, however, cells treated with a low concentration of POLA appeared to secrete the smallest proportion of their total intracellular cholesterol (Figure 2.22b). LDL showed the same pattern regarding the proportion of total TAG secreted as VLDL although none of these difference were significant (Figure 2.22c). No significant differences were seen in the proportion of total intracellular cholesterol secreted in LDLs (Figure 2.22d).

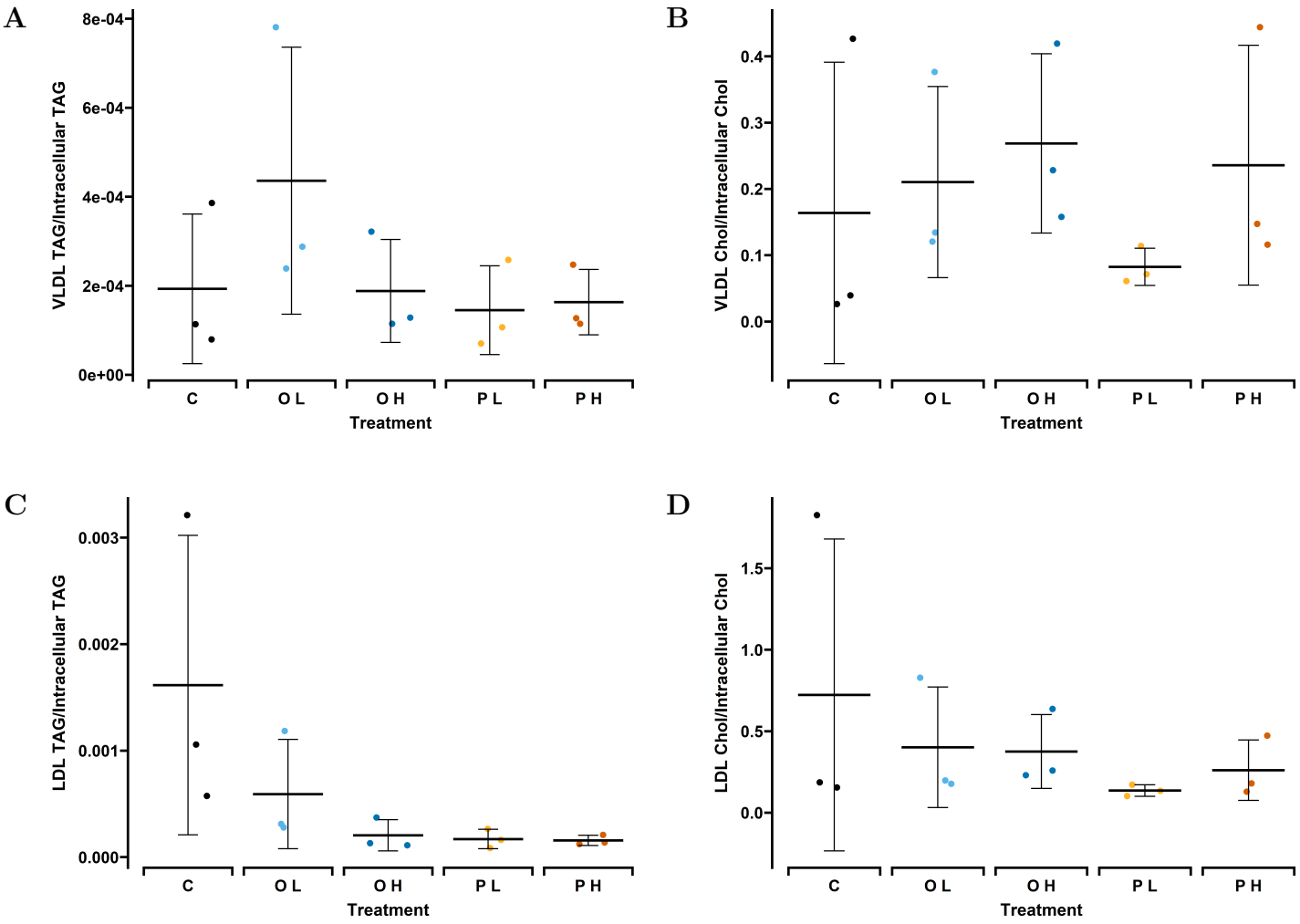


Figure 2.22: Export of triacylglycerol (TAG) and cholesterol by FA treated Huh7 cells adjusted for the intrahepatocellar TAG (IHTAG) or cholesterol concentration. A) VLDL-TAG adjusted to IHTAG; B) LDL-TAG adjusted to IHTAG; C) VLDL-cholesterol adjusted to intracellular cholesterol; D) LDL-choleseterol adjusted to intracellular cholesterol. Data presented as mean +/- SD, n = 3 per treatment unless stated otherwise. Abbreviations: C, no fat control; OL, low (200µM) concentration OPLA, OH, high (800µM) concentration OPLA; PL, low (200µM) concentration POLA; PH, high (800µM) concentration POLA.

2.3.8 Confocal imaging of FA treated Huh7 cells

A histological analysis was conducted to visualise the potential impact of FA composition of the treatment media on LDs morphology. The results showed significant morphological differences between these two conditions. Figure 2.23a shows Huh7 cells treated for 7 days with low concentrations of OPLA, with a heterogeneous population of LDs observed. Figure 2.23b shows Huh7 cells treated for 7 days with a higher concentration of OPLA and appears to show a greater amount of LDs of heterogeneous sizes when compared with cells treated with low concentrations of OPLA. Figure 2.23c shows Huh7 cells treated for 7 days with a low concentration of POLA ad shows a heterogenous population of LDs. In contrast to the LDs seen at either concentration of OPLA or a low concentration of POLA, cells treated with high concentrations of POLA show a homogeneous pattern of small LDs throughout the cells (Figure 2.23d. Figure 2.23e shows Huh7 cells treated with a no-fat control, with no LDs to be seen.

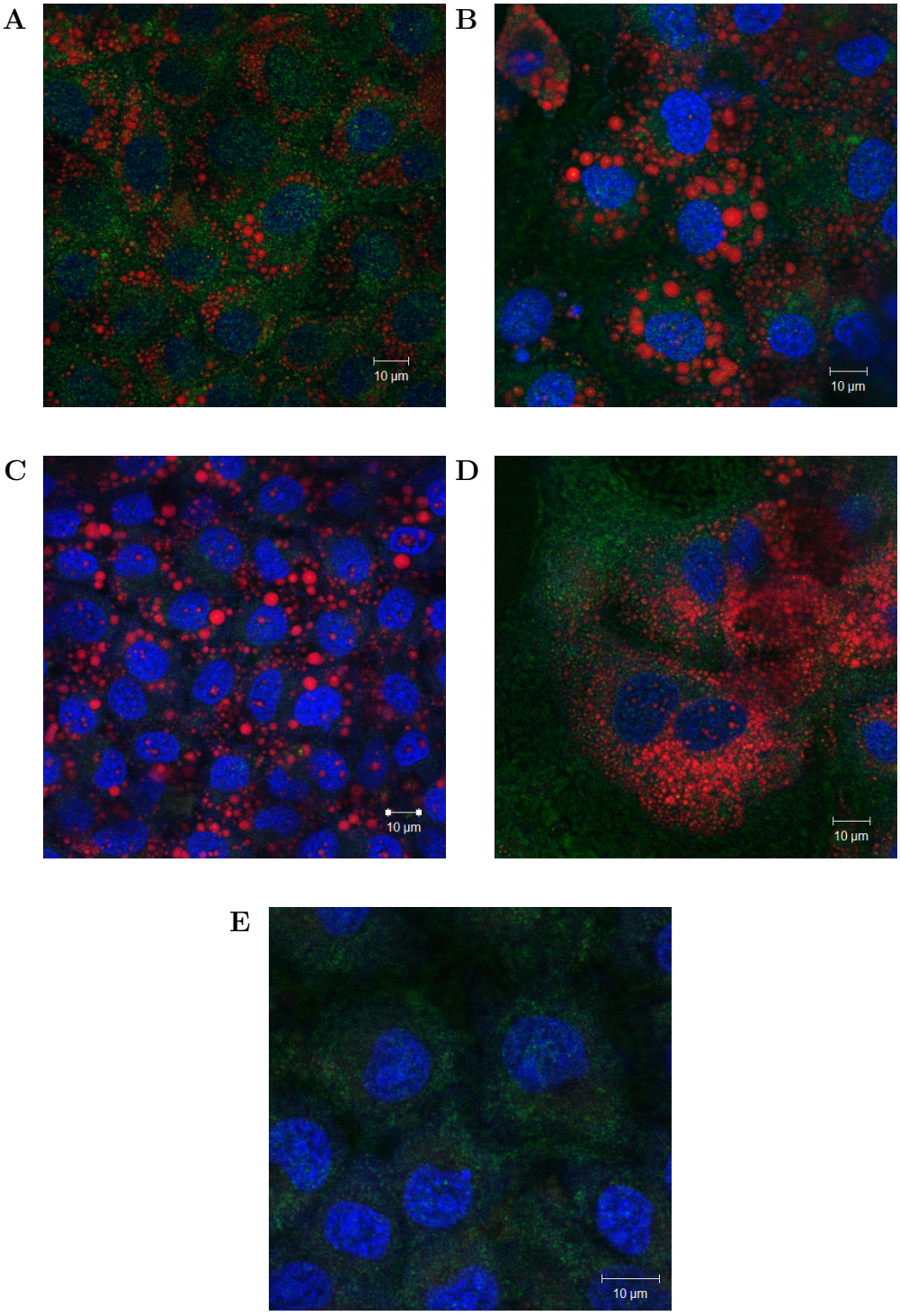


Figure 2.23: Confocal imaging of fluorescent stained lipid droplets (LDs) in fatty acid (FA) treated Huh7 cells. Cells were treated for 7 days with either a low concentration (200µM) or high concentration (800) of OPLA or POLA or a no-fat control. For all images, green is a α Tubulin stain in green, red is lipotox LD stain, blue is DAPI nuclear staining. A) OPLA FA treatment at low concentration; B) OPLA FA treatment at high concentration; C) POLA FA treatment at a low concentration; D) POLA FA treatment at high concentration; E) Treatment with a no-fat control.

2.3.9 Quantification of ATGL in FA treated Huh7 cells

In hepatocytes, adipose triglyceride lipase (AGTL) is the major lipase allowing access to hepatic LDs, regulated in part by ubiquitination by peroxin 2 (PEX2). Figure 2.24a, shows the Western blot for non-ubiquitinated ATGL. Figure 2.24b shows the quantification of the ATGL Western blot adjusted for total protein. There was a trend towards increased presence of non-ubiquitinated ATGL for cells treated with high concentrations of POLA compared to other conditions, but this difference was not significant.

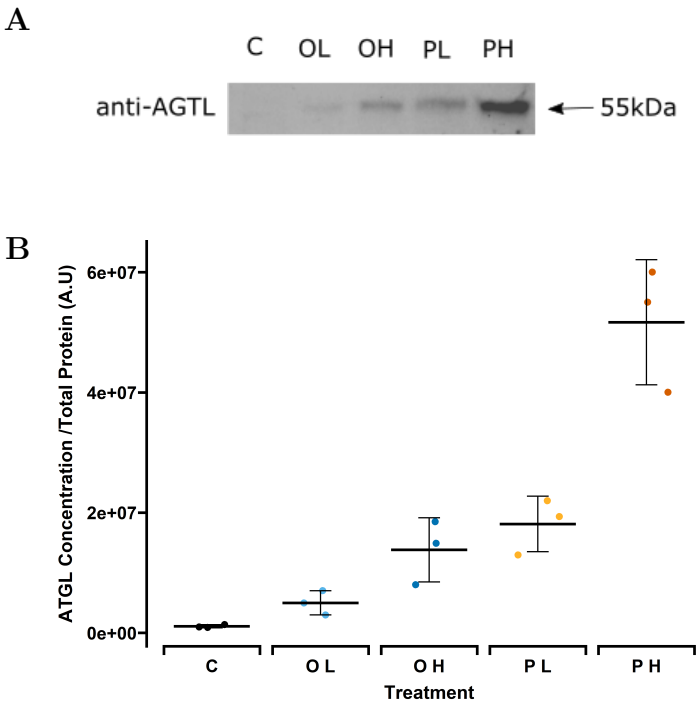


Figure 2.24: Quantification of the amount of ubiquitinated adipose triglyceride lipase (ATGL) in fatty acid (FA) treated Huh7 cells. A) Western Blot of non-ubiquitinated ATGL; B) Quantification of non-ubiquitinated ATGL compared to total protein. Data presented as mean +/- SD, n = 3 per treatment unless stated otherwise. Abbreviations: C, no fat control; OL, low (200µM) concentration OPLA, OH, high (800µM) concentration OPLA; PL, low (200µM) concentration POLA; PH, high (800µM) concentration POLA.

2.4 Discussion

The liver plays a central role in the homeostasis of circulating lipid and glucose levels. Within the liver, exogenous FAs mix with those derived endogenously from adipose tissue lipolysis and synthesized intracellularly, they are then partitioned into either esterification pathways for storage as TAG in LDs or secretion in VLDL, or into oxidation pathways (Trefts et al. 2017). Similarly, intracellular glucose can be stored (as glycogen), oxidised (via glycolysis) or secreted into systemic circulation (via glycogenolysis or gluconeogenesis (Agius 2008; Hanson et al. 2013).

Studying these pathways and their interactions in humans *in vivo* is challenging, thus there is a need for robust physiological *in vitro* cellular models. Although the group have previously established an *in vitro* model of IHTAG accumulation using nutritional substrates at physiological concentrations (Gunn et al. 2020), the impact of different FA compositions on lipid and glucose metabolism were not investigated. Therefore, the aim of this chapter was to investigate how altered FA composition and concentration affected hepatocellular FA metabolism and function. In Huh7 cells, the two FA compositions, OPLA and POLA were reflected in the intracellular TAG and the PL pools. These altered media compositions and also resulted in significant differences in the morphology of LDs. In PHH cells, they reflected the media FA composition to a lesser degree, which was likely influenced by the phenotype and possibly genotype of the donor.

Previous *in vitro* studies have suggested that treatment with SFAs (namely palmitic acid) compared to UNSFAs (namely oleic acid) to be cytotoxic, leading to reduced cell viability and metabolic activity as well as disruption in lipid metabolism, oxidative stress and intrahepatocellular calcium levels. Specifically, palmitic acid treatment has been demonstrated to increase apoptosis and ROS formation, with lower IHTAG content compared to exclusive oleate treatment (Nissar et al. 2015). This work demonstrated that these cytotoxic effects can be mitigated with the use of a mixture of FA, thus these observations support the rationale for the use of mixture of FAs, in physiological ratios when modeling hepatic steatosis *in vitro*.

These ratios were chosen based on analysis of total blood fat (Hodson et al. 2008), with more recent work highlighting the influence that consumption of different dietary fats has on blood plasma showing similar ranges to those chosen for this work (Gallego et al. 2018; Hodson et al. 2009).

Although there was a significant increase in NEFA uptake when Huh7 were cultured with high POLA compared to high OPLA, there were no differences in IHTAG. This is in contrast to a number of *in vitro* studies, using both HepG2 and Huh7 cells(Gunn et al. 2020; Mei et al. 2011) where increasing treatment with oleic acid and decreasing intrahepatic palmitic acid concentrations resulted in increased TAG content in cells cultured with single FA. However, these studies typically cultured cells for 6 to 24 hours, raising potential for an acute responses to changing nutrition source. Additionally, the majority of these have quantified TAG using histological Oil Red O staining, where data was rarely normalised to cell number, nor was information provided about cellular health, therefore raising further questions regarding the translatability of these models to human hepatic metabolism.

Human dietary intervention studies have previously reported that the consumption of a diet enriched in SFA as opposed to UNSFA results in a greater increase in IHTAG (Parry et al. 2017). It is well documented that SFA enriched diets, compared to PUFA enriched diets, can elevate adipose tissue lipolysis in humans (Yki-Järvinen et al. 2021), potentially leading to increased plasma NEFA levels, which in turn may contribute to greater hepatic NEFA uptake and subsequent TAG storage. Moreover, the intracellular partitioning of FAs into oxidation and VLDL secretion pathways may differ depending on FA saturation. We have previously shown that postprandial whole-body oxidation of linoleate is greater than palmitic acid (Parry et al. 2017), a phenomenon which may explain the differences observed in IHTAG accumulation between PUFA and SFA enriched diets in humans.

Oxidation was assessed in Huh7 cells in a number of ways, including tracing the fat of the stable-isotope labelled fatty acids D33 oleate and D31 palmitic acid through oxidation, and quantification of media acetate which is a proxy for

peroxisomal oxidation (Wanders et al. 2023). The greatest differences in oxidation were observed between the respective FA treatments and peroxisomal oxidation, with greater oxidation observed in cells treated with OPLA, particularly at higher concentrations, than POLA. Given that increased peroxisomal oxidation has been previously associated with a corresponding increase in ubiquitination of ATGL via PEX 2 (Ding et al. 2021), this could potentially explain the differences in LD size, with increased peroxisomal activation potentially limiting access to the LD, therefore allowing them to get bigger.

The PL composition observed in Huh7 cells reflected that of the treatment medias. This observation is noteworthy because the composition of the membrane can affect its fluidity, potentially leading downstream metabolic consequences including alterations in export and disposal pathways as well as changes in protein interactions with the membranes (Hashidate-Yoshida et al. 2015; Casares et al. 2019). The export of TAG relies on the formation of lipoproteins, which are secreted via exocytosis, a process dependent on membrane fluidity. Additionally, excess TAG is stored within LD in the cytoplasm, which are coated in PLs (Côté et al. 2014; Parks et al. 1999). Changes in the fluidity of the PL membrane could account for differences in the size of these LD and also may also affect the accessibility the of TAG for cellular metabolic processes, particularly oxidation.

While glucose remained consistent across treatments, Huh7 cells exhibited increased glucose production, when subjected to high concentration of POLA. Culturing cells with low POLA levels, also resulted in increased intracellular glycogen content. Previous studies have reported that treating HepG2 cells with 0.25 mM palmitic acid for 24 hours resulted in 30% reduction in glycogen content and decreased pAKT, pGSK and GS activity, suggesting alterations in insulin signaling (Gao et al. 2010). This is consistent with an *in vivo* human study showing that in healthy, non-obese individuals, elevated plasma NEFA levels interfered with insulin suppression of glycogen breakdown (Steiner et al. 1996). In contrast, in isolated rat liver perfusions, both palmitic acid and oleic acid impaired insulin signaling but had no effect on glycogen content (Su et al. 2019). It would be intriguing to

investigate and compare hepatic glycogen content and metabolism in individuals with metabolic vs genetic MASLD, as they are reported to have notably distinct liver FA compositions (Luukkonen et al. 2016).

This work has some limitations to note. While we used Huh7 cells, a well-established human hepatocyte cell line, it is essential to acknowledge that they do not fully recapitulate *in vivo* human liver function due to being an hepatoma-derived line (Kawamoto et al. 2020). Although Huh7 cells are reported to show traits associated with tumor metabolism, such as rapid glucose consumption and elevated lipogenesis, it is worth mentioning that both our research and that of others have revealed that culturing hepatoma cells in HS, as opposed to FBS, can improve metabolic functionality rendering more akin to PHH. In previous work, we demonstrated that culturing Huh7 cells in HS lowers DNL levels to those reported in human liver, while also improving insulin sensitivity, VLDL secretion and FA oxidation (Gunn et al. 2017). It is essential to recognize, however, that this model does not modulate the 'meal frequency' experienced by the hepatocytes *in vivo*. Nevertheless, ongoing research within our group, has explored alterations in feeding schedules, revealing a similar trend between these models (Nagarajan et al. 2022). Additionally, it is pertinent to mention that this model did not include the use of insulin, a well-known regulator of fat and glucose metabolism. Nonetheless, other researchers within the group are actively investigating this aspect.

PHH also come with significant issues despite being considered a gold standard *in vitro* model: they are costly, with high inter-donor variability and are frequently sourced from older donors with pre-existing liver diseases and prior medical treatments. Additionally, these cells do not survive long outside of the body, restricting experiments to a maximum duration of 5 days. This limitation bears particular significance in our study, due to the seeding protocol requiring that these cells are seeded onto collagen coated plates, which entail the retention of dead cells, consequently allow them to be incorporated into measurements. This may have significantly contributed to the observed data variation, particularly given the varying composition of pre-existing LDs in these cells.

2.5 Conclusion

Our study has demonstrated that Huh7 cells, when exposed to a physiological mix of FAs, maintain their cellular viability and sustain normal glucose and lipid metabolic pathways despite accruing IHTAG. As a result, this cellular model displays several characteristics of resembling early stage MASLD in an *in vitro* setting. By further manipulating the nutritional and hormonal substrates, coupled with prolonged exposure, this model could be used to further investigate the effect of IHTAG accumulation of differing compositions and the impact on both lipid and glucose pathways, in addition to exploring any other pertinent questions that may arise in this context.

3

Transcriptome analysis of mRNA in an *in vitro* Huh7 or PHH model of IHTAG using FA treatments enriched in UNSFA or SFA

3.1 Introduction

With IHTAG accumulation, is it suggested that key genes may be altered. RNA sequencing provides the opportunity to further explore the effect of both phenotype and lifestyle changes on hepatic metabolism. To date, the majority of studies investigating hepatic gene expression have been limited by small sample sizes, particularly when considering the different stages of MASLD, which have been of previous focus. This chapter will focus on the effect of FA treatment composition on the mRNA transcriptome.

Investigating changes in RNA sequencing across the MASLD spectrum, Sudunhi et al assessed differences between patients presenting with both MASLD and obesity. They quantified 795 genes hypothesised to be involved in hepatic fibrosis, inflammation and steatosis in liver tissue from 318 adults (76% female, 24% male, median age 44 years, 75% BMI >40, dyslipidemia (36%), T2DM (29%) and categorised using the 4 stages of MASLD: healthy liver (n = 76, 24%), steatosis (n = 88, 28%), MASH without fibrosis or MASH (n = 72, 23%), and MASH with fibrosis (n = 82, 26%). Analysis was done with a linear model developed and adjusted

for covariates (sex, diabetes and BMI) (Subudhi et al. 2022). Subunhi et al showed that as MASLD progresses, distinct gene expression changes occur. These are associated with inflammation, the compliment and coagulation pathways and tissue remodelling. Of particular relevance to this project, they identified 29 differentially expressed genes when comparing early stage MASLD with healthy livers. This number increased to 188 differently expressed genes in patients presenting with MASH. In early stage MASLD, upregulation was seen in genes associated with inflammation: CXCL9 and CXCL8. Early stage MASLD was also associated with the down-regulation of genes involved in the compliment and coagulation cascades (C9, C8b, C3BPB, FGG, GFA, SERPINA 1, SERPING1, FBG, SERPINC1, C3, CFB, C5, KNG1 MASP2) (Subudhi et al. 2022). There was also a downwards trend in PON3, a protein associated with modulation of oxidative stress and also HDL formation which has been demonstrated to be protective of cancerous cells, enabling their progression by by protecting the cells against oxidative stress and apoptosis) (Furlong et al. 2016; Subudhi et al. 2022). Dysregulation of extracellular remodelling genes was only seen in advance stage fibrosis (Subudhi et al. 2022).

Comparison between lipid profile and gene expression within tissue or cell samples is something that has not been reported often. From the limited data available, Arendt et al, have shown a small (n=20 with simple steatosis, n=19 MASH patients, and n=24 healthy control participants) cross-sectional study that hepatic gene expression differed mainly between healthy controls and patients with disease (both simple steatosis and MASH). 22 genes were differentially expressed between MASH and simple steatosis of which most were correlated with disease severity and related more to cancer progression rather than to lipid metabolism. Regarding the FA profile, they noted that long-chain PUFA (eicosapentaenoic acid and docosahexaenoic acid and arachidonic acid) were lower in MASH compared to patients with simple steatosis and postulated that this may be related to the overexpression of FADS1, FADS2 and PNPLA3 in MASH. It is unclear whether gene expression modulates PUFA content, or whether PUFA content modulates the gene expression of the liver (Arendt et al. 2015). Additionally, studies investigating dietary influence on

MASLD gene expression have predominately been carried out in animal models of MASLD, which poses questions about how translatable these finding are for human disease (Alshawsh et al. 2022; Kim et al. 2016)

Investigations into the changes in RNA in *in vitro* cellular models, has been limited with focus on metabolic pathways, with an aim of establishing therapeutic targets rather than generating a more complete understanding of the molecular mechanisms underlying the disease (Long et al. 2019; Wang et al. 2022; Lee et al. 2021). The role of miRNA has been reviewed extesively by Gjorgjieva et al where dysreulgated miRNA have been associated with metabolic pathways. Of note, miRNAs have been found to be associated with increased DNL, increased plasma lipid uptake, diminished hepatic export of lipid and or impaired oxidation. Alterations have also been observed in glucose metabolism initiated by miRNAs. On top of this, cellular processes have been shown to be dysregulated e.g. autophagy, ER stress and the unfolded protein response and these dysregulations have been demonstrated to be under the control of miRNAs (Gjorgjieva et al. 2019).

The aim of this chapter was to investigate the effects of exposing Huh7 and PHH cellular models to different FA compositions (OPLA and POLA) and assessing changes in RNA expression to determine potential targets for further investigation. Understanding FA composition derived changes will allow for a targeted approach in future metabolic studies.

3.2 Methods

Cells were cultured as described in Chapter 2 Section 2.2.1 and Section 2.2.1.6. Cells were treated with both OPLA and POLA FA treatments as well as a no-fat control. Huh7 cells were treated with only a high concentration of OPLA or POLA whereas PHH cells were treated with both a high and a low concentration of OPLA and POLA.

3.2.1 RNA extraction

Two different methods were used for RNA extraction for the Huh7 cells and PHH cells. This decision made due to resource availability and not due to different cellular requirements.

3.2.1.1 Huh7 RNA extraction

Cells were cultured in 6-well plates as described in Chapter 2 Section 2.2.1.6. RNA extraction was carried out using the RNAeasy kit (Qiagen, 74104) as per the manufacturer's instructions. Briefly, lysis was carried out *in situ*: a highly denaturing guanidine-thiocyanate- containing buffer was added followed by 350µL of RLT buffer which inactivated the RNAses to ensure the RNA remained intact. Homogenisation was then necessary to reduce the viscosity of the lysates generated by the disrupting lysis buffer. Additionally, homogenisation shears high-molecular weight genomic DNA and other cellular components. Samples were vortexted to ensure complete homogenisation, to reduce the risk of inadequate binding of RNA to the column and potential clogging of the column. An equal volume of 70% ethanol was added (made in RNAse free water) to create appropriate binding conditions. Sample (700µL) was then applied to the RNeasy mini spin column where total RNA bound to the membrane. The spin column was then attached to the vacuum manifold and a vacuum applied until transfer was complete. Sample were washed with 700µL of RW1 and a vacuum applied until transfer was complete. Two washes with RPE buffer were then carried out with a vacuum step following each wash. Columns were then centrifuged dry for 1 minute on a bench-top centrifuge at 12000xg. 30-50µL

RNase-free water was added and columns were centrifuged at 1 minute at 12000xg to elute the RNA. No clean up protocols were required for any of these samples.

3.2.1.2 Primary cell RNA extraction

Prior to extraction, cells were cultured as described Chapter 2 Section 2.2.1.3 in 24-well plates. Cells were then washed with PBS before they were harvested using Trizol reagent at 200µL per well. Cells were scraped and transferred to elution tubes where 50µL of chloroform was added and shaken vigorously. Samples were left at room temperature for 5 minutes then centrifuged at 1200xg at 4°C for 15 minutes. The top aqueous phase was transferred to a second elution tube already containing 2µL of glycol blue (ThermoFisher, AM9516). An equal volume of isopropanol was added to the elution tube and briefly vortex. Samples were incubated overnight at -20°C or for 1 hour at -80°C. Samples were then centrifuged at 1200xg at 4°C for 30 minutes. The supernatant was then removed and 200µL of 80% ethanol (made up in RNAse free water) added before samples were gently shaken to dislodge the pellet from the elution tube wall. Samples were centrifuged at 1200xg at 4°C for 15 minutes and 80% ethanol wash and spin steps repeated. Following the second ethanol wash, as much ethanol is removed by pipette as possible and the pellet allowed to air dry. 15µL of RNAse free water was then added to re-suspend the pellet. Samples were then incubated in fridge for a minimum of 3 hours before further analysis. Many of these samples required clean up following this protocol.

3.2.1.3 RNA specifications

For both the Huh7 cells and the PHH, RNA sequencing was carried out by Novagene.

The following specifications were required:

- Amount of RNA: minimum 200ng of RNA in 20µL.
- RNA integrity number (RIN) greater than 4.
- RNA to DNA ratio measured with absorbance at 260/280 between 1.8 to 2.2.
- Organic matter contamination measured with absorbance at 260/230 and must be above 1.8.

3.2.1.4 RNA clean-up

For RNA which did not meet the required specifications a clean-up was performed. The protocol was as follows: First, the volume of RNAse free water was increased to 100µL before 300µL of chloroform was added and the samples were shaken then incubated on ice for 5 minutes. The samples were then centrifuged for 30 minutes at 1200xg, 4°C. The upper solvent phase was then transferred to an elution tube and 30µL NaAc (10%v/v) was added and the samples vortexed. 900µL of 100% ethanol was added and samples incubated either overnight at -20°C or for 1 hour at -80°C. Samples were then centrifuged at 1200xg, 4°C for 15 minutes to precipitate the pellet. The protocol then follows the initial extraction protocol: Twice through 200µL of 80% ethanol wash was added and samples centrifuged at 1200xg at 4°C for 15 minutes before the supernatant removed. Following the second wash, the sample was left to air dry before being re-suspended in RNAse free water (10-30µL depending on expected concentration).

3.2.1.5 In-house quality control checks for Huh7 and PHH cell sequencing

To ascertain whether the samples were suitable to be sequenced by Novogene, several in-house quality control checks were carried out. Firstly, samples were analysed with a nanodrop spectrophotometer to assess the concentration, and the absorbance ratios

for RNA to DNA (260/280nm) and for other organic contamination (260/230nm). RNA was also measured on the 2200 TapeStation (Agilent, G2964AA) to generate a RIN number. All samples were cleaned until they had the desired specifications.

3.2.1.6 Novogene protocols for Huh7 and PHH cell sequencing

Novogene completed the following pipeline for RNA sequence analysis; quality control confirmation, quantification and sample; library construction and quality control of the library. Documentation provided by Novogene on this process and their analysis can be found in Appendix A.2.1. For library construction: mRNA was purified from total RNA using poly-T oligo-attached magnetic beads. cDNA was then synthesised from this mRNA. The library was checked with Qubit and RT PCR for quantification and bioanalyzer for size distribution detection. Quantified libraries were pooled and sequenced on Illumina platforms according to the effective library concentration and data amount. The clustering of the index-coded samples was performed according to the manufacturer's instructions. After cluster generation, the library preparations were sequenced on an Illumina platform and paired-end reads were generated.

Raw data (raw reads) of FASTQ format were firstly processed by Novogene through in-house perl scripts. In this step, clean data (clean reads) were obtained by removing reads containing adapter, poly-N regions and low-quality reads from raw data. At the same time, Q20 (99% accurate) , Q30 (99.9% accurate) and G/C content the clean data were calculated (see Appendix A.2.1). All the downstream analyses were based on the clean data with high quality. Reference genome (Hg38) and gene model annotation files were downloaded from genome website browser (NCBI/UCSC/Ensembl) directly. Index of the reference genome was built using Hisat2 v2.0.5 and paired-end clean. Two reads were aligned to the reference genome using Hisat2 v2.0.5. They selected Hisat2 as the mapping tool for that Hisat2 can generate a database of splice junctions based on the gene model annotation file and thus a better mapping result than other non-splice mapping tools.

Alignments were parsed using Tophat program. Gene fusion and difference of alternative splicing event were detected by Star-fusion and rMATS software. Indexes of the reference genome was built using STAR (v2.5) and paired-end clean reads were aligned to the reference genome using STAR. STAR used the method of Maximal Mappable Prefix (MMP) which can generate a precise mapping result for junction reads. HTSeq v0.6.1 was used to count the read numbers mapped of each gene for Huh7 and featureCounts v1.5.0-p3 was used to count the reads numbers mapped to each gene for PHH and then FPKM of each gene was calculated based on the length of the gene and reads count mapped to this gene. FPKM, Reads Per Kilobase of exon model per million mapped reads, considers the effect of sequencing depth and gene length for the reads count at the same time, and is currently the most commonly used method for estimating gene expression levels (Mortazavi et al. 2008).

Fusion gene refers to the two genes of all or part of the sequences where fusion has been performed resulting in a chimeric gene, usually caused by reasons such as chromosome translocation. Novogene used Star-fusion (0.8.0 for Huh7 and 1.9.0 for PHH) software analysis (including SATR alignment, SATRfusion.predict, SATR-fusion.filter) for detection of fusion genes to ensure the accuracy of the results. Alternative Splicing is an important mechanism for regulate the expression of genes and the variable of protein. rMATS (3.2.1 for Huh7 and 4.1.0 for PHH) software was used to analysis alternative splicing events.

3.2.2 Data analysis

3.2.2.1 Data normalisation

The following was carried out on all datasets. Data as counts and gene ID were analysed in R (version 4.3.1). Data were first filtered to remove genes with low expression and then normalised using the TMM method, a scaling normalisation method, with EdgeR (version 3.42.4) (Robinson et al. 2010). Data were then converted into log(Counts per million (CPM)). All data for both Huh7 cells and and PHH cells had an adjusted log(CPM) between 0 and 15. Figure 3.1, shows data spread for PHH cells. All samples showed adequate amounts of data for analysis.

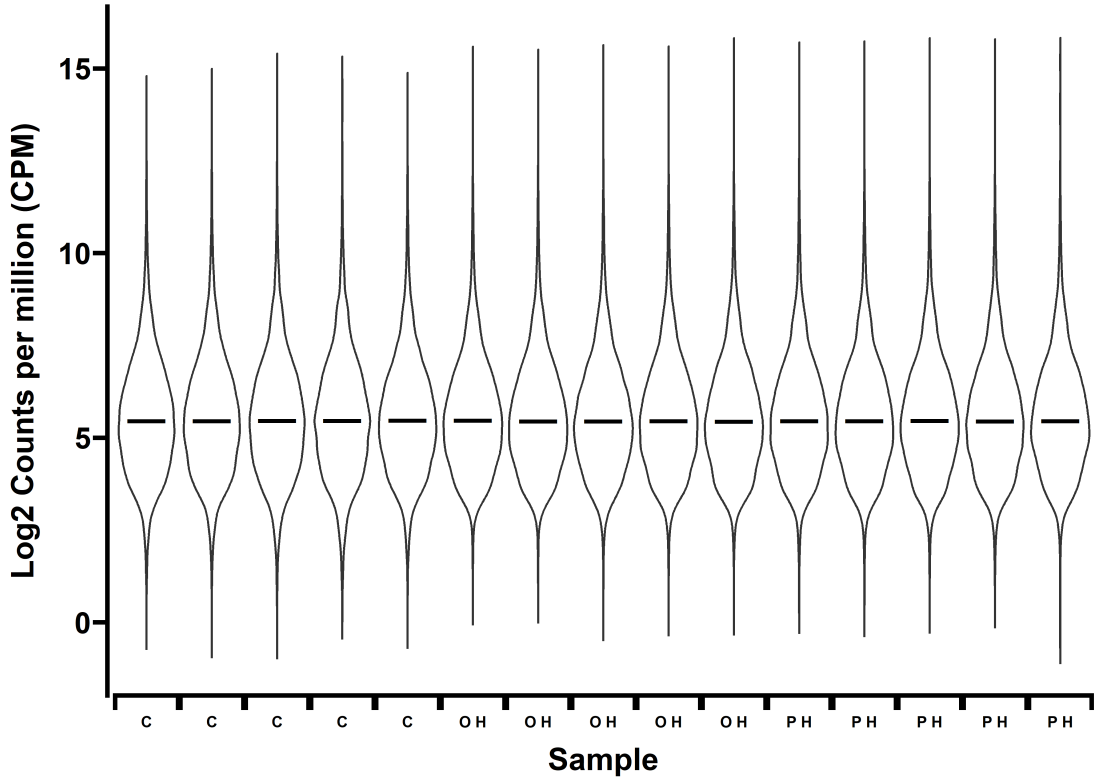


Figure 3.1: TMM normalisation with the EdgeR (v3.42.4) package on PHH cells. Abbreviations: C is a no-fat control, OH are cells treated with OPLA at a high concentration of 800µM FA and PH are cells treated with POLA at a high concentration of FA at 800µM. Data are spread, with line as median

3.2.2.2 Data visualisation

RNA-Seq Principal Component Analysis (PCA) is a data analysis method used in genomics to simplify and visualize high-dimensional gene expression data. PCA reduces the complexity of RNA sequencing data by identifying patterns and relationships among genes, highlighting the most significant variations between samples. By projecting the data into a lower-dimensional space, PCA allows researchers to identify key sources of variation, such as biological differences or experimental effects. This simplification aids in data interpretation, revealing insights into gene expression patterns and facilitating the discovery of genes that are biologically relevant or respond to specific conditions, without the need for extensive computational expertise. FactoMineR (version 2.8) and factoextra packages were used to generate and visualize PCA (version 1.0.7).

Differentially expressed genes were visualised with Venn diagrams, volcano plots and heatmaps. Venn diagrams were generated with the package ggvenn (version 0.1.10). Volcano plots were generated using EnhancedVolcano (version 1.18.0). Volcano plots show the scatter plot juxtaposing statistical significant, p-value, against the magnitude of biological relevance - the log fold change between experimental groups. Cuts offs were applied for p values greater than 0.01 and change size of 0.15, the application of which was to help reduce the false discovery rate. Heatmaps were generated using gplots (version 3.1.3) enhanced heatmap function.

3.2.2.3 Differential gene expression analysis

PHH, by nature, exhibit inherent biological variability arising from the genotype and phenotype of the donor and environmental influences. These variations can make interpretation of smaller data sets more challenging. Therefore, a sophisticated statistical approach is required and a mixed effects model, also known as a multilevel or hierarchical model, provides a flexible framework to handle biological variability by explicitly incorporating random effects. Random effects capture and allow the separation of individual-specific differences, treatment effects, or batch effects

(as more relevant for Huh7 models), thus accounting for inter-sample and intra-sample variations. By considering these random effects, use of a mixed effects model enabled a more accurate estimation of gene expression changes, resulting in improved statistical power and reliable inference.

A mixed effect model was used on both datasets, describing treatment as the fixed effect, accounting for both the composition and the concentration of the FA given (combined into one variable). Limma package (version 3.56.2) was used to extract the differentially expressed genes, using the package 'voomwithqualityweight', owing to the large sample variability. These previous steps remove heteroscedascity from the count data, with the adjustment in data distribution shown in Figure 3.2. For analysis of the Huh7 RNA sequencing data, the batch number was considered a random effect, (something which has an impact on the data but one which we are not interested in). For the PHH dataset, the individual whom the cells came from was considered a random variable. Genes were considered to be differentially expressed if the false discovery rate (FDR) was less than 0.01.

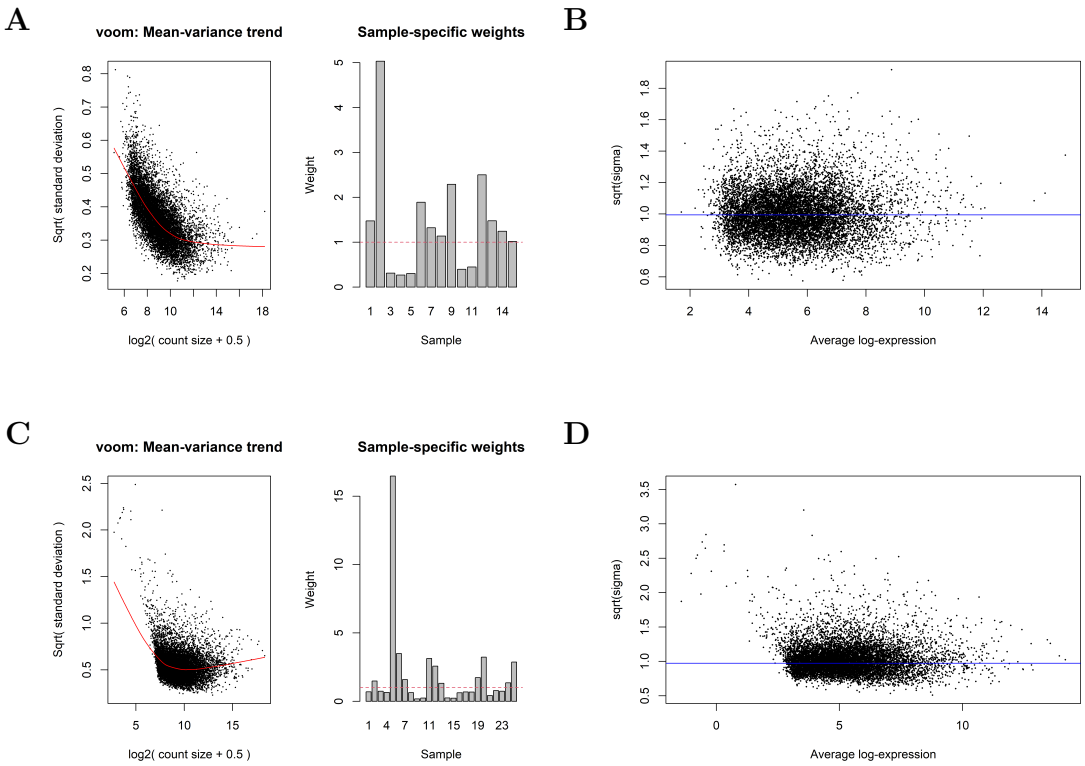


Figure 3.2: Relationship between the standard errors and the average log-counts of the genes in the differential expression analysis of fatty acid (FA) treated Huh7 cells and primary human hepatocytes (PHH).. Each point on the plot corresponds to a sample, and the position or size of the point reflects the sample-specific weight assigned to that particular sample. Plots show data after applying the mixed effects model. A) Variation in RNA sequencing of Huh7 cells; B) Average log expression from sequencing Huh7 cells; C) Variation in RNA sequencing of PHH cells; D) Average log expression from sequencing PHH cells.

3.2.2.4 Pathway analysis

Pathway analysis of the differentially expressed genes was carried out using fgsea (version 1.26.0) to detect significantly enriched pathways within h.all.v2023.1.Hs.symbols.gmt database. Entrez ID was converted using the org.Hs.eg.db database using clusterProfiler (version 4.8.1) and gene look up was done using GenomeInfoDbData (version 1.2.10).

3.3 Results

In this section, the results from Huh7 RNA Sequencing will be followed by the PHH RNA sequencing data.

3.3.1 RNA sequencing in Huh7 cells

3.3.1.1 Factor analysis

Factor analysis, is a statistical method used to identify underlying factors or latent variables that explain patterns of relationships within a set of observed variables. In factor analysis, eigenvalues are associated with the factors extracted from the data. An eigenvalue represents the variance explained by each factor with high eigenvalues indicating that the corresponding factor explains a significant amount of variance in the data. A scree plot is a graphical representation of eigenvalues and shows the eigenvalues in descending order along with determining the optimal number of factors to retain for analysis as the point where the eigenvalues level off which is often described as the 'elbow' of the curve indicating the number of meaningful factors to keep. Figure 3.3a, shows the scree plot of the RNA sequencing data obtained from the treated Huh7 cells and suggests that consideration only needed to be taken of the first 2 factors, which together account for 88.4% of the variation.

PCA is a graphing technique related to factor analysis that transforms data into a new coordinate system, revealing patterns and relationships between data and allowing the size and contribution of the effect of a factor to be visualised. Data were plotted according to the pre-determined factors established from the scree plot. Figure 3.3b, shows the interaction between the Huh7 treated samples across the first two dimensions. The weighting, or contribution and impact of each PCA factor can be seen in Figure 3.3c, visually demonstrating that the largest effect was explained by the addition of FA to the media, regardless of composition. The composition of the FA was explained by the second PCA dimension, with the third dimension again demonstrating variation resulting from the differing treatment FA compositions.

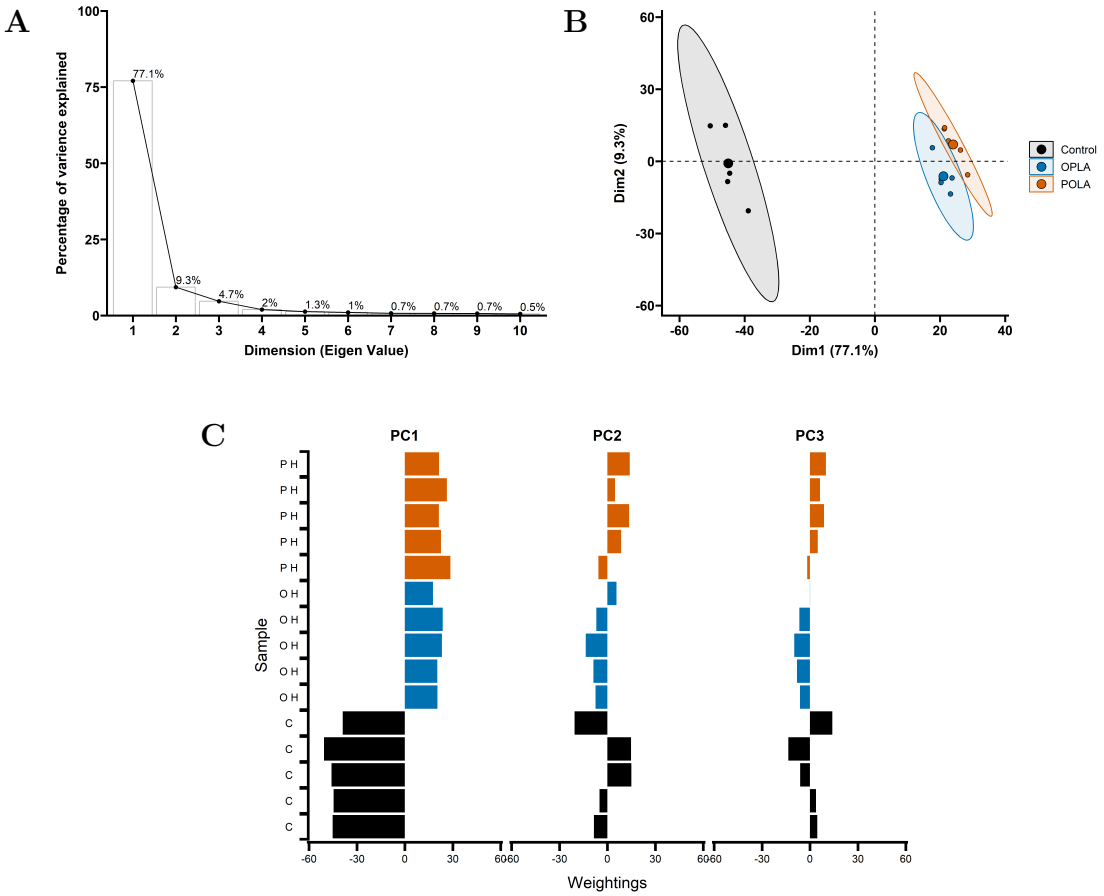


Figure 3.3: Factor analysis in RNA expression from fatty acid (FA) treated Huh7 cells. A) Scree plot of eigenvalues from sequencing of Huh7 cells; B) principle component analysis (PCA) plot between the first and second dimension from sequencing Huh7 cells; C) Weighting of the first 3 PCA factors. Abbreviations: C, no fat control; , OH, high (800µM) concentration OPLA; PH, high (800µM) concentration POLA (PH).

3.3.1.2 Differential gene expression

Venn diagrams were utilised to determine the quantity of differentially expressed genes. Data were generated using a cut-off of 0.01 p-value and a cut-off of 0.2 fold change. Figure 3.3.1.2 genes which are differentially expressed in Huh7 when comparing those cells treated with either a high concentration of OPLA or POLA against a no-fat control, categorising them as either genes which are down-regulated, or up-regulated with the addition of the FA treatments. Data show that the majority of the genes which are differentially expressed are so with both the FA compositions.

Volcano plots were generated to visualise the size and direction of gene expression changes. Figures 3.5a and 3.5a, show the volcano plots for both OPLA versus the no-fat control samples and POLA versus the no fat control samples. Where positive values show RNA was found at a greater concentration in cells treated with either FA composition when compared to the no-fat control, and negative fold changes values show RNA expressed at a greater level in no-fat treated control cells. Overall, data showed a significant number of genes were expressed at both higher and lower amounts comparing cells treated with the no-fat control versus either high concentrations of OPLA or POLA (Figures 3.5a and 3.5a).

Figure 3.5b shows the volcano plot comparing cells treated with OPLA versus POLA. Positive fold change values show RNA expressed at a higher level in cells treated with POLA compared with those treated with OPLA and negative fold change values show RNA expressed at a greater level in OPLA treated cells. Genes showing the greatest fold-change and significance have been highlighted on the graph. Expressed in a higher level in POLA compared to OPLA are the genes SPON2, AHSG, SERPINE1, TRIBE3 and A2M and expressed in a higher level in OPLA compared to POLA treated cells are FOLH1, SLC1A3, NAPEPLD, SI and CHORDC1.

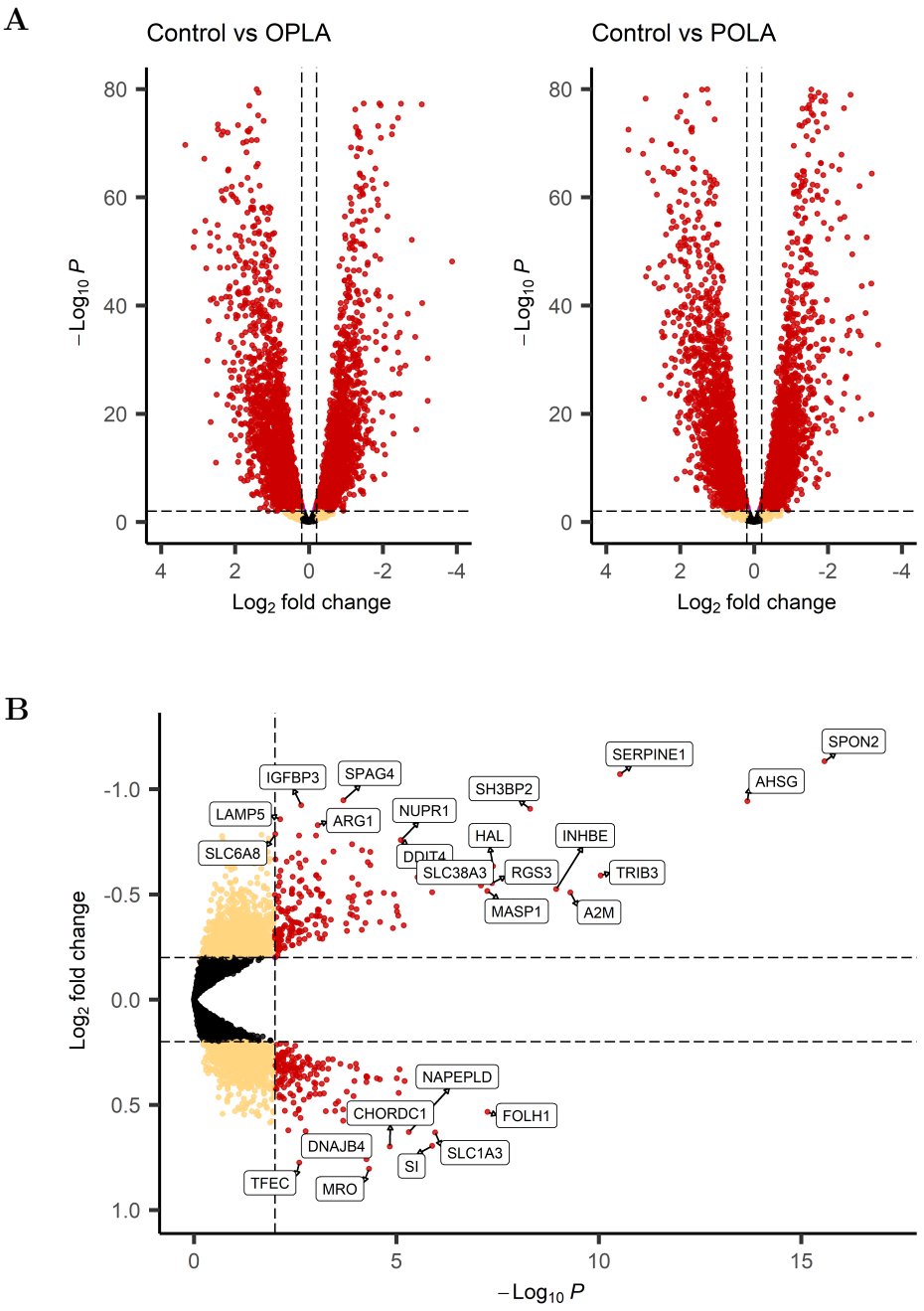


Figure 3.5: Volcano plots of extracted RNA from fatty acid (FA) treated Huh7 cells. A) Volcano plot showing differentially regulated genes between cells treated with either high OPLA compared to the no-fat control or high POLA compared to a no fat control. Positive values show RNA found at a greater level in cells treated with either FA treatment composition when compared to the no-fat control, and negative fold changes values show RNA expressed at a greater level in no-fat treated control cells; B) Differentially expressed genes found when comparing expression data between cells treated with High concentrations or OPLA or High concentrations of POLA. Positive fold change values show RNA expressed at a higher level in cells treated with POLA compared with those treated with OPLA and negative fold change values show RNA expressed at a greater level in OPLA treated cells.

3.3.1.3 Go terms and KEGG pathways

KEGG is a database resource used to describe known interactions between proteins and genes relating to different processes, conditions or diseases; it provides a good starting point for interpreting RNA sequencing results. Figure 3.6a shows pathways associated with differentially expressed genes identified when comparing cells treated a FA treatment (either OPLA or POLA) with the no fat control. Relevant to IHTAG accumulation, FA treatment resulted in activated DNA repair pathways, activated cell cycle whereas ER protein processing, autophagy and protein export were found to be suppressed. Figure 3.7a, shows the associated pathways to genes activated and suppressed with POLA compared to OPLA treatment. In cells treated with POLA opposing pathways were identified with both cell cycle pathways and cellular senescence pathways activated to a greater extent compared to those cells treated with OPLA. Additionally, higher amounts of genes associated with cancer were upregulated with POLA when compared to cells treated with OPLA. Only ER protein processing pathways were found to be activated to a greater extent in OPLA treated cells compared to POLA. However, KEGG pathways are considered a blunt tool and often identify processes that may be irrelevant, but may involve overlapping proteins. For example, comparing cells treated with either FA composition compared to the no-fat control, the KEGG analysis identified RNA changes being involved in HERPES simplex virus 1 infection. While this may be in reference to the small incidence (<1%) of herpes induced hepatitis (Chávez et al. 2021) it is unlikely to be relevant to this model.

Gene Ontology (GO) pathway analysis, another analytical tool used to investigate RNA changes within known pathways, was also performed. This analysis methodology offers a structured framework for categorizing genes into biologically relevant functional groups aiming to provide biological context. GO pathway analysis also faces the same limitations of KEGG, including the potential for oversimplification, dependence on data completeness, sensitivity to statistical thresholds, and the inability to establish causality. Figure 3.6b, shows the results of GO pathway analysis comparing the effects of treatment with either high concentrations of OPLA

or POLA with a no- fat control. Identified are pathways more relevant to metabolism within the hepatocyte (oxidation, oestrogen), as well as pathways associated with some of the adverse changes seen in MASLD (ER stress, inflammation, hypoxia). Figure 3.7b, shows the same analysis but this time comparing high POLA with high OPLA was analysed to look at gene upregulated in FA treated cells versus control, or look at genes upregulated with POLA compared to OPLA.

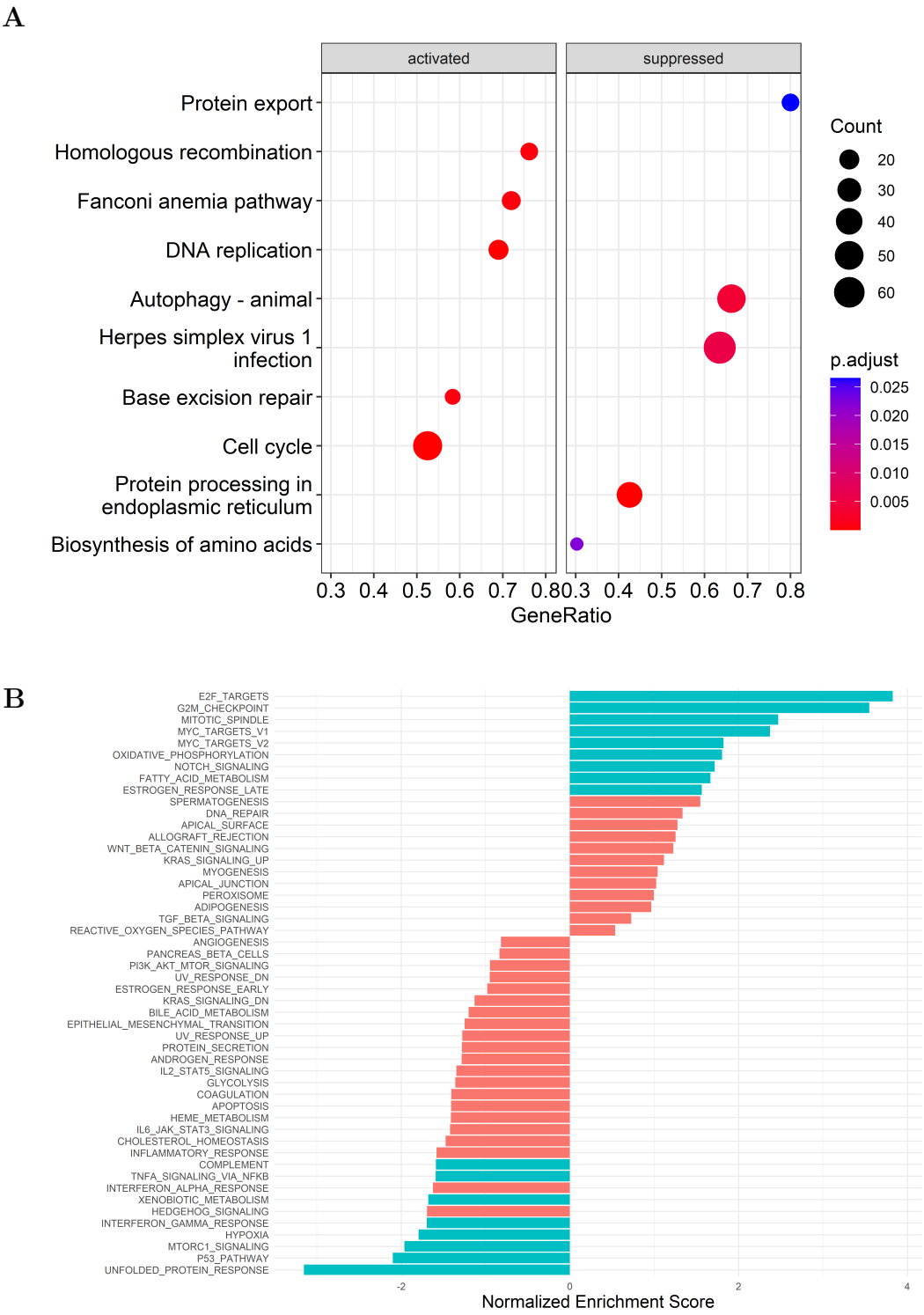


Figure 3.6: KEGG and GO pathway analysis of RNA extracted from fatty acid (FA) treatment versus no-fat control in Huh7 cells. A) KEGG pathway analysis showing pathways enriched in samples treated with FA treatments, either OPLA or POLA comparison to those treated with a no-fat control; B) GO pathways analysis for the same comparison. Abbreviations: C, no fat control; , HF, high FA treatment (800µM) of either OPLA or POLA.

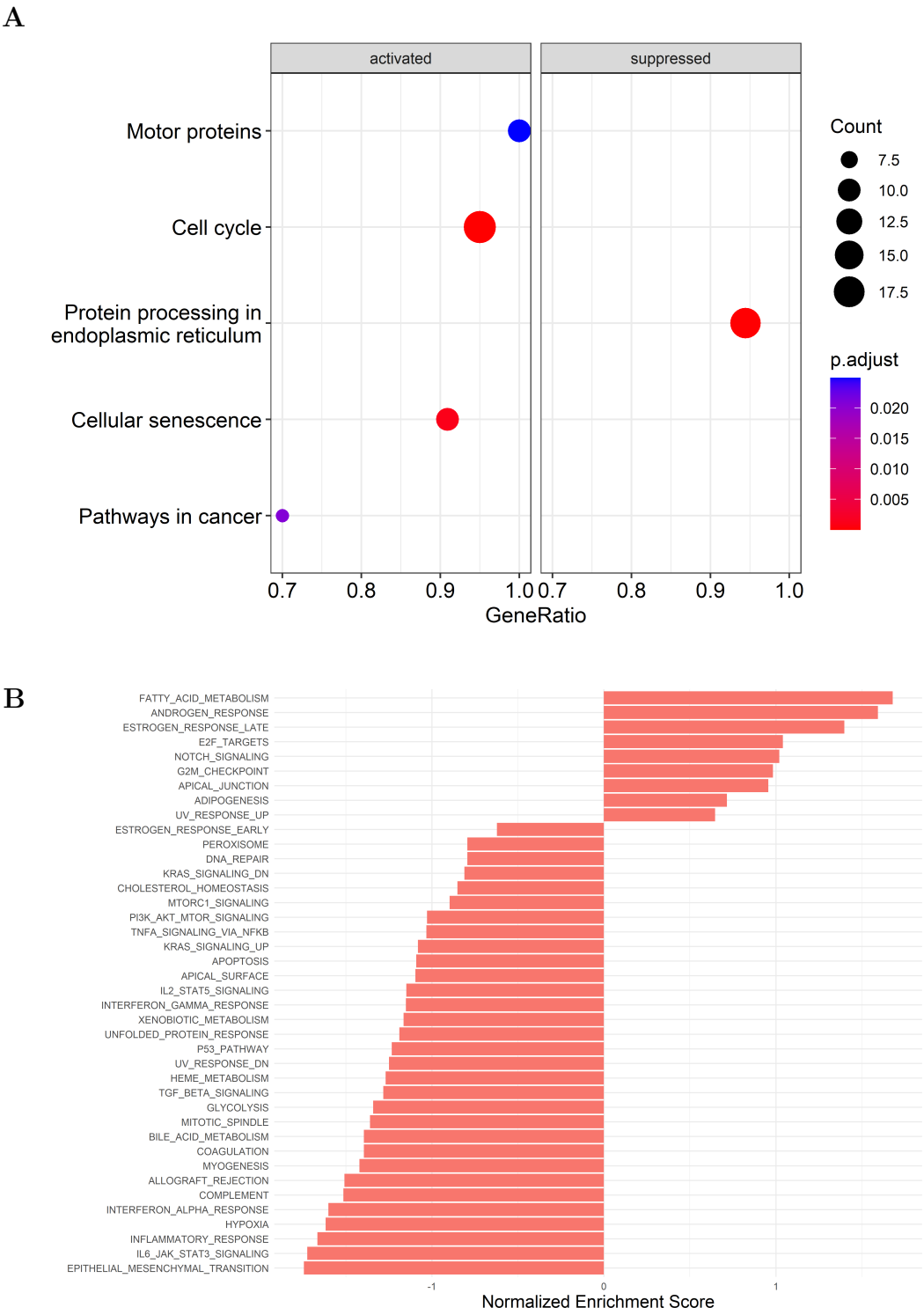


Figure 3.7: KEGG and GO pathway analysis for RNA extracted from Huh7 cells treated with OPLA fatty acids (FA) versus POLA FAs. A) KEGG pathway analysis showing pathways enriched in samples treated OPLA comparison to those treated with a POLA. Data show those enriched in following treatment with POLA; B) GO pathways analysis for the same comparison. Abbreviations: O, high (800µM) concentration OPLA; P, high (800µM) concentration POLA.

Heatmaps were generated to visualise the differentially expressed genes between each condition. Figure 3.8a shows the top 20 genes which are differentially expressed when comparing cells treated with either OPLA or POLA at a high concentration with a no-fat control. Figure 3.8b shows the top 20 genes differentially expressed between OPLA and POLA, visualised looking at the individual treatment groups.

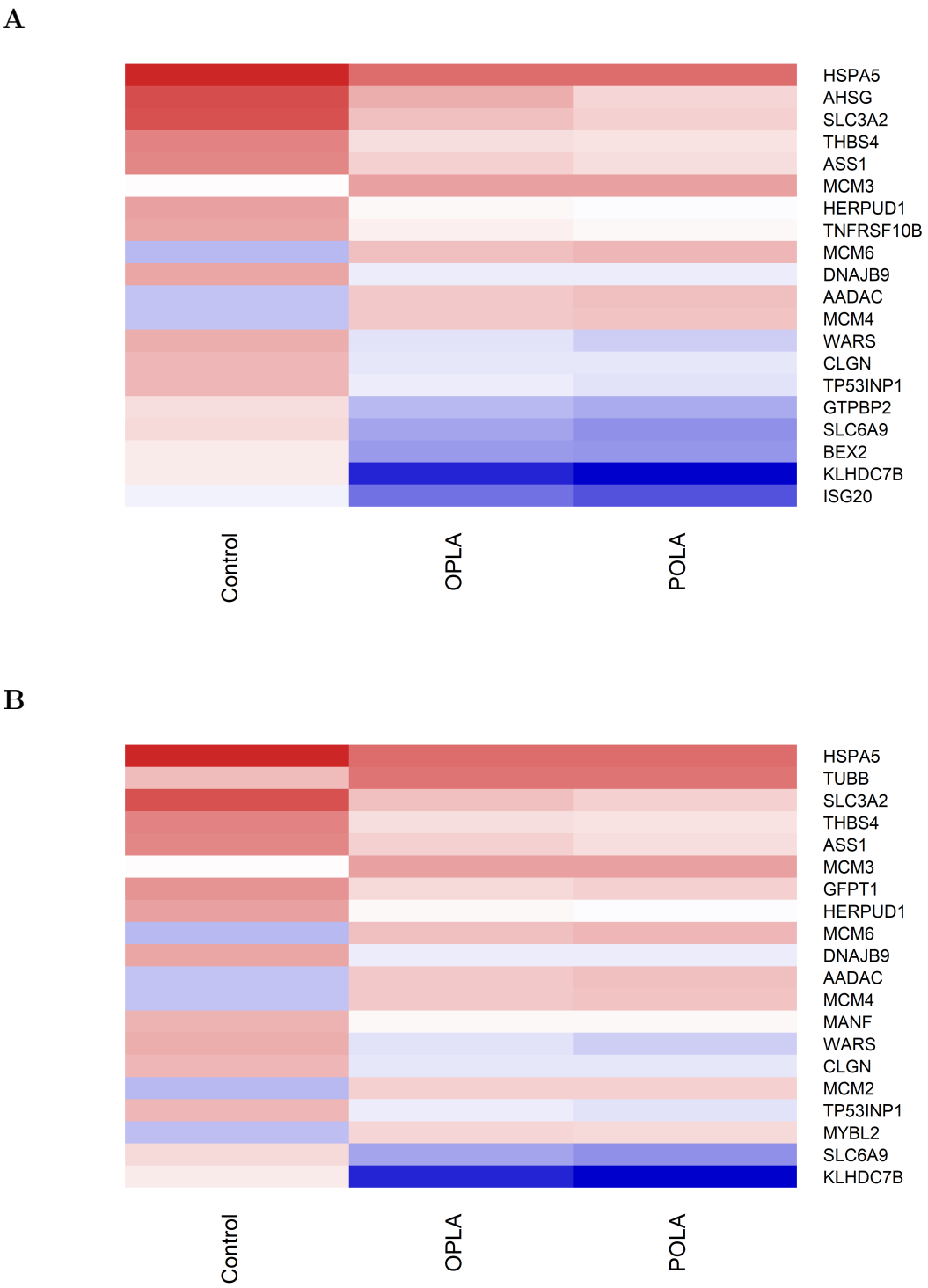


Figure 3.8: Heatmap of most differentially expressed genes RNA extracted from fatty acid (FA) treated Huh7 cells A) Differentially expressed genes comparing treated with either OPLA or POLA FA treatment with the no-fat control; B) Differentially expressed genes visualised from comparing OPLA and POLA RNA expression.

3.3.1.4 Huh7 RNA sequencing pathway analysis

From the KEGG and GO pathway analyses, all the significantly different relevant pathways were further investigated. The pathway most commonly appearing as altered was protein processing. Figure 3.9a shows the changes in RNA within the unfolded protein response (UPR) following treatment with a high concentration of either OPLA or POLA and comparing between these conditions. Figure 3.10a shows the compliment and coagulation cascade with genes indicated where they are differentially expression resulting from treatment with either high concentrations of OPLA or POLA. Figure 3.11a shows signaling through the p53 pathway and differential expression between cells treated with OPLA.

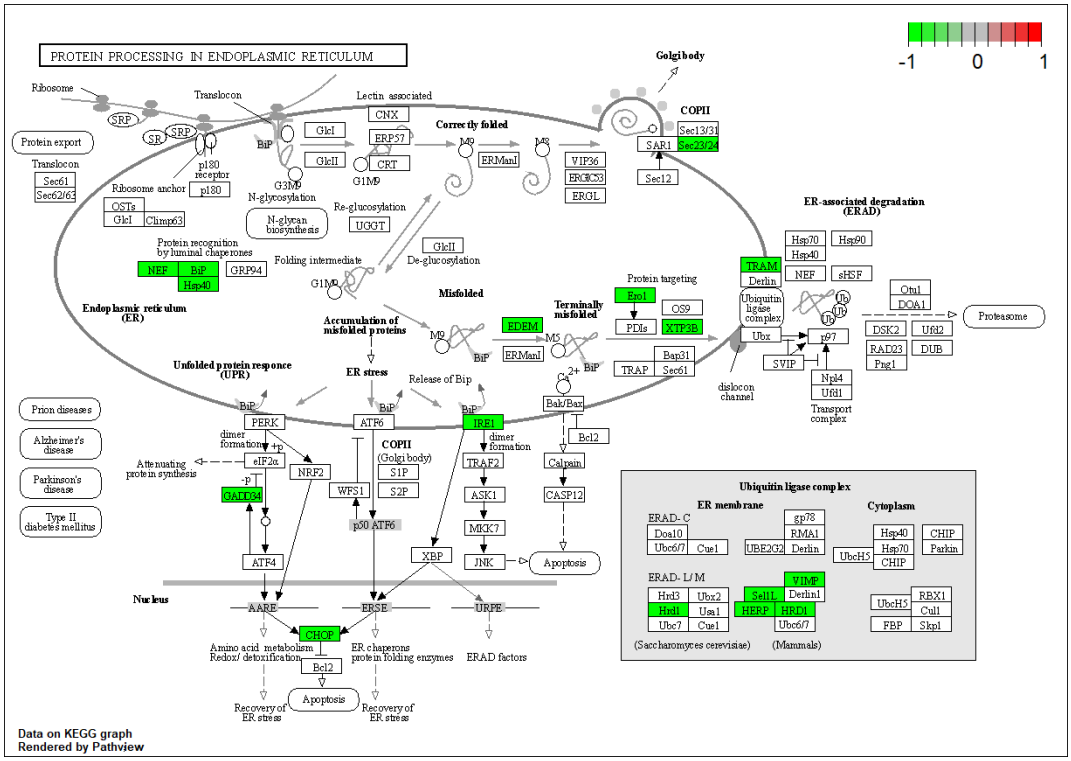


Figure 3.9: Pathway enrichment for the unfolded protein response (UPR) in RNA extracted from fatty acid (FA) treated Huh7 cells. Green indicates those genes which are upregulated in cells treated with OPLA FA treatment compared to POLA FA treatment and red shows cells which are upregulated in POLA compared to OPLA.

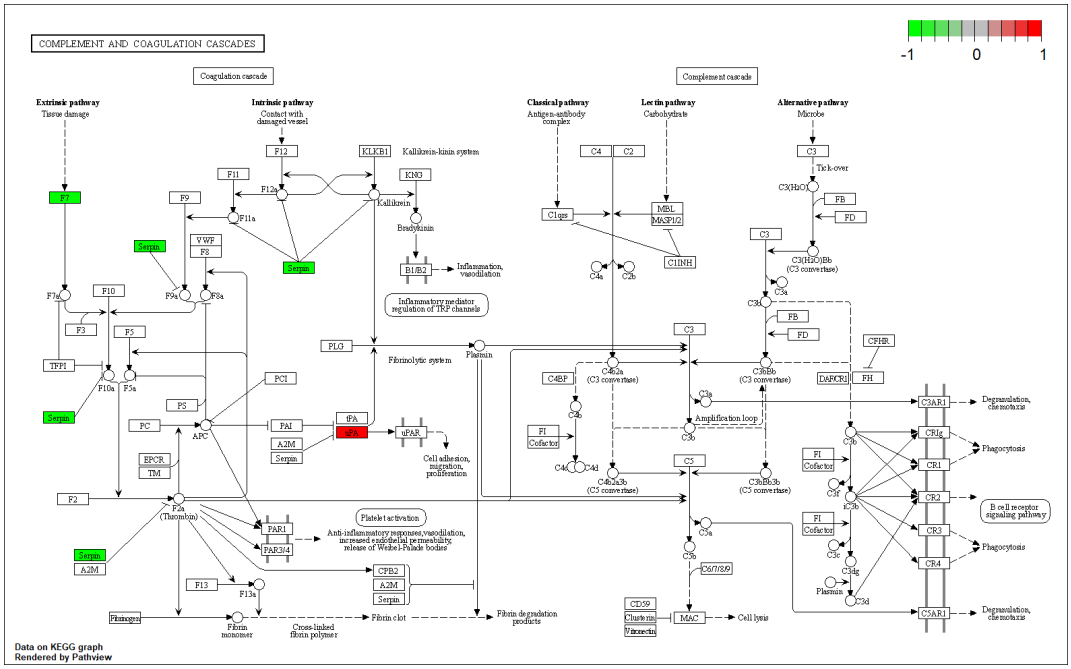


Figure 3.10: Pathway enrichment for the compliment and coagulation pathway in RNA extracted from fatty acid (FA) treated Huh7 cells. Green indicates those genes which are upregulated in cells treated with OPLA FA treatment compared to POLA FA treatment and red shows cells which are upregulated in POLA compared to OPLA.

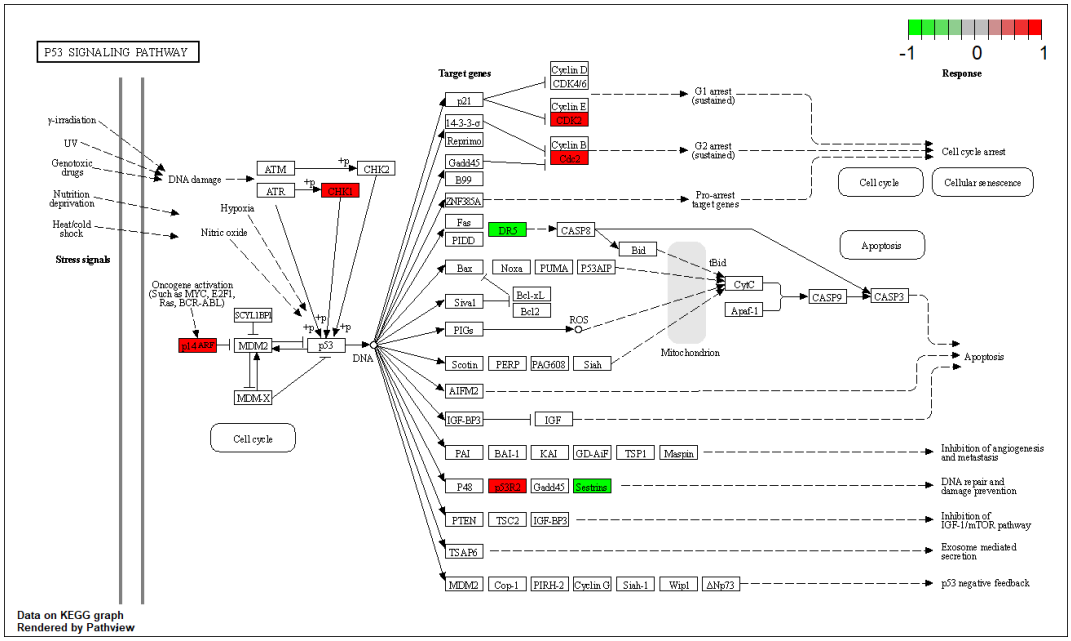


Figure 3.11: Pathway enrichment for p53 signalling in RNA extracted from fatty acid (FA) treated Huh7 cells.. Green indicates those genes which are expressed at a higher level in cells treated with OPLA FA treatment compared to POLA FA treatment, red indicates those expressed at a higher level in POLA compared to OPLA.

3.3.2 Results from PHH RNA sequencing analysis

PHH cells from five individuals were treated as described in Methods 2.2.1.3 and a subsequent mRNA sequencing analysis was performed.

3.3.2.1 Factor analysis

A factor analysis was performed to simplify the data set and probe underlying relationships from the RNA sequencing in PHH cells. Figure 3.12a, shows a scree plot of the PHH cells following treatment with either a no-fat control, low concentrations of either OPLA or POLA or high concentrations of either OPLA or POLA. The scree plot informs that it is the first three factors that contribute most to the variation observed within the data, accounting for 86.9% of the variation.

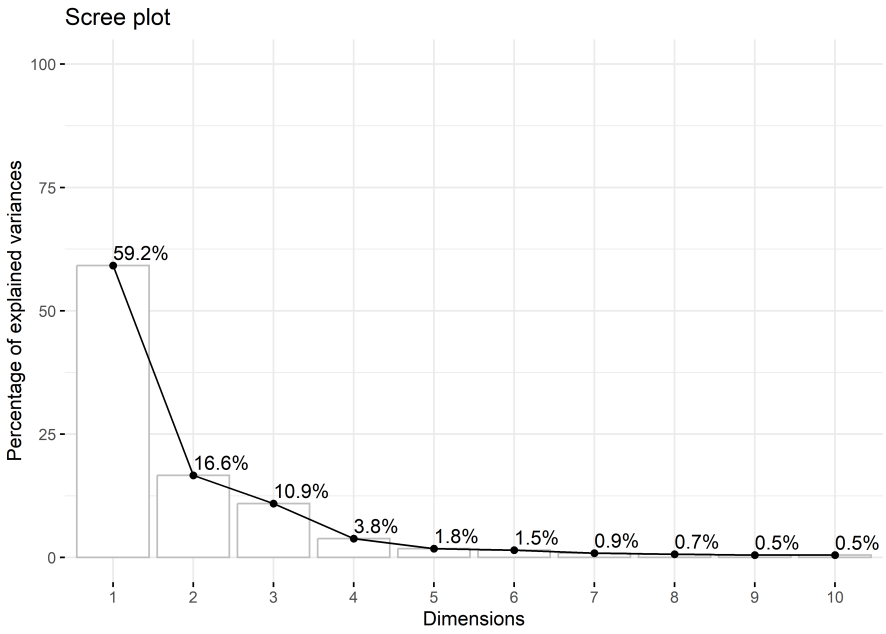


Figure 3.12: Factor analysis in RNA expression from fatty acid (FA) treated primary human hepatocytes (PHH). Figure shows a scree-plot of eigenvector values for PHH cells RNA sequencing analysis.

Figure 3.13 shows multiple PCA plots looking at the relationship between the treatments and the RNA sequencing data. The interaction between the different factors are described as the dimensions of the plot, with the dimensions corresponding to the factors, i.e. dimension 1 is the first eigen factor. How these dimensions are displayed depends on how the data is categorised. Figures 3.13a, 3.13b and 3.13c show the data spread between the first three dimensions (1v2, 1,v3 and 2v3 respectively) categorise the data by both the composition of the treatment and also the concentration of the FA treatment. Data show with this categorisation, although there was some variation in 3D space, there were still significant overlaps and therefore similarities within the data.

Categorising the data by the concentration of FA provided in the treatment regardless of composition across the first three dimensions (1v2, 1,v3 and 2v3) for Figures 3.13d, 3.13e,3.13f respectively, showed a very similar pattern of data organisation, but perhaps with greater distance, and therefore less data similarity between the groups. However, splitting the data according to the composition of the treatment

provided resulted in more graphical overlap of the data and therefore more data similarity. Figures 3.13g, 3.13h,3.13i showed the spread of data according to the first three factors (1v2, 1,v3 and 2v3) respectively.

Another way to categorise the data is by the source of the cells, i.e. the donor. For the first three factors (1v2, 1,v3 and 2v3), Figures 3.13j, 3.13k,3.13l graphically show the similarity between the data. Here, the data separate into more distinct groups, indicating greater dissimilarity between the donors, thus implicating that the origin of the cells has the strongest effect on the data.

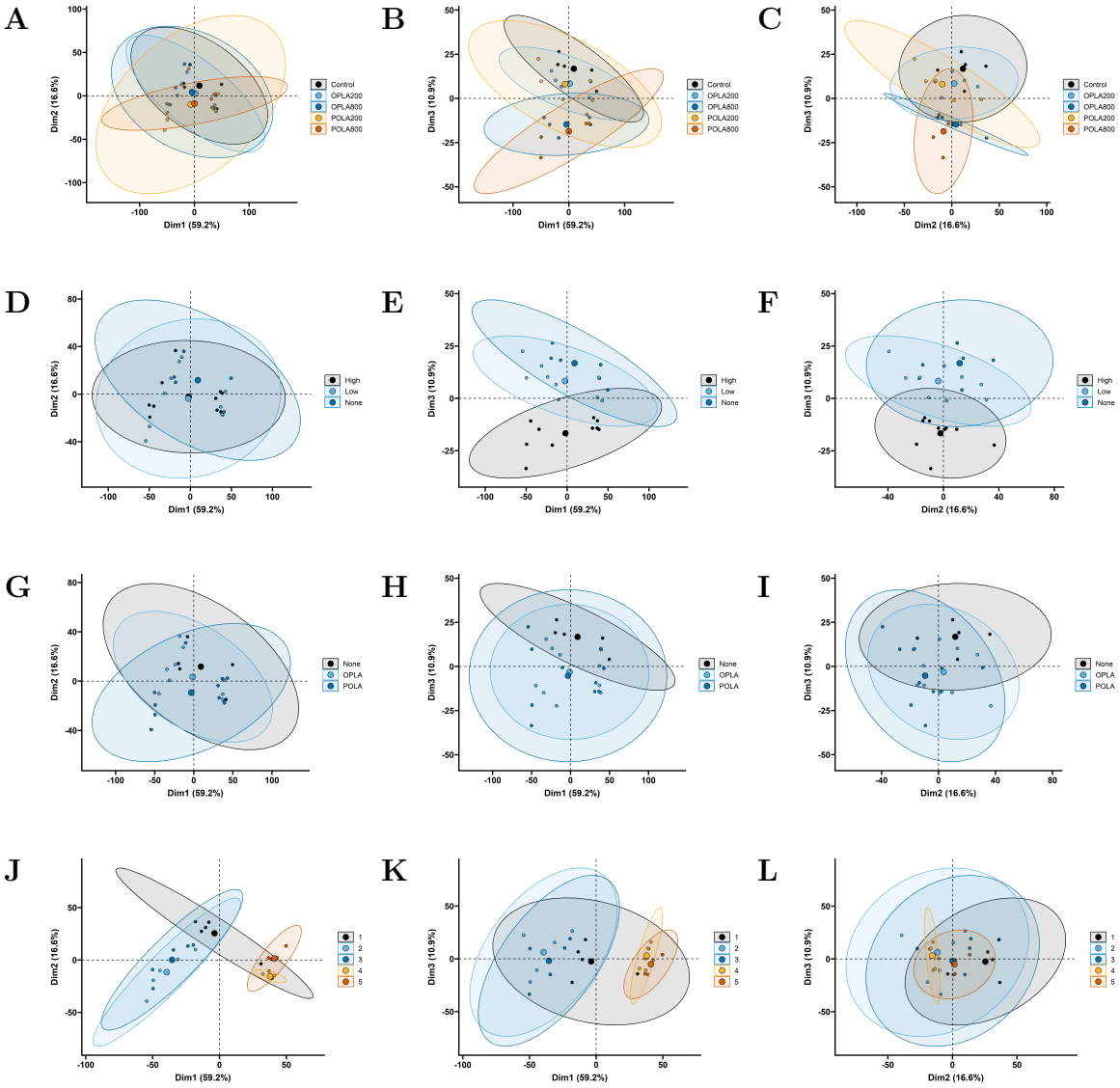


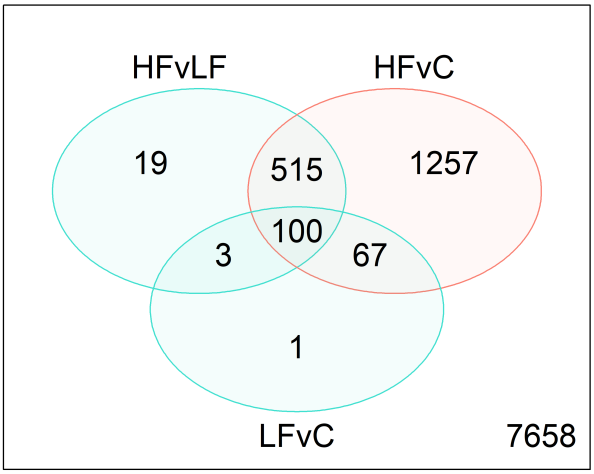
Figure 3.13: Principle component analysis (PCA) in RNA expression from fatty acid (FA) treated primary human hepatocytes (PHH). A) First and second dimension PCA plot, grouped by treatment; B) First and third dimension grouped by treatment condition; C) Second and third dimension grouped by treatment; D) First and second dimension grouped by treatment concentration; E) First and third dimension grouped by treatment concentration; F) Second and third dimension grouped by treatment concentration; G) First and second dimension grouped by treatment composition; H) First and third dimension grouped by treatment composition; I) Second and third dimension grouped by treatment composition; J) First and second dimension grouped by donor; K) First and third dimension grouped by donor; L) Second and third dimension grouped by donor.

3.3.2.2 Differential gene expression

Following the application of a mixed random effects model to the data, the number of differentially expressed genes was probed following treatment with OPLA, POLA (at either high or low concentrations) and a no-fat control. Examining the effect of concentration of FA in the treatment, Figure 3.14a, shows the number of genes which are differentially expressed comparing the following: control versus FA treatment, control versus low concentration FA treatment, control versus high concentration FA treatment. Figure 3.14a identifies the number of genes which had altered expression in common between these comparisons.

Focusing specifically on the effect of FA treatment composition across the different concentrations, Figure 3.14b shows a Venn diagram of genes differentially expressed in the chosen comparisons and how many of these differentially expressed genes are shared between comparisons: POLA versus OPLA, low concentrations of POLA versus low concentrations of OPLA, high concentrations of POLA versus high concentrations of POLA.

A



B

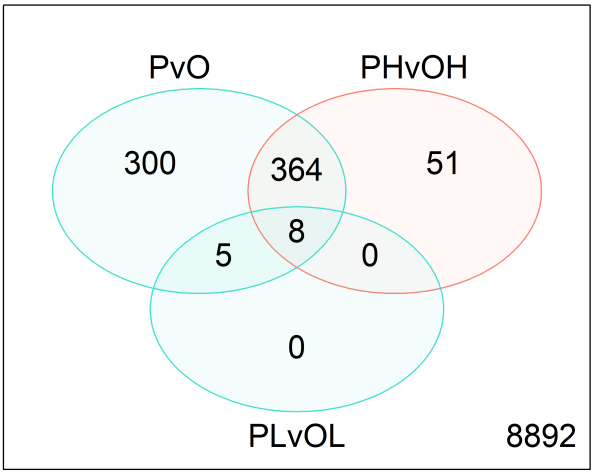


Figure 3.14: Venn diagram of differentially expressed genes in RNA extracted from fatty acid (FA) treated primary human hepatocytes (PHH). A) Differentially expressed genes according to amount of treatment FA given; B) Differentially expressed genes according to composition at different treatment concentrations. Where C is no-fat control, LF is low Fat, HF is High Fat, OL is Low OPLA, PL is low POLA, OH is high OPLA and PH is high POLA.

Volcano plots were generated to visualise the size and direction of gene expression changes showing log fold changes compared with the significance of the change. Figure 3.15a shows the volcano plot for the comparison of cells treated with a low concentration of either OPLA or POLA with cells treated with the no-fat control. Figure 3.15b shows the volcano plot for the comparison of cells treated with a high concentration of either OPLA or POLA with cells treated with a no fat control. Comparing these volcano plots (Figure 3.15a and 3.15b), there were notably more genes differentially expressed between those treated with a high FA concentration versus those treated with a low concentration of FA, when compared to a no-fat control. There are also a distinct set of genes identified as the most significantly changed between these two comparisons.

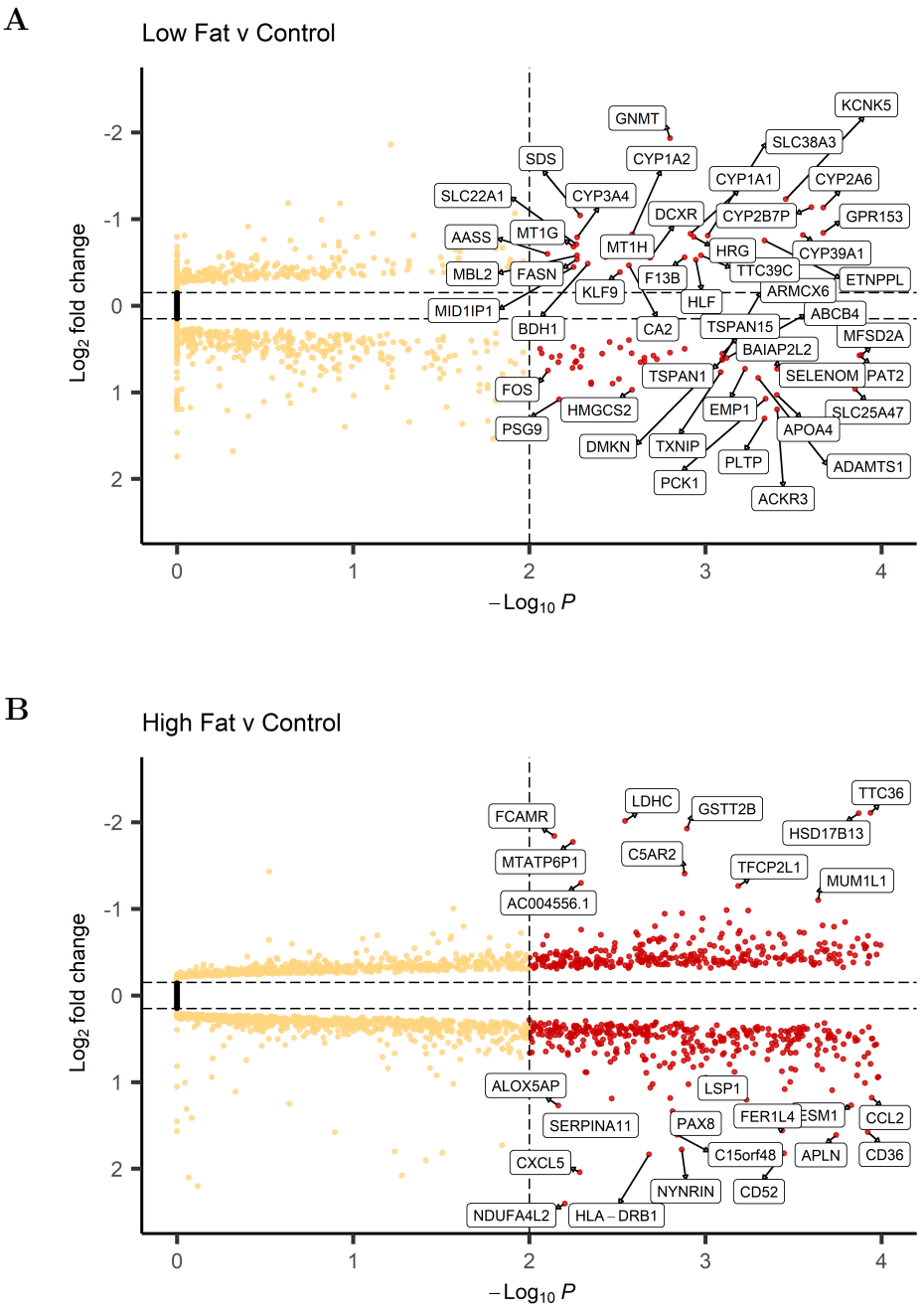


Figure 3.15: Volcano plots of extracted RNA from fatty acid (FA) treated primary human hepatocytes (PHH) comparing treatment with low fat concentration (LF) versus control, or high fat concentration (HF) versus control. V A) LF versus Control, where a negative log fold change values indicate a gene is enriched in the Control treatment and positive log fold change values indicate genes are enriched in the cells treated with LF; B) HF versus control, where a negative log fold change values indicate a gene is enriched in the Control treatment and positive log fold change values indicate genes are enriched in the cells treated with HF.

Figure 3.16a represents the spread of genes differentially expressed when comparing cells treated with a high concentration of FA versus those treated with a low concentration of FA, regardless of composition. Although not identical, there was overlap in the genes identified between those identified in the comparisons between a concentration amount (high or low) and a no fat control. Figure 3.16b compares the effect of FA treatment composition, regardless of concentration on differential gene expression. Notably, the p values identified comparing compositions were generally less significant for those identified genes when compared to those identified when looking at the effect of FA concentration of gene expression.

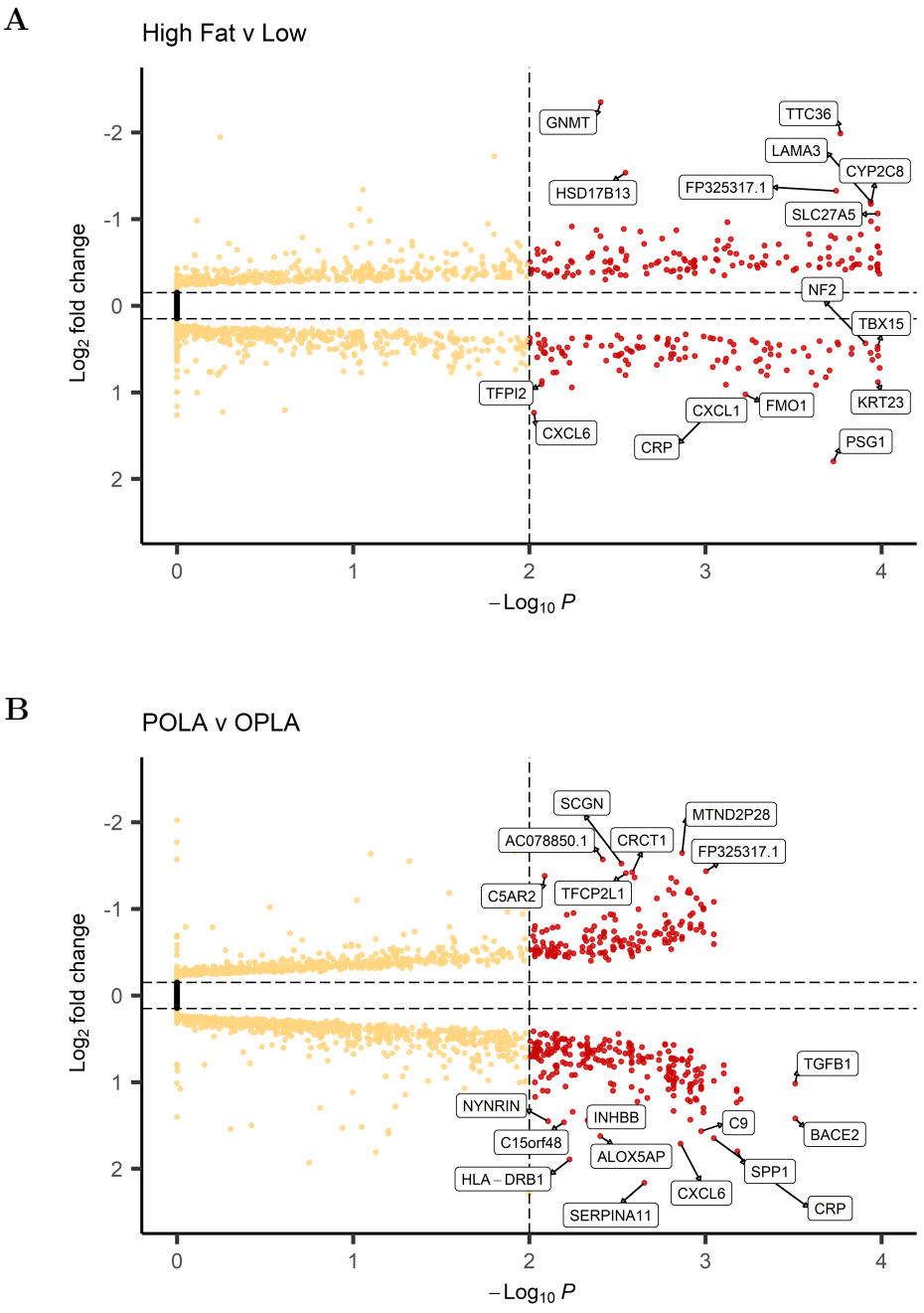


Figure 3.16: Volcano plots of extracted RNA from fatty acid (FA) treated primary human hepatocytes (PHH) comparing high fat concentration (HF) to low fat concentration (LF) and OPLA and POLA FA treatments. A) HF versus LF, where a negative log fold change values indicate a gene is enriched in the LF treatment and positive log fold change values indicate genes are enriched in the cells treated with HF; B) OPLA versus POLA, where a negative log fold change values indicate a gene is enriched in the OPLA treatment and positive log fold change values indicate genes are enriched in the cells treated with POLA.

When investigating the effect of the concentration which the different FA compositions (OPLA or POLA) were applied to the PHH cells we found that at a low concentration very few genes were differentially expressed between cells treated with low concentrations of OPLA and POLA, indeed only two were identified: PECAM and STAB1 (Figure 3.17a). At a high concentration more genes were differentially expressed (Figure 3.17b).

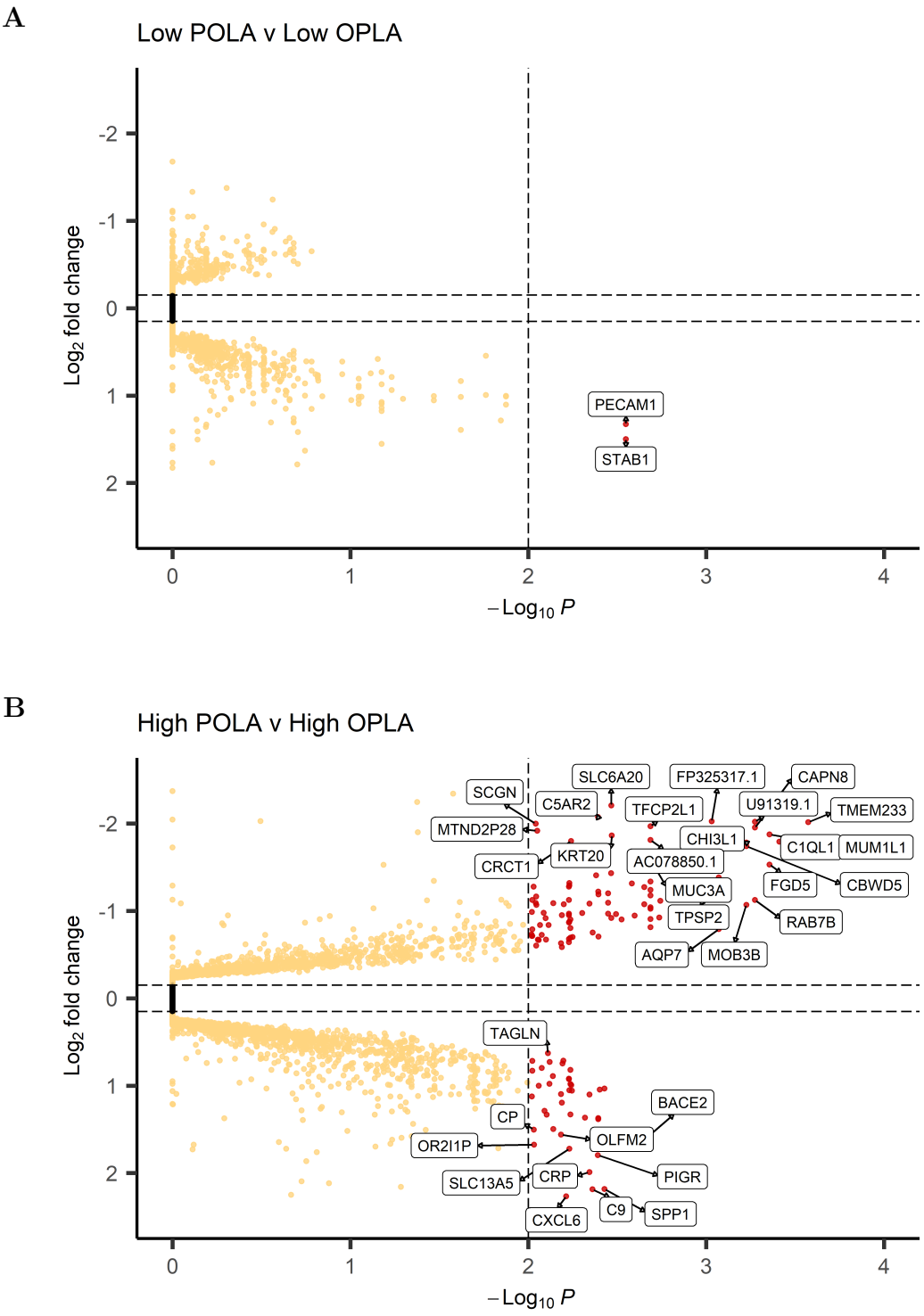


Figure 3.17: Volcano plots of extracted RNA from fatty acid (FA) treated primary human hepatocytes (PHH) comparing treatment with low OPLA concentration (OL) versus low POLA concentration (PL), or high OPLA concentration (OH) versus high POLA concentration (PH). A) Comparing OL with PL, where a negative log fold change values indicate a gene is enriched in the OL treatment and positive log fold change values indicate genes are enriched in the cells treated with PL; B) Comparing OH with PH, where a negative log fold change values indicate a gene is enriched in the OH treatment and positive log fold change values indicate genes are enriched in the cells treated with PH.

3.3.2.3 Hall mark and functional gene enrichment scores

Investigating the pathway enrichment seen when comparing those cells treated with low FA concentrations against control, very few pathways are identified, however, all of them are relevant to hepatic health and metabolism. From the KEGG analysis, activated by treatment with low FA concentrations upregulated PPAR signalling, and suppressed are other metabolic pathways, although the analysis does not specify which. Also suppressed was the metabolism of xenobiotic compounds by cytochrome P450 and the activation of the chemical carcinogenesis receptor (Figure 3.18a). Although a GO pathway analysis was performed, and pathways were identified, none were significant (Figure 3.18).

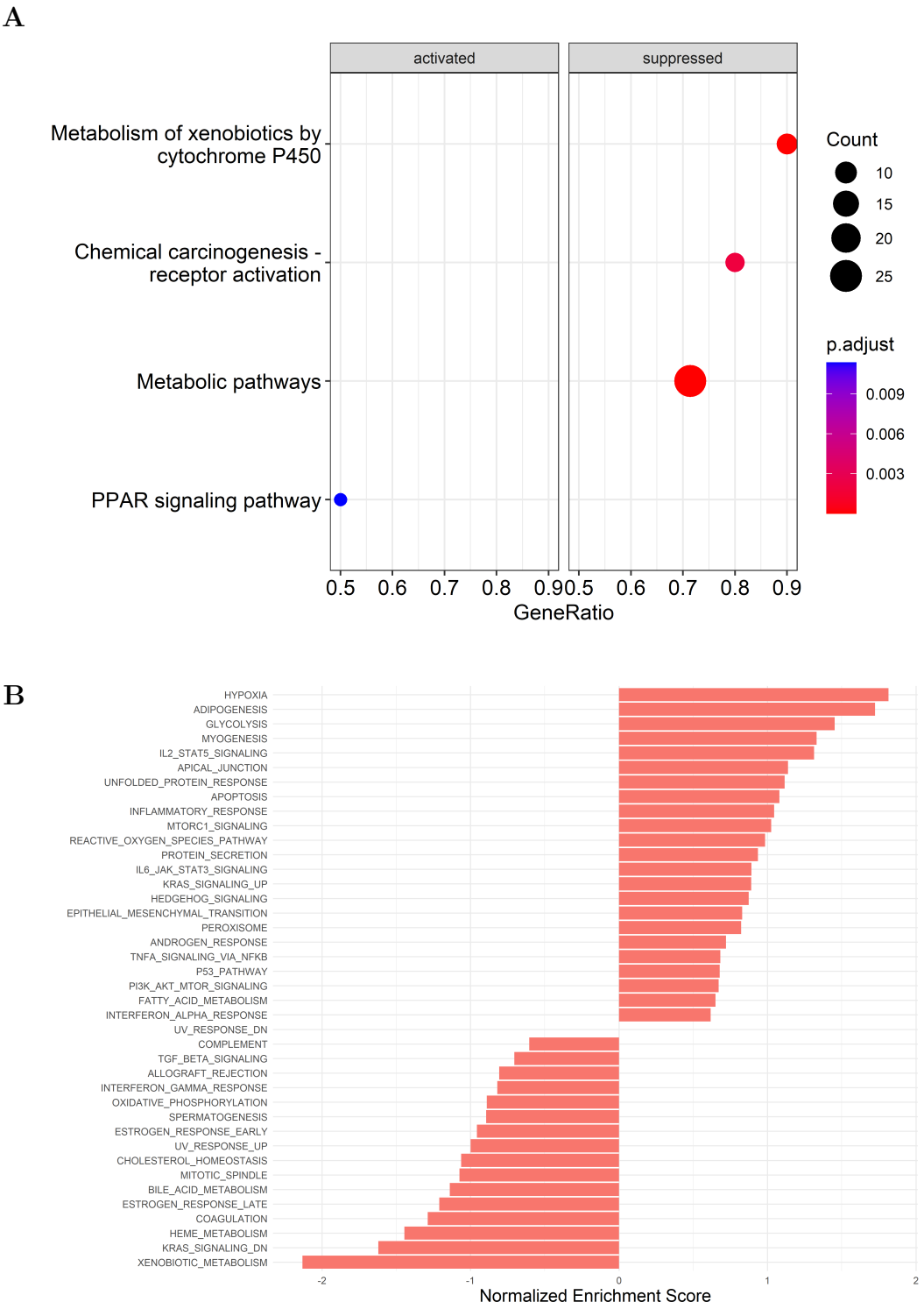


Figure 3.18: KEGG and GO pathway analysis of RNA extracted from fatty acid (FA) treatment versus no-fat control in primary human hepatocytes (PHH) comparing low FA (LF) concentration treatment with no-fat control. A) KEGG pathway analysis showing pathways activated in samples treated with no-fat control compared to those treated with low FA (LF) treatments, either OPLA or POLA; B) GO pathways analysis for the same comparison. Suppression indicated that those pathways are activated to a greater extent in the FA treated cells, and activation shows that those pathways are activated to a greater extent in the no-fat treated control. Abbreviations: C, no fat control; , LF, low FA treatment (200µM) of either OPLA or POLA.

More pathways have been identified when comparing the pathway enrichment between cells treated with a high concentration of FA with those treated with no-fat control. Figure 3.19a, shows the pathways identified in a KEGG pathway enrichment analysis and of relevance to hepatic metabolism and MASLD, were differences between both general metabolism as well as two inflammatory pathways: TNF signalling and IL-17 signalling. Figure 3.19b, shows the resulting GO pathway enrichment analysis between cells treated with a high concentration of FA with those treated with no-fat control. Both metabolic and inflammatory pathways identified a suppression of FA metabolism in cells treated with no-fat control compared to those treated with high concentrations of FA, with the corresponding increase in FA metabolism mRNA likely to enable the PHH cells to process the provided FAs. The inflammatory pathways were expressed to a greater extent in cells treated with a no-fat control compared to cells treated with a high concentration of FA suggesting that to some extent, receiving extra nutrition is beneficial.

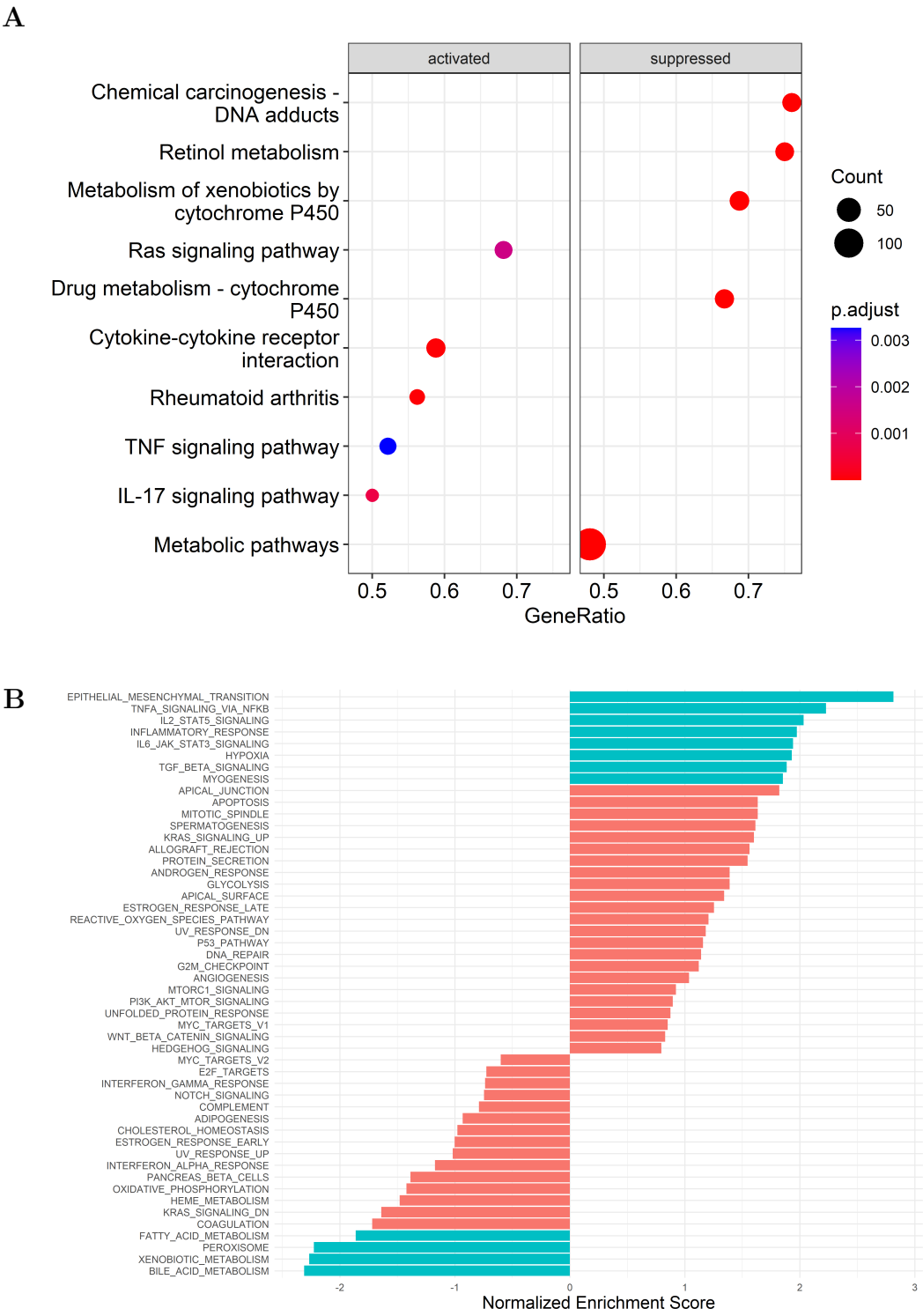


Figure 3.19: KEGG and GO pathway analysis of RNA extracted from fatty acid (FA) treatment versus no-fat control in primary human hepatocytes (PHH) comparing high FA (HF) concentration treatment with no-fat control. A) KEGG pathway analysis showing pathways activated in samples treated with High FA treatments, either OPLA or POLA comparison to those treated with a no-fat control; B) GO pathways analysis for the same comparison. Suppression indicated that those pathways are activated to a greater extent in the FA treated cells, and activation shows that those pathways are activated to a greater extent in the no-fat treated control. Abbreviations: C, no fat control; , HF, high FA treatment (800µM) of either OPLA or POLA.

Comparing cells treated with a high concentration of FA versus those treated with a low concentration of FA, Figure 3.20a shows the pathways enriched by KEGG analysis. The corresponding GO analysis, Figure 3.20b identified that oxidation pathways were upregulated to a greater extent in cells treated with a lower concentration of FA, but inflammation pathways were activated to a greater extent in those cells treated with higher FA concentrations.

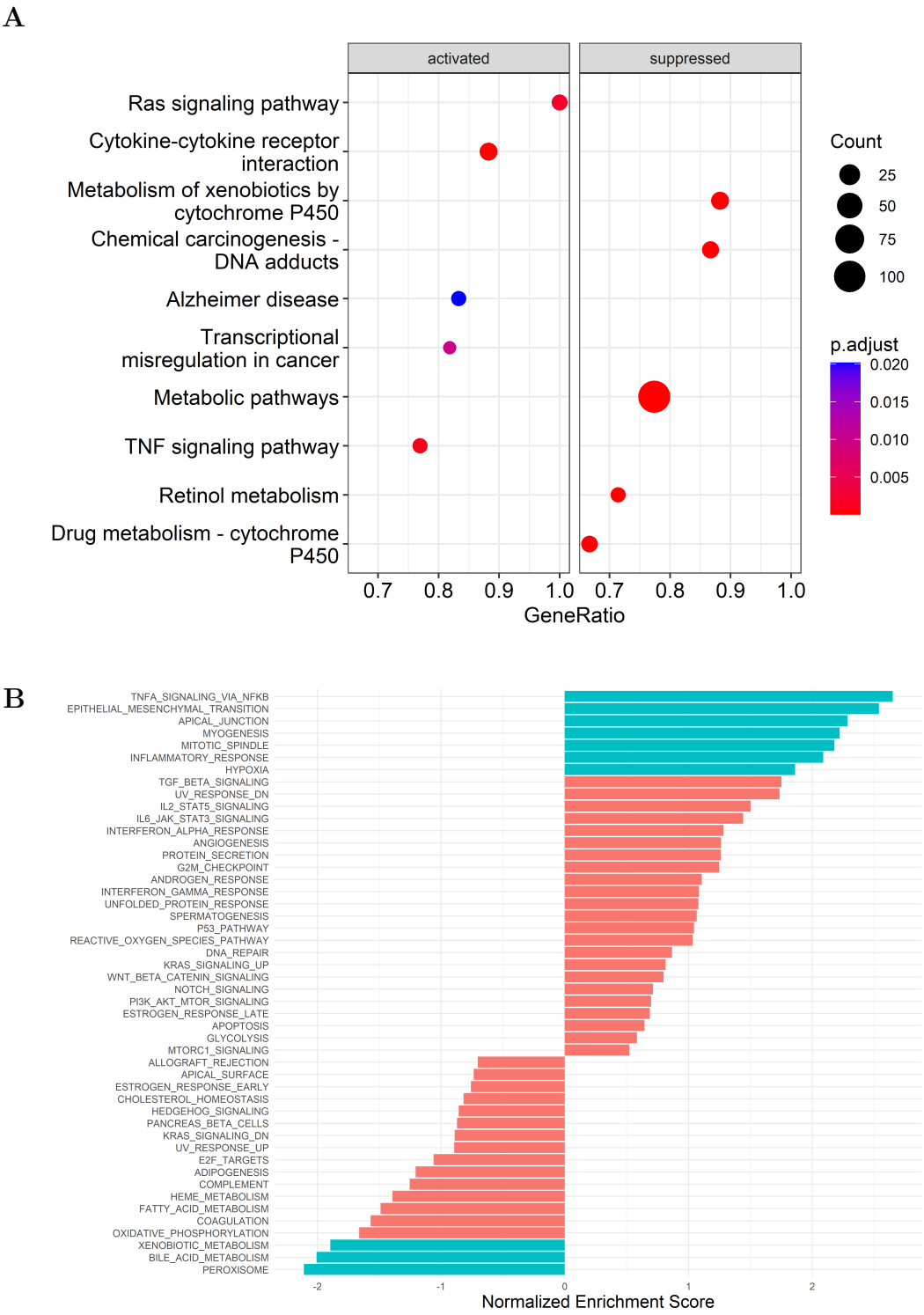


Figure 3.20: KEGG and GO pathway analysis of RNA extracted from fatty acid (FA) treatment versus no-fat control in primary human hepatocytes (PHH) comparing high FA (HF) concentration treatment with low FA (LF) concentration treatment. A) KEGG pathway analysis showing pathways activated in samples treated with High FA treatments, either OPLA or POLA comparison to those treated with Low FA; B) GO pathways analysis for the same comparison. Suppression indicated that those pathways are activated to a greater extent in the low FA treated cells, and activation shows that those pathways are activated to a greater extent in the high FA treated cells. Abbreviations: HF, high FA treatment (800µM), LF, low FA treatment (200µM) of either OPLA or POLA.

Comparing pathways upregulated to a greater extend in POLA compared to OPLA, Figure 3.21a shows the KEGG pathways analysis with the majority of pathways identified being activated with POLA compared to OPLA. Figure 3.21b shows the corresponding GO analysis which showed that OPLA treated cells had a greater activation of FA metabolism pathways, and oestrogen associated pathways, whereas POLA treated cells had greater activation of coagulation related pathways.

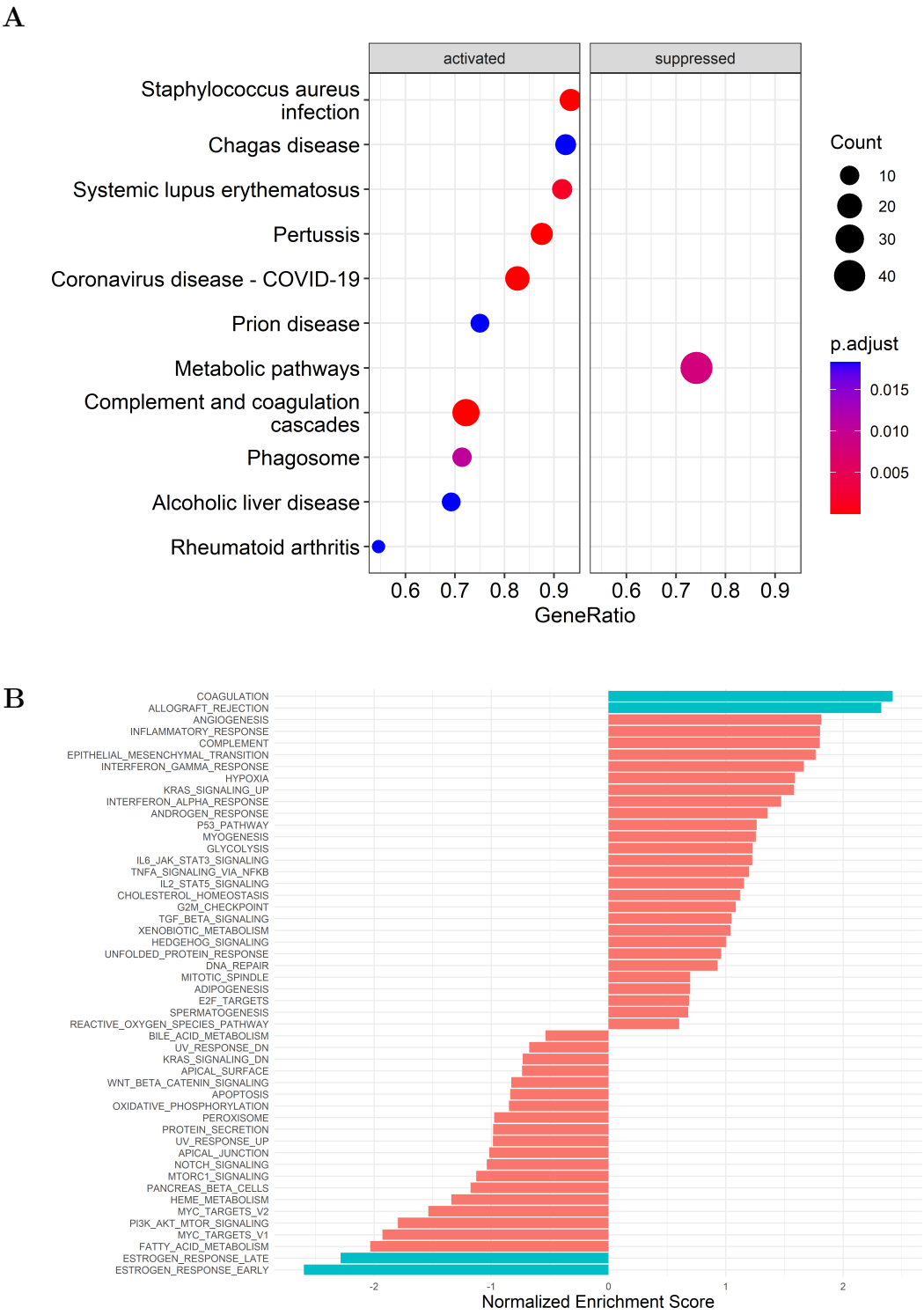


Figure 3.21: KEGG and GO pathway analysis of RNA extracted from fatty acid (FA) treatment versus no-fat control in primary human hepatocytes (PHH) comparing OPLA FA treatment with POLA FA treatment. A) KEGG pathway analysis showing pathways activated in samples treated with OPLA versus POLA, at either a high concentration or a low concentration; B) GO pathways analysis for the same comparison. Suppression indicated that those pathways are activated to a greater extent in the OPLA treated cells, and activation shows that those pathways are activated to a greater extent in POLA treated cells. Abbreviations: O, OPLA at either a high (800µM) or low (200µM) concentration; P, POLA at either a high (800µM) or low (200µM) concentration.

For pathway enrichment in cells treated with low concentrations of OPLA or POLA, comparison was challenging as fewer genes were differentially expressed. As shown in Figure 3.22a,the KEGG pathway analysis with POLA treated cells showed more inflammation associated pathways but, OPLA treated cells showing more metabolic activity. There were not enough differentially expressed genes to perform a GO pathway analysis.

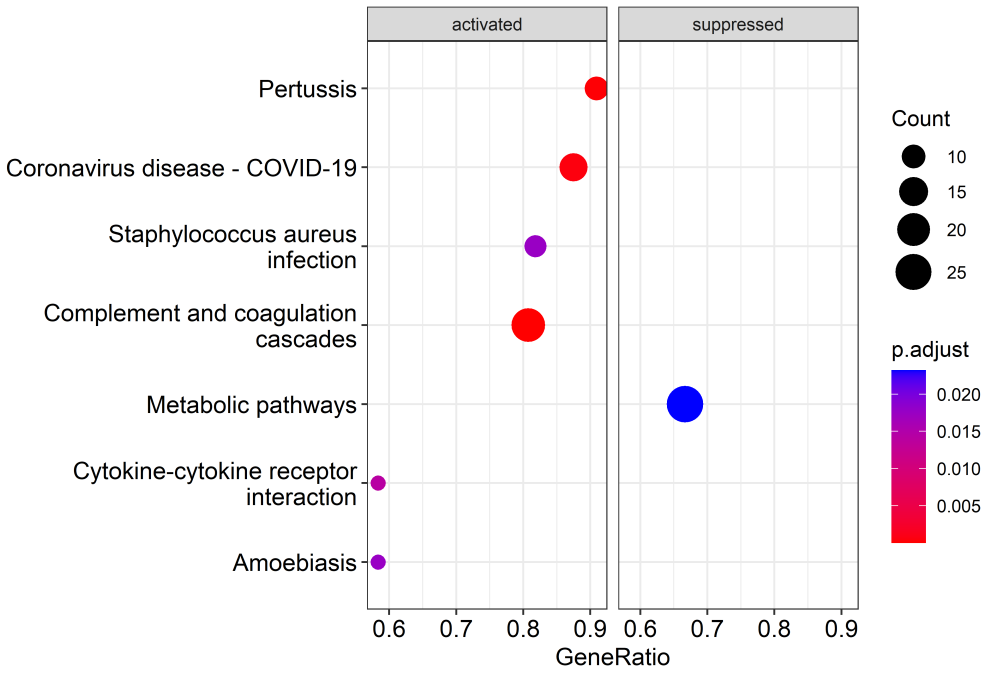


Figure 3.22: KEGG and GO pathway analysis of RNA extracted from fatty acid (FA) treatment versus no-fat control in primary human hepatocytes (PHH) comparing low concentration OPLA (OL) FA treatment with low POLA (PL) FA treatment. KEGG pathway analysis showing pathways activated in samples treated with Low OPLA versus Low POLA no-fat control. Suppression indicated that those pathways are activated to a greater extent in the OPLA treated cells, and activation shows that those pathways are activated to a greater extent in POLA treated cells. Abbreviations: LO, OPLA at a low (200µM) concentration; PL, POLA at a low (200µM) concentration.

For cells treated with a high concentration of either OPLA or POLA, Figure 3.23a shows the KEGG enrichment pathway analysis which shows the same patterns as those cells treated with low concentrations or either concentrations of OPLA and POLA. Figure 3.23b shows the GO pathway analysis comparing differentially expressed genes from cells treated with either high concentrations of OPLA or high concentrations of POLA, however, although pathways were identified, none reached statistical significance.

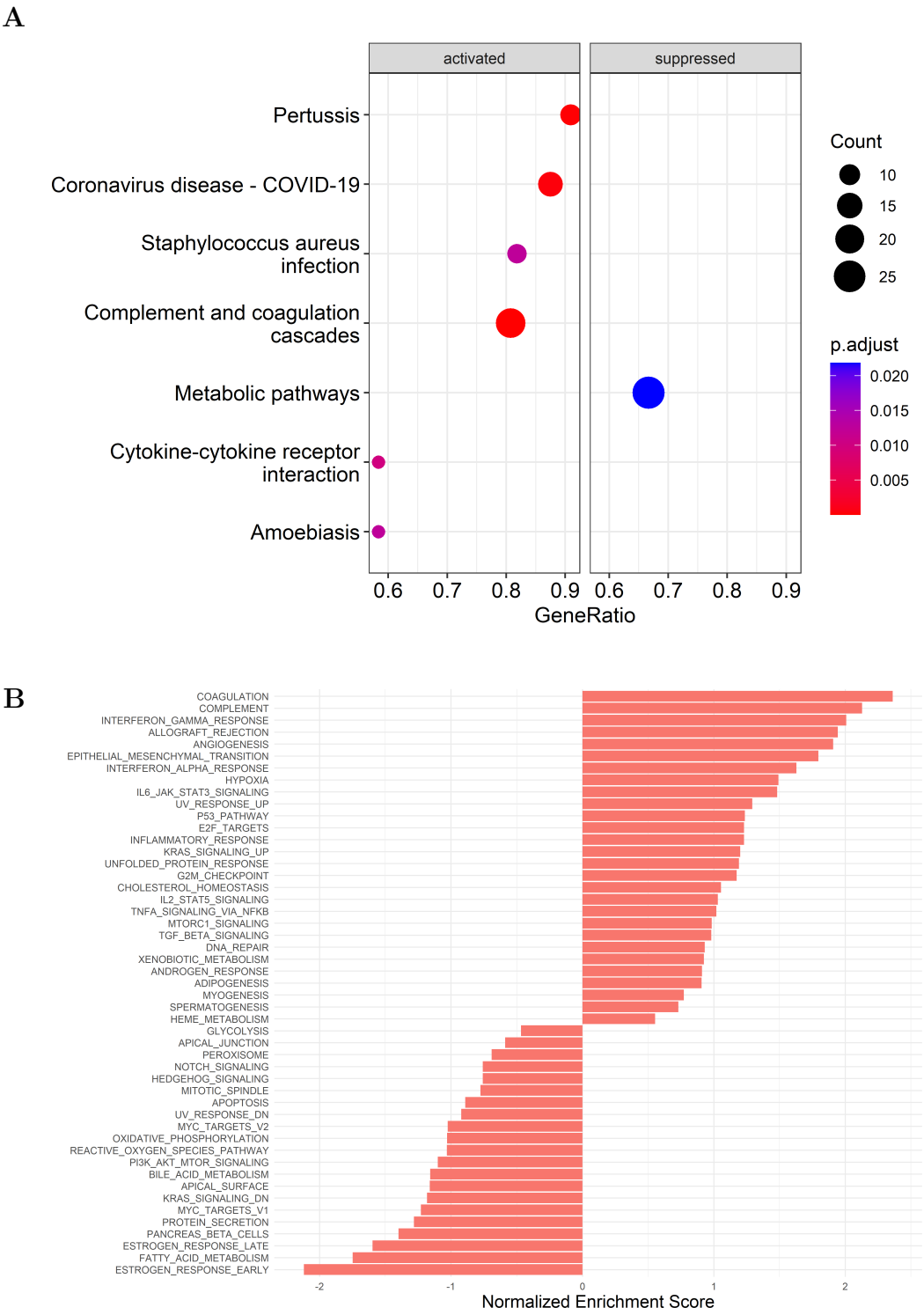


Figure 3.23: KEGG and GO pathway analysis of RNA extracted from fatty acid (FA) treatment versus no-fat control in primary human hepatocytes (PHH) comparing high concentration OPLA (OH) FA treatment with high POLA (PH) FA treatment. A) KEGG pathway analysis showing pathways activated in samples treated with high OPLA versus high POLA no-fat control; B) GO pathways analysis for the same comparison. Abbreviations: OH, OPLA at a high (800µM) concentration; PH , POLA at a high (800µM) concentration.

3.3.2.4 Top gene analysis

Heatmaps have also been generated to look at the response of the different conditions for the top candidates identified through differential gene analysis. Figure 3.24a shows the top candidates when comparing low with high gene expression. Figure 3.24b, shows the differentially expressed genes found when comparing POLA with OPLA and displaying the patterns of expression across all treatment conditions.

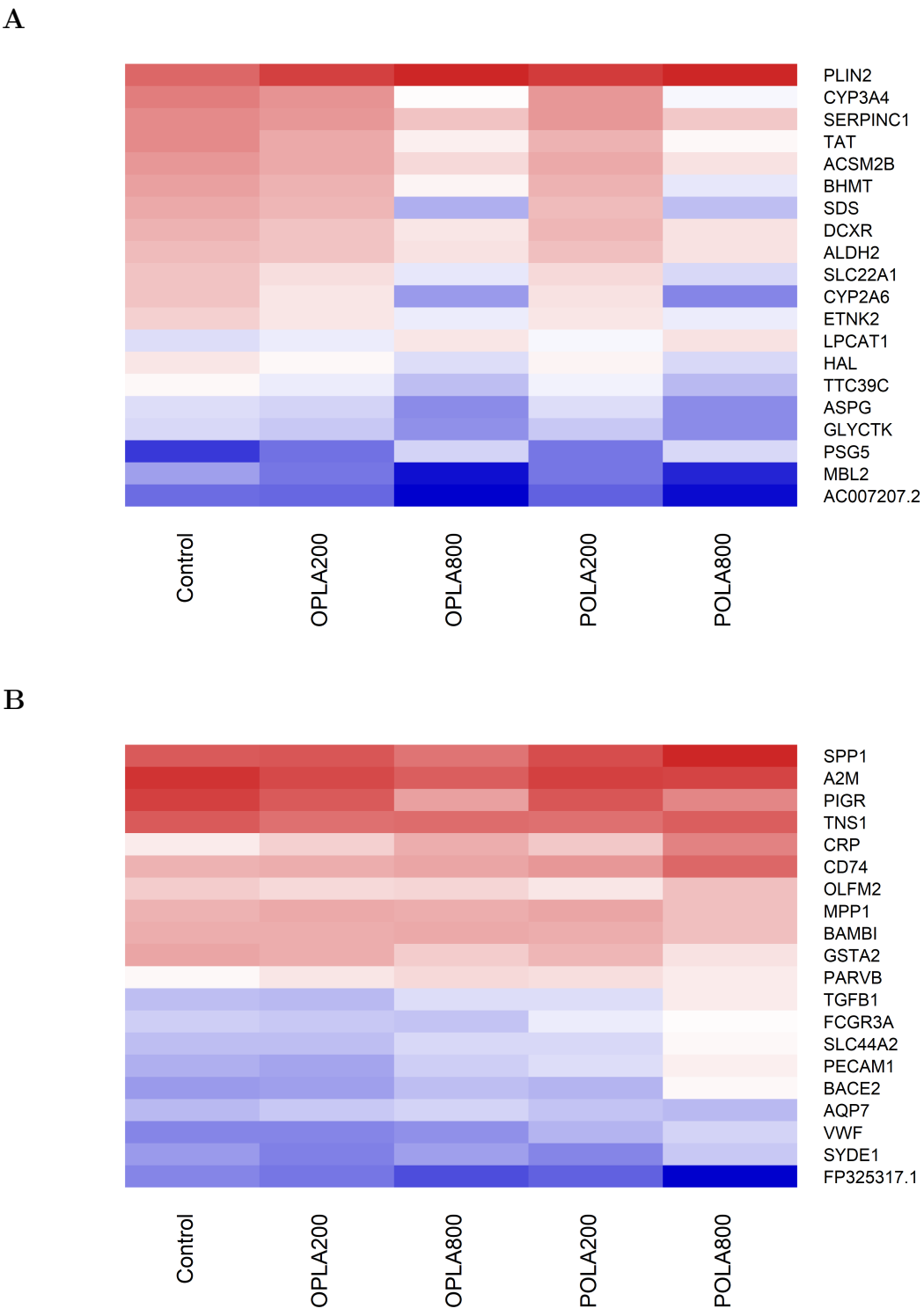


Figure 3.24: Heatmap of most differentially expressed genes RNA extracted from fatty acid (FA) treated Huh7 cells comparing cells treated with OPLA FA treatment with POLA FA treatment and cells treated with high concentration of FAs versus those treated with low concentration of FAs. A) Heatmap showing top candidates found from comparing cells treated with either OPLA or POLA comparing treatment with a high or a low concentration; B) Heat map of top candidate genes identified when changes between PHH cells treated with either a high or a low concentration of FA as either OPLA or POLA.

Figure 3.25a shows a heat map of the top candidates identified when comparing those cells treated with low concentrations of OPLA and POLA. There are a limited number of genes identified here, and they mostly seem to be expressed differently in those cells treated with high concentrations of POLA. Top candidates identified comparing those cells treated with high concentrations of OPLA and POLA can be seen in Figure 3.25b.

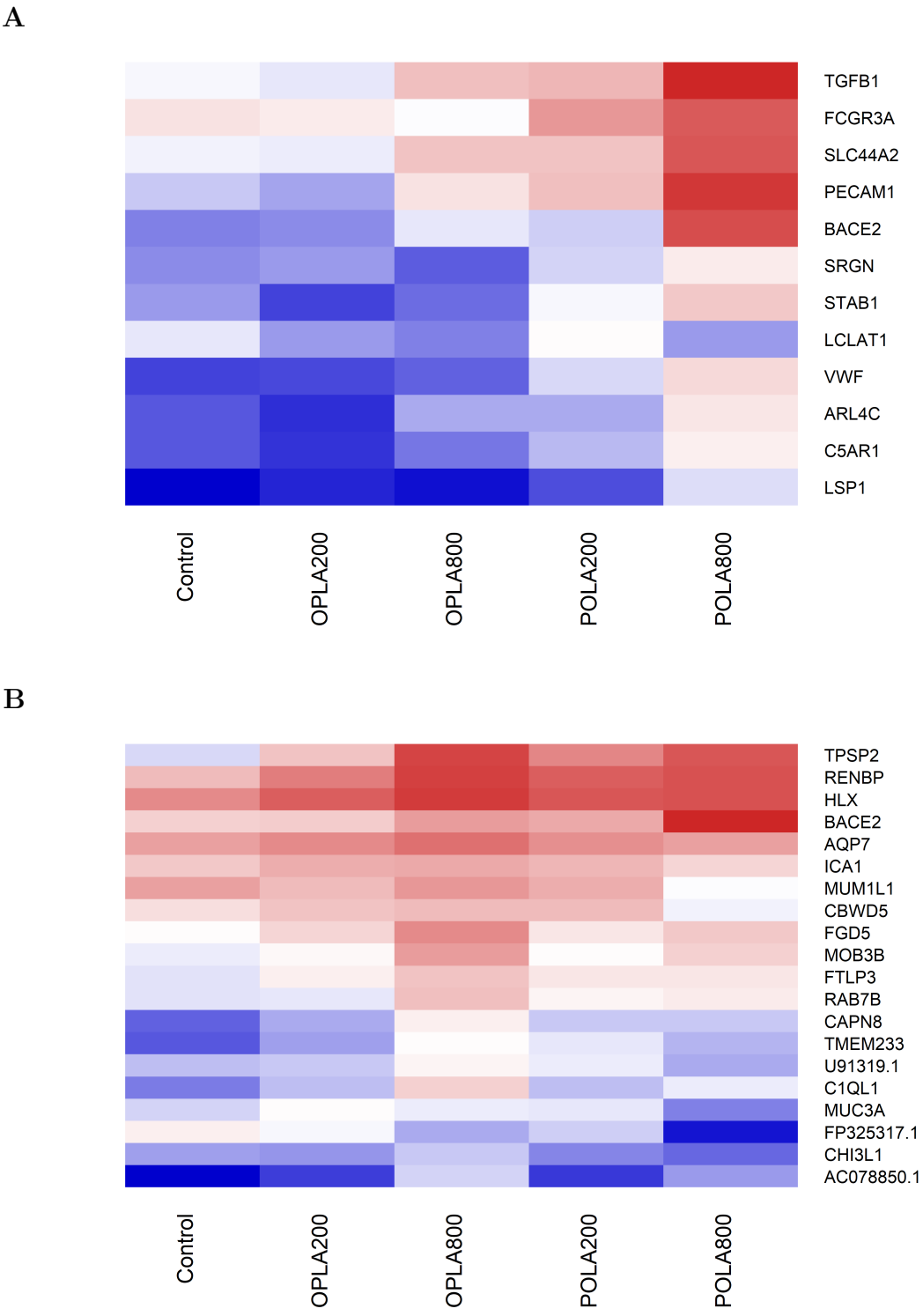


Figure 3.25: Heatmap of most differentially expressed genes RNA extracted from fatty acid (FA) treated Huh7 cells comparing cells treated with low concentration of OPLA FA treatment with low concentration POLA FA treatment and cells treated with high concentration of OPLA FA treatment with high concentration POLA FA treatment. A) Heatmap showing top candidates found from comparing cells treated with low concentrations of OPLA or POLA; B) Heat map of top candidate genes identified when comparing fold changes between PHH cells treated with high concentration of OPLA or high concentration of POLA.

3.4 Discussion

Using RNA sequencing techniques, this chapter aimed to investigate the effect of culturing both Huh7 cells and PHH cells with different compositions and concentrations of FA treatment on the RNA transcriptome of hepatocytes. The majority of the observed differences in gene expression were evident to a greater extent with changes in the quantity, rather than composition of FA provided in the treatment. However, the composition of the FA treatment did have some effect. Comparing Huh7 and PHH cells, there was little overlap in the genes that were differentially expressed following treatment with OPLA and POLA (at a high concentration). Some of the identified differences were divergent, with the coagulation cascades down regulated in Huh7 treated with OPLA when compared to POLA and the opposite observed in PHH cells. Moreover, changing FA compositions resulted in less inflammation related genes being upregulated in the Huh7 cells following treatment, compared to the PHH FA treated cells where there was more transcriptome changes associated with inflammation and fibrosis. Although RNA sequencing has identified different genes, in both Huh7 and PHH cells, with many of the changes observed with POLA associated with the development and progression of MASLD, it is not possible with these data to determine the underlying mechanisms concerning why a diet enriched with SFA resulted in more IHTAG *in vivo*.

Pathway enrichment data from Huh7 comparing cells treated with OPLA compared to POLA, implicated upregulation of protein processing genes within the ER. Whether this is adverse or protective will require further investigation. Although GO pathway analysis identified additional differentially expressed pathways, none of these were altered to a significant level between the two FA compositions. The top candidates identified when comparing Huh7 cells treated with OPLA compared to POLA are discussed below. For this discussion, only those top candidates previously associated with MASLD are included in the following:

- **HSPA5**, also known as BiP, is sequestered and therefore dissociated from the three ER-transmembrane transducers of ER stress enabling their activation (Malhi et al. 2011). HSPA5 was expressed at a higher concentration in OPLA compared to POLA. This increase in transcription of HSPA5 needs further mechanistic investigation to elucidate the effect on ER stress within this model. Additionally, whether the UPR works in a protective or detrimental capacity regarding MASLD likely depends on the stage of disease, and the timescale by which this pathway is elevated for.

- **AADAC, arylacetamide deacetylase**, an ER lipase, sharing protein sequence homology with HSL in the active site. In humans, it is expressed in the liver and intestine (Hirosawa et al. 2021) and expresses preference for DAG over TAG. Overexpression in rat hepatoma cells which lacked endogenous AADAC resulted in a decrease in TAG accumulation and increase in FA oxidation (Lo et al. 2010). AADAC is expressed at a higher level in Huh7 cells treated with POLA compared to OPLA, which would suggest a decrease in TAG accumulation and an increase in FA oxidation. However, these effects were not evident within this model (see Chapter 3).

- **MANF, Mesencephalic asterocyte-derived neutrophic factor**, a secreted factor associated with inflammation and lipid metabolism was expressed to a greater extent in cells treated with OPLA compared to those treated with POLA, implicating a protective mechanism for cells treated with OPLA. MADF is known to be decreased in a murine MASH model following the induction of a western diet. Down regulation of MANF was shown *in vivo* in mice to exacerbate hepatic lipid accumulation, inflammation and fibrosis with over expression mitigating these pathogenic features (Sousa-Victor et al. 2019). In human and murine primary cells, MANF was knockdown to result in increased hepatic steatosis and inflammation which subsequent over expression then attenuated. It is suggested to work by modulating SREBP1 expression and inhibiting SREBP1 in primary hepatocytes blocked the previously seen

lipid accumulation following MANF down regulation. MANF has been shown to decrease the expression of proinflammatory cytokines by inhibiting NF-κB phosphorylation (Yan et al. 2022). 24 hour NEFA stimulation of HepG2 cells increased MANF protein expression 1.3 fold, lowering to a 0.66 fold increase after 72 hours. MANF deficiency up-regulated genes involved in FA synthesis, cholesterol synthesis and FA uptake and aggravated cell steatosis while the reverse was true with MANF over expression, with suppressed lipid deposition. MANF has therefore been identified as a potential therapeutic target (He et al. 2020).

- **Argininosuccinate synthase, ASS1**, is a rate limiting enzyme in the ornithine cycle, ASS1 is a biomarker of HCC prognosis as well as a predictor of susceptibility to arginine deprivation therapy. In our Huh7 cellular model, there was increased transcription of ASS1 in cells treated with OPLA compared to those treated with POLA, given that increased expression is associated with better outcomes for HCC, it is plausible that at earlier stages of MASLD that over expression could also be protective, or perhaps reduce the probability of HCC developing. Changes in DNA methylation significantly reduce the expression of this enzyme in HCC patients, and silencing of ASS1 has been shown to enhance both cell migration and invasion with knockdown associated with HCC metastasis (Du et al. 2022). Yao et all showed that in HFD fed rats, ASS1 is downregulated associated with upregulated cytokines expression and impaired endotoxin clearance, with ASS1 suggested as a potential target for therapeutics (Yao et al. 2018; Zhang et al. 2020).

Considering the PHH model, the only pathway significantly enriched at a higher level with OPLA compared to POLA treatment was oestrogen signalling. Whilst this *in vitro* model did not contain oestrogen signalling has been implicated in maintaining metabolic homeostasis and cellular function in various tissues, including the liver (Mauvais-Jarvis 2011). Oestrogen is known to have anti-inflammatory and antioxidant effects in extra-hepatic tissues (Fan et al. 2021). Whether these

changes associated with oestrogen signalling are protective or deleterious towards MASLD, and whether these same pathways are altered by dietary FA composition *in vivo* remains to be determined.

Conversely, upregulated in POLA compared to OPLA treated PHH are: the allograft rejection pathway and the compliment and coagulation cascade pathways. Allograft rejection is particularly topical as there is a current shortage of livers available for transplants, and significant work, both from academic institutes and from industry is being undertaken to try and increase the number of livers available for transplant to account for the shortfall (Arulraj et al. 2011; Clarke et al. 2023; Mergental et al. 2024). Thus knowing that within this *in vitro* context, a POLA composition of treatment media is associated with activation of pathways relating transplant rejection may provide a useful insight. The compliment and coagulation cascade, typically discussed together and are primarily associated with the immune response and blood clotting and both of these pathways can contribute to liver inflammation and damage (Amara et al. 2008). Additionally MASLD is associated with a number of extra hepatic comorbidities, including CVD, with a higher prevalence of coagulation disorders in patients with liver disease, potentially relating to the necessity of coagulation factors being synthesised hepatically (Virović-Jukić et al. 2021). Moreover, hepatic injury may lead to a pro-coagulant state, due to an increased production of inflammatory mediators e.g. PAI-1 (Bajt et al. 2008).

Top gene candidates identified from comparing PHH treated with OPLA or POLA are discussed below if they have been previously associated with MASLD. SPP1 and PECAM1 has been associated with MASLD, where SPP1 plays a protective role, and PECAM1 through alterations in the RUNX1 protein plays a deleterious role, however these changes are typically seen in macrophages and endothelial cells respectively so shall not be discussed here (Han et al. 2023; Kaur et al. 2019).

- **Alpha 2-macroglobulin, A2M** is produced by the liver and is a major plasma protein with various functions including ion transport, carrier protein, and the inhibition of proteinases. A2M transcription is increased in PHH cells

treated with POLA compared to OPLA. Comparing, HepG2 cells treated with oleic acid and palmitic acid, silencing HIF-1α was associated with increased lipid metabolism and an increase in lipid deposits and a corresponding increase in A2M (He et al. 2021). Similar downstream activation of A2M has been observed in MASLD and inrodent models (Liu et al. 2016), however, the whether A2M enrichment is deleterious for MASLD has not been determined.

- **PIGR, Polymeric immunoglobulin receptor** is a receptor involved in cellular immune functions (Xu et al. 2023). PIGR has been expressed more in PHH cells treated with a lower concentration of OPLA or POLA compared to a higher concentration, however cells treated with a higher concentration of POLA did express more PIGR when compared to those treated with OPLA. The consequences of elevated PIGR are unknown. Plasma profiling of 48 patients presenting with either health livers, MASLD or cirrhosis, showed an increase in PIGR, in both cohorts with MASLD and cirrhosis. This finding was validated in a mouse model. Mechanistic studies have not been undertaken, but thus far PIGR has more been implicated as a marker of disease, rather than causative (Niu et al. 2019).

- **CRP, C-reactive protein**, an inflammatory marker has been extensively studied and is suggested to be a good marker for the severity of MASLD (Kumar et al. 2020; Foroughi et al. 2016). PHH RNA data showed significantly higher levels of CRP in cells treated with higher concentrations of POLA, potentially implicating a transcriptome which is more similar to advanced MASLD.

- **CD74**, is a invariant chain antigen presenting protein, involved in macrophage recruitment, T cell activation and B cell differentiation. CD74 is expressed at significantly higher levels in cells treated with POLA than OPLA. Human liver transcriptome data from MASLD patients was investigated by Li et al who found CD74 was correlated with infiltrating immune cells in hepatic tissue

(Li et al. 2023). Mishra et all used a rodent model to investigate the role of this protein in a high fat high fructose diet for 12 weeks and demonstrated that a CD74 mouse knockout model, did not develop hepatic steatosis and immune cells remained unaltered (Mishra et al. 2016)

- **OLFM2, olfactomedin 2**, a secreted glycoprotein has been studied by Bertran et al have shown that OLFM2 was expressed at higher mRNA expression in MASH patients and also demonstrated positive correlations between hepatic OLFM2 and glucose and cholesterol levels (Bertran et al. 2022). In PHH cells, cells treated with higher concentrations of POLA showed increased expression of OLFM2 compared to the OPLA, with the lowest expression with cells treated with a low concentration of POLA. It has also been studied in adipose tissue but implicated in hepatic lipid accumulation (Barrientos-Riosalido et al. 2023).

- **BAMBI, BMP and activin membrane bound inhibitor** is a transmembrane protein structurally related to TGFβ but without the kinase domain, thus functioning as an TGC-β1R antagonist. It is essential to processes which are regulated by TGF-β1R signalling, which, is associated with liver fibrosis. Hepatic BAMBI is downregulated in rodent models of liver injury suggesting that a low BAMBI level has a role in liver fibrosis (Weber et al. 2023). BAMBI mRNA is expressed at a lower level in cells treated with POLA compared to those treated with OPLA, however, the mechanistic consequences of this remain to be determined.

- **GSTA2, glutathione S-transferase α2** is a oxidative stress associated gene and is expressed in FA treated PHH at a lower level in POLA compared to OPLA treated cells. A dietary intervention study by Miyata et al, investigated the effects of selenoneine,an organic selenium compound found in fish, on hepatocellular injury and hepatic steatosis in a mouse MASLD model where they demonstrated that selenonenine, showed a significant decrease in GSTA2

and other similar proteins which resulted in attenuated hepatic steatosis and hepatocellular injury (Miyata et al. 2020). However, the role of GSTA2 has yet to be investigated in human hepatocytes.

- **TGFB1, transforming growth factor β-1**, is a proinflammatory cytokine associated with all stages of MASLD progression, with expression levels increasing with MASLD severity (Ahmed et al. 2022) TGFB1 shows significantly greater expression in PHH cells treated with POLA compared to OPLA, potentially implicating deleterious mechanisms.

- **AQP7, Aquaporin 7** is a plasma membrane channel and allows movement of water, glycerol and urea across the cellular membrane. Fu et al, demonstrated that in a HepG2 model of steatosis, oleic acid incuded an increase of lipogenic genes through an oestrogen mediated pathway (Fu et al. 2016). In FA treated PHH cells, AQP7 is expressed at a lower level in POLA when compared to OPLA treated cells, which indicates a potential mechanism for increased lipogenic gene expression. However, the relevance to this *in vivo* needs consideration, particularly as oestrogen displays sexual and age dimorphism in its expression and was not included in the culturing medium. However, AQP7 has also been implicated in driving phenotype increased lipolysis in adipose tissue with increased levels promoting higher lipolysis in the visceral fat, which would in turn impinge on hepatic metabolism (Rodríguez et al. 2015).

- **VWF, Von Willebrand factor**, is a multimeric adhesive protein, which allows platelets to adhere to the side of blood vessel walls during injury. A number of studies have associated VWF with MASLD as discussed by Valenti et al (Valenti et al. 2022). VWF is a ligand for GPIbα, and data have showed that mice lacking VWF, or alternative ligands, develop MASH after 6 months on a high fat diet (Blenner et al. 2014). The role of GP1bα in MASH is to orchestrate the inflammation response, however, given that there are a number

of ligands which can activate it, it is unclear whether this increase of VWF would have any molecular consequences (Malehmir et al. 2019). However, other data suggest that procoagulation activation is associated with activation of stages of fibrogenesis (Valenti et al. 2022). VWF shows significantly greater expression in PHH cells treated with POLA compared to OPLA, potentially implicating deleterious mechanisms. .

All of the above changes discussed demonstrate, that when comparing cells treated with OPLA compared to POLA in PHH cells, POLA appears to have a potentially more deleterious effect regarding MASLD disease development and prognosis. Although mechanistic insights are needed to confirm that these changes are driving forces behind the observations seen *in vivo*, they do provide a starting point for future investigations.

There are a number of limitations posed by this work. Whilst these observations highlight transcriptonal differences between cells treated with different FA compositions, any findings will need to be replicated on a protein level to ensure that changes are translated. Moreover, as discussed before, Huh7 cells are a hepatoma derived cell line (Kawamoto et al. 2020), and therefore they can only go so far in explaining observations seen in MASLD patients. PHH cells, although of human origin and considered the gold standard, come with their own issues, namely, they are hindered by phenotype, genotype, and their inability to survive for long periods outside the body. Moreover, when studying patient biopsy samples, it is likely that they will contain different cell types, and not just an isolated pool of hepatocytes. Additionally, *in vivo*, hepatocellular mRNA expression will not only be governed by nutrient supply but also by a range of hormonal factors which are challenging to recapitulate *in vitro*, especially regarding diurnal variation and particularly for PHH cells, which present literature suggest require high sugar concentrations in their culturing media, potentially influencing sequencing results. Cells also derive genetic expression cues from the physical environment - through cell-cell interactions and pressure and oxygen availability. These are difficult to recapitulate *in vitro*, but

as research progresses, experimental set ups, such as organoids, co-cultures and chip devices may help overcome these issues (Zeilinger et al. 2016).

3.5 Conclusions

From this sequencing data in both PHH and Huh7 cells treated with OPLA and POLA compositions, it is not possible to suggest which model is more physiologically relevant to liver steatosis, as both have identified previously considered candidates thought to be altered in MASLD. Comparison with other *in vitro* transcriptomic datasets as and when they are generated will be important in further interpreting this data. However, the data discussed here indicate that both the composition and concentration of the FA treatments impacted on Huh7 and PHH cells at a transcriptional level, which may translate over time into functional changes that alter MASLD risk.

4

Characterisation of IHTAG turnover *in vitro* in Huh7 cells cultured with FA enriched in UNSFA or SFA

4.1 Introduction

For individuals with MASLD, lifestyle changes remain the primary method of treatment (Ray 2013). Specifically, patients are advised to consume a diet with more low-glycemic index foods (fruits, vegetables, and whole grains), while reducing FA intake, and of the FA consumed, ensuring it is enriched in MUFA and PUFA as opposed to SFA (Kargulewicz et al. 2014; Marchesini et al. 2016). Whilst there is significant evidence documenting the positive effect of altering both diet and lifestyle to reflect the advice given (Mundi et al. 2020), the underlying changes within the hepatocytes themselves are not understood, specifically, how changing a diet from one enriched in SFA to one enriched in MUFA might reduce hepatic steatosis *in vivo* (Friedman et al. 2018; Kargulewicz et al. 2014).

The majority of *in vitro* cellular models investigating IHTAG accumulation, do so by providing a high fat treatment condition for a 24 hour period, or up to a week as described in the model at the beginning of this thesis, observing the formation of LDs and then investigating whether there are changes in metabolic pathways (Pramfalk et al. 2020; Tian et al. 2016; Nagarajan et al. 2019). Thus far, no *in vitro*

experiments to date, have looked at the impact of macronutrients on hepatocytes when they have already been exposed to nutritional stimulation, as would be seen in a human when dietary changes are induced following a previous diet, rather they look at cells which have been previously kept under control conditions. The most applicable experimental set-up to investigate the effect of compounding diets, have been carried out using livers which were rejected from transplant. Some studies have been undertaken where the livers are in a steatotic state at the beginning of the experiment, however, the goal of these investigations has typically been to induce FA turn-over or 'defat' them, with the aim of using these techniques to make more livers suitable for transplantation (Šeda et al. 2019; Nagrath et al. 2009).

Although a number of pharmacological agents have been demonstrated to improve parameters such as plasma TAG, hepatocyte viability, cellular oxidation on a whole organ level, none result in a significant reduction in hepatic TAG, even in an *in vitro* environment (Du et al. 2022; Pais et al. 2016). Thus, at present, it is not possible to explore any metabolic changes in an *in vitro* environment which may occur following the loss of FA from a previous state of being enriched in IHTAG. The work described in this chapter aimed to investigate the effect of changing both FA composition and or concentration in an *in vitro* model of hepatic steatosis where IHTAG of a known composition had already accumulated.

4.2 Method

Refer to Chapter 2 for: cell culturing, protein assay, lipid extraction, glucose assay, glycogen assay, oxidation techniques, DNL analysis methodologies and imaging techniques.

All experiments in this chapter have been performed using Huh7 hepatocytes.

4.2.1 Cellular experiment timeline

The model presented in this chapter is an extension of the model outlined within Chapter 3 as the treatment is kept the same for the first period, then a second phase is undertaken. For all experiments within this chapter, except the imaging experiments, for the first 7 days, either deuterated water or stable-isotope FA (D31 palmitic acid and D33 oleic acid) were used. For days 7-14 label free media was used. Stable-isotope labels were used to monitor mobilisation and utilisation of FAs as either the composition or concentration, or both changed. The media change timeline can be seen in Figure 4.1 and follows: After seeding and a 24 hour incubation, the first media change was carried out and cells were cultured in media containing stable-isotope labels, with changes occurring every other day except the second change which happened after 3 days. On the 7th day, the media was changed to be label free and they were maintained for 7 days with the media changed every 2 days until the 14th day. The cells were then harvested for analysis.

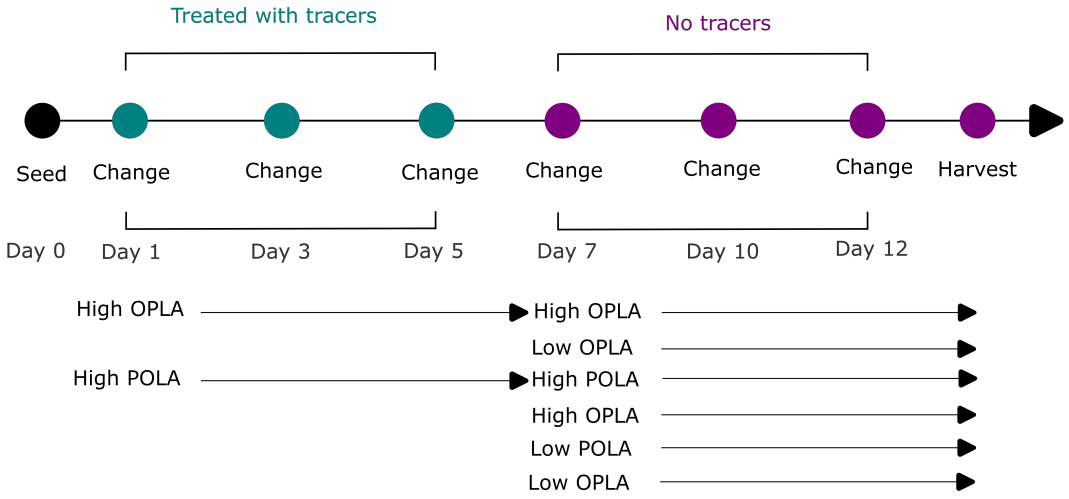


Figure 4.1: Experimental timeline for Chapter 4. Figure shows the seeding and media change schedule. Cells were seeded on Day 0, then underwent three media changes on days 1, 3 and 7. This first media contained labelled fatty acids (FA)(D33 oleic acid and D31 palmitic acid) as tracers. On day 7 the media was changed to be tracer free. Tracer free media was then used for the following changes which occurred on day 10 and day 12. On day 14 the cells were harvested for further experimentation. For the first 7 days, the tracer containing media was either a high concentration of POLA (PH) or a high concentration of OPLA (OH). This media was then changed as follows: PH treated cells were then treated wither either PH again, a low concentration of POLA (PL), a high concentration of OH, or a low concentration of OPLA (OL). Cells treated initially with OPLA were subsequently treated with either OH or OL

4.2.2 Gas chromatography

For GC results, data included in this chapters show the relative contribution of these FA to the total TAG amount. GC methodologies can be seen in Chapter 2 Section 2.2.4.3. A breakdown by molar amount corresponding to each of the ratios provided in this chapter are presented in the Appendix Section (A.3).

4.2.3 Cell profiler

An analysis of LD size was carried out using images acquired as described in Chapter 2 Section 2.2.8. For each condition, 10 images were taken at the same magnification. Open source Cell profiler software (Stirling et al. 2021) was used to analyse the images to calculate the area of the cells. For this thesis, the following pipeline was used: Images were converted to greyscale, Enhance and suppress function applied, watershed function applied and quantification performed. Figure 4.2.3 shows the process.

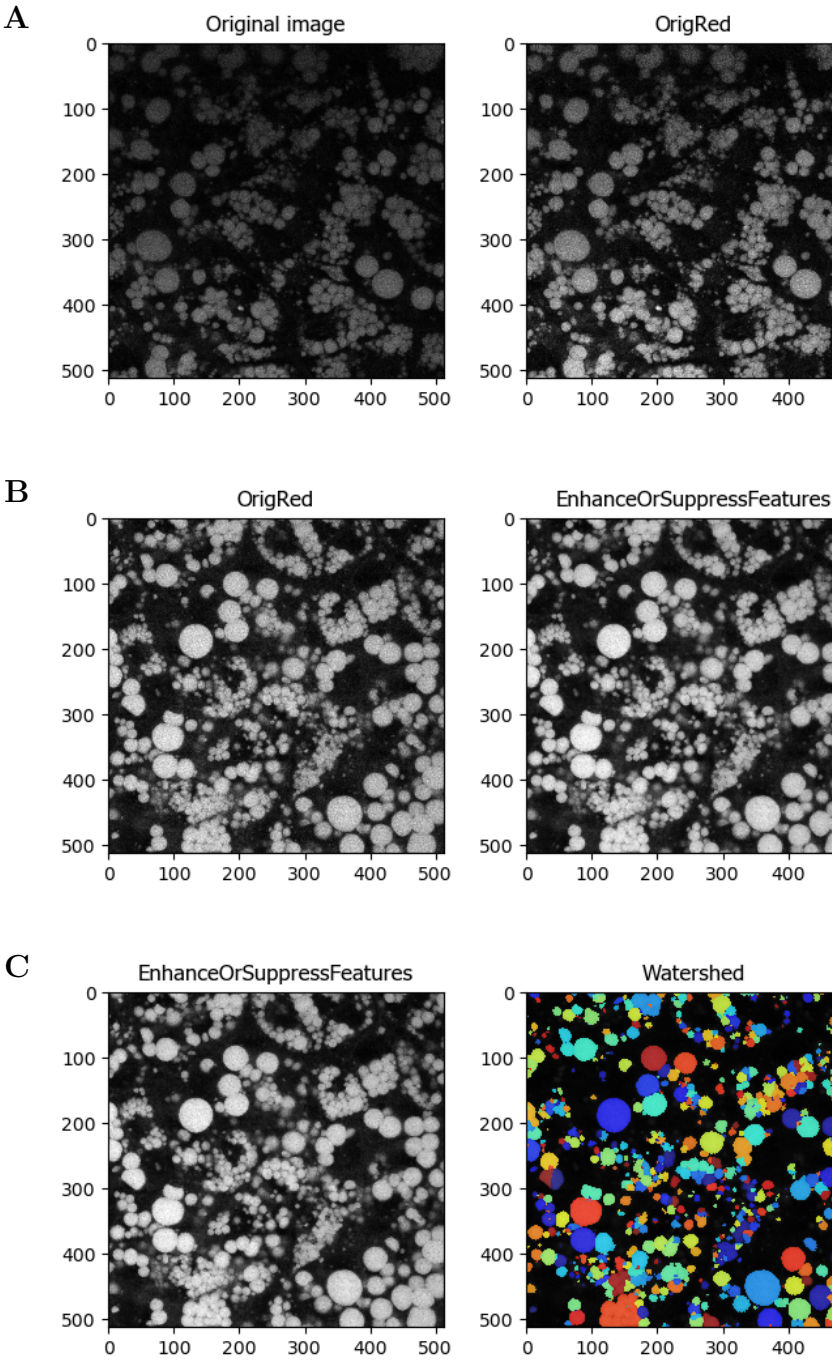


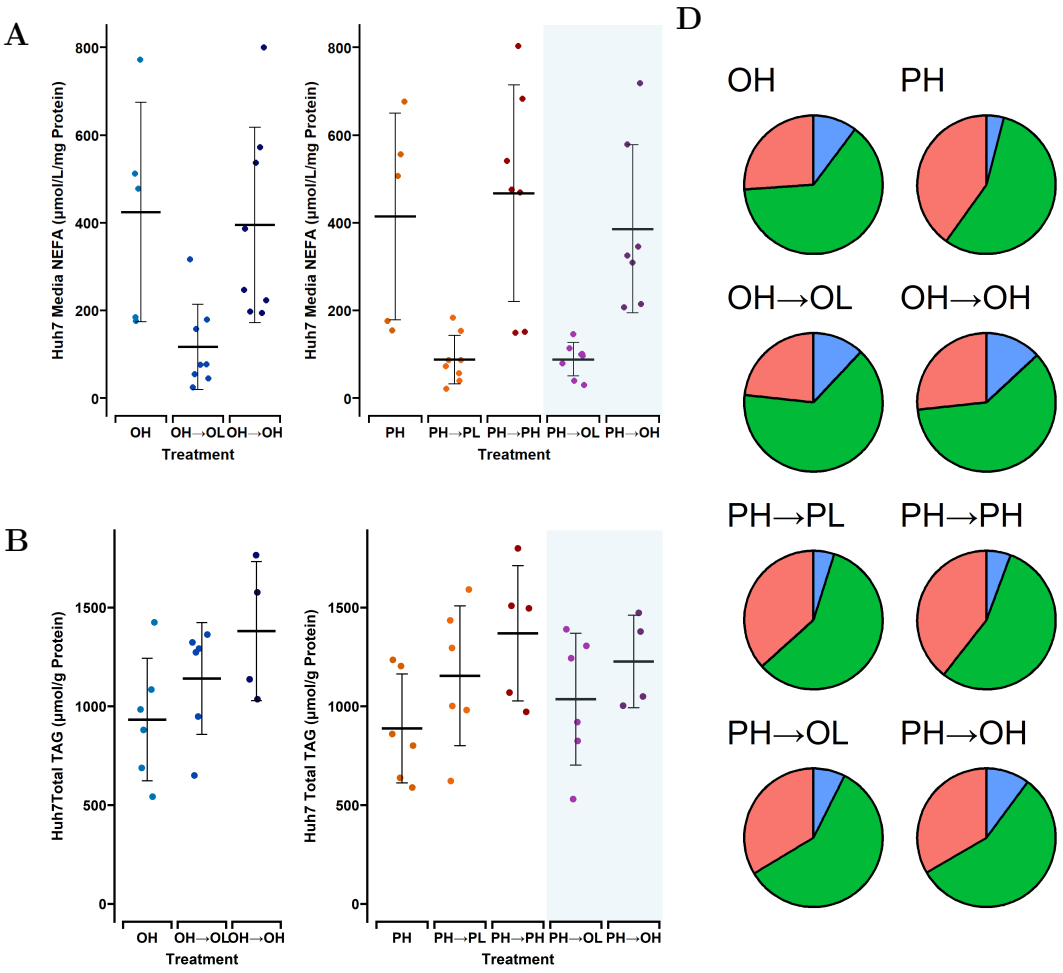
Figure 4.2: Methodology for analysing lipid droplet size using Cell Profiler in Huh7 cells Images were taken on a confocal microscope using one fluorescent colour for lipid droplets before being analysed by Cell Profiler software (Stirling et al. 2021). A) Conversion of image to greyscale, B) Enhance and Suppress function, C) Application of Watershed function. Images taken from cell profiler application (Stirling et al. 2021).

4.3 Results

4.3.1 Quantification of Huh7 TAG following 14 days of FA treatment

As none of the previous experiments for this thesis required cells to be cultured for more than one week, we firstly established that the cells were still capable of responding to the nutrient stimulation over a 14 day period. Figure 4.3a shows media NEFA uptake and under all conditions, media NEFA was reduced at the end of the treatment period (14 days) indicating NEFA uptake. Cells cultured with 200µM of NEFA between days 7 and 14 took up a smaller amount of NEFA compared to those cultured withe 800µM of NEFA. Cells retained their capacity for NEFA uptake across the 14 day treatment. There was no significant difference in the total protein content for each sample under different culturing conditions (data not shown), implying no significant difference in cellular proliferation resulting from the different FA treatments over the two week treatment period.

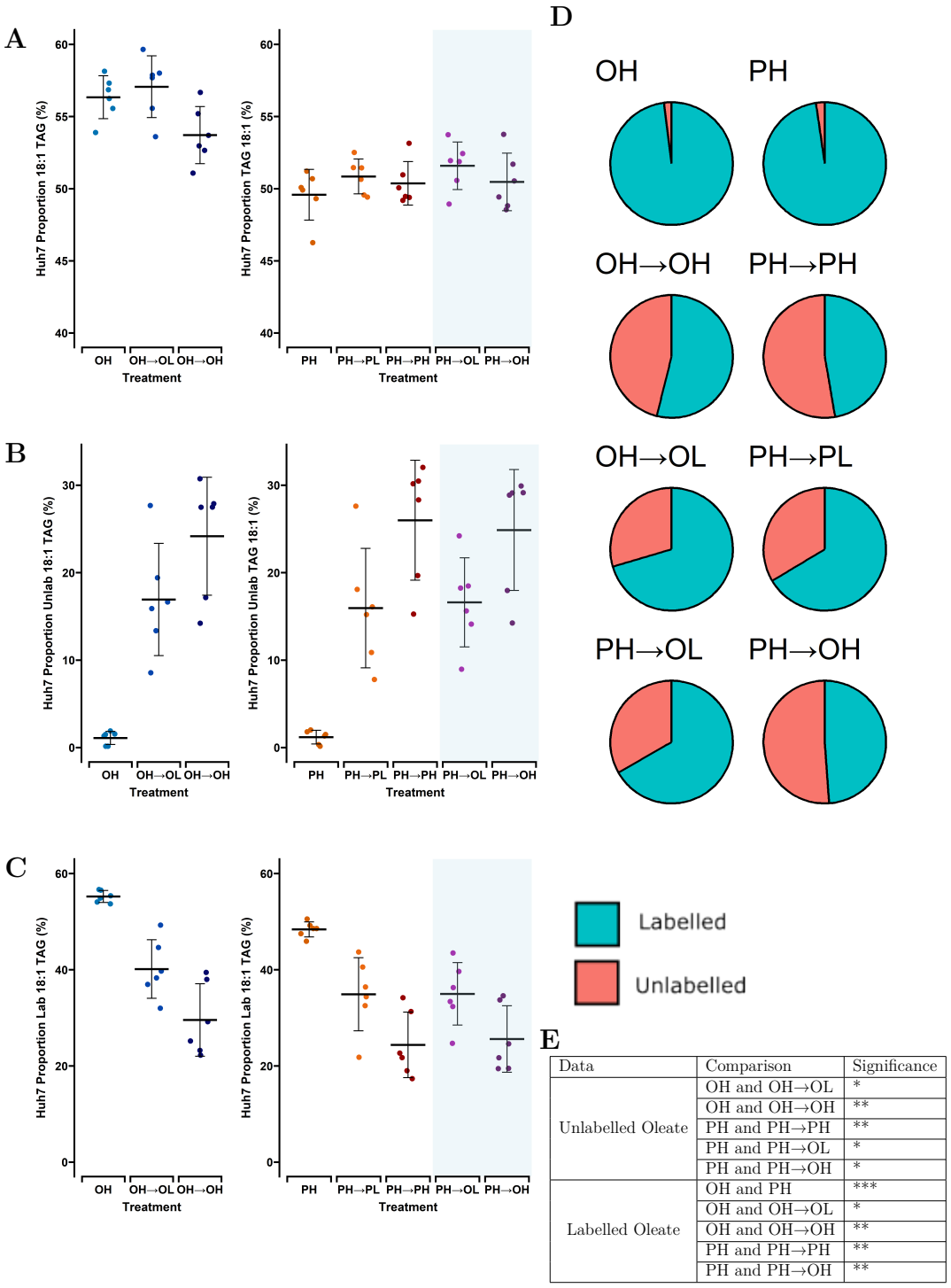
As shown in Figure 4.3b, culturing Huh7 cells for an additional 7 days increased the total TAG content for those cells treated with FA for 14 days compared to 7 days, although this difference was only significant for cells treated with high concentrations of OPLA, comparing 7 days in a high concentration of OPLA with cells treated in a high concentration of OPLA for 14 days. The FA composition of the TAG pool reflected that of the treatment media. Figure 4.3c, shows the contribution of the FA constituents of OPLA or POLA to total mean TAG.



Data	Comparison	Significance
Total TAG	OH & OH→OH	*
Media NEFA	OH→OL & OH→OH	*
	PH→PL and PH→PH	*
	PH→OL and PH→OH	*

Figure 4.3: Huh7 cells intrahepatic triacylglycerol (IHTAG) content in Huh7 cells following treatment with fatty acids (FA). A) NEFA uptake by Huh7 cells quantified by clinical biochemistry analyser; B) Total IHTG content of Huh7 cells quantified by gas chromatography; C) Pie charts depicting the mean contribution of each constituent FA of OPLA or POLA (excluding α-linolenic acid as it contributed less than 1% of treatment media); D) Table of statistics Data show proportion of linoleic acid, oleic acid and palmitic acid (colours, green, red and blue respectively). Data presented as mean +/- SD, n = 6 per treatment unless stated otherwise. Abbreviations: OH→OL, first week at high (800µM) and second week at low (200µM) of OPLA; OH→OH, two weeks at high of OPLA; PH→PL, first week at high and second week at low of POLA; PH→PH, two weeks at high of POLA; PH→OL, first week at high POLA and second week at low of OPLA; PH→OH, first week at high of POLA and second week at high of OPLA. Significance levels indicated are * $p<0.05$, ** $p<0.01$ and *** $p<0.001$.

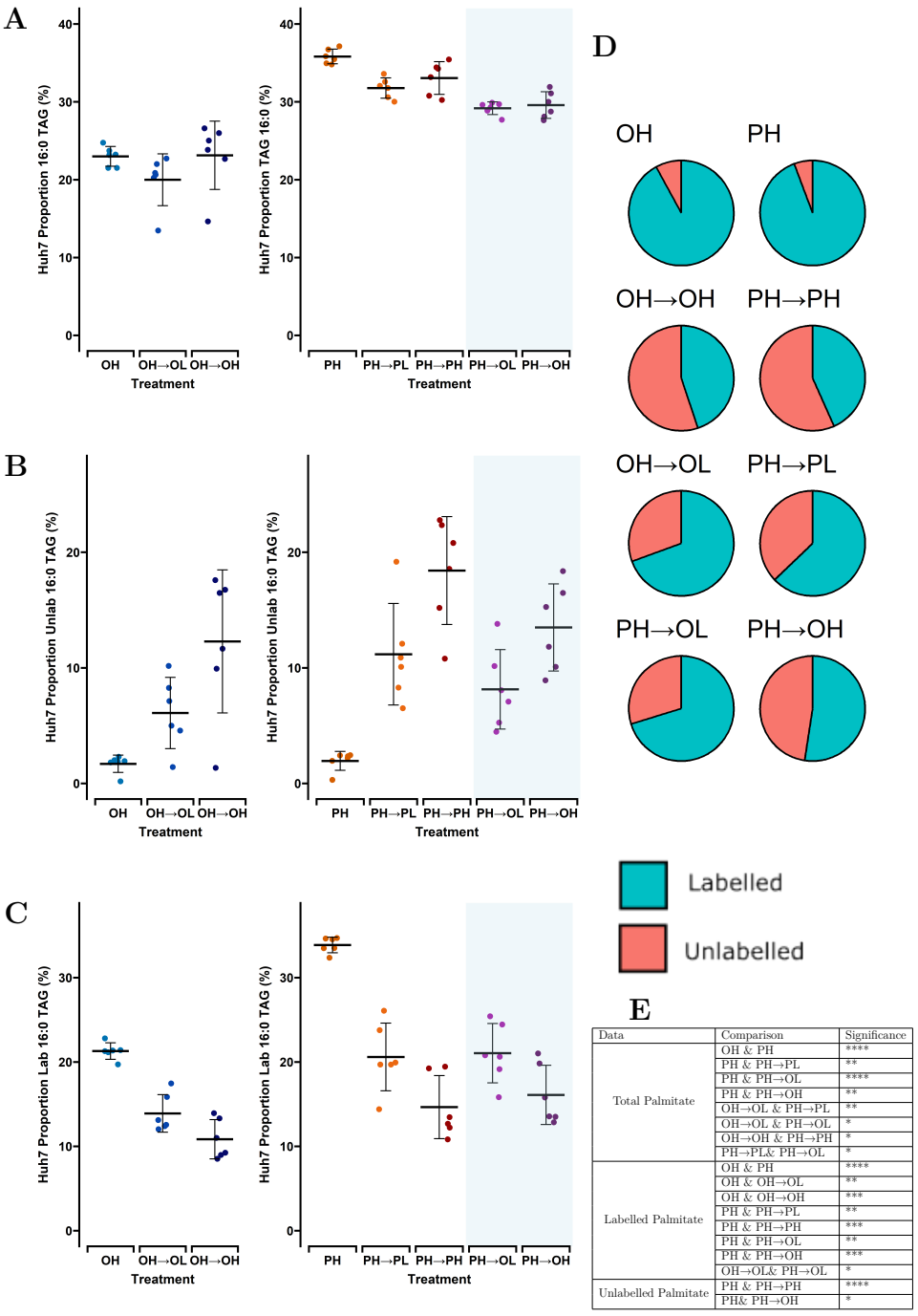
There were no significant differences between any of the treatment conditions, with either length of treatment, composition or concentration for the proportion of total TAG constituted by oleic acid, either stable-isotope labelled oleic acid or unlabelled oleic acid (Figure 4.4a). Figure 4.4c, shows the proportion of labelled D33 oleic acid constituted of total TAG and Figure 4.4b, shows the proportion unlabelled oleic acid constituted of the total TAG present. Changing the composition of the treatment media, resulted a shift in cellular TAG composition to reflected that of the treatment composition provided on days 7-14. Unlabelled oleic acid significantly increased in cells treated for 14 days (with 7 days treated with stable-isotope labelled oleic acid then 7 days unlabelled oleic acid), when compared to cells treated with 7 days of stable-isotope labelled oleic acid for all conditions, except for cells treated with low concentrations of POLA for days 7-14. Accordingly, the proportion of stable-isotope labelled oleic acid significantly decreased when cells were cultured for an additional 7 days (days 7-14) with unlabelled oleic acid when compared to cells treated for 7 days with stable-isotope labelled oleic acid (Figure 4.4c). Despite the decrease in proportion of total TAG constituted by stable-isotope labelled oleic acid, the concentration of stable-isotope labelled oleic acid within the cells did not decrease with the extended treatment timeline (see Appendix Figure A.9a). The changes in the proportion of total oleic the labelled and unlabelled oleic acid constitute can be seen in Figure 4.4d.



Data	Comparison	Significance
Unlabelled Oleate	OH and OH→OL	*
	OH and OH→OH	**
	PH and PH→PH	**
	PH and PH→OL	*
	PH and PH→OH	*
Labelled Oleate	OH and PH	***
	OH and OH→OL	*
	OH and OH→OH	**
	PH and PH→PH	**
	PH and PH→OH	**

Figure 4.4: Huh7 intrahepatocellular triacylglycerol (TAG) derived oleic acid composition following treatment with fatty acids (FA). Data quantified by gas chromatography. A) Proportion of total TAG constituted by either labelled or unlabelled oleic acid (18:1n-9), B) Proportion of total TAG constituted by unlabelled oleic acid (18:1n-9), C) Proportion of total TAG constituted by stable-isotope labelled oleic acid (D-33 18:1n-9). D) Pie chart depicting the mean contribution of either labelled or unlabelled oleic acid. E) Table of statistics Data presented as mean +/- SD, n = 6 per treatment unless stated otherwise. Abbreviations: OH→OL, first week at high (800µM) and second week at low (200µM) of OPLA; OH→OH, two weeks at high of OPLA; PH→PL, first week at high and second week at low of POLA; PH→PH, two weeks at high of POLA; PH→OL, first week at high POLA and second week at low of OPLA; PH→OH, first week at high of POLA and second week at high of OPLA. Significance levels indicated are * $p<0.05$, ** $p<0.01$ and *** $p<0.001$.

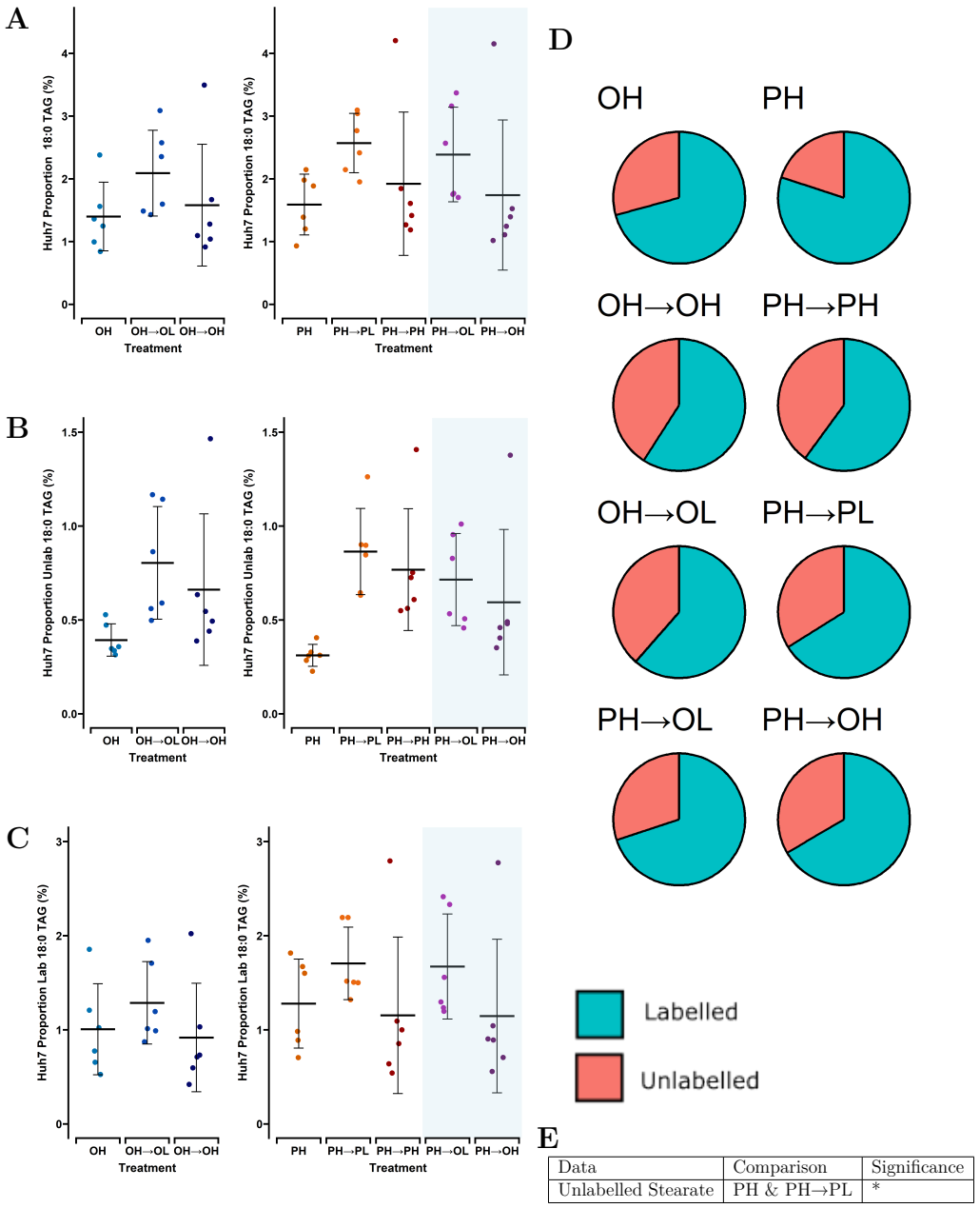
Treatment with POLA resulted in a significant increase in palmitic acid proportion of total TAG compared to OPLA treatment across both the 7 and 14 day period. Changing the media composition from POLA to OPLA for days 7-14 resulted in significant decrease in palmitic acid when comparing composition changes at both high and low concentrations of OPLA with those cells treated with POLA (Figure 4.5a). As stable-isotope labelled palmitic acid was provided for the first 7 days, and unlabelled palmitic acid provided for days 7-14, the relative contribution of the remaining labelled palmitic acid was examined. Considering turnover of the stable-isotope labelled palmitic acid (Figure 4.5c), there was a decrease in proportion of the labelled palmitic acid constituting total TAG, for cells treated for 14 days compared to those treated with just the labelled palmitic acid for 7 days. Conversely, an increase was seen in the proportion of total TAG constituted by unlabelled palmitic acid for cells treated for 14 days compared to cells for 7 days, and this difference was singificant for cells treated with a high concentration of POLA (Figure 4.5b). There were no significant differences in the proportion of unlabelled palmitic acid between the different treatment conditions. Figure 4.5d, shows the relative proportions of labelled and unlabelled palmitic acid making up the total intracellular pool of palmitic acid.



Data	Comparison	Significance
Total Palmitate	OH & PH	****
	PH & PH→PL	**
	PH & PH→OL	****
	PH & PH→OH	**
	OH→OL & PH→PL	**
	OH→OL & PH→OL	*
	OH→OH & PH→PH	*
	PH→PL& PH→OL	*
Labelled Palmitate	OH & PH	****
	OH & OH→OL	**
	OH & OH→OH	***
	PH & PH→PL	**
	PH & PH→PH	***
	PH & PH→OL	**
	PH & PH→OH	***
	OH→OL& PH→OL	*
Unlabelled Palmitate	PH & PH→PH	****
	PH& PH→OH	*

Figure 4.5: Huh7 intrahepatocellular triacylglycerol (TAG) derived palmitic acid composition following treatment with fatty acids (FA). Data quantified by gas chromatography. A) Proportion of total TAG constituted by either stable-isotope labelled or unlabelled palmitic acid (16:0), B) Proportion of total TAG constituted by unlabelled palmitic acid (16:0), C) Proportion of total TAG constituted by labelled palmitic acid (D-31 16:0). D) Pie chart depicting the proportion of labelled or unlabelled palmitic acid. E) Table of statistics. Data presented as mean +/- SD, n = 6 per treatment. Abbreviations: OH→OL, first week at high (800µM) and second week at low (200µM) of OPLA; OH→OH, two weeks at high of OPLA; PH→PL, first week at high and second week at low of POLA; PH→PH, two weeks at high of POLA; PH→OL, first week at high POLA and second week at low of OPLA; PH→OH, first week at high of POLA and second week at high of OPLA. Significance levels indicated are * $p<0.05$, ** $p<0.01$ and *** $p<0.001$.

Hepatocytes can elongate palmitic acid to stearic acid. There were no significant differences between the treatment conditions for the proportion stearic acid constituted of total TAG over the 14 day experiment (Figure 4.6a). However, there was a statistical trend towards an increased proportion of total TAG constituted by stearic acid for cells treated with a lower concentration of FA for days 7-14, regardless of treatment composition. As the cells received both stable-isotope labelled palmitic acid and unlabelled palmitic acid, both stable-isotope labelled stearic acid and unlabelled stearic acid were produced. There were no significant differences between either the stable-isotope labelled stearic acid or the unlabelled stearic acid and the proportion of total TAG they constitute between conditions (Figures 4.6c and 4.6b). Figure 4.6d, shows the relative proportion of stearic acid constituted by stable-isotope labelled or unlabelled stearic acid.

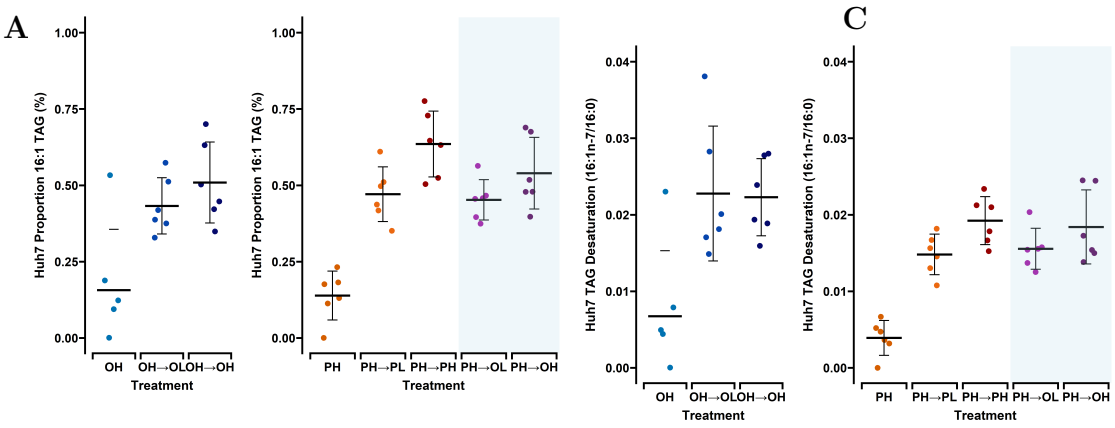


Data	Comparison	Significance
Unlabelled Stearate	PH & PH→PL	*

Figure 4.6: Huh7 intrahepatocellular triacylglycerol (TAG) derived stearic acid composition following treatment with fatty acids (FA). Data quantified by gas chromatography. A) Relative contribution of stearic acid to total intracellular TAG B) Proportion of total TAG constituted by unlabelled stearic acid (18:0), C) Proportion of total TAG constituted by labelled oleic acid (D-31 18:0). D) Pie chart depicting the mean contribution of labelled or unlabelled stearic acid. E) Table of statistics. Data presented as mean +/- SD, n = 6 per treatment unless stated otherwise. Abbreviations: OH→OL, first week at high (800µM) and second week at low (200µM) of OPLA; OH→OH, two weeks at high of OPLA; PH→PL, first week at high and second week at low of POLA; PH→PH, two weeks at high of POLA; PH→OL, first week at high POLA and second week at low of OPLA; PH→OH, first week at high of POLA and second week at high of OPLA. Significance levels indicated are * $p<0.05$, ** $p<0.01$ and *** $p<0.001$.

Figures 4.7a and 4.7b, show the relative contribution of palmitoleic acid and linoleic acid to total TAG respectively. There were significant differences in the proportion of palmioleic acid when comparing between cells treated for the first 7 days with POLA followed by any of the other treatments for the next 7 days and cells treated with with POLA for 7 days. The proportions of linoleic acid were reflective of the proportions of linoleic acid in the treatment mediums (Figure 4.7b). Linoleic acid constituted a greater proportion of total TAG in cells treated with OPLA, compared to those treated with the same concentration of POLA for the same time period. Changing media composition from POLA for the first 7 days to OPLA for the next 7 days resulted in a significant increase in the proportion of linoleic acid when treatment medias were given at a high concentration.

The ratio of palmitoleic acid to palmitic acid (16:1n-7/16:0), is a marker of FA desaturation and significant differences were only seen when comparing cells treated for 7 days in high POLA with those treated with FAs for another 7 days (Figure 4.7c). Other ratios: 18:0/16:0, 18:0/18:1n-9, and 18:1n-7 ad 16:1n-7, reflecting, elongation, desaturation and elongation respectively showed no significant differences.



D

Data	Comparison	Significance
Palmitoleic acid	PH & PH→PL	**
	PH & PH→PH	***
	PH & PH→OL	***
	PH & PH→OH	**
Linoleic acid	OH & PH	***
	OH & OH→OH	*
	PH & PH→PH	*
	PH & PH→OH	**
	OH→OL & PH→PL	**
	OH→OH & PH→PH	***
	PH→PH& PH→OH	*
16:0/18:0	PH & PH→PL	***
	PH & PH→PH	***
	PH & PH→OL	***
	PH & PH→OH	**

Figure 4.7: Huh7 intrahepatocellular triacylglycerol (TAG) derived palmitoleic acid composition following treatment with fatty acids (FA). Data quantified by gas chromatography. A) Relative contribution of palmitoleic acid to total TAG. B) Proportion of TAG constituted by linoleic acid. C) Desaturation ratio of 16:1n-7 to 16:0. D) Pie chart depicting the mean contribution of labelled and unlabelled palmitoleic acid. E) Table of statistics. Data presented as mean +/- SD, n = 6 per treatment unless stated otherwise. Abbreviations: OH→OL, first week at high (800µM) and second week at low (200µM) of OPLA; OH→OH, two weeks at high of OPLA; PH→PL, first week at high and second week at low of POLA; PH→PH, two weeks at high of POLA; PH→OL, first week at high POLA and second week at low of OPLA; PH→OH, first week at high of POLA and second week at high of OPLA. Significance levels indicated are * $p<0.05$, ** $p<0.01$ and *** $p<0.001$.

4.3.2 Quantification of Huh7 PL following 14 days of FA treatment

The PL profile of the Huh7 hepatocytes which had been treated for 14 days with FA was also assessed using gas chromatography. Figure 4.8a, shows the total amount of PL adjusted for cellular protein. There were no significant difference between treatment groups. Figure 4.8b, shows the relative contribution of the main FA constituents of OPLA and POLA to total PL.

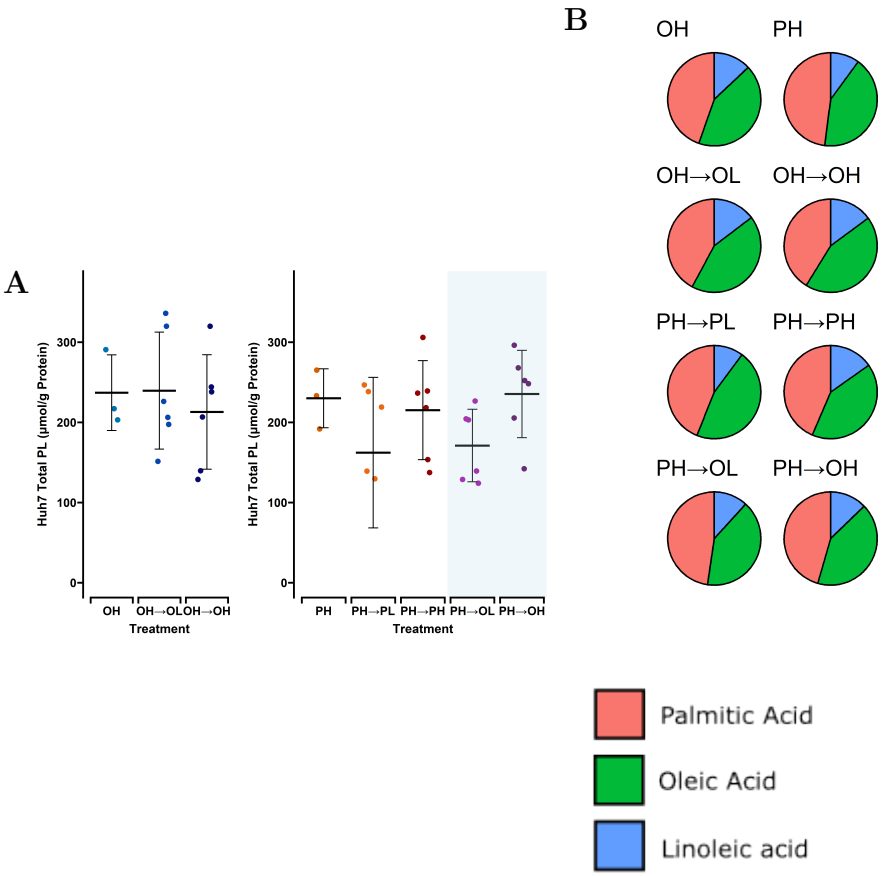
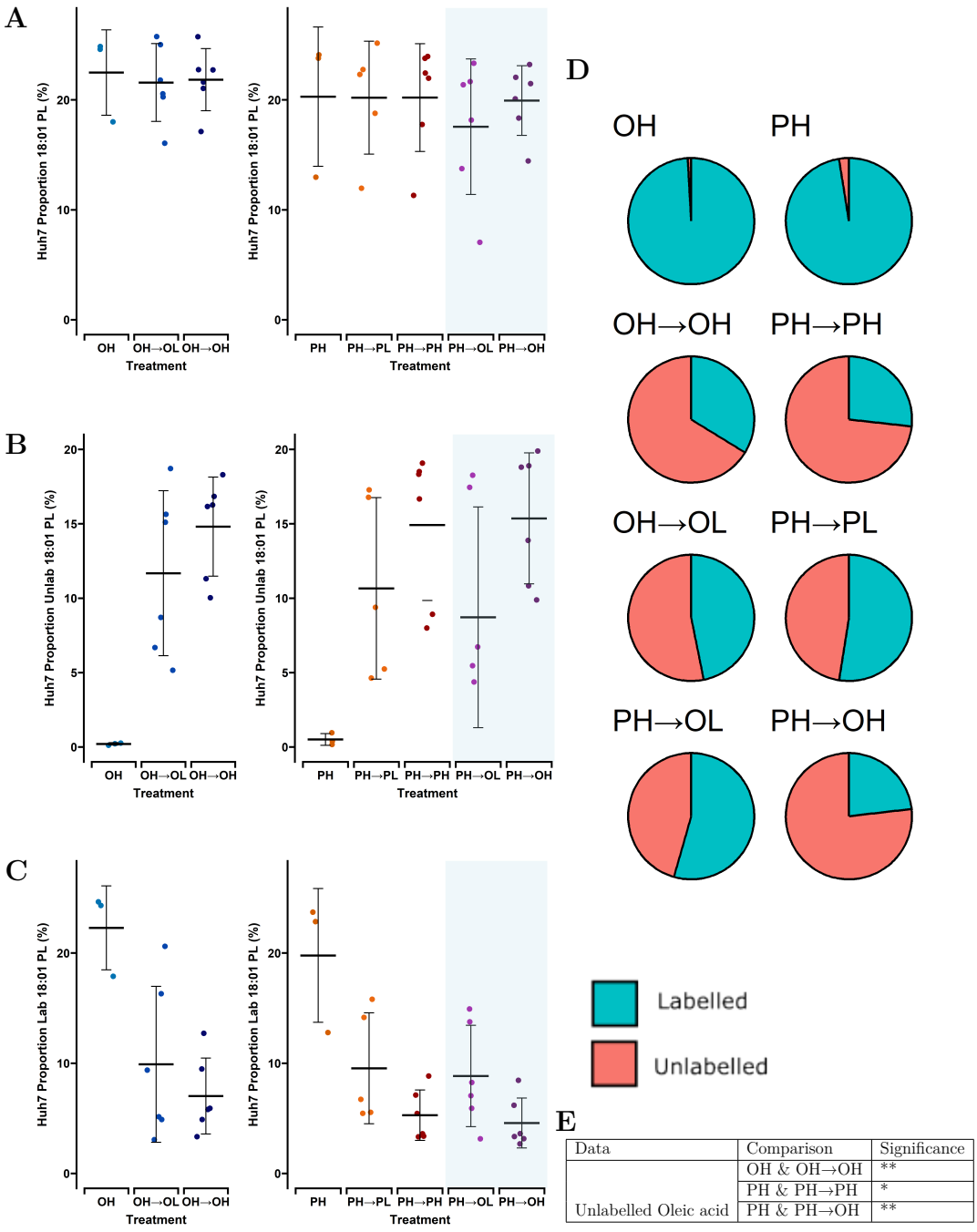


Figure 4.8: Huh7 cells intrahepatic phospholipid (PL) content in Huh7 cells following treatment with fatty acids (FA). Data quantified by gas chromatography. A) Total intrahepatic PL content of Huh7 cells. B) Pie charts depicting the mean contribution of each constituent FA of OPLA or POLA (excluding α-linolenic acid as it contributed less than 1% of treatment media). Data show proportion of linoleic acid, oleic acid and palmitic acid (colours, green, red and blue respectively. Data presented as mean +/- SD, n = 6 per treatment unless stated otherwise. Abbreviations: OH→OL, first week at high (800µM) and second week at low (200µM) of OPLA; OH→OH, two weeks at high of OPLA; PH→PL, first week at high and second week at low of POLA; PH→PH, two weeks at high of POLA; PH→OL, first week at high POLA and second week at low of OPLA; PH→OH, first week at high of POLA and second week at high of OPLA.

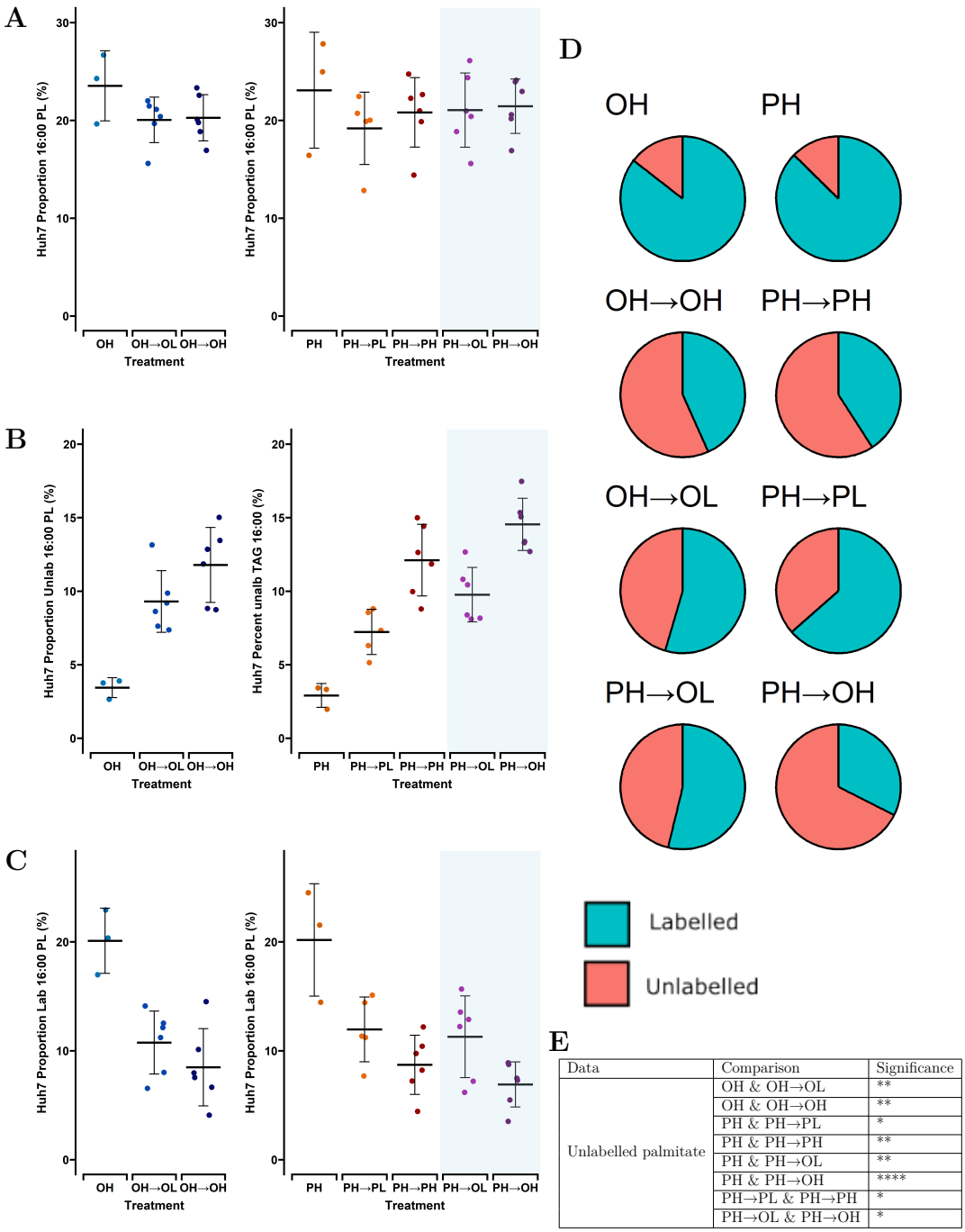
Neither treatment composition, nor concentration altered the contribution of oleic acid to the total PL pool (Figure 4.9a) and when considering the contribution of the stable-isotope labelled oleic acid to the PL pool, where no significant differences were seen (Figure 4.9b). There was a significant increase in unlabelled oleic acid in cells treated with high concentrations of either OPLA or POLA from days 7-14 when compared to those treated for 7 days regardless of OPLA or POLA respectively (Figure 4.9c). There were no changes in total PL concentration (see Appendix Figure A.7a), this reflects a shift in the PL composition. Figure 4.9d shows the mean proportions of stable-isotope labelled oleic acid and unlabelled oleic acid resulting from each treatment condition.



Data	Comparison	Significance
Unlabelled Oleic acid	OH & OH→OH	**
	PH & PH→PH	*
	PH & PH→OH	**

Figure 4.9: Huh7 intrahepatocellular phospholipid (PL) derived oleic acid composition following treatment with fatty acids (FA). Data quantified by gas chromatography. A) Relative contribution of oleic acid to total PL, B) Proportion of total PL constituted by unlabelled oleic acid (18:1n-9), C) Proportion of total PL constituted by labelled oleic acid (D-33 18:1n-9). D) Pie chart depicting the mean contribution of either labelled or unlabelled oleic acid to the PL oleic acid fraction. E) Table of statistics. Data presented as mean +/- SD, n = 6 per treatment unless stated otherwise. Abbreviations: OH→OL, first week at high (800µM) and second week at low (200µM) of OPLA; OH→OH, two weeks at high of OPLA; PH→PL, first week at high and second week at low of POLA; PH→PH, two weeks at high of POLA; PH→OL, first week at high POLA and second week at low of OPLA; PH→OH, first week at high of POLA and second week at high of OPLA. Significance levels indicated are * $p<0.05$, ** $p<0.01$ and *** $p<0.001$.

No significant differences were seen in the contribution of total palmitic acid to the total PL pool (Figure 4.10a), nor were there any significant differences in the proportion of total PL constituted specifically by the labelled palmitic acid (Figure 4.10b). Significant proportions of unlabelled palmitic acid contributed to the IHPL pool for all treatments compared to the respective 7-day treated controls (Figure 4.10c). There was a significant decrease in the proportion of unlabelled palmitic acid in cells treated with a lower concentration of FA for days 7-14, compared to those treated with a high concentration, when treated with the same compositions for cells treated with POLA for the first 7 days.



Data	Comparison	Significance
Unlabelled palmitate	OH & OH→OL	**
	OH & OH→OH	**
	PH & PH→PL	*
	PH & PH→PH	**
	PH & PH→OL	**
	PH & PH→OH	****
	PH→PL & PH→PH	*
	PH→OL & PH→OH	*

Figure 4.10: Huh7 intrahepatocellular phospholipid (PL) derived palmitic acid composition following treatment with fatty acids (FA) . Data quantified by gas chromatography. A) Relative contribution of palmitic acid to theIHPL pool, B) Proportion of total PL constituted by unlabelled palmitic acid, C) Proportion of total PL constituted by labelled palmitic acid (D31). D) Pie chart depicting the mean contribution of either labelled or unlabelled palmitic acid to the PL palmitic acid fraction. E) Table of statistics. Data presented as mean +/- SD, n = 6 per treatment unless stated otherwise. Abbreviations: OH→OL, first week at high (800µM) and second week at low (200µM) of OPLA; OH→OH, two weeks at high of OPLA; PH→PL, first week at high and second week at low of POLA; PH→PH, two weeks at high of POLA; PH→OL, first week at high POLA and second week at low of OPLA; PH→OH, first week at high of POLA and second week at high of OPLA. Significance levels indicated are * $p<0.05$, ** $p<0.01$ and *** $p<0.001$.

There were no significant differences in the proportion of stearic acid (labelled or unlabelled), to the total PL pool (Figure 4.11a). The relative proportions of total PL made up by either stable-isotope labelled stearic acid, or unlabelled stearic acid can be seen in Figures 4.11c and 4.11b respectively. Figure 4.11d, shows the mean contribution from either labelled or unlabelled stearic acid to total amount of stearic acid.

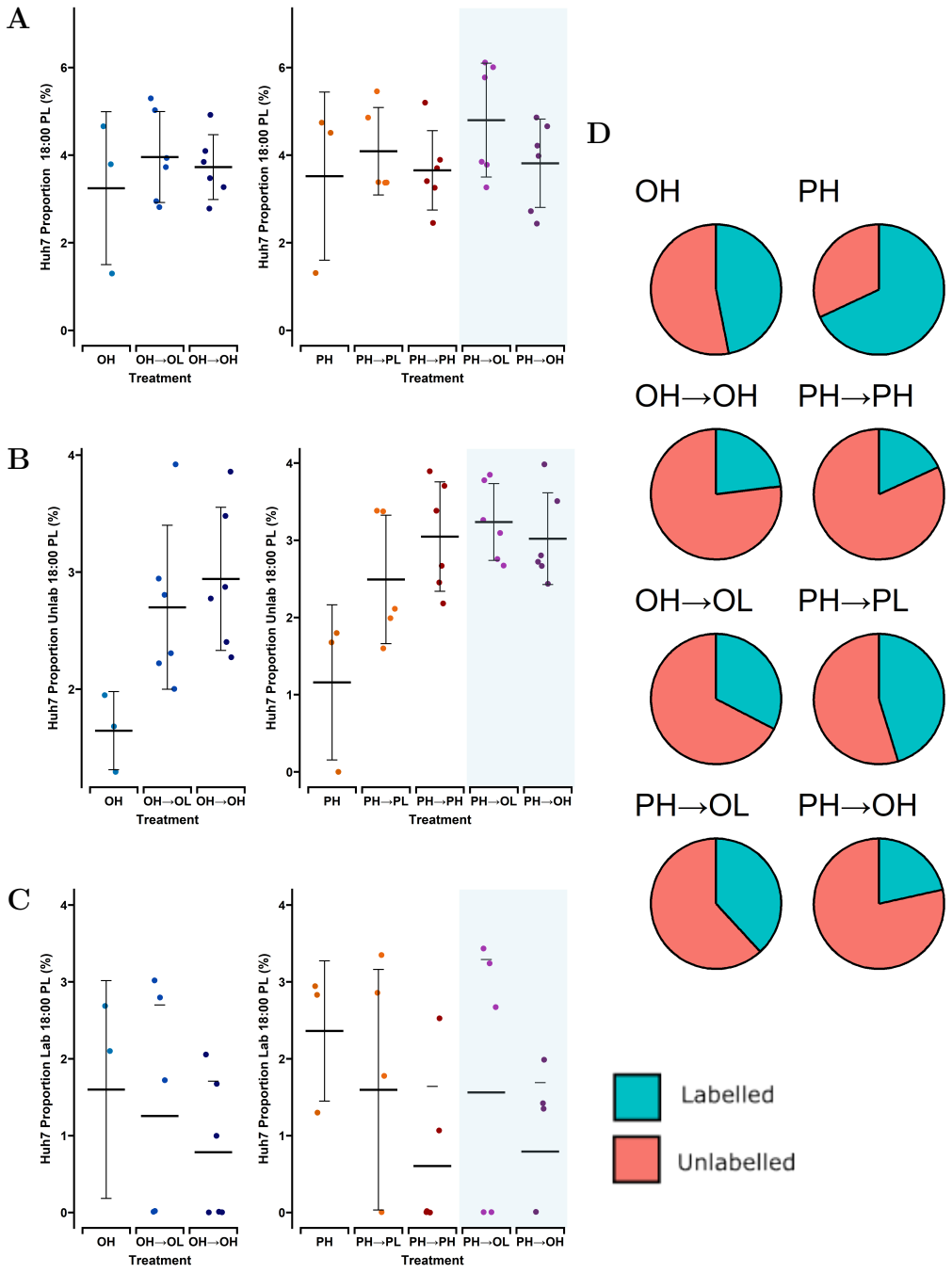
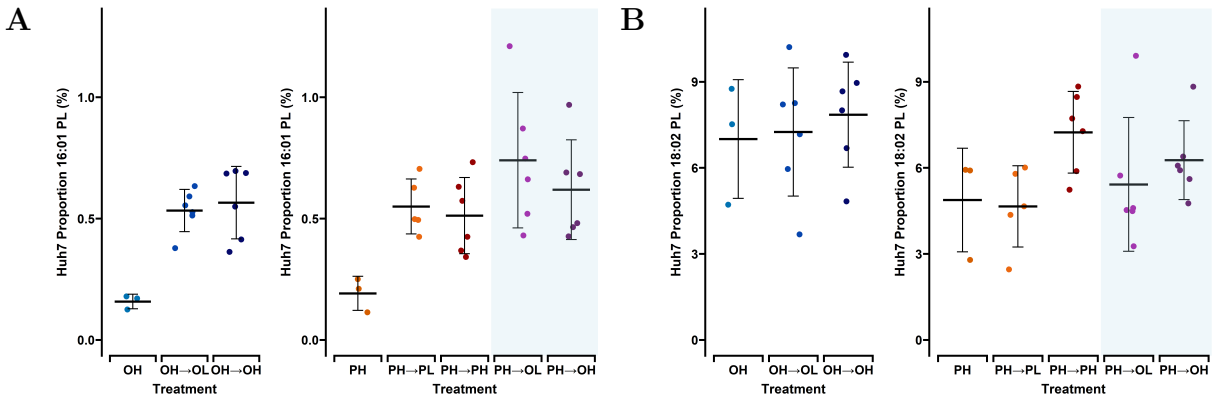


Figure 4.11: Huh7 intrahepatocellular phospholipid (PL) stearic acid composition following treatment with fatty acids (FA) . Data quantified by gas chromatography. A) Proportion of total PL constituted by either labelled or unlabelled stearic acid, B) Proportion of total PL constituted by unlabelled stearic acid, C) Proportion of total PL constituted by labelled stearic acid (D-33 18:1n-9). D) Pie chart depicting the mean contribution of either labelled or unlabelled stearic acid to the PL stearic acid fraction. Data presented as mean +/- SD, n = 6 per treatment unless stated otherwise. Abbreviations: OH→OL, first week at high (800µM) and second week at low (200µM) of OPLA; OH→OH, two weeks at high of OPLA; PH→PL, first week at high and second week at low of POLA; PH→PH, two weeks at high of POLA; PH→OL, first week at high POLA and second week at low of OPLA; PH→OH, first week at high of POLA and second week at high of OPLA. Significance levels indicated are * $p<0.05$, ** $p<0.01$ and *** $p<0.001$.

There was no significant difference in the contribution of linoleic acid to the total PL pool between treatments (Figure 4.12a). There was however, a significant increase in the proportion of palmitoleic acid in the IHPL pool comparing cells treated with OPLA for 7 days with those treated for days 7-14, with either high OPLA or low OPLA. In cells treated with POLA for the first 7 days there was a significant difference between cells treated with another 7 days at a low concentration of POLA and cells treated for just 7 days with POLA (Figure 4.12b).



C

Data	Comparison	Significance
Palmitoleic acid	OH & OH→OL	**
	OH & OH→OH	*
	PH & PH→PL	*

Figure 4.12: Huh7 intrahepatocellular phospholipid (PL) palmitoleic acid composition following treatment with fatty acids (FA). Data quantified by gas chromatography. A) Proportion of total PL constituted by palmitoleic acid, B) Proportion of total PL constituted by linoleic acid. D) Pie chart depicting the mean contribution of either labelled or unlabelled palmitoleic acid to the PL palmitoleic acid fraction. E) Table of statistics. Data presented as mean +/- SD, n = 6 per treatment unless stated otherwise. Abbreviations: OH→OL, first week at high (800µM) and second week at low (200µM) of OPLA; OH→OH, two weeks at high of OPLA; PH→PL, first week at high and second week at low of POLA; PH→PH, two weeks at high of POLA; PH→OL, first week at high POLA and second week at low of OPLA; PH→OH, first week at high of POLA and second week at high of OPLA. Significance levels indicated are * $p<0.05$, ** $p<0.01$ and *** $p<0.001$.

4.3.3 Analysis of cellular treatment media

The composition of the treatment media after culturing the cells was considered on the last day of the timeline, day 14. Figure 4.13a, shows the total amount of FA in the media (all FA species). Data show that there was no significant difference in the amount of media FA, despite the culturing media initially containing different amount of FA and can be seen in Appendix Figure A.9a.

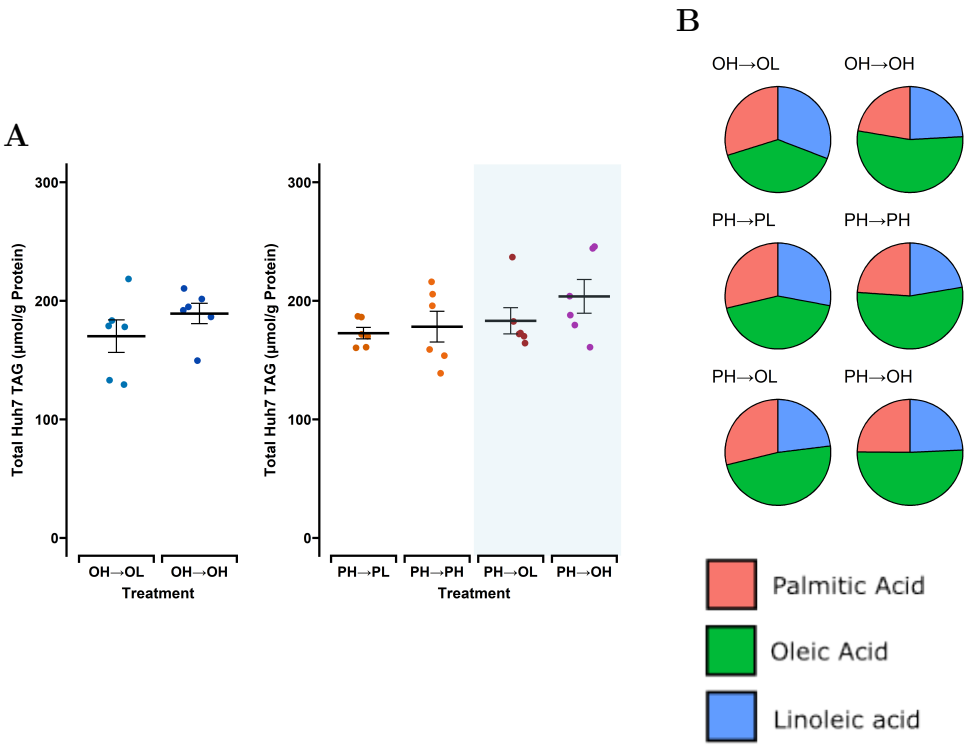
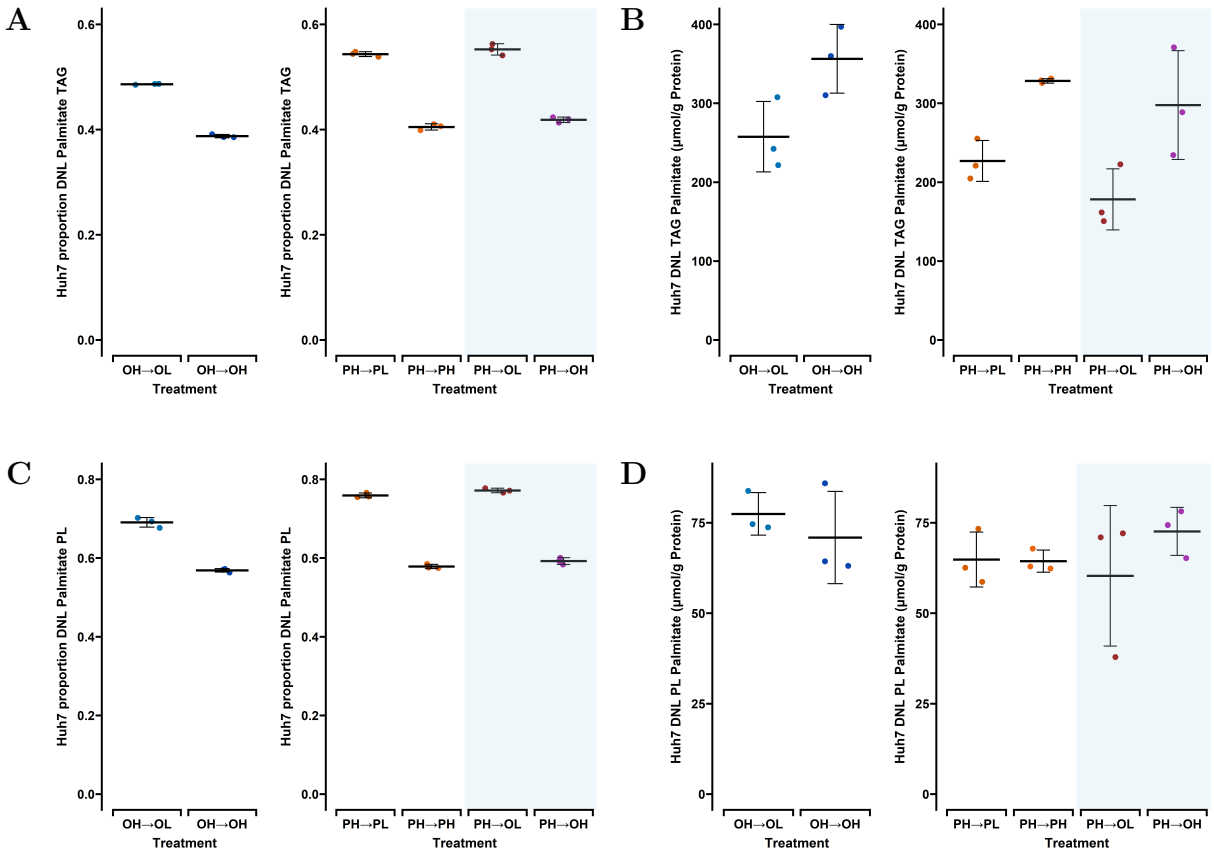


Figure 4.13: Huh7 media triacylglycerol (TAG) content in Huh7 cells following treatment with fatty acids (FA). Data quantified by gas chromatography. A) Total Media FA B) Pie charts depicting the mean contribution of each constituent FA of OPLA or POLA (excluding ∝-linolenic acid as it contributed less than 1% of treatment media). Data show proportion of linoleic acid, oleic acid and palmitic acid (colours, green, red and blue respectively. Data presented as mean +/- SD, n = 6 per treatment unless stated otherwise. Abbreviations: OH→OL, first week at high (800µM) and second week at low (200µM) of OPLA; OH→OH, two weeks at high of OPLA; PH→PL, first week at high and second week at low of POLA; PH→PH, two weeks at high of POLA; PH→OL, first week at high POLA and second week at low of OPLA; PH→OH, first week at high of POLA and second week at high of OPLA. Significance levels indicated are * $p<0.05$, ** $p<0.01$ and *** $p<0.001$.

4.3.4 Contribution of DNL in to intrahepatocellular fat

The effect of extending the cellular treatment to 14 days, and changing the FA treatment composition and concentration on the contribution of DNL derived palmitic acid to IHTAG was assessed. Deuterated water was provided for the initial 7 days but not days 7-14, thus any labelled DNL derived palmitic acid was synthesised using the provided deuterated water in the first 7 days only. In the IHTAG pool, there was a significantly higher ratio of labelled DNL derived palmitic acid compared to unlabelled palmitic acid in cells which were exposed to a lower concentration of FA between days 7-14 and treatment composition had no significant effect on the ratio of labelled DNL derived palmitic acid to unlabelled palmitic acid (Figure 4.14a). Adjusting for the amount of palmitic acid present in the cell, i.e. accounting for the increase in treatment FA and changes in composition, there was a trend towards an increase in the amount of DNL derived palmitic acid for those cells treated with a higher concentration of FA between days 7-14, although this was not significant (Figure 4.14b). Investigating DNL-derived palmitic acid within the PL fraction revealed that cells treated with lower concentrations of FA showed an increased ratio of labelled DNL derived palmitic acid compared to unlabelled palmitic acid in the PL fraction, but no significant differences were seen when adjusting for the concentration of palmitic acid within the cells (Figures 4.14c, 4.14d).



E

Data	Comparison	Significance
TAG DNL F factor	OH→OL & OH→OH	***
	PH→PL & PH→PH	****
	PH→OL & PH→OH	**
PL DNL F factor	OH→OL & OH→OH	**
	PH→PL & PH→PH	****
	PH→OL & PH→OH	****

Figure 4.14: Huh7 contribution of *de novo* lipogenesis (DNL) to intrahepatic triacylglycerol (TAG) or phospholipid (PL) content following treatment with fatty acids (FA). Data determined by gas chromatography and mass spectrometry. A) F factor for TAG DNL; B) DNL derived palmitate TAG; C) F factor for PL DNL; D) DNL derived palmitate PL; E) Table of statistics. Data presented as mean +/- SD, n = 3 per treatment unless stated otherwise. Abbreviations: OH→OL, first week at high (800µM) and second week at low (200µM) of OPLA; OH→OH, two weeks at high of OPLA; PH→PL, first week at high and second week at low of POLA; PH→PH, two weeks at high of POLA; PH→OL, first week at high POLA and second week at low of OPLA; PH→OH, first week at high of POLA and second week at high of OPLA. Significance levels indicated are * $p<0.05$, ** $p<0.01$ and *** $p<0.001$.

4.3.5 Huh7 cellular oxidation

The oxidation of FA was also measured and no significant differences were observed with either treatment composition or concentration (Figure 4.15a). Additionally, there was no significant difference in media concentrations of 3OHB (Figure 4.15b).

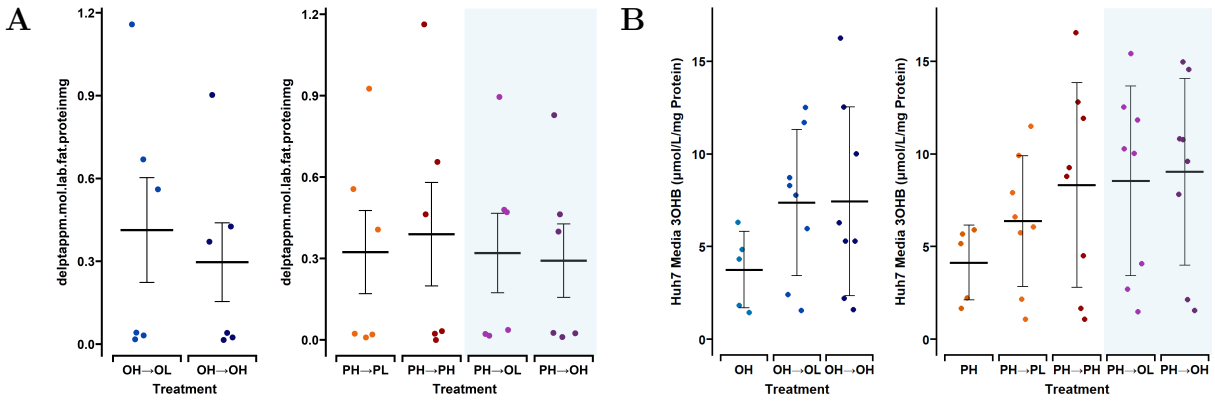


Figure 4.15: Huh7 cellular oxidation following treatment with fatty acids (FA). A) Oxidation as measured by isotope-ratio mass spectrometry (IRMS), B) Media 3OHB quantified with a clinical biochemistry analyser. Data presented as mean +/- SD, n = 6 per treatment unless stated otherwise. Abbreviations: OH→OL, first week at high (800µM) and second week at low (200µM) of OPLA; OH→OH, two weeks at high of OPLA; PH→PL, first week at high and second week at low of POLA; PH→PH, two weeks at high of POLA; PH→OL, first week at high POLA and second week at low of OPLA; PH→OH, first week at high of POLA and second week at high of OPLA. Significance levels indicated are * $p<0.05$, ** $p<0.01$ and *** $p<0.001$.

4.3.6 Huh7 glucose metabolism

Figure 4.16a, shows the glucose uptake adjusted for protein content with no significant differences between the treatment groups. Additionally, there were no significant differences between the treatment conditions in media lactate concentrations (Figure 4.16b). Figure 4.16c, shows intracellular glycogen content, with no significant differences arising from changes in composition or concentration of FA treatment. However, there was a trend towards increased glycogen concentration between cells treated for 14 days with high concentrations of OPLA between days 7-14 compared to those treated with low concentrations of OPLA for days 7-14. Moreover, there were no significant differences in cellular glucose release when cells were stimulated with or without insulin or glucagon following any FA treatment (Figure 4.16d).

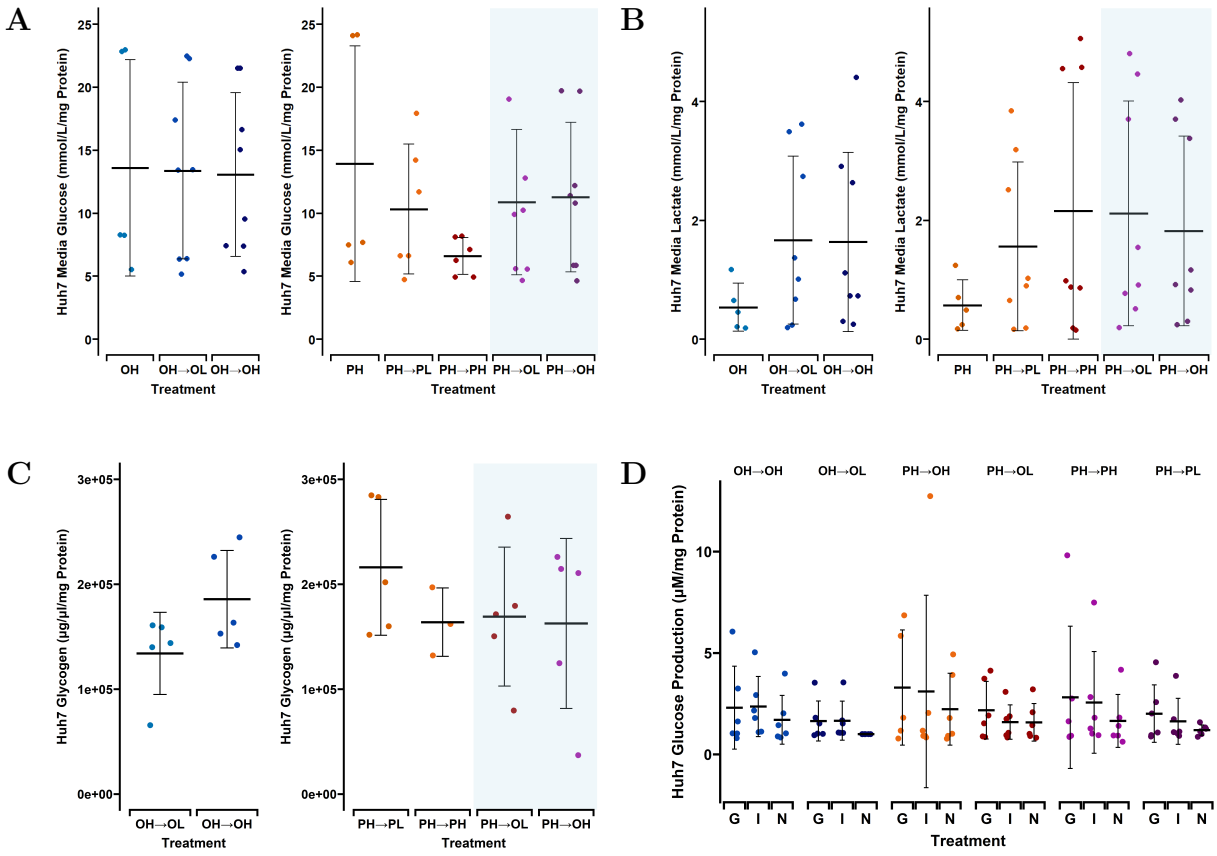


Figure 4.16: Huh7 quantification of glucose metabolism following treatment with fatty acids (FA). A) Media glucose uptake measured by clinical biochemistry analyser; B) Media lactate measured by clinical biochemistry analyser; C) Intracellular glycogen; D) Glucose production. Data presented as mean +/- SD, n = 6 per treatment unless stated otherwise. Abbreviations: OH→OL, first week at high (800µM) and second week at low (200µM) of OPLA; OH→OH, two weeks at high of OPLA; PH→PL, first week at high and second week at low of POLA; PH→PH, two weeks at high of POLA; PH→OL, first week at high POLA and second week at low of OPLA; PH→OH, first week at high of POLA and second week at high of OPLA. Significance levels indicated are * $p<0.05$, ** $p<0.01$ and *** $p<0.001$.

4.3.7 Confocal imaging of Huh7 FA treated cells

Cells were visualised as described in Chapter 2 Section 2.2.8 shown in Figures 4.17a - 4.19a. These images of cells treated with different FA concentrations and compositions showed distinct variation in LD size and quantity, with POLA treated cells showing more small LDs and OPLA treated cells showing larger LDs. There was a visual increase in LD quantity with increased FA treatment. LD area was quantified with Cell Profiler and data are shown in Figure 4.20a. As Cell Profiler data was comprised on technical replicates, statistical analysis was not undertaken but data recapitulate the morphological patterns observed.

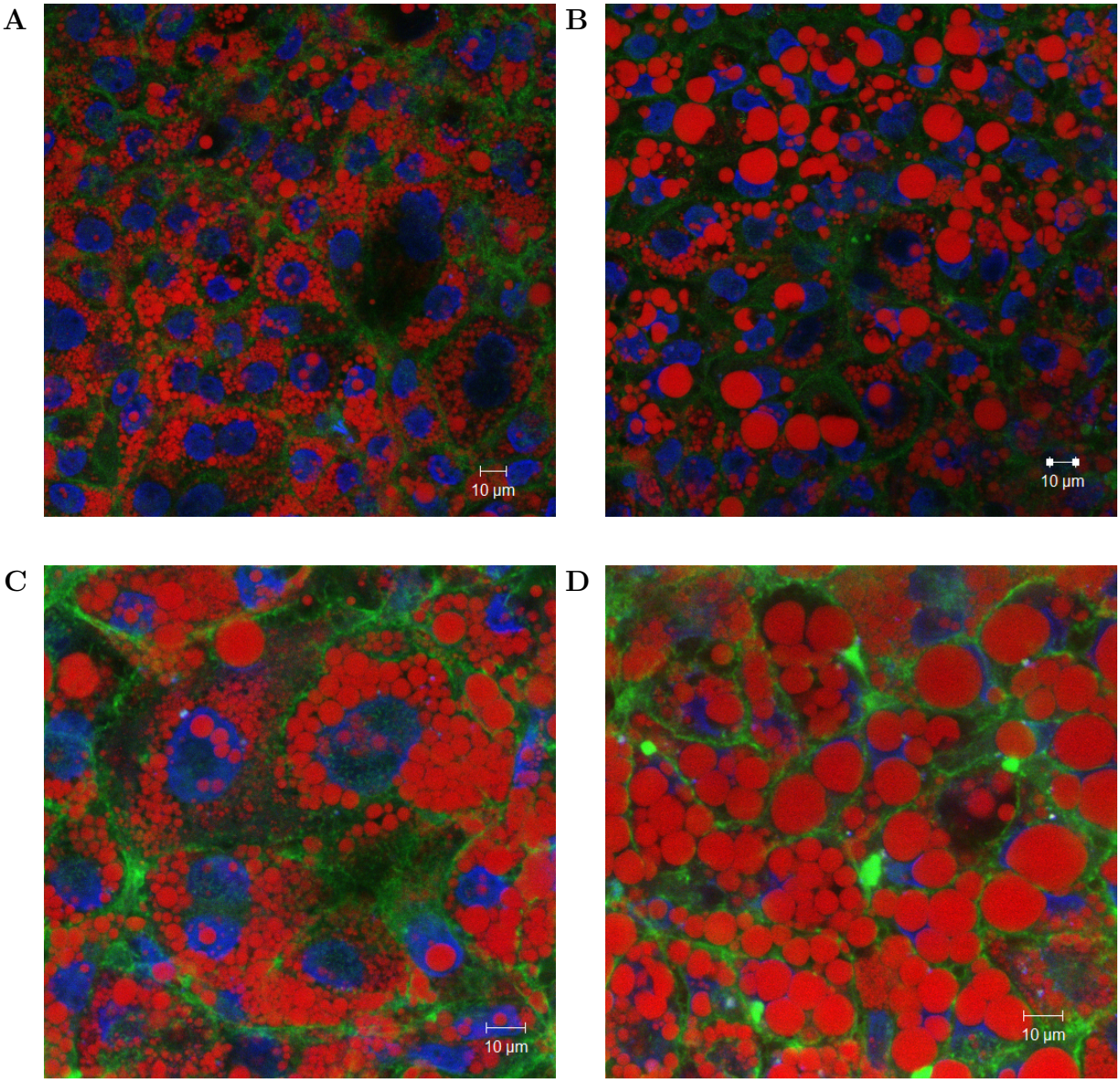


Figure 4.17: Confocal imaging of fluorescent stained lipid droplets (LDs) in Huh7 cells treated for 2-weeks with OPLA of at either high concentration (OH), or high then low concentration (OL). A) OH→OL; B) OH→OL; C) OH→OH; D) OH→OH; Staining: a α-Tubulin stain in green, red lipotox lipid droplet stain, blue DAPI nuclear stain.Abbreviations: OH→OL, first week at high (800µM) and second week at low (200µM) of OPLA; OH→OH, two weeks at high of OPLA; PH→PL, first week at high and second week at low of POLA; PH→PH, two weeks at high of POLA; PH→OL, first week at high POLA and second week at low of OPLA; PH→OH, first week at high of POLA and second week at high of OPLA. Significance levels indicated are * $p<0.05$, ** $p<0.01$ and *** $p<0.001$.

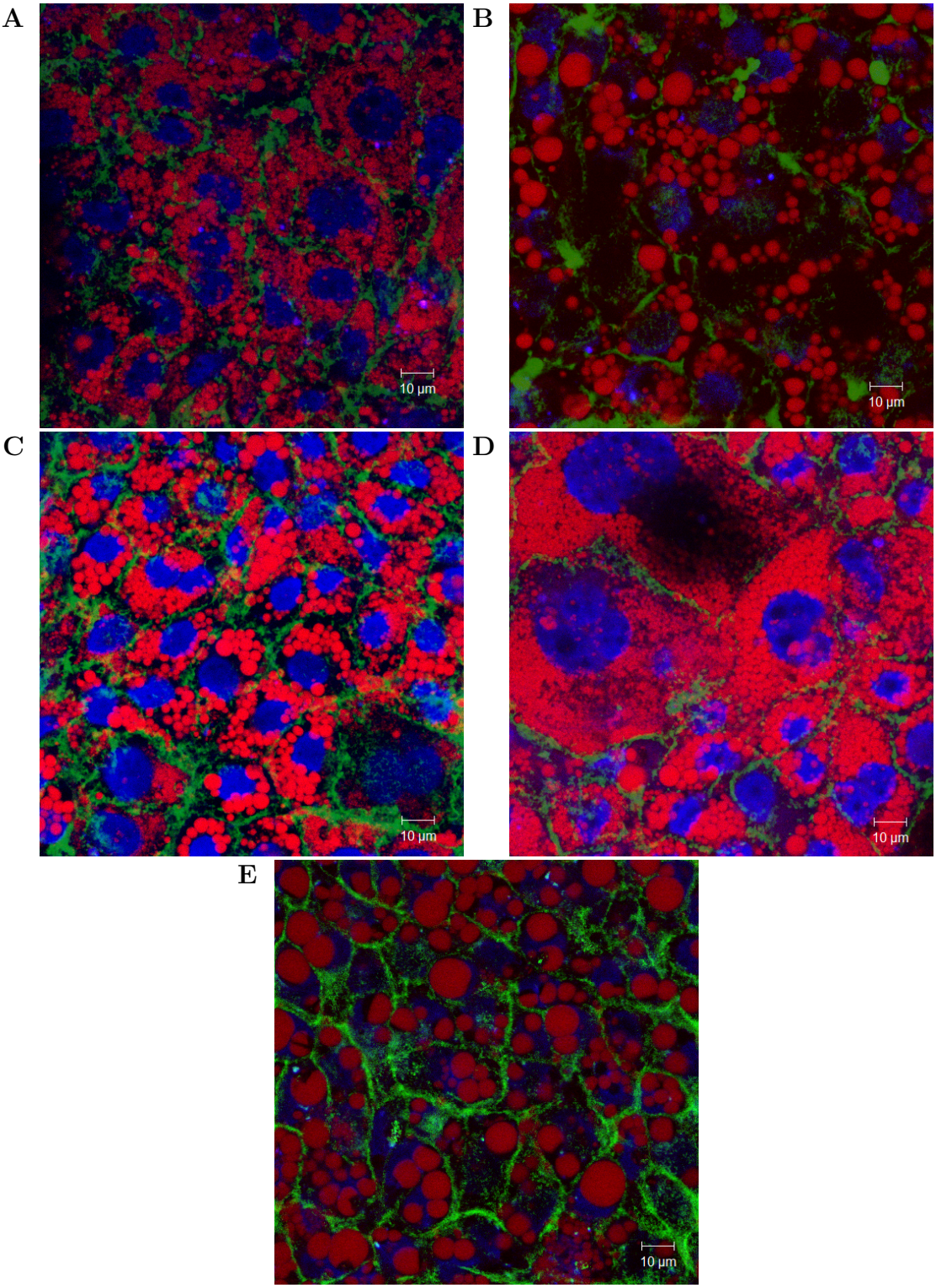


Figure 4.18: Confocal imaging of fluorescent stained lipid droplets (LDs) in Huh7 cells treated for 2-weeks with POLA of at either high concentration (PH), or high then low POLA concentration (PL) or low OPLA concentration (OL). A) PH→PL; B) PH→PL; C) PH→PH; D) PH→PH; E) PH→OL; F) PH→OL; Staining: a α-Tubulin stain in green, red lipotox lipid droplet stain, blue DAPI nuclear stain.Abbreviations: OH→OL, first week at high (800µM) and second week at low (200µM) of OPLA; OH→OH, two weeks at high of OPLA; PH→PL, first week at high and second week at low of POLA; PH→PH, two weeks at high of POLA; PH→OL, first week at high POLA and second week at low of OPLA; PH→OH, first week at high of POLA and second week at high of OPLA. Significance levels indicated are * $p<0.05$, ** $p<0.01$ and *** $p<0.001$.

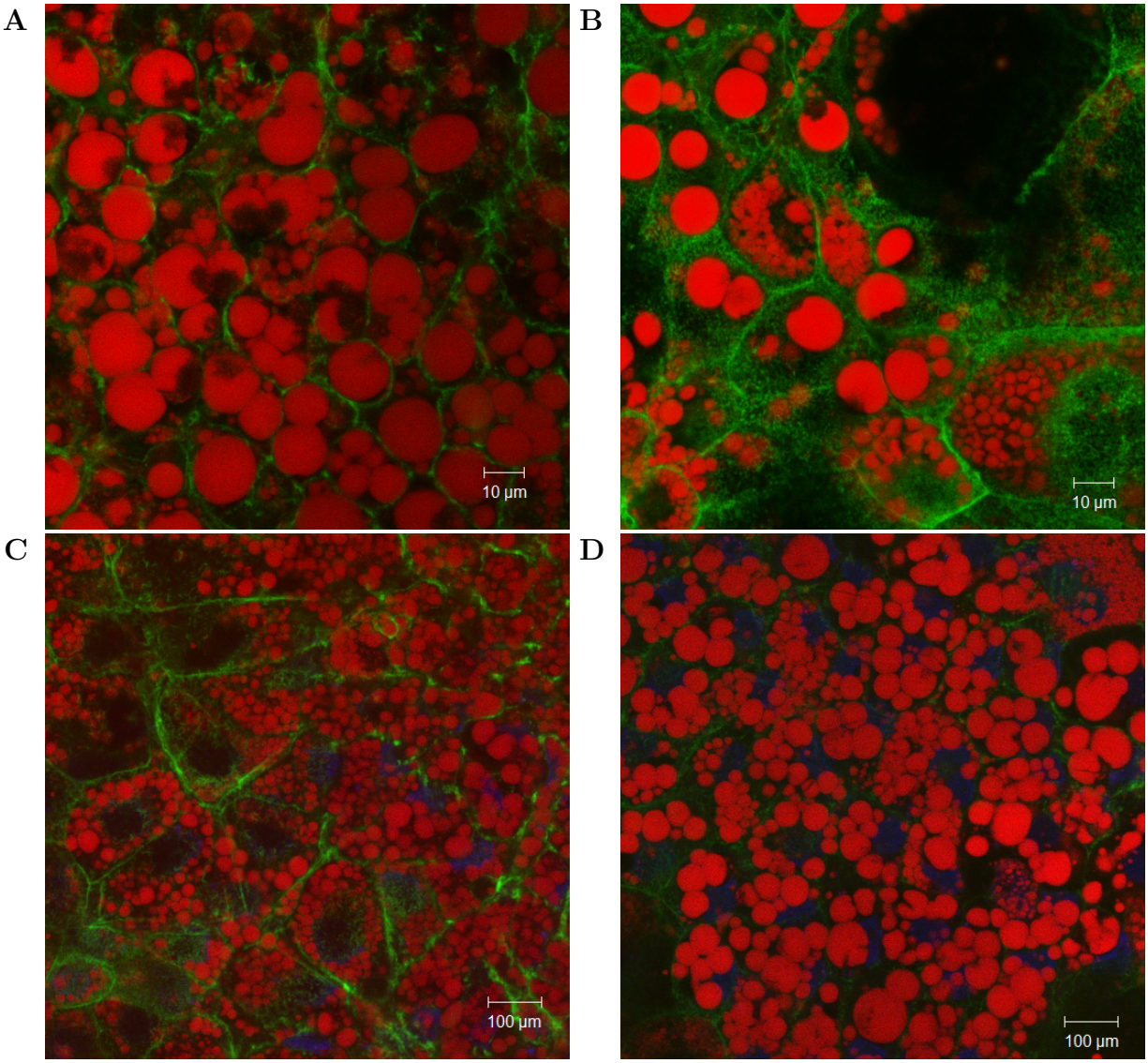


Figure 4.19: Confocal imaging of fluorescent stained lipid droplets (LDs) in Huh7 cells treated for 2-weeks with POLA of at a high concentration (PH) then OPLA at a high concentration (OH). A) PH→OH; B) PH→OH; C) PH→OH; D) PH→OH. Staining: a α-Tubulin stain in green, red lipotox lipid droplet stain, blue DAPI nuclear stain.Abbreviations: OH→OL, first week at high (800µM) and second week at low (200µM) of OPLA; OH→OH, two weeks at high of OPLA; PH→PL, first week at high and second week at low of POLA; PH→PH, two weeks at high of POLA; PH→OL, first week at high POLA and second week at low of OPLA; PH→OH, first week at high of POLA and second week at high of OPLA. Significance levels indicated are * $p<0.05$, ** $p<0.01$ and *** $p<0.001$.

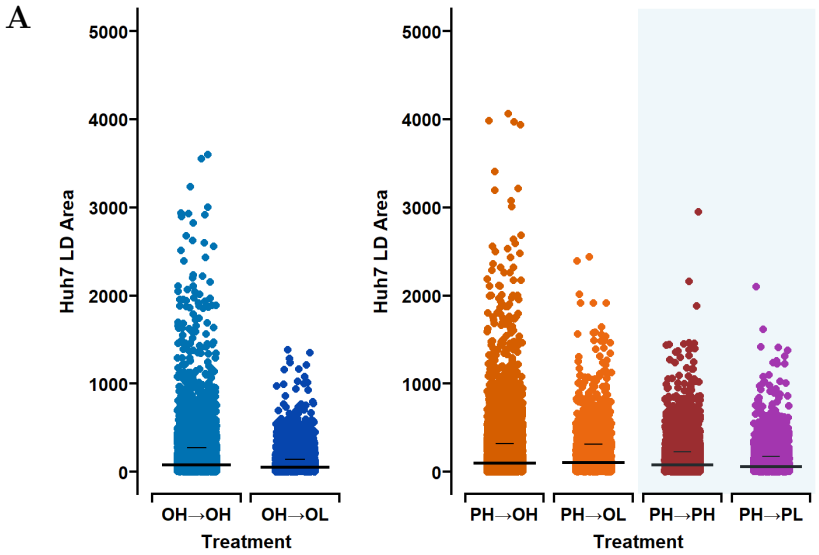


Figure 4.20: Huh7 quantification of lipid droplet (LD) size following treatment with fatty acids (FA). Quantified using cell profiler (section 4.2.3). A) quantification of LD area. Droplets are pooled from analysis of two cover slips, with 5 images taken per cover slip. No Lipid droplets were present in a no-fat control to quantify.Abbreviations: OH→OL, first week at high (800µM) and second week at low (200µM) of OPLA; OH→OH, two weeks at high of OPLA; PH→PL, first week at high and second week at low of POLA; PH→PH, two weeks at high of POLA; PH→OL, first week at high POLA and second week at low of OPLA; PH→OH, first week at high of POLA and second week at high of OPLA. Significance levels indicated are * $p<0.05$, ** $p<0.01$ and *** $p<0.001$.

4.4 Discussion

This chapter characterised potential changes in the metabolism and storage of fat and glucose in Huh7 cells which had been exposed to two consequetive FA treatment periods each 7 days long differing by FA tracer, aiming to investigate the effects of changing FA composition and concentration within the context of preexisting IHTAG accumulation, of either a more SFA composition (POLA) or more MUFA composition (OPLA). Understanding the effects of preexisting TAG accumulation within cells is often under-considered, particularly given that the predominant treatment of MASLD is through lifestyle changes, with the context of pre-existing hepatic steatosis (Ray 2013). Data illustrated how the fat makeup of the hepatocytes shifted to resemble that of the current FA treatment, implying non selective uptake of the provided treatment NEFA. As the changes in treatment composition did not completely match that of the new FA treatment we can infer that the FA provided the week before was not turned over (through secretion or oxidation) within the period between 7-14 days, aligning with the observed increase in IHTAG across the 14 days.

Data showed that following 14 days of FA treatment, DNL was altered by the concentration of FA provided with increasing DNL derived palmitic acid concentration with increasing treatment concentration. It would typically be expected in a healthy liver for an increase in IHTAG to reduce DNL. The reduced ratio of labelled DNL derived palmitic acid to unlabelled palmitic acid is likely increased in cells treated with low concentrations of FA because they receive less fat to lower the ratio, rather than an increase in DNL.

Despite no increase in glucose uptake between the conditions, the appears to be an increase in cellular glycogen in cells treated with high concentrations of OPLA compared to low concentrations of OPLA for days 7-14 suggests that the amount of FA provided in the treatment is altering glucose handling although further work is needed. Considering glucose production, all treatments resulted in a blunted response to hormonal stimulation, again more influenced by FA treatment

concentration rather than composition. With higher FA treatment, cells appear to be storing more glucose, as either glycogen or lipid through DNL and secreting less, despite having excess energy from the FAs.

In Chapter 3, it was observed that treatment with POLA resulted in numerous small LDs and larger LDs were seen with OPLA treatment. Extending the treatment period to 14 days instead of 7, again resulted in numerous small LDs in cells treated with POLA throughout the 14 days, particularly at a higher concentration. The addition of OPLA to the cells previous treated with POLA resulted in large LDs forming, implying that the changing media composition influenced the mechanism underlying the smaller size of the LDs with POLA. One plausible mechanism for the enlargement of LDs is through peroxisomal activity where OPLA may upregulate peroxisomal activation and consequently the LDs become larger through a PEX2 induced mechanism as discussed in Chapter 3 (Ding et al. 2021). However, cells treated with a higher concentration of POLA followed by a higher concentration of OPLA, displayed variation in LD size between cells with some maintaining only the pattern induced by POLA treatment with small LDs and others expanding the LDs to be more similar to the OPLA cells. The causes of the variation in cells LD pattern in cells treated with POLA then OPLA have yet to be elucidated.

4.5 Conclusion

When extending the treatment period and altering both the FA composition and concentration of the treatment media, cells exhibit an in-adaptive response by continuously absorbing FA, the composition of which reflects that of the current treatment media. The prolonged exposure to FA resulted in the expansion of LDs when exposed to OPLA compared to POLA. Treatment with increased FA also resulted in trends towards increased glucose storage, either as glycogen or as palmitic acid and a blunted response in glucose production with hormone stimulation implying lost flexibility in glucose metabolism and potentially aberrant storage and reduced oxidation.

5

In vitro model of uptake of TAG-rich remnants enriched in either UNSFA or SFA by Huh7 cells

5.1 Introduction

Dietary fat enters the circulation and travels to liver via two distinct pathways: either as CM derived spill over NEFA or as TAG within CM remnants (Cooper 1997; Hagenfeldt et al. 1972). Despite the two distinct pathways for delivery of dietary FA, the majority of research has only considered the contribution of NEFA to hepatic FA metabolism and storage. TAG-rich remnants (CM and VLDL remnants), have long been speculated to play a significant role in intrahepatic lipid metabolism, including contribution to the development of MASLD, however the potential mechanisms and size of the contribution from this FA source remain unclear (Côté et al. 2014). TAG-rich remnants are taken up by the LDL receptor via endocytosis, and once within the liver, travel to the endosome to be hydrolysed (Havel et al. 1988). However, these pathways require further study to resolve the temporal-spatial movements of the TAG-rich remnants within the cells. Whilst research has focused on the kinetics of the LDL receptor, including investigating the time it takes for these receptors to release the TAG-rich remnants and recycle back to the plasma membrane (Pompey et al. 2013), the fate of the TAG-rich remnant derived FA

requires further elucidation; it remains unknown how hepatocytes process these FA and whether they are prioritised for particular metabolic fates. Additionally, it remains unknown whether there are differences in the handling of the different TAG-rich remnant lipoproteins. Any potential differences in the handling of TAG-rich remnant derived FA may effect their contribution to IHTAG accumulation or affect other cellular metabolic pathways including, FA oxidation and glucose metabolism.

Individuals who present with CM retention disease, characterised by the inability to secrete CMs from enterocytes, present with: failure to thrive, diarrhea, vomiting, abnormal distention and malabsorption of fat (Burnett et al. 1993), indicating the key role CMs have on delivering dietary fat on a whole-body level. The significance of TAG-remnant derived FA to hepatocytes remains to be elucidated. For individuals presenting with dysfunctional adipose tissue metabolism, such as is seen in obesity, a consequence may be that the liver receives a greater flux of TAG-rich remnants, and they may contain a higher amount of TAG if the adipose tissue is inadequately hydrolysing them (Piché et al. 2018).

The lack of knowledge regarding the effect of TAG-rich remnants on hepatic metabolism is not without reason; they are challenging to study as they are isolated from post-prandial blood samples and cannot be stored for a long time. Although synthetic lipoproteins are available, they are predominately used clinically for purposes such as use as drug delivery agents (Müller et al. 2016; Santhekadur et al. 2018; Huang et al. 2015). Moreover, human-derived lipoproteins contain associated proteins, which cannot easily be added to synthetically produced lipoprotein-like particles, and changing the lipid composition (including both TAG and PL fractions) of these particles is challenging (Redgrave et al. 1988). To date, the majority of the limited studies that have investigated differences in TAG-rich remnant metabolism, have used TAG-rich remnants isolated from animals, (Takahashi 2017; Raymond et al. 1986), with very few studying hepatic lipid metabolism. Tabas et al. used a murine model to investigate the interaction between rabbit VLDLs, and human LDL on mouse peritoneal macrophages, investigating the conversion of macrophages to foam cell, initiated by receptor mediated endocytosis of lipoproteins. Tabas et

al., using non-transferable dyes to track the pathways of lipoproteins to deliver cholesterol to microsomal ACAT and they established that the VLDL binds the LDL receptor with greater affinity and induces foam cell formation to a greater extent compared to LDL. VLDL and LDL also demonstrated a different diffusion pattern within the cells with fluorescence emitted by the LDL lipoproteins being within the center of the cell, and fluorescence emitted by the VLDL being diffuse throughout the cytoplasm. These differences were seen as early as two minutes into the experiment and persisted throughout, which may explain why only VLDL and not LDL was able to induce transformation of the macrophage into a foam cell (Tabas et al. 1990).

Hepatic lipase (HL) has been suggested to promote the uptake of CM remnants, with enzymatic activity modifying the surface lipoproteins to expose epitopes of ApoE. HL has also been suggested to act as a glycosaminoglycan anchored lipid to help coordinate the TAG-rich remnant binding to the hepatic plasma membrane. Additionally, LPL is also involved in the process of CM remnant uptake and competes with HL for the remnants and may also compete for remnant internalisation (Diard et al. 1994). Using mice as a model organism, Mortimer et al, investigated TAG-rich remnant metabolism in mice lacking the LDL receptor and ApoE. Despite the lack of LDLR, these mice demonstrated the ability to clear CM remnants through an ApoE independent pathway although this was notably slower (Mortimer et al. 1995).

Zhang et al, investigated differences in the method of FA delivery to the liver in a murine model, incubating for either 3 or 6 hours using either 6mM of oleic acid complexed with albumin, 0.5-20% intralipid or saline. Both fat infusions showed similar increases in plasma fat concentration, however, plasma TAG only significantly increased after infusion of between 4-20% Intralipid. ApoB secretion was increased by 6 hour infusions of either oleic acid or between 4-20% Intralipid. Despite a concentration of 0.5-2% intralipid delivering more lipid to the plasma than the 6mM of oleic acid did, it did not stimulate ApoB secretion but the NEFA infusion did although neither infusion altered ApoB mRNA concentration. Hepatic microsomal TAG transfer protein (MTTP) mRNA was significantly lower after the 6 hour infusions with the oleic acid when compared to either the saline

control of the maximum concentration (20%) of Intralipid, associated with reduced IHTAG following the 6 hour infusion with oleic acid (Zhang et al. 2004). These data illustrate that there are metabolic distinctions within the murine hepatocyte depending on the mode of fat delivery.

Research investigating the effect of different FA composition of lipoprotein metabolism has been carried out by López-Soldado et al, who generated CM-remnant-like-particles (CRLP), using either palm, olive or corn oil which produced particles enriched in SFA, UNSFA, or n-6 PUFA respectively. Particles were then bound to rat ApoE and added to the culture media of primary rat hepatocytes for 5 hours (0.3µmol of TAG/ml) before a CRLP-free media was added for 16 hours. It was found that TAG secretion increased following treatment with SFA or PUFA CRLPs when compared to UNSFA CRLPS or a CRLP-free control. Apolipoprotein B RNA expression in primary rat hepatocytes decreased following treatment with UNSFA and PUFA CRLPS. HMG-CoA mRNA was increased with SFA CRLPS and this was associated with the production of cholesterol. Thus, the increase in secreted TAG was possibly because of the secretion of larger particles for those cells treated with PUFA TAG CLRPs (López-Soldado et al. 2009a). Whether the same effect would be seen in human hepatocytes remains to be seen.

Another study carried out by Soldado et al used CRLPs, generated from either palm or fish oil, enriched in SFA or n-3 PUFA respectively, in the culture media for rat hepatocytes for 24 hours. Consequently, HNF-4α protein and RNA were significantly decreased by CRLPs enriched in n-3 PUFA but not changed with CRLPs enriched with SFA and the mRNA expression of the target genes were consequentially lowered (HNF-1α, apolipoprotein B and MTTP). This decrease may explain the previously observed decrease in VLDL secretion seen following a diet enriched in omega-3 PUFAs (López-Soldado et al. 2009b).

This chapter aimed to study the effect of dietary derived TAG-rich remnants on hepatocytes and whether there were any differences in hepatic uptake of TAG-rich remnants if the hepatocytes have already accumulated IHTAG. This chapter also

aimed to investigate whether there were any differences in uptake of TAG-rich remnants if the TAG composition varied to be either enriched in SFA of UNSFA.

5.2 Methods

Clinical work to obtain TAG-rich remnants was carried out thanks to the help of clinical research nurses Sarah White and Diana Mantripp at OCDEM.

Refer to general methods (Chapter 2) for routine cell culturing, lipid extraction techniques and analysis of metabolites (glucose, 3-OHB, urea, lactate, TAG, NEFA).

5.2.1 Volunteers

Three men volunteered to take part in this study. All were free from any known metabolic disease, aged between 28-58 years, body mass index >25 and <30kg/m^2, were not taking medication known to affect lipid or glucose metabolism and did not smoke or consume alcohol above recommended limits (Chalasani et al. 2012). Volunteers gave written informed consent, and the study was approved by the University of Oxford Medical Sciences Interdivisional Research Ethics Committee (IDREC) (R75046/RE001).

5.2.2 Dietary intervention

Participants undertook two, 3-day dietary intervention periods prior to a post-prandial study day with a 3-week washout period between dietary interventions. The intervention diets were the same in macronutrient composition but differed in FA composition, with one being enriched with SFA, the other with UNSFA. The diets were designed (by Paige O'Rourke) to be as close as possible to the compositions of OPLA and POLA that were used in all *in vitro* cellular experiments. The order in which participants consumed the SFA and UNSFA diets was randomized, and the total calories provided were in line with their habitual energy expenditure (EE), which was calculated using the following formula:

$$EE = (10 \times weight(kg)) + (6.25 \times height(cm)) - (5 \times age(years)) + 5$$

*Thermic effect of food not included in estimation **A physical activity adjustment was included as 1.4 for those who lead a sedentary life, and 1.7 for those who are moderately active.

The diets aimed to provide macronutrients at the ratios of 25-30% CHO, 10-15% protein, 55% FA as a percent of total caloric intake with FA as either 20% SFA and 80% UNSFA for the diet enriched in UNSFA, or 55% SFA and 45% UNSFA for the diet enriched in SFA. It proved challenging to keep the protein and CHO consistent between diets and the UNSFA enriched diet had a higher protein intake compared to the SFA enriched diet, but both were within range.

5.2.3 Post-prandial study day

Following consumption of the experimental diet, participants had a post- prandial study day. For 24 hour before the study day, participants were asked to avoid particularly strenuous exercise. On the study day, after an overnight fast participants came to the clinical research unit and a cannula was inserted into an antecubital vein, and baseline (time 0) blood and breath samples taken. Whole blood was collected into heparinized syringes (Starstedt) and breath samples were collected in an EXETAINER® tube (LabcoLtd, High Wycombe, UK). Participants were fed a mixed test meal, consisting of 40g Rice Krispies (Kelloggs), 200g skimmed milk and a chocolate drink containing 40g oil (test meal contained 42g fat, 44g carbohydrate). The proportions of the fat in chocolate drink were altered to match the composition of the dietary intervention - either enriched with UNSFA (25% palmitate, 42% oleate, 30% linoleate, 1% stearate) or SFA (32% palmitate, 35% oleate, 27% linoleate, 5% stearate). These FA proportions were confirmed with GC (data not shown). 200mg of $U^{13}C$ palmitic acid was added to the chocolate drink to trace the fate of the dietary FA.

After consumption of the mixed meal, repeated blood and breath samples were taken at the following time intervals: 120, 180, 240, 300, 360 minutes post-prandial. Following collection, blood was immediately centrifuged at 4xg for 10 minutes. At each time point, 3mL of plasma was collected in LP4 tubes with added preservative: 2µL EDTA (VWR, 100935) at 0.5mol/L ph7.4, 1µL PMSF (Sigma, 93482), (10mmol/L in propan-2-ol(Anhydrous) (VWR, 83677.230), 5µL trasylol (Bayer), (10,000 KIE/ml). Remaining plasma was frozen until required

for analysis. At time 0, and 180 minutes, VO_2 max calculations were performed on the metalizer (Cortex). Measurements were taken over a 10 minute period to determine whole body CO_2 production and whole body respiratory exchange ratio (RER), and net carbohydrate and fat oxidation rates.

5.2.4 Remnant isolation

Remnant isolation was carried as has previously been done within the group (Hodson et al. 2007). The density of the plasma was increased using NaBr to d1.10kg/l by adding 0.5ml of NaBr (d1.42kg/l) for each mL of plasma, ignoring the volume of preservative. 4mL of this density adjusted plasma were reverse pipetted into ultra-clear centrifuge tube (Beckman, 344060) coated in poly-vinyl-alcohol (PVA). A density gradient made with NaCl was generated above the plasma using syringes with a internal diameter less than 0.7 mm angled with the bevel against the side of the tube and the following were added: 3mL of 1.063kg/L, 1.02kg/L, 1.006kg/L, sequentially.

Separation of the TAG-rich remnants used chylomicron-Svedberg flotation rate (Sf) >400 and VLDL-rich fraction (Sf20-400) which were made by sequential flotation using density gradient ultracentrifugation (Hodson et al. 2007). Ultracentrifugation was performed in a SW40Ti swinging bucket rotor (Beckman Instruments) at 40,000rpm at 14°C. The gradients were run for 32 minutes to float Sf >400, for 3 hours 28 minutes to float VLDL 1 lipoproteins and for a further 16 h to float Sf 20 – 250 VLDL2 lipoproteins. Between each run the tubes were topped up with 1.006kg/L NaCl.

5.2.5 LDL receptor expression

As TAG-rich remnants are taken up by receptors, we checked that Huh7 cells expressed the LDL receptor. We found that Huh7 cells expressed LDLR in a pilot experiment where we collect TAG-rich remnants from multiple donors, we found that cells took up TAG-rich remnants (data not shown).

5.2.6 Labeling of isolated fraction

To establish a method of *ex vivo* labelling of the remnant particles, protocols from Kalyani G. Bharadwaj were adapted for this study (Bharadwaj et al. 2010). Following the isolation of the remnants, the addition of a ^{13}C tri-palmitin (ThermoFisher, 10608074) label was optimised. To begin, two amounts of ^{13}C tri-palmitate were used: 5mg and 50mg, which were dissolved in 200µL of chloroform. The chloroform was left to evaporate, leaving the ^{13}C tri-palmitin coating the bottom of a 4.5mL glass tube to which the aspirated remnants were added. For the pilot protocol, two incubation times were tested: i) a shorter period of 1 hour, and ii) an overnight incubation at 37°C on a shaker. Additionally, a re-isolation step, using the same isolation protocol as before was tested compared to not re-isolating the TAG-rich remnants.

5.2.7 Cell treatment

Prior to treatment of Huh7 cells with TAG-rich remnants, cells were cultured with the treatment medias described in Chapter 2. Experimental proceedure can be seen in Figure 5.1. Cells were either treated with a no-fat control, containing low-glucose DMEM (5.5mM), 1% P/S, and 2% HS or cells were treated with FAs. For this chapter, 400µM of FA were used in the treatment mixture to account for the additional FA added in the form of TAG-rich lipoproteins. The FA treatments added were either OPLA or POLA to match the composition of the diet given to the participants prior to collecting and isolating the TAG-rich remnants. Cells were then cultured for 48 hours. TAG-rich remnants were then applied to the cells and cultured for 2 days.

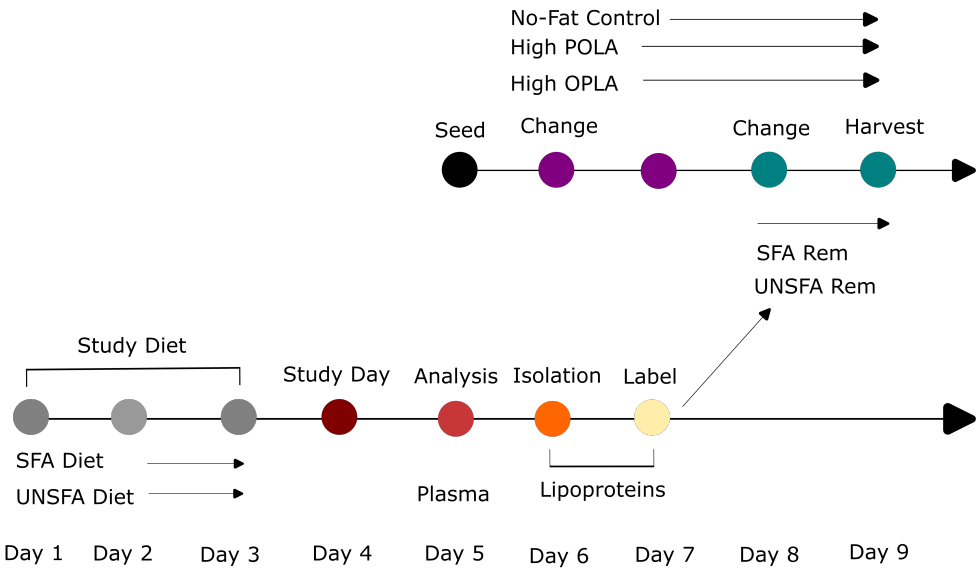


Figure 5.1: Experimental protocol for Chapter 5. This chapter is based around isolating triacylglyercol (TAG)-rich lipoprotein remnants for analysis and application to cells. Following piloting, the main study was carried out as follows: Participants took part in a 3 day study diet consuming either a diet high in SFA or UNSFA. Participants then underwent a post parandial study day. During the study day plasma was collected for analysis. Lipoproteins were also isolated from this plasma and then labelled. Both the initially labelled lipoprotein remnants and the labelled lipoproteins were analysed by gas chromatography mass spectrometry. The labelled lipoproteins were added to cells which had been previously cultured in either a no-fat control, a high concentration of OPLA or a high concentration of POLA for 2 days. The composition of the culturing free fatty acids (FA) was matched to that of the study diet. The cells were cultured with the labelled lipoproteins for 2 days before being harvested for analysis.

5.2.8 Quantification of ^{13}C tri-palmitin and U^{13}C palmitic acid

Following treatment with NEFA and labelled TAG-rich lipoprotien remnants, cellular TAG was quantified for the amount of label present, and analysed by GC and GCMS. Here the following ions were measured: 270m/z for unlabelled palmitate, 271, for ^{13}C tri-palmitin derived palmitic acid from the *ex vivo* labeling and 286 for the U^{13}C palmitic acid from the chocolate drink.

5.2.9 Imaging of uptake

Live cell imaging of the uptake of the TAG-rich remnant particles was carried out with expert help from Dr Katrina Viloria and Professor David Hodson. Based on protocols by Tabas et al., TAG-rich remnants were pre-labeled with fluorescent dye, 3,3'-Dioctadecyloxacarbocyanine (perchlorate), DiOC$_{18}$(3) at 200µL of 2mg/ml overnight at 4°C (Tabas et al. 1990). A re-isolation step was tested, but not enough fluorescent label was recovered in the TAG-rich remnants for application onto cells. 24 hours before imaging, Huh7 cells, were seeded into glass-bottom collagen coated 96-well plates (Cellvis, P96-1.5H-N) (Chapter 2 Section 2.2.1). Cells were then stained with a lipophilic membrane dye (CellBrite® Orange) for one hour prior to imaging.

To image the cells, videos were taken on spinning disc confocal microscope with 60x magnification was used and images were taken every 3 seconds across a half an hour period. After 30 images had been taken, the particles were added. Dye, DiOC$_{18}$(3) has emission/excitation at 501 /484 nm for the TAG-rich remnants and Ex/Em 549/565nm for the membrane. Images were processed in image J.

5.2.10 Breath analysis

Fasting and postprandial breath samples were analysed using gas chromatography-combustion-isotope ratio mass spectrometry (GC-C-IRMS). A capillary column (CPPoraPLOTQ) was used to separate CO_2 from the presence of other gases. The column had dimensions of 30 m x 0.32 mm x 10 µm. Samples were injected at 10 µL

using the split injection mode at 110°C with the column flow kept at 2.0 mL/min. The sampling time was 10 mins with the oven temperature at 35 °C. From each sample, the machine generates a delta value (δ^{13}C 0/00), which was then converted into a TTR using the following equation (Chong et al. 2007):

$$TTR(^{13}C :^{12} C) = [(\delta^{13}C0/00/1000) + 1] \times 0.0112372$$

To account for the natural abundance of ^{13}C , the TTR of the fasting breath sample was later subtracted from the TTR of each postprandial sample. The $^{13}CO_2$ production rate was determined by multiplying the TTR for $^{13}CO_2$ of each breath sample by the CO_2 production rate (VCO_2 in mmol/min).

5.2.11 Plasma insulin concentration

Plasma insulin was quantified by ELISA (Enzyme-linked immunosorbent assay) using the Insulin Human ELISA Kit (Thermofisher, KAQ1251) according to the manufacturers instructions.

5.3 Results

5.3.0.1 *Ex vivo* labelling of TAG-rich remnants

To determine the best protocol for *ex vivo* labelling of TAG-rich remnants, different ^{13}C-tri-palmitin concentrations, incubation times and use of a re-isolation step were investigated. Figure 5.2a shows the difference between a incubation periods, with a more consistent labelling of the TAG-remnants being observed with the overnight incubation period, although there was no significant difference in amount of label incorporated. Figure 5.2c shows the TTR (271/270 m/z) in IHTAG, after culturing Huh7 cells with the TAG-rich remnants which had been incubated for either 1h or overnight prior to application to cells. Less variation was observed when cells were cultured with TAG-rich remnants labeled overnight compared to 1 hour, however there was no a significant difference in the amount of IHTAG enrichment.

Concerning the effect of re-isolation, regardless of label incubation period, there appeared to be an increase in the TTR (271/270 m/z) with re-isolation, however, this was not significantly different. The TTR was investigated for the different types of remnant fractions isolated and, with decreasing TAG content per TAG-rich remnant (i.e. CM, then VLDL1, then VLDL2), there was an increase in TTR, i.e more label is being taken up, although this was not significant (Figure 5.2d). Moreover, the TTR increased in cells treated with the VLDL1 fraction compared to those treated with the CM fraction. It is not clear whether this increase in cellular TTR was due to the increase in label taken up by the TAG-rich remnants themselves or because the cells were taking up a great amount of TAG-rich remnants. We decided to go for the longer incubation period but no re-isolation for this thesis.

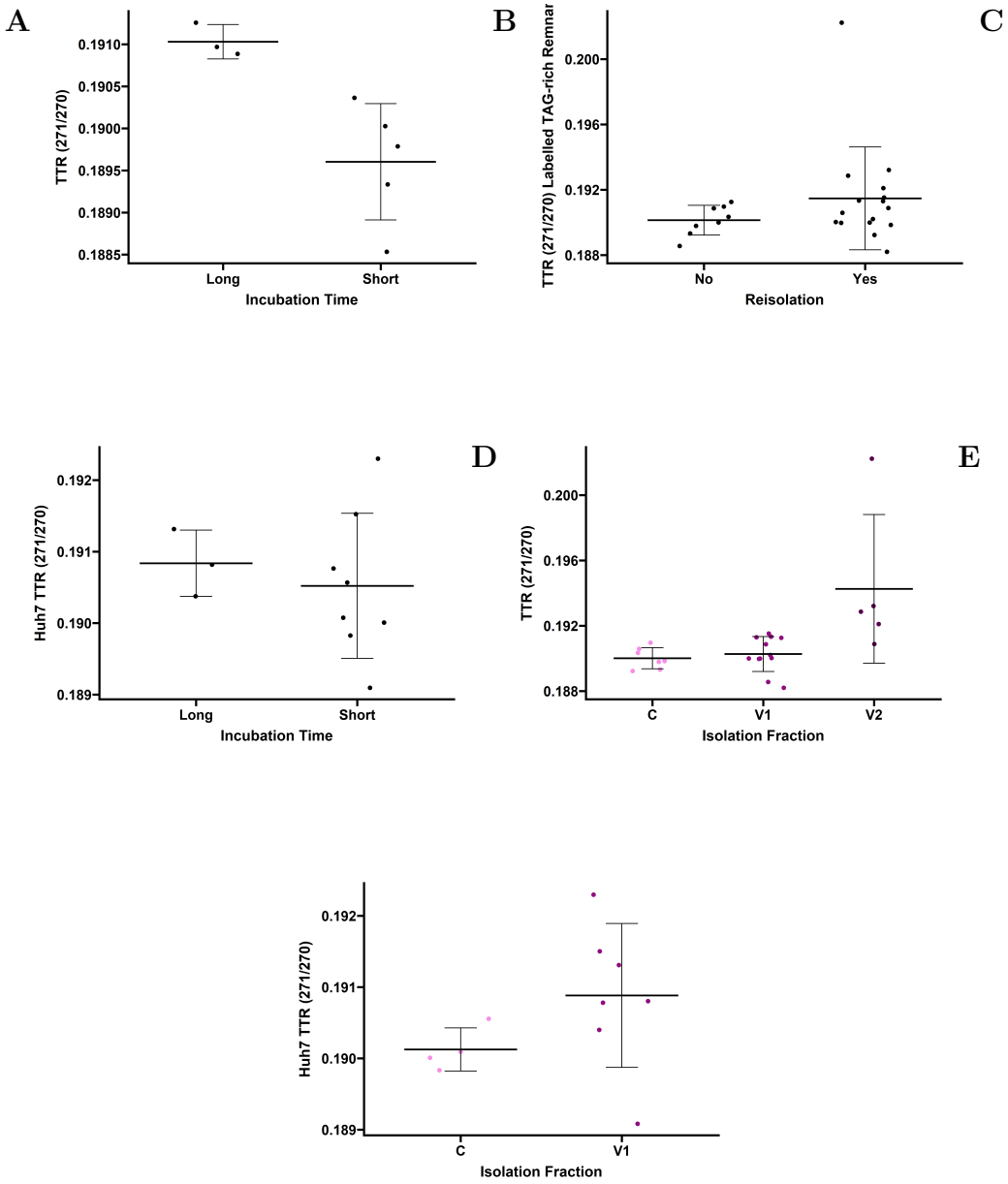


Figure 5.2: Analysis of the incorporation of a tripalmitin label into triacylglycerol (TAG) rich lipoproteins TTR and consequently into Huh7 cells. TAG-rich remnants were cultured with a ^{13}C tripalmitin label and the tracer to tracee ratio (TTR) of 271/270mz was determined with mass spectrometry, where 270 is the isotopic weight of unlabelled palmitate. A) TTR of isolated lipoproteins of any type following either a short incubation period (1 hour) with ^{13}C-tripalmitin or a long incubation period (12 hours). n=5 for the short incubation period, n= 3 for the longer incubation period; B) TTR of TAG-rich remnants before and after a reisolation step regardless of whether they had a short of long initial incubation period. n = 18 for the reisolation step, n= 7 for TAG-rich remnants which did not undergo a reisolation step; C) TTR of Huh7 cells treated with TAG-rich remnants which had undergone a labelling previously for either a short (1 hour) or long (12 hour) incubation period with a reisolation step. n=8 for the short incubation period, n=3 for the long incubation period; D) TTR of the TAG-rich remnants grouped by by lipoprotein fraction; E) TTR following a mass spec analysis of cells treated with TAG-rich labelled lipoproteins from either the C or V1 fraction, n=3 and n=7 respectively. N numbers were determined by the amount of lipoproteins collected from the volunteers at the beginning of this project. Abbreviations: C, chylomicron isolation fraction; V1, VLDL1 isolation fraction; V2, VLDL2 isolation fraction described in Section 5.2.4.

5.3.1 Plasma lipoprotein composition

Following the consumption of a diet enriched in either UNSFA, or SFA, the plasma TAG-rich remnant TAG composition was analysed and shown to reflect that of the diets provided. Figure 5.3a shows the contribution the predominant constituent FA used in the cellular FA treatment mixtures (OPLA and POLA). There was significantly more SFA in TAG-rich remnants generated from the consumption of a diet enriched in SFA compared to one enriched in UNSFA. There was no significant difference between the diets regarding the proportion of TAG that MUFA and PUFAs contributed to, although there appeared to be a reduced proportion resulting from diets enriched in SFA compared to those enriched in UNSFA. Figure 5.4a shows the proportions of TAG-rich remnant sub-divided by isolation fraction. Although none of these differences were significant, all TAG-rich remnants fractions from diets enriched in SFA showed an increased proportion of SFA and a decreased proportion of MUFA in TAG-rich remnants from a diet enriched in SFA compared to a diet enriched in UNSFA.

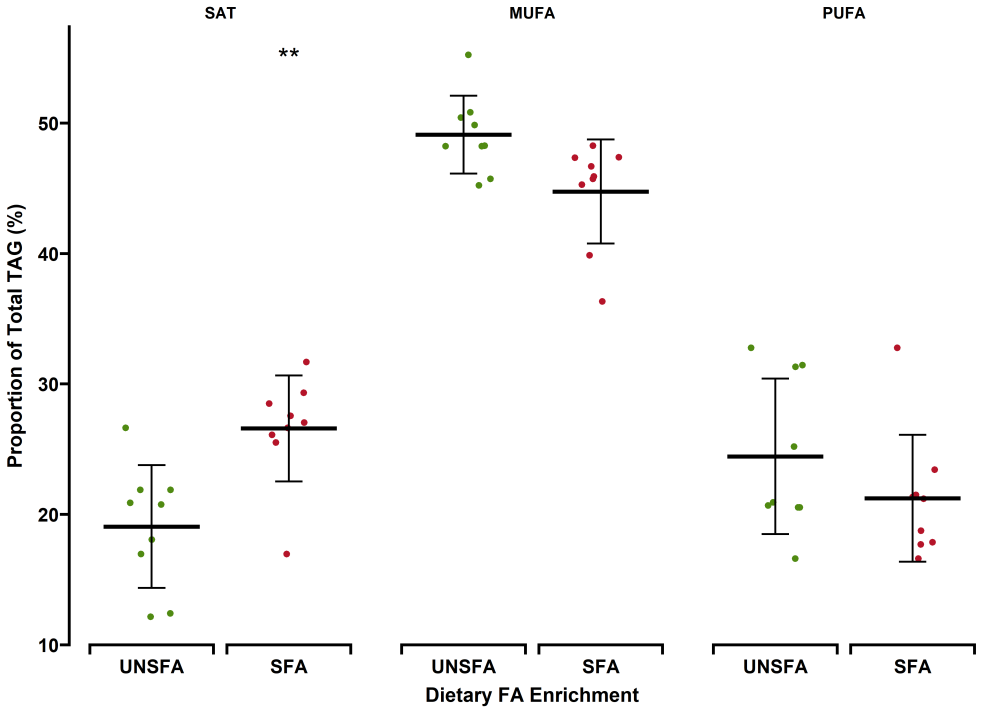


Figure 5.3: Composition of triacylglycerol (TAG) within isolated TAG-rich remnants. Data generated by gas chromatography. Figure shows the proportion of TAG-rich remnant derived TAG by degree of saturation as either saturated (SAT), mono-unsaturated (UNSFA), or polyunsaturated (PUFA). Data show mean +/- SD from 3 participants on two dietary interventions, n=9 for each group accounting for the different lipoprotein fractions. Significance levels indicated are * $p<0.05$, ** $p<0.01$ and *** $p<0.001$.

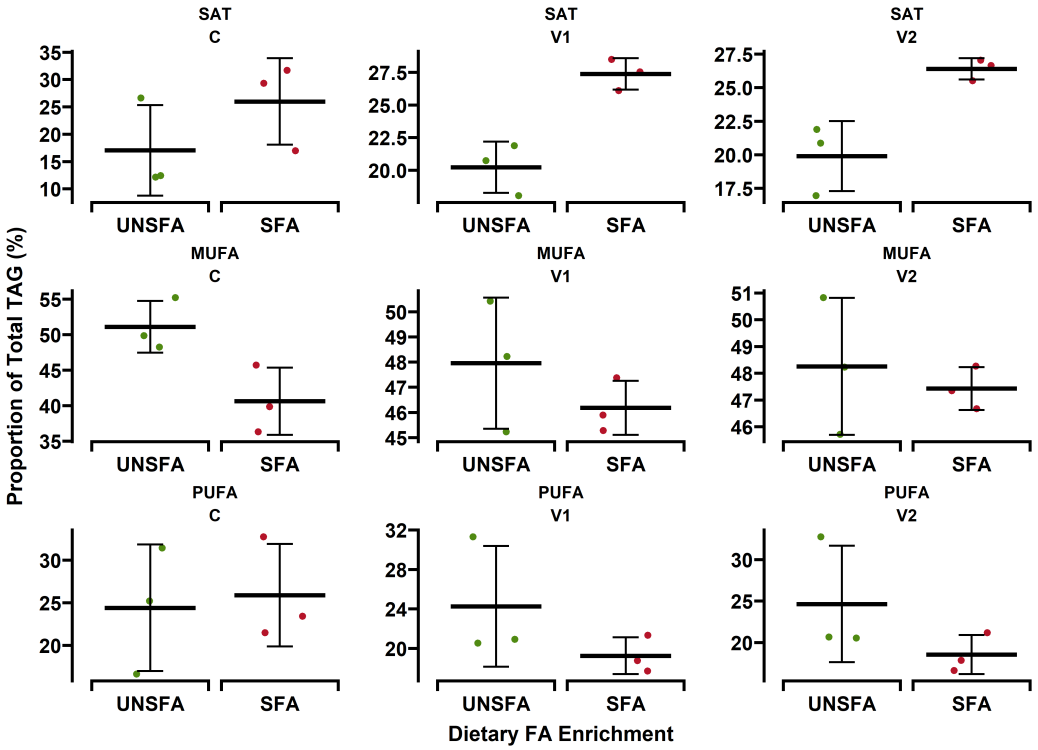


Figure 5.4: Composition of triacylglycerol (TAG) within isolated TAG-rich remnants by lipoprotein isolation fraction. Data generated by gas chromatography. Figure shows the proportion of TAG-rich remnant derived TAG by degree of saturation as either saturated (SAT), mono-unsaturated (UNSFA), or polyunsaturated (PUFA). Data show mean +/- SD from 3 participants on two dietary interventions, n=9 for each group accounting for the different lipoprotein fractions. Significance levels indicated are * $p<0.05$, ** $p<0.01$ and *** $p<0.001$. Abbreviations: C, chylomicron isolation fraction; V1, VLDL1 isolation fraction; V2, VLDL2 isolation fraction described in Section 5.2.4.

Figure 5.5a shows the composition of PL in the TAG-rich remnant lipoproteins by degree of saturation (SFA, UNSFA or PUFA) where there were no significant differences seen. Investigating the composition of TAG-rich remnant's PL further, Figure 5.6a describes the proportions of TAG-rich remnant's PL fraction subdivided by isolation fraction with no significant differences in PL composition between the diets.

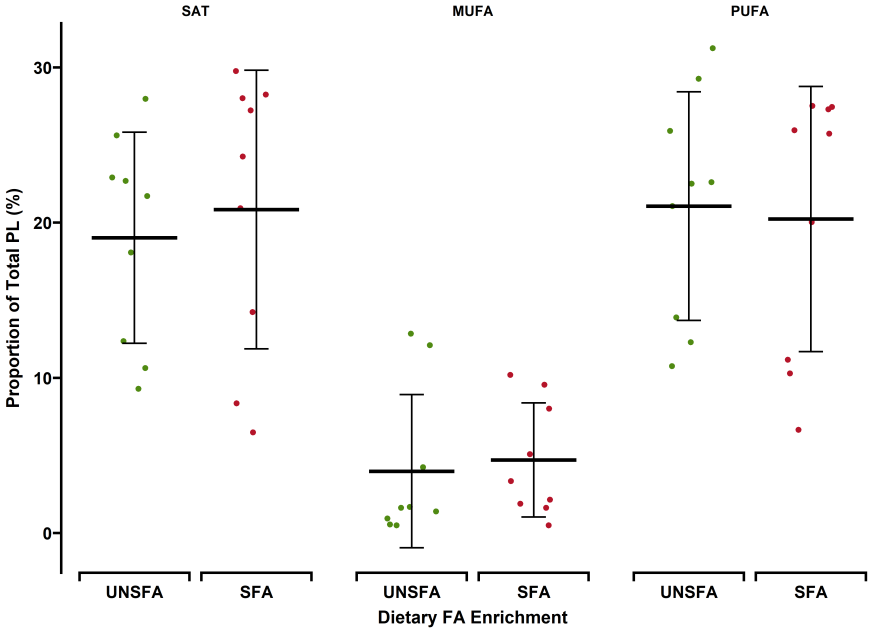


Figure 5.5: Composition of phospholipid (PL) within isolated triacylglycerol (TAG)-rich remnants. Data generated by gas chromatography. Figure shows the proportion of TAG-rich remnant derived PL by degree of saturation as either saturated (SAT), mono-unsaturated (UNSFA), or polyunsaturated (PUFA). Data show mean +/- SD from 3 participants on two dietary interventions, n=9 for each group accounting for the different lipoprotein fractions. Significance levels indicated are * $p<0.05$, ** $p<0.01$ and *** $p<0.001$.

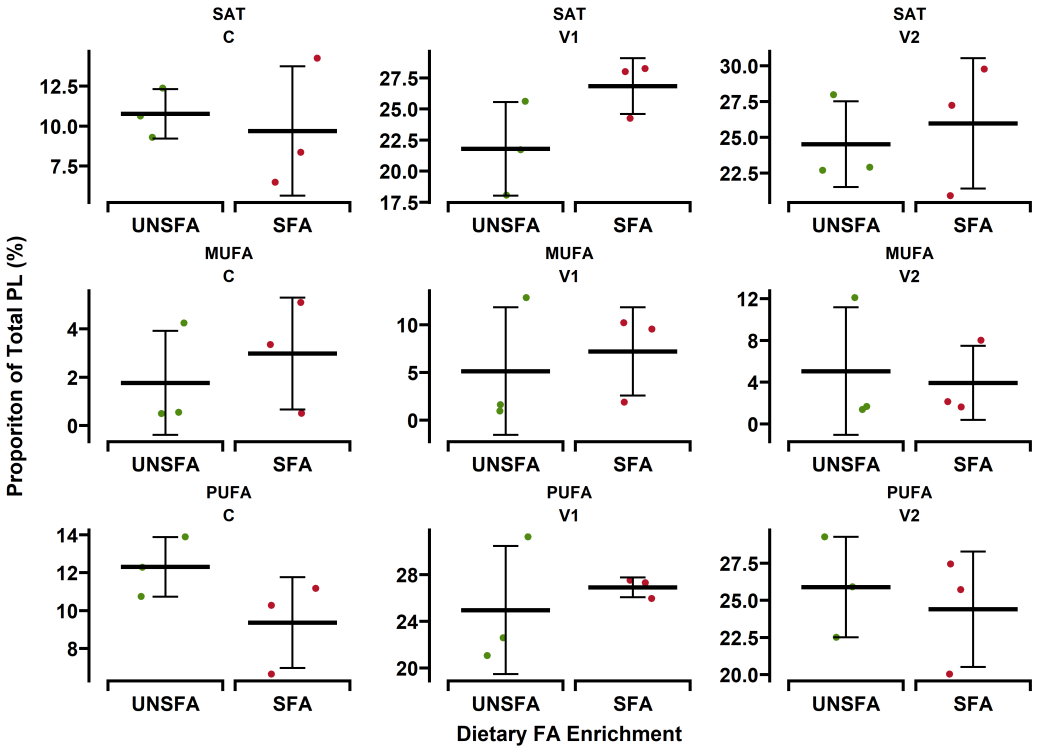


Figure 5.6: Composition of phospholipid (PL) within isolated triacylglycerol (TAG)-rich remnants grouped by lipoprotein isolation fraction. Data generated by gas chromatography. Figure shows the proportion of TAG-rich remnant derived PL by degree of saturation as either saturated (SAT), mono-unsaturated (UNSFA), or polyunsaturated (PUFA). Data show mean +/- SD from 3 participants on two dietary interventions, n=9 for each group accounting for the different lipoprotein fractions. Significance levels indicated are * $p<0.05$, ** $p<0.01$ and *** $p<0.001$. Abbreviations: C, chylomicron isolation fraction; V1, VLDL1 isolation fraction; V2, VLDL2 isolation fraction described in Section 5.2.4.

The incorporation of $U^{13}C$ palmitic acid from the chocolate drink into the different TAG-rich remnant isolation fractions. Figure 5.7a, showed that the CM remnants contained the ^{13}C label to a greater extent than VLDL1 and VLDL2 isolation fraction. Figure 5.7b, shows that there appears to be greater $U^{13}C$ palmitic labelling resulting from the diet enriched for UNSFA when compared to one enriched in SFA.

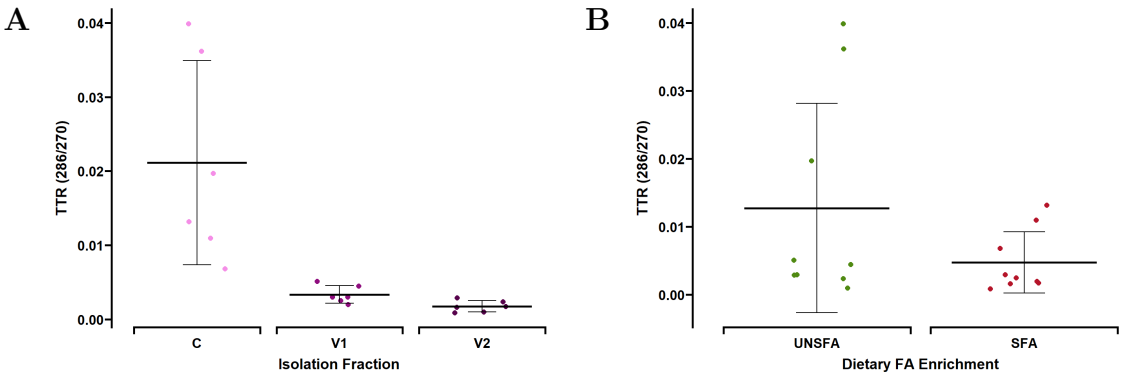


Figure 5.7: Analysis of the incorporation of dietary U^{13}C palmitic acid label into triacylglycerol (TAG) rich lipoproteins. Data shows the tracer to tracee ratio (TTR) of U^{13}C-palmitic acid compred to unlabelled palmitic acid generated by mass spectrometry. A) TTR (286/270 m/z) by isolation fraction of the TAG-rich remnant; B) TTR (286/270 m/z) by study diet composition. Data show mean +/- SD from 3 participants on two dietary interventions. Abbreviations: C, chylomicron isolation fraction; V1, VLDL1 isolation fraction; V2, VLDL2 isolation fraction described in Section 5.2.4.

5.3.2 Plasma biochemistry

Table 5.1, shows data following diets enriched in UNSFA or SFA, at time 0, before the meal was consumed. Data showed no significant differences between the study days. Figure 5.8a shows plasma TAG concentration across the post-prandial study day. Figure 5.8b shows plasma NEFA across the study day with no significant differences. Breath and Insulin data can be seen in Appendix Figures A.4.1 and A.4.2 respectively.

Table 5.1: Plasma Biochemistry of participants post diet

Name	**UNSFA**		**SFA**	
	Mean	**SD**	**Mean**	**SD**
Glucose (mmol/L)	4.70	0.60	5.54	0.763
Cholesterol (mmol/L)	3.90	0.22	4.76	1.3
HDL (mmol/L)	1.36	0.30	1.65	0.544
3OHB (µmol/L)	37.0	7.12	57.7	27.3
CRP (mg/L)	0.640	0.124	0.690	0.236
Lactate (mmol/L)	0.770	0.429	0.890	0.298
Glycerol (µmol/L)	82.0	6.53	132.	34.9
Urea (mmol/L)	5.6	1.42	4.80	0.462
ALT (U/L)	40.3	3.64	31.3	5.38

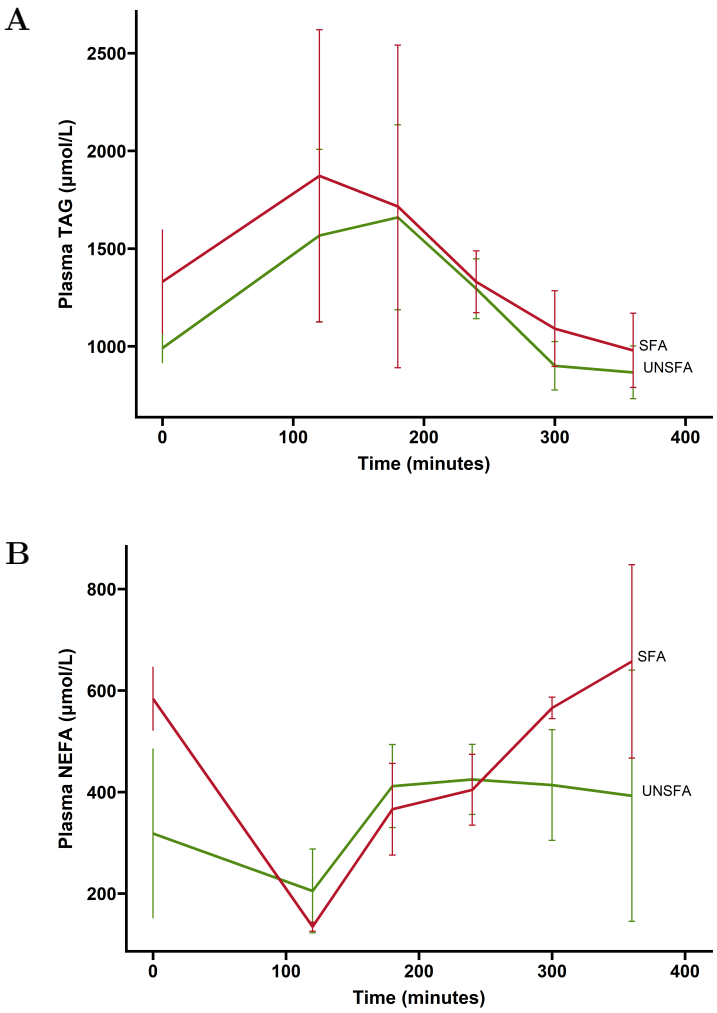


Figure 5.8: Post parandial plasma TAG and NEFA concentration in participants following consumption of a diet enriched in unsaturated fatty acids (UNSFA) or saturated fatty acids (SFA). Data measured on a clinical biochemical analyser. A) Plasma TAG; B) plasma NEFA. Green line indicates data from diet enriched in UNSFA, and orange line indicates diet enriched in SFA Data show mean +/- SD from 3 participants on two dietary interventions. Abbreviations: C, Chylomicron isolation fraction; V1, VLDL1 isolation fraction; V2, VLDL2 isolation fraction.

5.3.3 Culturing of cells with TAG-rich remnants

Following the initial pilot investigation, for this study, the TAG-rich remnants were labelled both through incorporation of U^{13}C palmitic acid into the study day diet and also through *ex vivo* labelling with ^{13}C-tripalmitin. Figure 5.9a shows the incorporation of ^{13}C-tripalmitin into the TAG-rich remnants relative to an unlabelled VLDL background sample. Incorporation of the U^{13}C palmitic acid label from the chocolate drink was measured and shown to be enriched in TAG-rich remnants isolated in the CM fraction compared to the VLDL1 and VLDL2 isolation fractions (Figure 5.9b). The effect of dietary FA enrichment and consequential TAG-rich remnant composition on the remnant's ability to take up the label was considered (Figure 5.9c), with no difference between the two compositions.

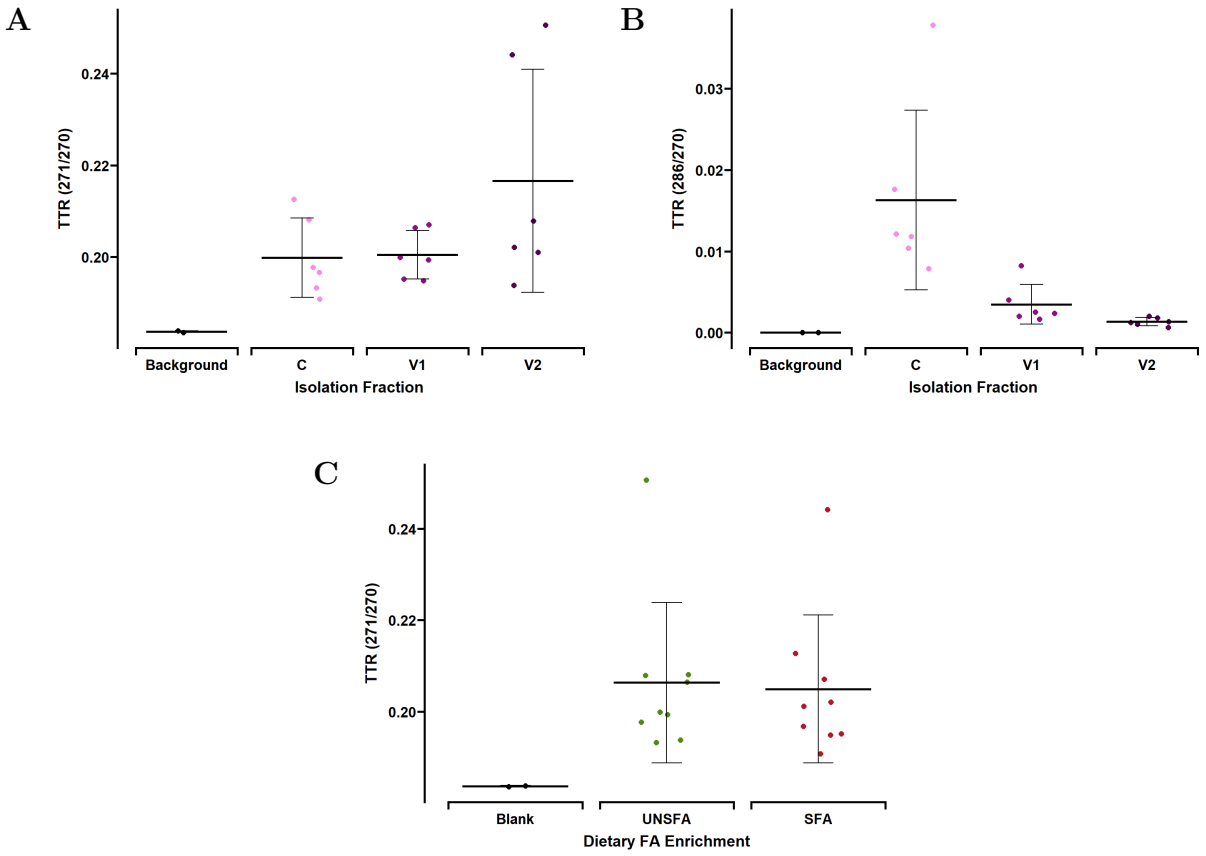
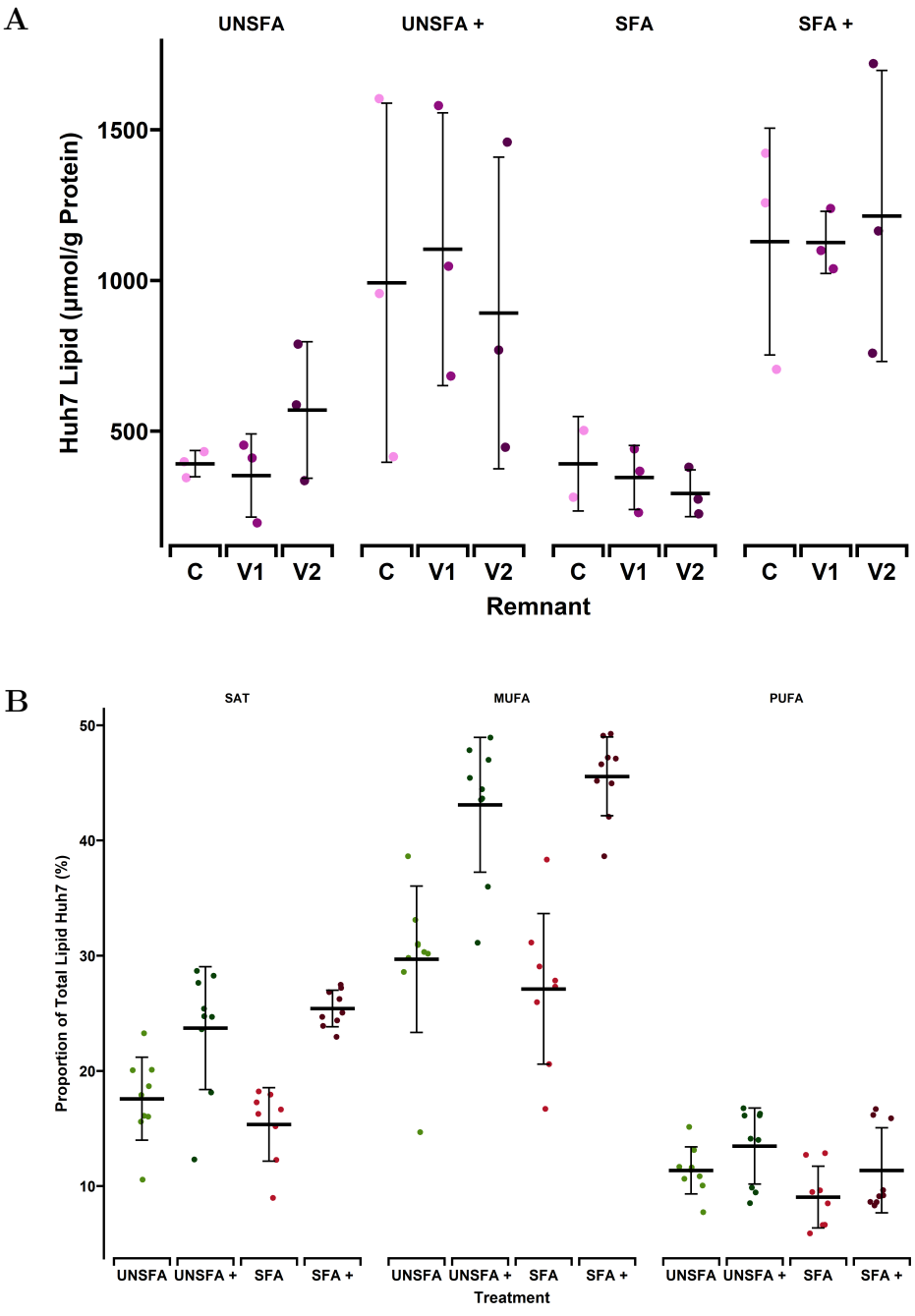


Figure 5.9: Analysis of the incorporation of dietary U^{13}C palmitic acid label and ^{13}C tripalmitin into triacylglycerol (TAG) rich lipoproteins] Data generated by mass spectrometry and analysed as tracer to tracee ratio (TTR) where the tracer is the Incorporated labelled fat and the tracee is the unlabelled fat. U^{13} palmitic acid results in a mz value of 286, and ^{13}C tripalmitin results in a mz value of 271 to compare to the unlabelled mz value of 270. A) TTR of 271/ 270 m/z to show the incorporation of ^{13}C tripalmitin into TAG-rich remnants; B) TTR of 286/270 m/z to show the incorporation of U^{13}C palmitic acid into TAG-rich remnants; C) TTR of 271/270 m/z to show the effect of dietary composition on the incorporation of ^{13}C tripalmitin into TAG-rich remnants. Data show mean +/- SD from 3 participants on two dietary interventions. Abbreviations: C, Chylomicron isolation fraction; V1, VLDL1 isolation fraction; V2, VLDL2 isolation fraction.

Following treatment of Huh7 cells with NEFA and TAG-rich remnants, total intracellular lipid was quantified. Cells cultured with additional NEFA (OPLA or POLA) had greater intracellular lipid compared to those treated with only TAG-rich remnants (Figure 5.10a). The lipid composition of either the TAG-rich remnants or TAG-rich remnants did not appear to alter cellular TAG accumulation. Figure 5.10b shows the proportion SFA, MUFA and PUFA constitute of total cellular lipid and shows that culturing with NEFA significantly increased the relative proportion of palmitic acid and oleic acid.



C

Lipid	Comparison	Significance
Total lipid	UNSFA & UNSFA + OPLA	*
	SFA & SFA + POLA	***
Percent SFA	UNSFA & UNSFA + OPLA	*
	SFA & SFA + POLA	****
Percent MUFA	UNSFA & UNSFA + OPLA	***
	SFA & SFA + POLA	***

Figure 5.10: Huh7 lipid composition after culturing with triacylclycerol (TAG)-rich remnants with or without additional free fatty acids (FA). All data were quantified by gas chromatography. A) Total intracellular lipid; B) Proportion of lipid grouped by dietary enrichment; C) Table of statistical differences. There were no statistical differences between the percentage of PUFA. Data show mean +/- SD from 3 participants on two dietary interventions with an n of three per condition. Additional FA treatment is indicated by '+'. Abbreviations: C, Chylomicron isolation fraction; V1, VLDL1 isolation fraction; V2, VLDL2 isolation fraction. Significance levels indicated are * $p<0.05$, ** $p<0.01$ and *** $p<0.001$.

Figure 5.11a shows the uptake of ^{13}C tripalmitin into the cell as measured by mass spectrometry, demonstrating that TAG-rich remnants were taken up into the cells. Figure 5.11b shows the proportion of the $U^{13}C$ palmitic acid within the cells. $U^{13}C$ palmitic acid was mainly present within CM remnants, cells treated with CM remnants had a greater proportion of $U^{13}C$ palmitic acid enrichment than cells treated with VLDL1 and VLDL2 TAG-rich remnants, although this difference was not significant (Figure 5.11c).

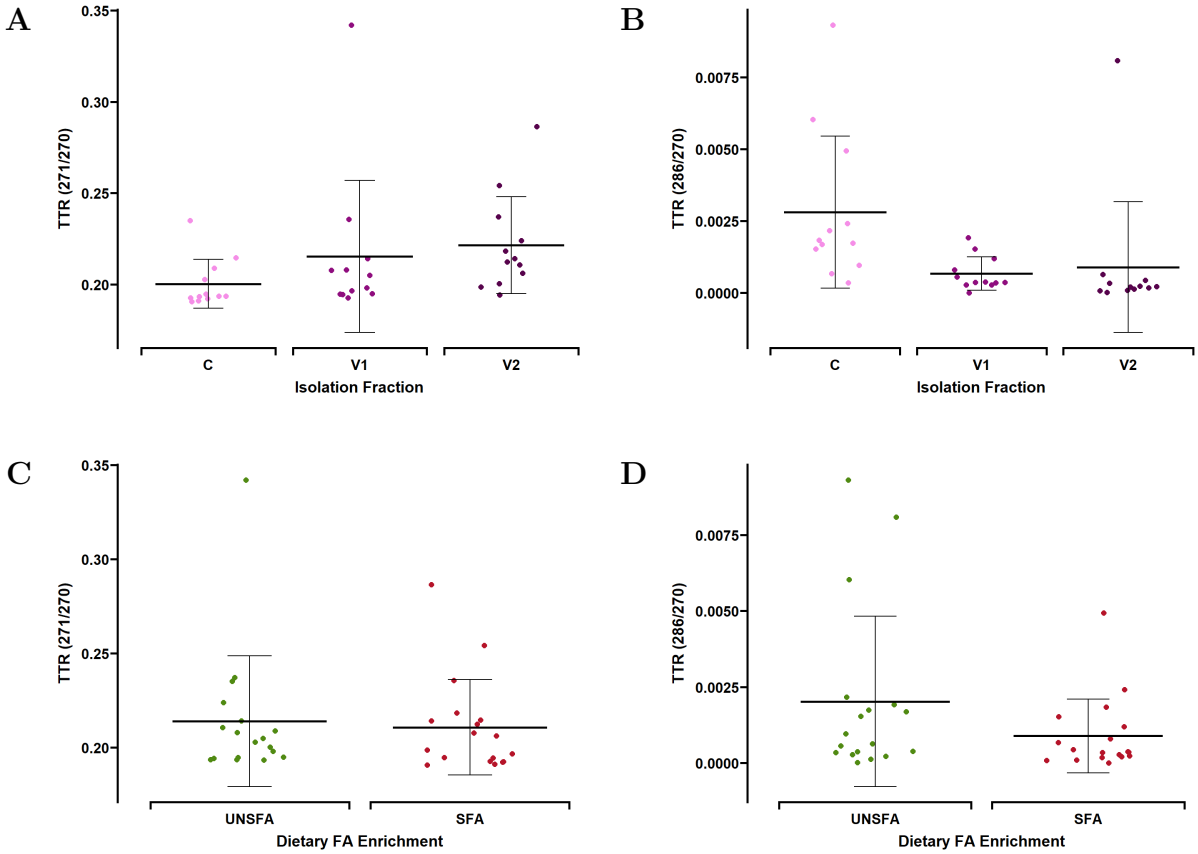
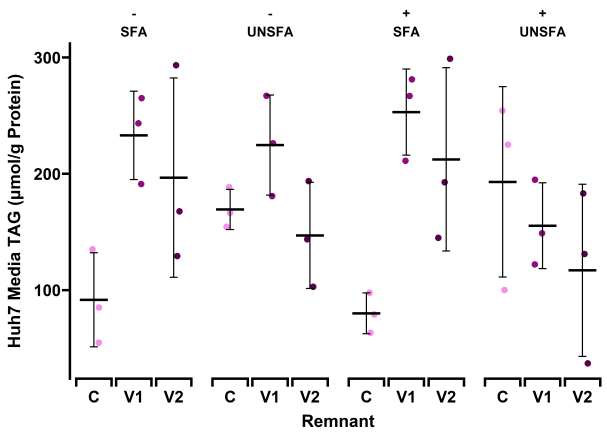


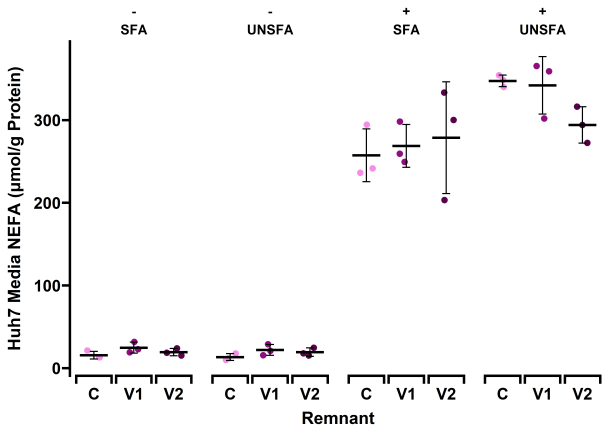
Figure 5.11: Analysis of the incorporation of dietary U^{13}C palmitic acid label and ^{13}C tripalmitin into Huh7 cells after treatment with triacylglycerol (TAG) rich lipoproteins. Data generated by mass spectrometry. A) TTR of 271/270 m/z to show the incorporation of ^{13}C tripalmitin into Huh7 cells grouped by lipoprotein isolation fraction (n=12); B) TTR of 286/270 m/z to show the incorporation of U^{13}C palmitic acid grouped by lipoprotein isolation fraction (n=12); C) TTR of 271/270 m/z of Huh7 cells grouped by composition of the study (n=18). D) TTR of 286/270 m/z of Huh7 cells grouped by composition of the study (n=18). Data show mean +/- SD from 3 participants on two dietary interventions . Abbreviations: C, Chylomicron isolation fraction; V1, VLDL1 isolation fraction; V2, VLDL2 isolation fraction.

Following treatment with the TAG-rich remnants, cellular media lipid was quantified using a automatic clinical biochemistry analyser to measure media TAG and NEFA. Figure 5.12a shows the concentration of TAG remaining in the media with no significant differences seen when comparing treatments. However, TAG-rich remnants enriched in SFA resulted in a greater remaining concentration of media TAG in the chylomicron isolation fraction compared to the V1 isolation fraction. Significant differences emerged comparing media NEFA concentrations, with greater amounts of NEFA measured in cells treated with OPLA or POLA NEFA mixtures as well as TAG-rich remnants when compared to cells treated with just TAG-rich remnants (Figure 5.12b). Figure 5.12c shows the amount of lipid present in the media after treatment with either CM, VLDL1 or VLDL2 fractions with or without the respective matching FA mixture (OPLA or POLA, matching TAG-rich remnants derived from the UNSFA and SFA diets respectively), although there were no significant differences between treatments.

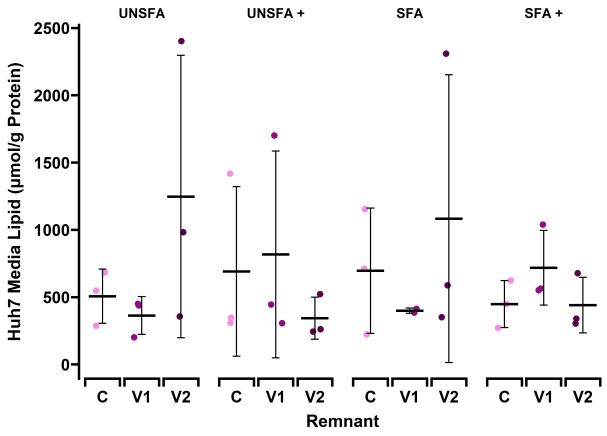
A



B



C

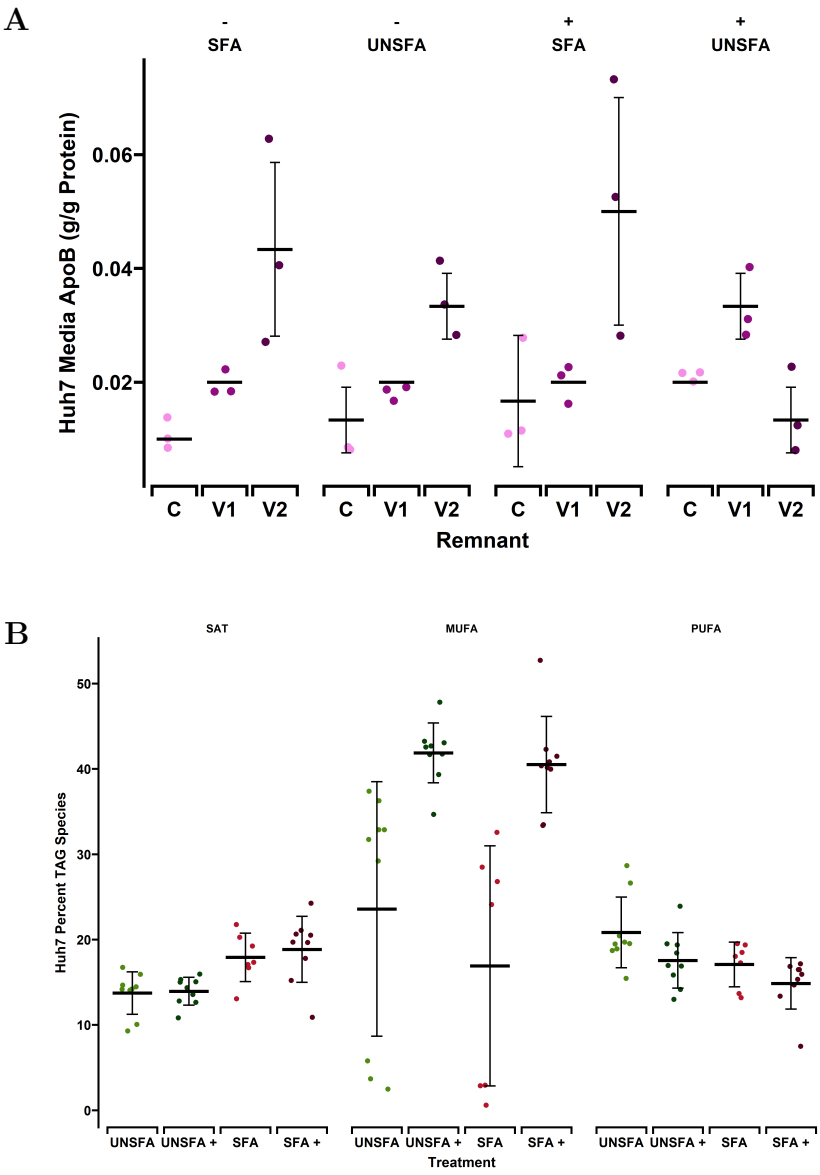


D

Metabolite	Comparison	Significance
NEFA	UNSFA & UNSFA + OPLA	***
	SFA & SFA + POLA	***
	UNSFA + OPLA & SFA +POLA	**

Figure 5.12: Huh7 media lipid composition after culturing with triacylclycerol (TAG)-rich remnants with or without additional free fatty acids (FA). All data were quantified by gas chromatography. A) Total media lipid; B) Concentration of media non esterified FA (NEFA) grouped by dietary enrichment; C) Proportion of media lipid grouped by dietary enrichment. D) Table of statistical differences. Data show mean +/- SD from 3 participants on two dietary interventions with an n of three per condition. Additional FA treatment is indicated by '+'. Abbreviations: C, Chylomicron isolation fraction; V1, VLDL1 isolation fraction; V2, VLDL2 isolation fraction. Significance levels indicated are * $p<0.05$, ** $p<0.01$ and *** $p<0.001$.

Media ApoB was measured (Figure 5.13a), although no significant differences were observed. Comparing the composition of the media total lipid by general degree of saturation (Figure 5.13b), the FA composition matches those of the remnants within the respective treatments: There was a significant increase in the proportion of total lipid constituted by SFA between TAG-rich remnants enriched in SFA compared to TAG-rich remnants enriched in UNSFA. Cells treated with additional NEFA (as OPLA or POLA appropriately) also showed a significant increase in SFA with cells treated with SFA enriched TAG-rich remnants and POLA compared to UNSFA enriched TAG-rich remnants and OPLA. The proportion total lipid comprised of MUFA was increased by the addition of NEFA, with no differences seen arising from the different compositions.

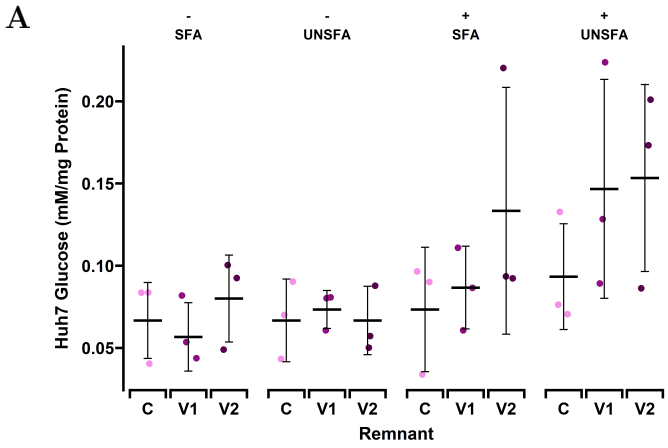


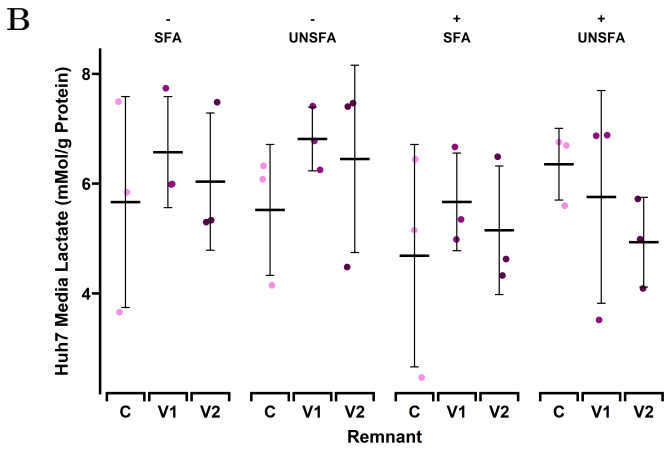
C

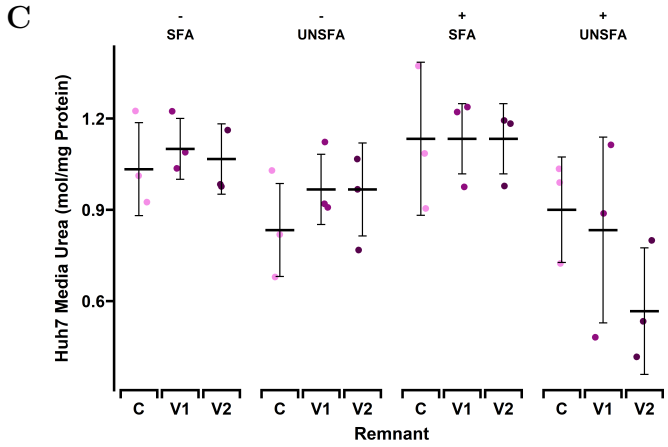
Lipid	Comparison	Significance
SFA	UNSFA & SFA	*
	UNSFA + OPLA & SFA + POLA	*
MUFA	UNSFA & UNSFA + OPLA	*
	SFA & SFA + POLA	*

Figure 5.13: Huh7 media Apolipoprotein B (ApoB) concentration and lipid composition after culturing with triacylclycerol (TAG)-rich remnants with or without additional free fatty acids (FA). A) Media ApoB concentration as measured on a clinical biochemistry analyser; B) Proportion of media lipid categorised by degree of saturation as measured by gas chromatography; C) Table of statistics. Data show mean +/- SD from 3 participants on two dietary interventions with an n of three per condition. Additional FA treatment is indicated by '+'. Abbreviations: C, Chylomicron isolation fraction; V1, VLDL1 isolation fraction; V2, VLDL2 isolation fraction. Significance levels indicated are * $p<0.05$, ** $p<0.01$ and *** $p<0.001$.

Figure 5.14a illustrates the glucose levels in the cell media after treatment. While overall remaining glucose concentration was minimal, cells treated with NEFAs and TAG-rich remnants, especially those enriched in UNSFA and given additional OPLA treatment, had significantly higher remaining glucose compared to cells treated solely with TAG-rich remnants. There were no significant differences in media lactate (Figure 5.14b). Comparing the concentration of urea in the media (Figure 5.14c), the concentration appears to be higher in cells treated with SFA enriched TAG-rich remnants compared to those enriched with UNSFA and this difference was significant in cells NEFA as well as TAG-rich remnants.







D

Metabolite	Comparison	Significance
Glucose	UNSFA & UNSFA + OPLA	*
Urea	UNSFA + OPLA & SFA + POLA	**

Figure 5.14: Huh7 media glucose, lactate and urea concentration after culturing with triacylclycerol (TAG)-rich remnants with or without additional free fatty acids (FA). Data measured on a clinical biochemistry analyser. A) Media glucose; B) Media lactate; C) Media urea; D) Table of statistics. Data show mean +/- SD from 3 participants on two dietary interventions with an n of three per condition. Additional FA treatment is indicated by '+'. Abbreviations: C, Chylomicron isolation fraction; V1, VLDL1 isolation fraction; V2, VLDL2 isolation fraction. Significance levels indicated are * $p<0.05$, ** $p<0.01$ and *** $p<0.001$.

5.3.4 Time lapse imaging of fluorescently stained TAG-rich remnants applied to flourescently stained Huh7 cells

To try and visualise the process of remnant uptake, videos were taken on a spinning disc confocal microscope. Here, fluorescent labelled TAG-rich remnants were added to the Huh7 visualised. Figure 5.15 shows a series of still images demonstrating the potential uptake of a TAG-rich remnant in a Huh7 hepatocyte.

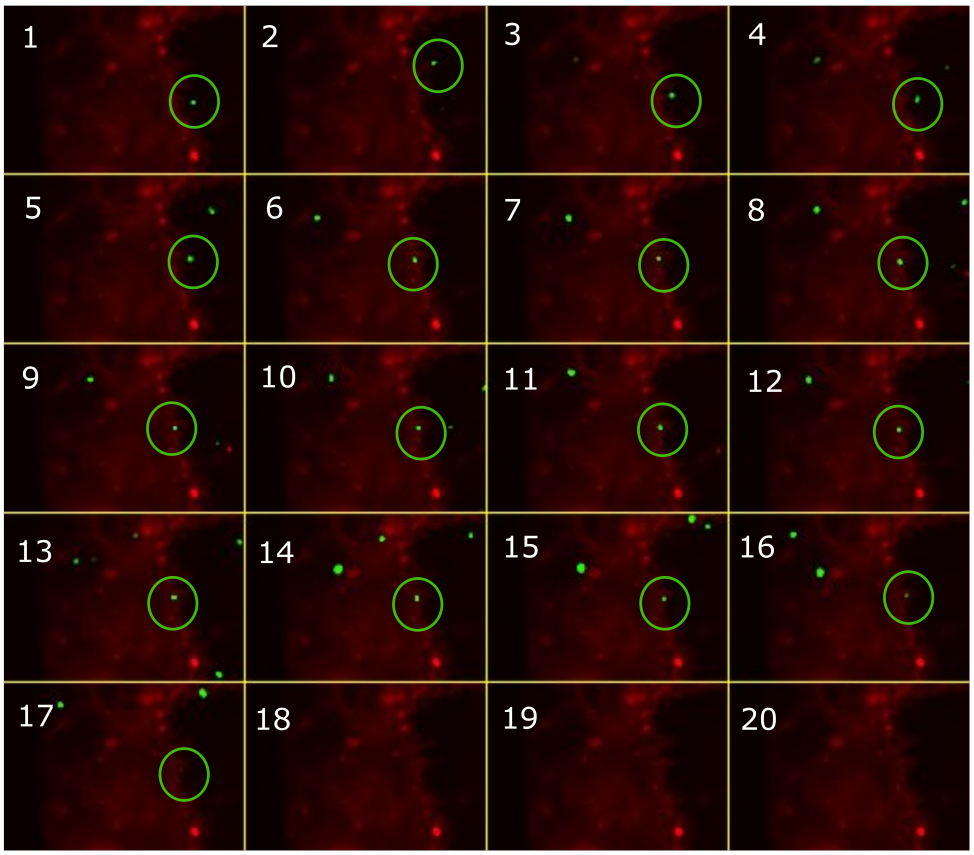


Figure 5.15: Time-lapse images taken of Huh7 cells immediatly after treatment with fluorescently labelled triacyglycerol (TAG)-rich lipoproteins. Images taken 3 seconds apart on spinning disc confocal microscope. TAG-rich lipoproteins are flourescently labelled green, cellular membrane is fluorescently labelled red. Green circle highlights a green TAG-rich lipoprotein as it appears to interact with the plasma membrane.

5.4 Discussion

This chapter aimed to establish the effect of changes in dietary FA composition on plasma TAG-rich remnants and whether there were any differences in uptake of TAG-rich remnants enriched in SFA of UNSFA. An initial question, was regarding the length of time an individual needed to be on a diet for their TAG-rich remnant compositions to reflect that of the diet. The time it takes depends on differences in clearance, differences in spillover, size of remnants and the interaction with the liver TAG pool. Three days were used here and this proved sufficient to change the lipoprotein compositions across all isolated fractions. TAG-rich remnants were successfully labelled with both U^{13}C palmitic acid and ^{13}C tripalmitin for uptake into cells and the label was observed to be taken up into cells, regardless of whether cells were cultured with additionally FAs or just TAG-rich remnants.

When provided to Huh7 hepatocytes, the cells showed no preferential uptake of TAG-rich remnants regarding their composition, with the final media composition reflecting the media composition provided as treatment. Although the cellular total lipid did not significantly change for enrichment in UNSFA or SFA following the respective treatments as had been seen previously (see Chapter 2 and Chapter 4), this may be a reflection of the shorter treatment period used here.

Although significant differences in the total glucose uptake were observed between the treatments, whether this is of significance for metabolic processes will require further elucidation. The difference in media urea concentration may be of interest as it may be a reflection of increased mitochondrial activity in UNSFA-enriched TAG-rich remnants, which would align with *in vivo* observations where diets enriched in PUFA, specifically linoleic acid, have been shown to increase FA oxidation when measured at a whole body level to a greater extent compared to diets enriched in SFA, specifically palmitate (Parry et al. 2021).

There are a number of limitations for the work described in this chapter. Firstly, the treatment media was adjusted for total TAG concentration post-isolation to ensure that cells received the same amount of fat, but this resulted in a different number

of TAG-rich remnants with this number depending on how lipidated the remnants were, being applied to the cells. The TAG-rich remnants also interacted with the stable-isotopes differently resulting in some variability in the amount of labelling used. It was not possible to determine an accurate estimate for how many particles were being used for cellular treatment. Moreover, it was not possible to provide the NEFA as a complete match to the fat composition of the TAG-rich remnants, however, they were as close as it was possible to get them. Another limitation with this study was that only male participants were measured, with male Huh7 cells receiving the treatment, and it is known but not completely understood, that there are gender differences in the handling of dietary fat (Koh et al. 2021; Varlamov 2017). Moreover, due to the limited shelf-life of TAG-rich remnants, cells cannot easily undergo an extended treatment with the lipoproteins.

However, regardless of the limitations, having a model to investigate the effect of the human-derived TAG-rich remnants contribution to the IHTAG accumulation could provide a platform to develop approaches to improve understanding of cellular processing of TAG-rich remnants. Future work, to elucidate the journey of FA originating from TAG-rich remnants within cells, fluorescent dyes could be used as a tool for tracking FA destination. Through the use of fluorescent dyes, the nuanced mechanisms involved in cellular uptake and utilization of lipoprotein-derived FA could be uncovered. Further metabolic characterisation of these TAG-rich remnant treated cells could also be undertaken. However, work on these lipoproteins will be hindered by practical challenges and progress will be slow in this area unless techniques to scale up and improve lipoprotein collection and use can be improved.

5.5 Conclusion

Described in this chapter, is the process of collecting, isolating and labeling TAG-rich remnant particles from humans for *in vitro* application. Data showed no preferential uptake of TAG-rich remnants regarding their FA composition and established that these experiments are feasible although limited by timeframes and abundance of

material. Further work will be required to unpick potential differences between TAG rich remnants enriched in either UNSFA or SFA.

6

General discussion and future directions

MASLD, characterised by excessive accumulation of IHTAG is becoming an increasing public health burden. Although, the exact pathogenesis of MASLD requires further research for a more detailed understanding, it is known that both genetic and lifestyle factors are involved both development and progression. Owing to the inaccessibility of the human liver, *in vivo* investigations of hepatocellular FA metabolism remain challenging. Therefore, the aims of this thesis were to optimise a physiological cellular model of FA metabolism and IHTAG accumulation reflecting different dietary compositions and delivery routes and to investigate the effect of specific dietary FA compositions and concentrations on intrahepatocellular metabolism and function.

6.1 Improving and Developing *in vitro* hepatocyte models

Hepatoma-derived cell lines are commonly used in MASLD research, although they present with a number of limitations including: rapid uptake and metabolism of glucose, poor mobilisation of stored TAG, low albumin secretion and minimal cytochrome P450 enzyme function (Green et al. 2020; Gunn et al. 2017). Previously, the group optimised the Huh7 cell-line to make a more physiologically-relevant model, and this was achieved by altering glucose concentration in the culturing

medium, culturing with HS and supplying exogenous FA enriched in UNSFA (Gunn et al. 2020). As *in vivo* human dietary studies have shown that consumption of diets enriched in SFA resulted in greater hepatic FA accumulation (Parry et al. 2017; Katan et al. 2010), this thesis aimed to establish an alternative FA treatment, enriched with SFA to the Huh7 cell-line model and to investigating how specific compositions of FA along with concentrations, affected hepatocellular metabolism and function *in vitro*.

The data ascertained from the Huh7 cells was compared to the gold standard for *in vitro* hepatic research: PHH cells which have been used previously to validate research carried out in hepatoma cell lines (Zeilinger et al. 2016). PHH cells are heavily relied upon by the pharmaceutical industry for investigations on hepatic metabolism. Whilst a number of pharmaceutical companies have accepted a culturing cocktail referred to as the 5C cocktail to be suitable for conducting physiologically relevant experiments on PHH cells, the effect of this medium on hepatic metabolism are yet to be fully defined as this media composition was decided based on transcriptional data rather than metabolic data (Xiang et al. 2019). Here we compared both metabolic data and transciptional data between the cell-line and PHH FA treated cells.

In the context of our investigation, the Huh7 cells demonstrated that the uptake of FA results in a cellular lipid composition which closely mirrors that of the treatment media. This observation suggests a lack of preferential uptake, indicating that the cells are not selectively internalizing specific FA. Consequently, there were notable disparities in LD morphology and glucose production, highlighting the impact that FA composition may have on cellular function. These differences in LD morphology may impact on cellular metabolism, with previous lipid accumulation previously associated with mechanical stress on the nucleus (Loneker et al. 2023). In contrast, PHH had fewer significant changes following treatment treatment and despite their uptake of FA, with the presence of pre-existing lipids within the cells made it challenging to disentangle the effects of treatment composition on the cells.

Comparing the transcptional data between FA treated Huh7 and PHH cells, although there was limited overlap in differentially expressed genes, a consistent narrative emerges—highlighting the POLA treatment as less favorable. Specifically implicated in Huh7 cells were changes in ER protein processing, which may prove to be of importance and ER stress has been associated with pathological process (Nissar et al. 2015). PHH cell transciptional data implicated the compliment and coagulation cascade as being significantly altered at a transciptional level with cells treated with differing FA compositions. Overall, the addition of FA compared to controls treated with no-fat had a greater effect on the transcription when compared to FA composition or concentration changes. Molecular studies are required to confirm whether these changes in transcriptional data are maintained at a protein level.

Additionally, transciptional data from PHH cells shows that they are predominantly influenced by the donor factors (phenotype and environmental), rather than that of the provided treatment, when looking at altered FA compositions. Whilst this could provide an opportunity to look at the interaction between the effect of nutrition on the transcriptome and genotype, for this thesis the genotype of the PHH cells was not established.

Investigating the impact of changing treatment media composition and concentration and extending the treatment model over two weeks demonstrated that the cells continue to have non-preferential uptake of FAs, although their metabolic responses became blunted. The most novel result here was the profound impact of dietary composition on LD morphology, where switching treatment FA reversed the effects of POLA on lipid morphology.

TAG-rich remnant particles pose a challenge in research due as they cannot be synthetically generated to reflect human TAG-rich lipoprotein remnants. Despite their difficulty to study, their impact is believed to be substantial (Nakajima et al. 2011; Parks et al. 1999). To understand how TAG-rich remnants contribute to IHTAG content and metabolism, a cellular model was established that incorporated two stable isotope labels within the TAG-rich remnant and our studies clearly

demonstrate uptake of these TAG-rich remnants by Huh7 cells, even in the presence of other FA in the media.

6.2 Future directions

For the initial model described in Chapter 3, further work could be undertaken to look at the effects of LD morphology. Specifically, the interaction between the peroxisome and the LD. To confirm that the peroxisome is impinging on LD size, ATGL or Pex2 could be knocked down within the Huh7 cell-line and the effects on LD morphology monitored. This would allow for investigations into which pathways are involved in determining LD size.

Studies could also be undertaken on EVs within this model and whether they are helping the cells manage the additional SFA content as they have been previously implicated in this manner (Garcia-Martinez et al. 2023; Hirsova et al. 2016). Understanding whether there are changes in the composition and or number of EVs from these FA treated cells would provide insight into whether the cells are trying to actively reduce the amount of SFA and whether changing the treatment composition would alter this disposal route. A particularly informative experimental technique would be the ability to trace FA turnover, particularly considering its location and whether there are differences in turnover of LDs depending on the size of them.

Considering the turnover of FA, ideally a 'defatting' agent which would look at the effects of historical IHTAG would be developed. Additionally the *in vitro* model looking at the turnover of FA could be further developed to incorporate other elements associated with MASLD e.g. higher concentrations of insulin. Moreover, fluorescent dyes, such as the laudin dyes, which report on membrane compositions and the degree of saturation, could be used to help looking at organelle specific changes induced by changing the treatment FA composition.

As hepatocytes are typically not in isolation, co-cultures could be established with other hepatic cells, particularly macrophages which would allow for further observations into the involvement of the immune system in the development of MASLD.

Studying the effect of TAG-rich remnants, there are a number of metabolic processes that are yet to be measured. If it could be established, an extended timeline, i.e. where the cells are able to undergo a number of media changes with TAG-rich remnants over multiple days may allow for greater IHTAG accumulation and further metabolic distinctions between the different FA compositions. Additionally, the TAG-rich remnant derived FAs could be labelled and their destination within the cells traced. When this model is more established, different phenotypes could be considered and factored into the *in vitro* model, i.e. gender, ratio of spillover NEFA and TAG-rich remnants.

6.3 Conclusion

In this thesis work, I have used hepatocyte models to study the effect of differing compositions of FA treatment towards IHTAG accumulation and explored the metabolic consequences of altering FA treatment media composition.

To the MASLD field in general, I have contributed the development of culture conditions which more closely mimic physiology. Some of this work has since been published (Appendix **??**).

Overall, I developed physiologically-relevant models of hepatocellular metabolism and steatosis, reflecting differences in dietary composition. Data showed that although FA composition did not alter IHTAG accumulation, it did alter a number of metabolic pathways, including oxidation, glucose handling, and significantly it had a strong effect on LD morphology.

Appendices

A

A.1 Supplementary Material for Chapter 2

A.1.1 PHH phenotypic factors

Table A.1: Primary human hepatocytes (PHH) donor phenotype

Donor ID	Gender	Race	Age (Yr)	BMI	Tobacco History	Alcohol History	Drug History	Cause of Death	Other
HU8339-A	Female	African American	31	18.9	Yes	Yes	Marijuana	Asphyxiation	N/A
HU2016	Female	African American	65	39.59	Yes	Yes	Bydureon, Amlodipine, Carvedilol, Losartan, Hydrochlorothiazide, Clonidine, Atorvastatin, Asprin, Clopidogrel, Cholecalciferol	N/A	N/A
Hu8356	Male	Caucasian	46	32.1	1 pack/day x 34 yrs	2-3 drinks/month	Cannabis x 30 yrs, cocaine x 1 yr	Asphyxiation	N/A
Huh8345-A	Male	Asian	47	23.9	1 pack/day x 20 yrs	6 beers/day x 20yrs	Cannabis daily x 20 yrs	Anoxia/CVA	N/A
Hu8148	Female	Caucasian	55	22.8	2-3 cigarettes/day x 2months	4 drinks/day x 32 yrs, stopped 10yrs before death	Cannabis daily x 5 yrs, stopped 30 years before death	CNA	Brain Tumor

A.1.2 Molar quantities of TAG in Huh7 cells

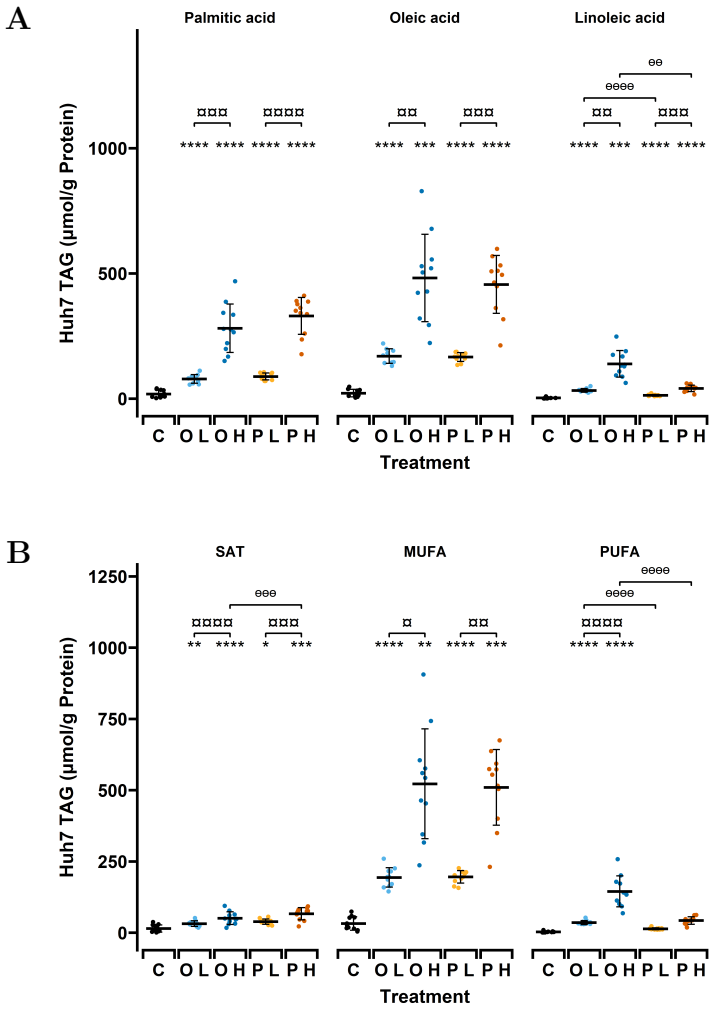


Figure A.1: Intrahepatocellular triacylglycerol (IHTAG) concentration and composition in Huh7 cells following treatment with different FA compositions. A) Concentration of total TAG after culturing with OPLA and POLA, by OPLA and POLA FA (α- linoleic acid not included as represents <1 mol% and did not change with treatment); B) Concentration of total IHTAG by degree of saturation. Data presented as mean +/- SD, n = 9 per treatment unless stated otherwise. Abbreviations: C, no fat control; OL, low (200µM) concentration OPLA, OH, high (800µM) concentration OPLA; PL, low (200µM) concentration POLA; PH, high (800µM) concentration POLA. Significance is indicated by '*' for comparison of treatment with control, '¤' for OPLA and POLA between concentrations, and 'θ' for OPLA verse POLA at the same concentration. Significance levels indicated are * $p<0.05$, ** $p<0.01$ and *** $p<0.001$ with the symbol changing appropriately.

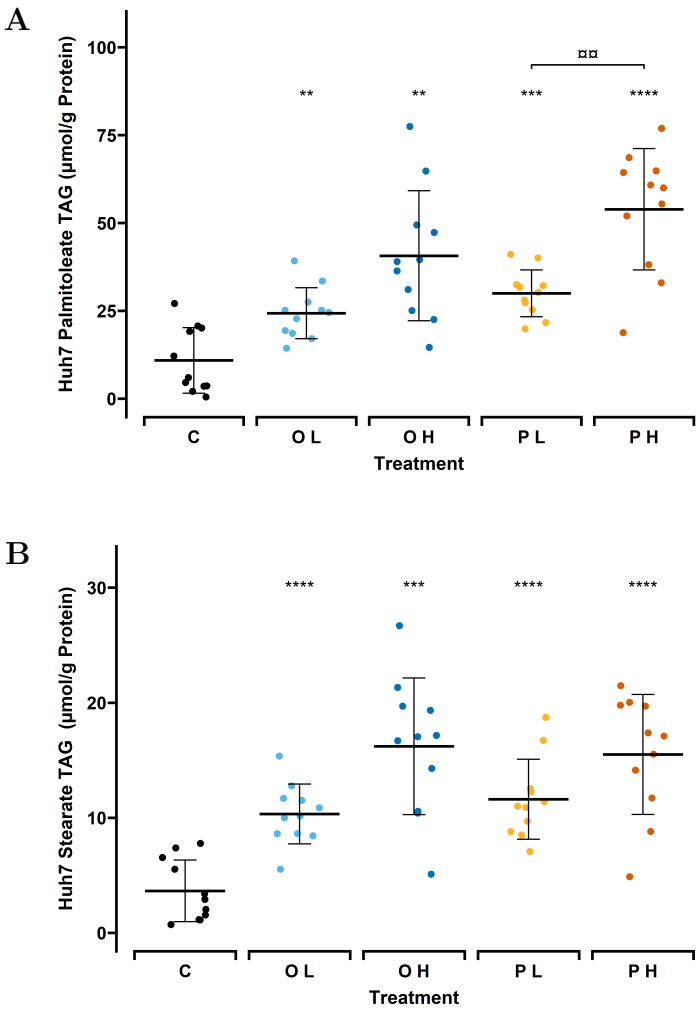


Figure A.2: Huh7 concentration of triacyglycerol (TAG) derived palmitoleic acid and stearic acid in fatty acid (FA) treated Huh7 cells. A) Concentration of palmitoleic acid in FA treated Huh7 cells; B) Concentration of stearic acid in FA treated Huh7 cells. Data presented as mean +/- SD, n = 9 per treatment unless stated otherwise. Abbreviations: C, no fat control; OL, low (200µM) concentration OPLA, OH, high (800µM) concentration OPLA; PL, low (200µM) concentration POLA; PH, high (800µM) concentration POLA. Significance is indicated by '*' for comparison of treatment with control, '¤' for OPLA and POLA between concentrations, and 'θ' for OPLA verse POLA at the same concentration. Significance levels indicated are * $p<0.05$, ** $p<0.01$ and *** $p<0.001$ with the symbol changing appropriately.

A.1.3 Molar quantities of PL in Huh7 cells

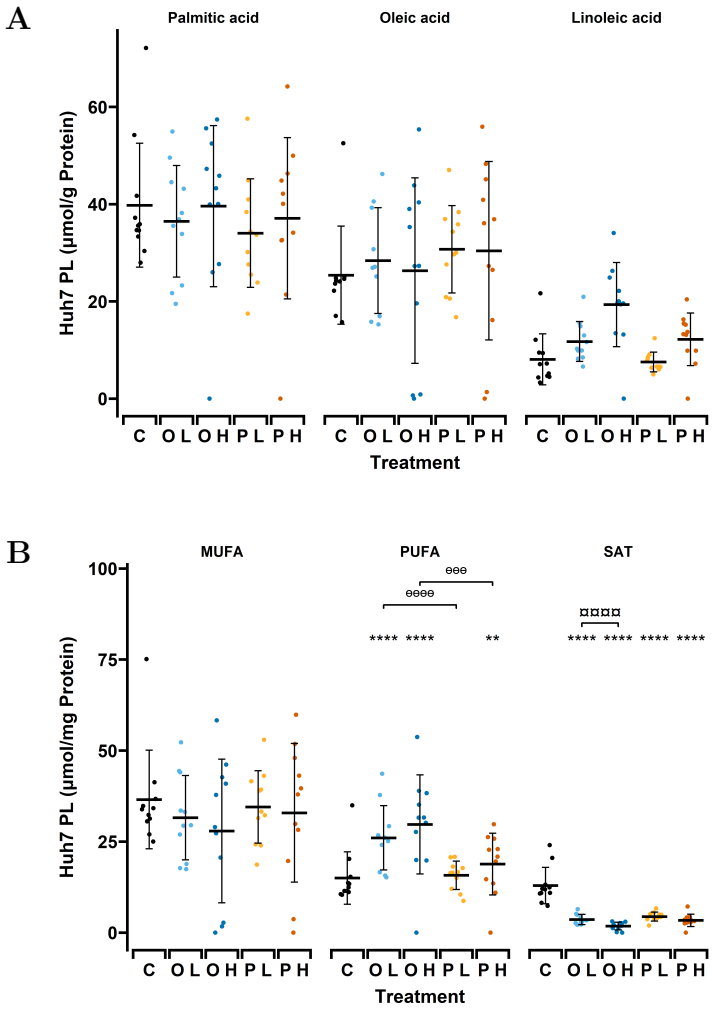


Figure A.3: Intrahepatocellular phospholipid (PL) concentration and composition in Huh7 cells following treatment with different FA compositions. A) Concentration of total PL after culturing with OPLA and POLA, by OPLA and POLA FA (α- linoleic acid not included as represents <1 mol% and did not change with treatment); B) Concentration of total intrahepatocellular PL by degree of saturation. Data presented as mean +/- SD, n = 9 per treatment unless stated otherwise. Abbreviations: C, no fat control; OL, low (200µM) concentration OPLA, OH, high (800µM) concentration OPLA; PL, low (200µM) concentration POLA; PH, high (800µM) concentration POLA. Significance is indicated by '*' for comparison of treatment with control, '¤' for OPLA and POLA between concentrations, and 'θ' for OPLA verse POLA at the same concentration. Significance levels indicated are * $p<0.05$, ** $p<0.01$ and *** $p<0.001$ with the symbol changing appropriately.

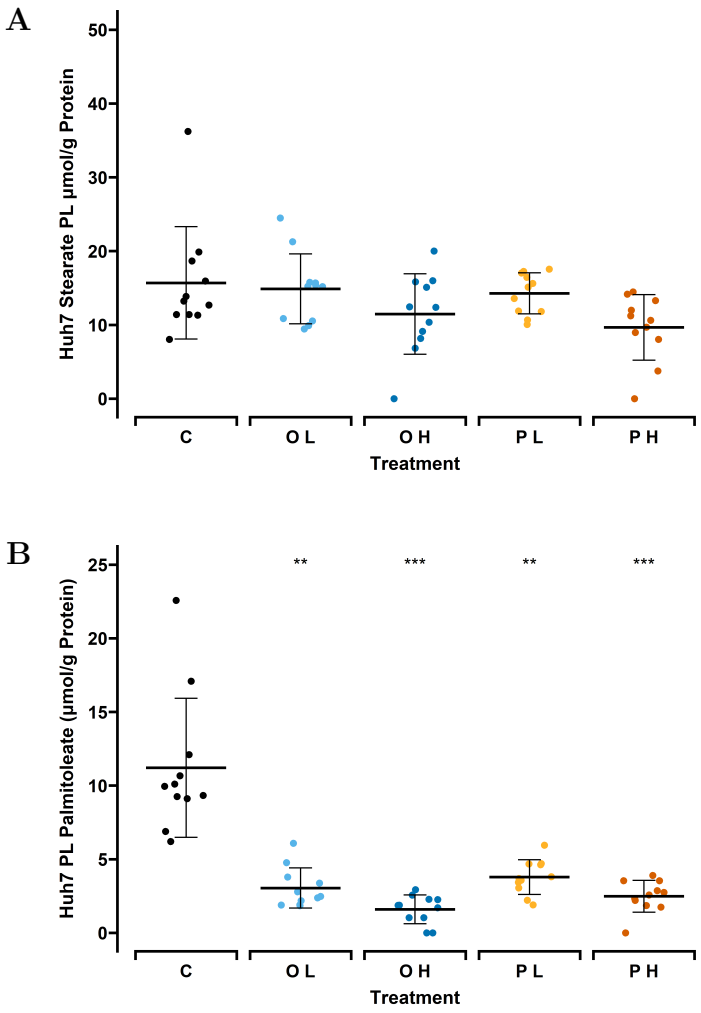


Figure A.4: Huh7 concentration of phospholipid (PL) derived palmitoleic acid and stearic acid in fatty acid (FA) treated Huh7 cells. A) Concentration of palmitoleic acid in FA treated Huh7 cells; B) Concentration of stearic acid in FA treated Huh7 cells. Data presented as mean +/- SD, n = 9 per treatment unless stated otherwise. Abbreviations: C, no fat control; OL, low (200µM) concentration OPLA, OH, high (800µM) concentration OPLA; PL, low (200µM) concentration POLA; PH, high (800µM) concentration POLA. Significance is indicated by '*' for comparison of treatment with control, '¤' for OPLA and POLA between concentrations, and 'θ' for OPLA verse POLA at the same concentration. Significance levels indicated are * $p<0.05$, ** $p<0.01$ and *** $p<0.001$ with the symbol changing appropriately.

A.1.4 Molar quantities of TAG in PHH

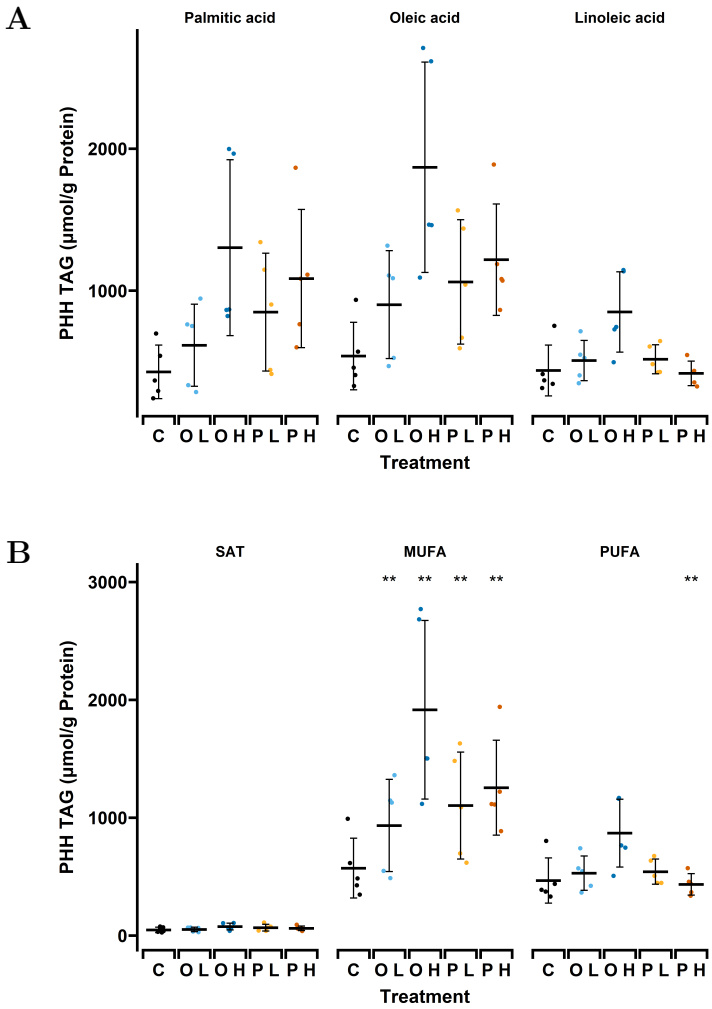


Figure A.5: Intrahepatocellular triacylglycerol (IHTAG) concentration and composition in PHH following treatment with different FA compositions. A) Concentration of total TAG after culturing with OPLA and POLA, by OPLA and POLA FA (α- linoleic acid not included as represents <1 mol% and did not change with treatment); B) Concentration of total IHTAG by degree of saturation. Data presented as mean +/- SD, n = 9 per treatment unless stated otherwise. Abbreviations: C, no fat control; OL, low (200µM) concentration OPLA, OH, high (800µM) concentration OPLA; PL, low (200µM) concentration POLA; PH, high (800µM) concentration POLA. Significance is indicated by '*' for comparison of treatment with control, '¤' for OPLA and POLA between concentrations, and 'θ' for OPLA verse POLA at the same concentration. Significance levels indicated are * $p<0.05$, ** $p<0.01$ and *** $p<0.001$ with the symbol changing appropriately.

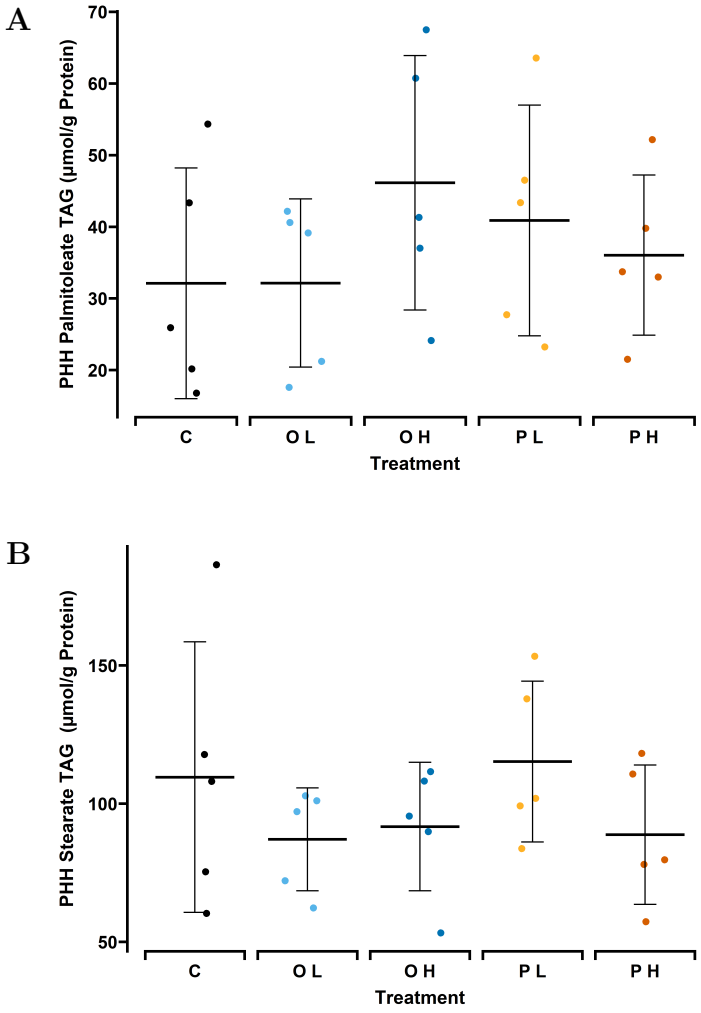


Figure A.6: PHH concentration of triacyglycerol (TAG) derived palmitoleic acid and stearic acid in fatty acid (FA) treated Huh7 cells. A) Concentration of palmitoleic acid in FA treated Huh7 cells; B) Concentration of stearate in FA treated PHH cells. Data presented as mean +/- SD, n = 9 per treatment unless stated otherwise. Abbreviations: C, no fat control; OL, low (200µM) concentration OPLA, OH, high (800µM) concentration OPLA; PL, low (200µM) concentration POLA; PH, high (800µM) concentration POLA. Significance is indicated by '*' for comparison of treatment with control, '¤' for OPLA and POLA between concentrations, and 'θ' for OPLA verse POLA at the same concentration. Significance levels indicated are * $p<0.05$, ** $p<0.01$ and *** $p<0.001$ with the symbol changing appropriately.

A.1.5 Molar quantities of PL in PHH

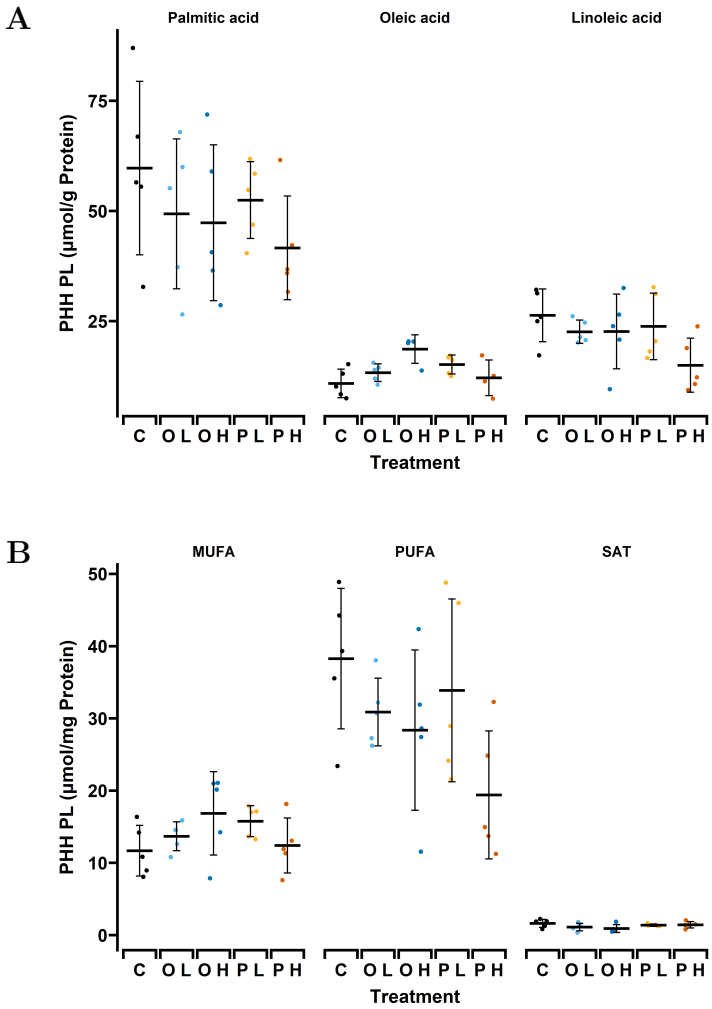


Figure A.7: Intrahepatocellular phospholipid (PL) concentration and composition in PHH following treatment with different FA compositions. A) Concentration of total intrahepatocellular PL by degree of saturation. Data presented as mean +/- SD, n = 9 per treatment unless stated otherwise. Abbreviations: C, no fat control; OL, low (200µM) concentration OPLA, OH, high (800µM) concentration OPLA; PL, low (200µM) concentration POLA; PH, high (800µM) concentration POLA. Significance is indicated by '*' for comparison of treatment with control, '¤' for OPLA and POLA between concentrations, and 'θ' for OPLA verse POLA at the same concentration. Significance levels indicated are * $p<0.05$, ** $p<0.01$ and *** $p<0.001$ with the symbol changing appropriately.

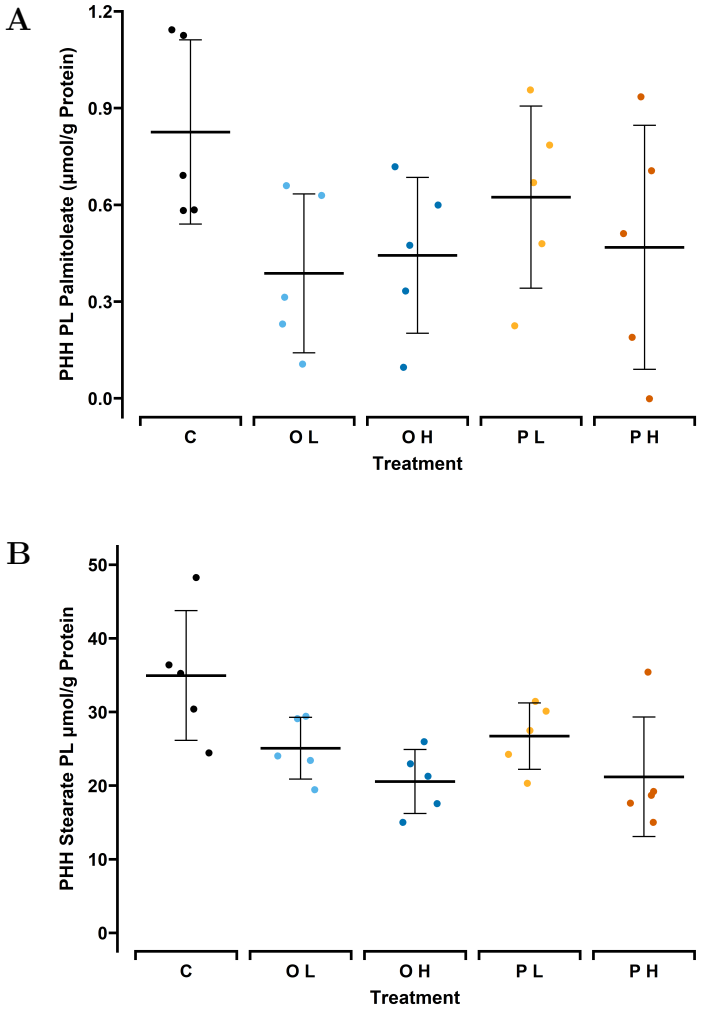


Figure A.8: Huh7 concentration of phospholipid (PL) derived palmitoleic acid and stearic acid in fatty acid (FA) treated Huh7 cells. A) Concentration of palmitoleic acid in FA treated Huh7 cells; B) Concentration of stearic acid in FA treated PHH cells. Data presented as mean +/- SD, n = 9 per treatment unless stated otherwise. Abbreviations: C, no fat control; OL, low (200µM) concentration OPLA, OH, high (800µM) concentration OPLA; PL, low (200µM) concentration POLA; PH, high (800µM) concentration POLA. Significance is indicated by '*' for comparison of treatment with control, '¤' for OPLA and POLA between concentrations, and 'θ' for OPLA verse POLA at the same concentration. Significance levels indicated are * $p<0.05$, ** $p<0.01$ and *** $p<0.001$ with the symbol changing appropriately.

A.2 Supplementary Material for Chapter 3

A.2.1 Publication by Novogene, describing their methods for RNA sequencing

Method

Sample Quality Control

Please refer to QC report for methods of sample quality control.

Library Construction, Quality Control and Sequencing

Messenger RNA was purified from total RNA using poly-T oligo-attached magnetic beads. After fragmentation, the first strand cDNA was synthesized using random hexamer primers, followed by the second strand cDNA synthesis using either dUTP for directional library or dTTP for non-directional library.

For the non-directional library, it was ready after end repair, A-tailing, adapter ligation, size selection, amplification, and purification(**Figure A**).

For the **directional** library, it was ready after end repair, A-tailing, adapter ligation, size selection, **USER enzyme digestion**, amplification, and purification(**Figure B**).

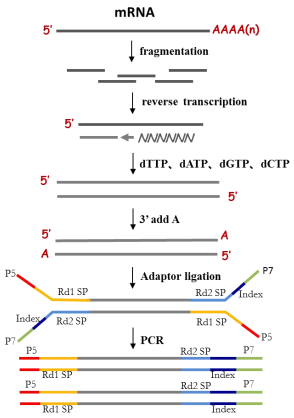


Figure A Workflow of non-directional library construction

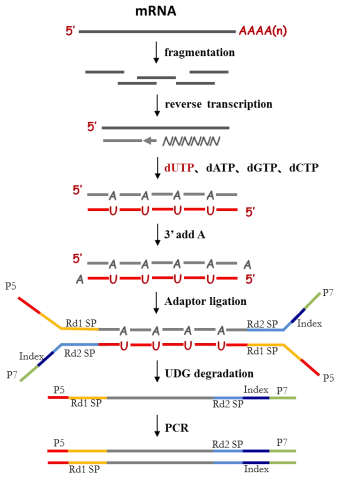


Figure B Workflow of directional library construction

The library was checked with Qubit and real-time PCR for quantification and bioanalyzer for size distribution detection. Quantified libraries will be pooled and sequenced on Illumina platforms, according to effective library concentration and data amount.

Clustering and sequencing

The clustering of the index-coded samples was performed according to the manufacturer's instructions. After cluster generation, the library preparations were sequenced on an Illumina platform and paired-end reads were generated.

Data Analysis

Quality control

Raw data (raw reads) of fastq format were firstly processed through in-house perl scripts. In this step, clean data (clean reads) were obtained by removing reads containing adapter, reads containing ploy-N and low quality reads from raw data. At the same time, Q20, Q30 and GC content the clean data were calculated. All the downstream analyses were based on the clean data with high quality.

Reads mapping to the reference genome

Reference genome and gene model annotation files were downloaded from genome website directly. Index of the reference genome was built using Hisat2 v2.0.5 and paired-end clean

reads were aligned to the reference genome using Hisat2 v2.0.5. We selected Hisat2 as the mapping tool for that Hisat2 can generate a database of splice junctions based on the gene model annotation file and thus a better mapping result than other non-splice mapping tools.

Quantification of gene expression level

featureCounts v1.5.0-p3 was used to count the reads numbers mapped to each gene. And then FPKM of each gene was calculated based on the length of the gene and reads count mapped to this gene. FPKM, expected number of Fragments Per Kilobase of transcript sequence per Millions base pairs sequenced, considers the effect of sequencing depth and gene length for the reads count at the same time, and is currently the most commonly used method for estimating gene expression levels.

Differential expression analysis

(For DESeq2 with biological replicates) Differential expression analysis of two conditions/groups (two biological replicates per condition) was performed using the DESeq2 R package (1.20.0). DESeq2 provide statistical routines for determining differential expression in digital gene expression data using a model based on the negative binomial distribution. The resulting P-values were adjusted using the Benjamini and Hochberg's approach for controlling the false discovery rate . Genes with an adjusted P-value <=0.05 found by DESeq2 were assigned as differentially expressed.

(For edgeR without biological replicates) Prior to differential gene expression analysis, for each sequenced library, the read counts were adjusted by edgeR program package through one scaling normalized factor. Differential expression analysis of two conditions was performed using the edgeR R package (3.22.5). The P values were adjusted using the Benjamini & Hochberg method. Corrected P-value of 0.05 and absolute foldchange of 2 were set as the threshold for significantly differential expression.

Enrichment analysis of differentially expressed genes

Gene Ontology (GO) enrichment analysis of differentially expressed genes was implemented by the clusterProfiler R package, in which gene length bias wascorrected. GO terms with corrected Pvalue less than 0.05 were considered significantly enriched by differential expressed genes. KEGG is a database resource for understanding high-level functions and

utilities of the biological system, such as the cell, the organism and the ecosystem, from molecular-level information, especially large-scale molecular datasets generated by genome sequencing and other high-through put experimental technologies (http://www.genome.jp/kegg/). We used clusterProfiler R package to test the statistical enrichment of differential expression genes in KEGG pathways. The Reactome database brings together the various reactions and biological pathways of human model species. Reactome pathways with corrected Pvalue less than 0.05 were considered significantly enriched by differential expressed genes. The DO (Disease Ontology) database describes the function of human genes and diseases. DO pathways with corrected Pvalue less than 0.05 were considered significantly enriched by differential expressed genes. The DisGeNET database integrates human disease-related genes. DisGeNET pathways with corrected Pvalue less than 0.05 were considered significantly enriched by differential expressed genes. We used clusterProfiler software to test the statistical enrichment of differentially expressed genes in the Reactome pathway, the DO pathway, and the DisGeNET pathway.

Gene Set Enrichment Analysis

Gene Set Enrichment Analysis (GSEA) is a computational approach to determine if a pre-defined Gene Set can show a significant consistent difference between two biological states. The genes were ranked according to the degree of differential expression in the two samples, and then the predefined Gene Set were tested to see if they were enriched at the top or bottom of the list. Gene set enrichment analysis can include subtle expression changes. We use the local version of the GSEA analysis tool http://www.broadinstitute.org/gsea/index.jsp, GO、KEGG、Reactome、DO and DisGeNET data sets were used for GSEA independently.

SNP analysis

GATK (v4.1.1.0) software was used to perform SNP calling. Raw vcf files were filtered with GATK standard filter method and other parameters (cluster:3; WindowSize:35; QD < 2.0 ; FS > 30.0; DP < 10.

AS analysis

Alternative Splicing is an important mechanism for regulate the expression of genes and the

variable of protein. rMATS(4.1.0) software was used to analysis the AS event.

PPI analysis of differentially expressed genes

PPI analysis of differentially expressed genes was based on the STRING database, which known and predicted Protein-Protein Interactions.

Fusion Analysis

Fusion gene refers to the chimeric gene formed by the fusion of all or part of the sequences of two genes, which is generally caused by chromosome translocation, deletion and other reasons. We used Starfusion software (1.9.0) to detect genes that are fused. Star-fusion is a software package uses fusion output results of STAR alignment to detect fusion transcripts, including SATR alignment, SATRfusion. predict, SATR-fusion.filter was used to correct the predicted results of Star-fusion to ensure the accuracy of the results.

A.3 Supplementary Material for Chapter 4

A.3.1 Huh7 media lipid following 14 days of culturing with FA treatments

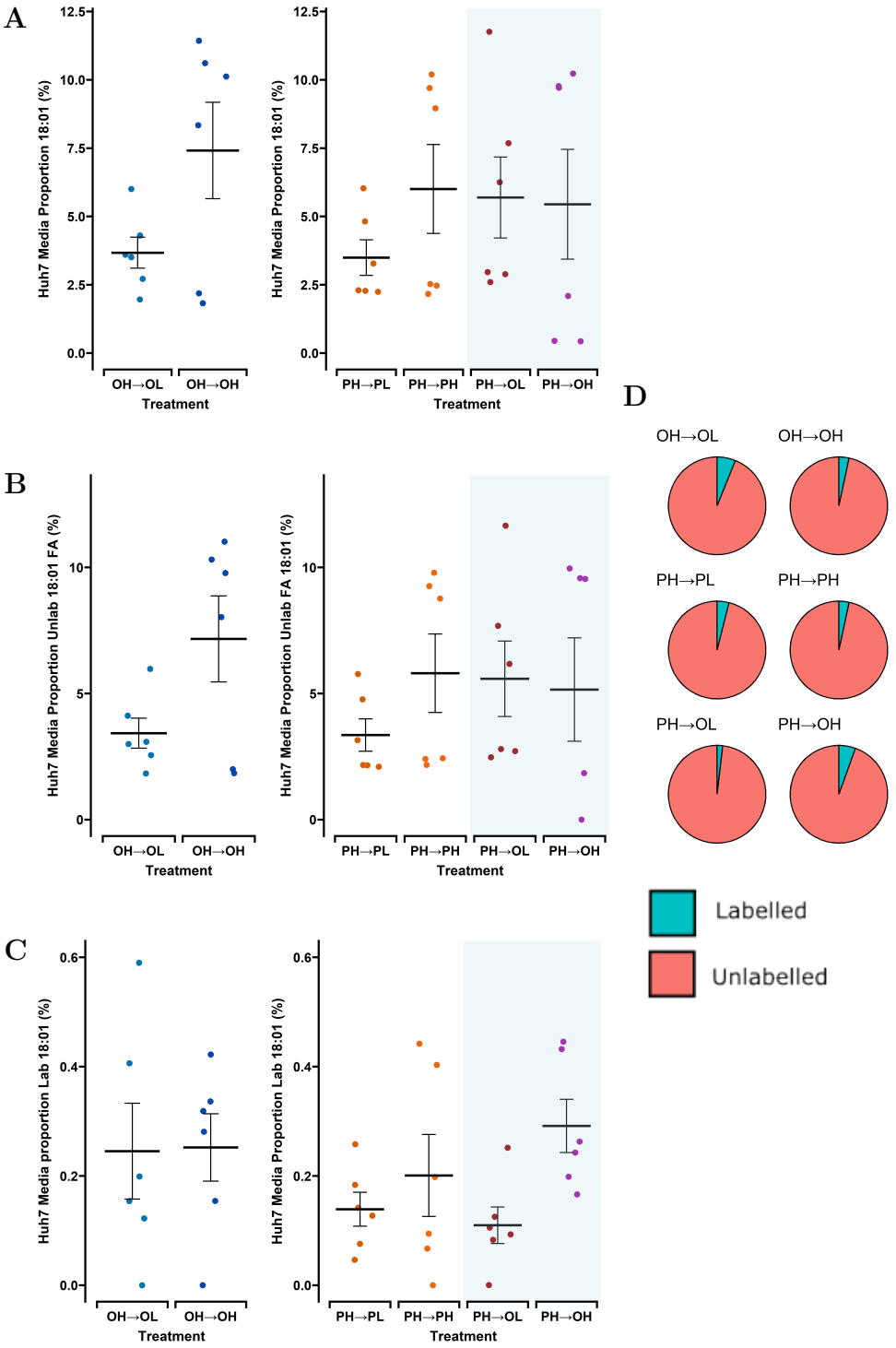


Figure A.9: Media Oleic acid FA content in Huh7 cells. A) Proportion of total FA constituted by either labelled or unlabelled oleic acid (18:1n-9), B) Proportion of total FA constituted by unlabelled oleic acid (18:1n-9),C) Proportion of total FA constituted by labelled oleic acid (D-33 18:1n-9). Data presented as mean +/- SD, n = 6 per treatment unless stated otherwise. Abbreviations: OH→OL, first week at high (800µM) and second week at low (200µM) of OPLA; OH→OH, two weeks at high of OPLA; PH→PL, first week at high and second week at low of POLA; PH→PH, two weeks at high of POLA; PH→OL, first week at high POLA and second week at low of OPLA; PH→OH, first week at high of POLA and second week at high of OPLA. Significance levels indicated are * $p<0.05$, ** $p<0.01$ and *** $p<0.001$.

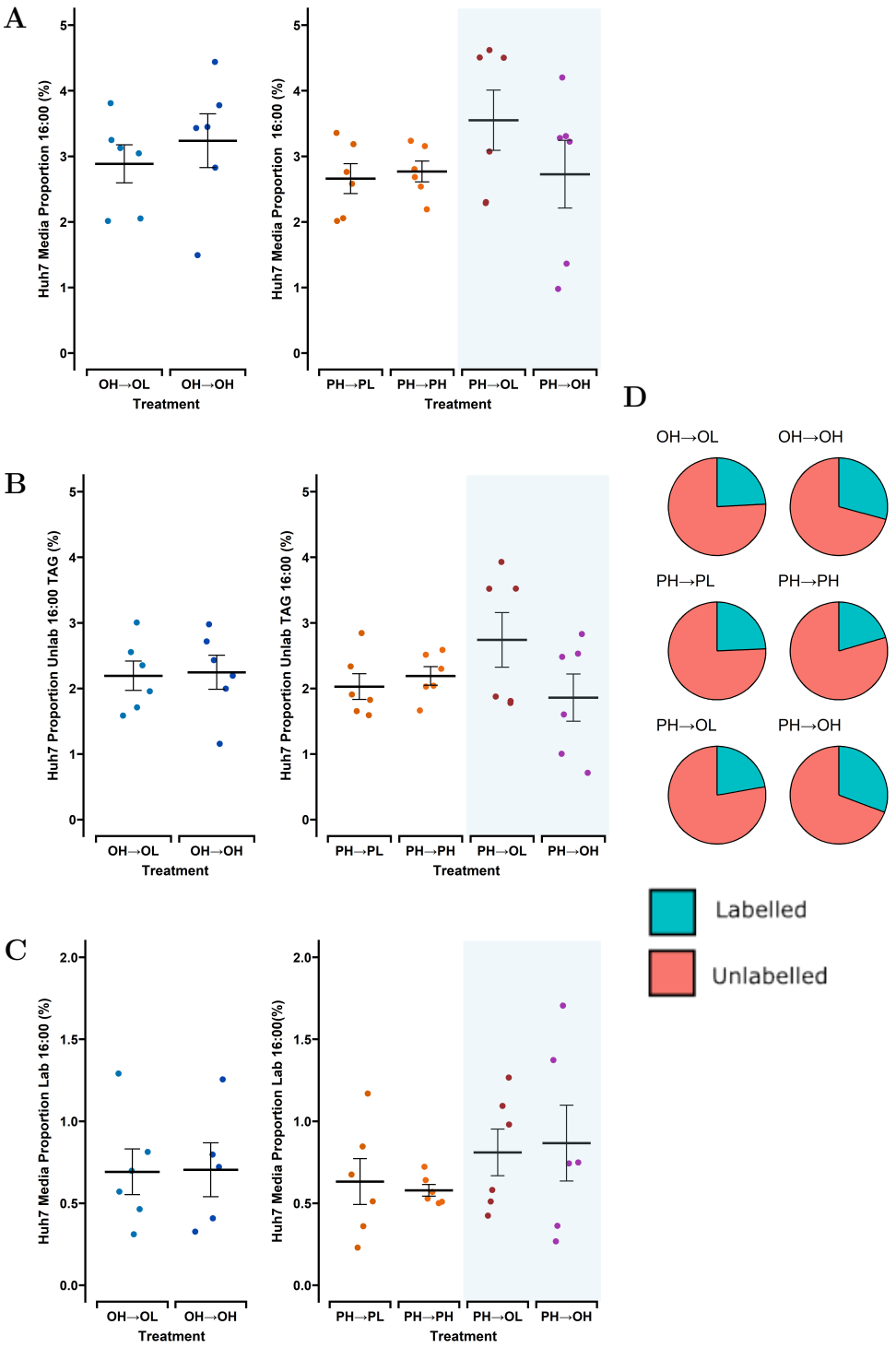


Figure A.10: Media palmitic acid FA content in Huh7 cells. A) Proportion of total FA constituted by either labelled or unlabelled palmitic acid or labelled palmitic acid (D31), B) Proportion of total FA constituted by unlabelled palmitic acid, C) Proportion of total FA constituted by labelled palmitic acid. Data presented as mean +/- SD, n = 6 per treatment unless stated otherwise. Abbreviations: OH→OL, first week at high (800µM) and second week at low (200µM) of OPLA; OH→OH, two weeks at high of OPLA; PH→PL, first week at high and second week at low of POLA; PH→PH, two weeks at high of POLA; PH→OL, first week at high POLA and second week at low of OPLA; PH→OH, first week at high of POLA and second week at high of OPLA.

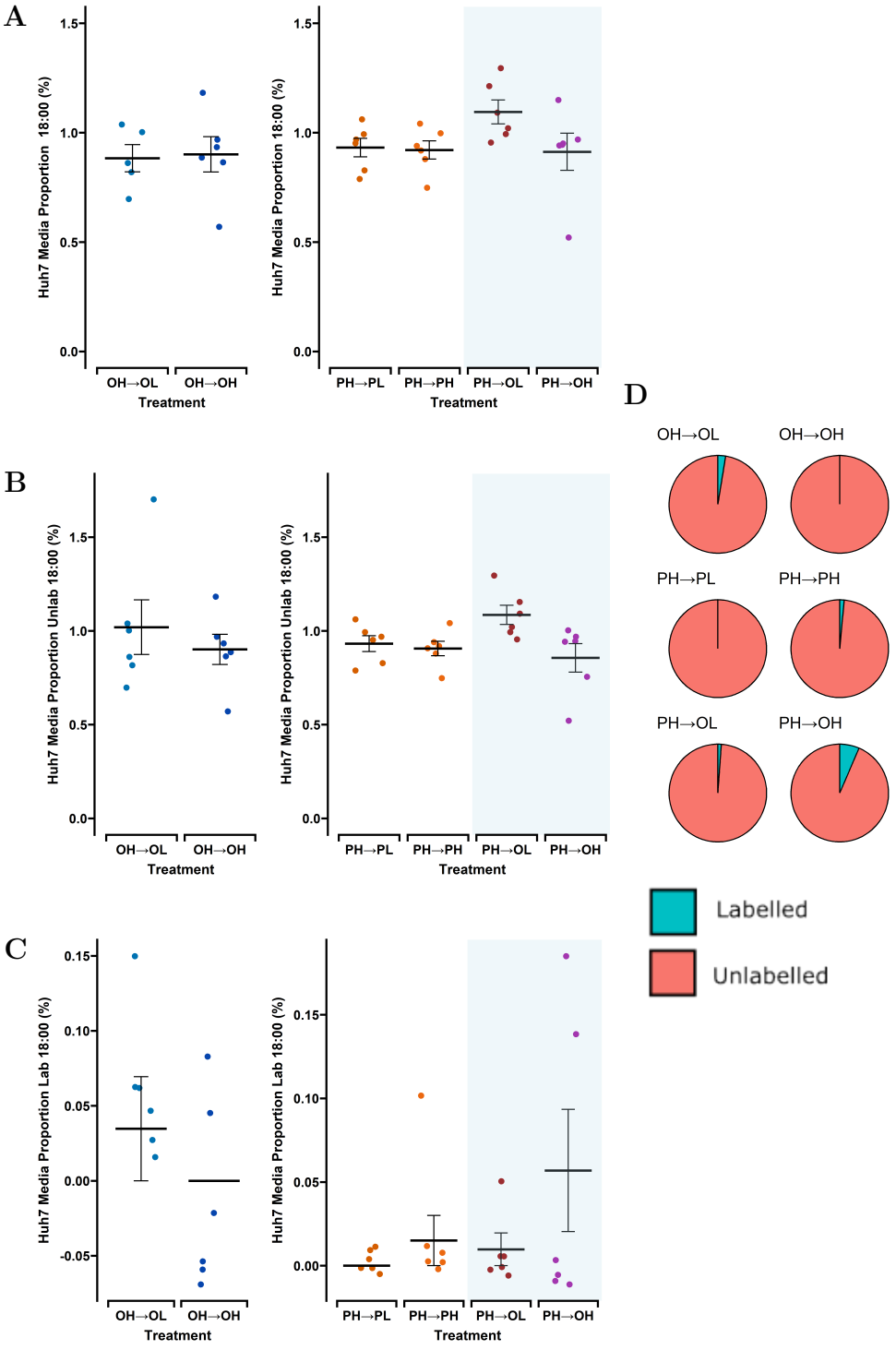


Figure A.11: Media stearic acid FA content in Huh7 cells. A) Proportion of total FA constituted by either labelled or unlabelled stearic acid , B) Proportion of total FA constituted by unlabelled stearic acid, C) Proportion of total TAG constituted by labelled stearic acid. Data presented as mean +/- SD, n = 6 per treatment unless stated otherwise. Abbreviations: OH→OL, first week at high (800µM) and second week at low (200µM) of OPLA; OH→OH, two weeks at high of OPLA; PH→PL, first week at high and second week at low of POLA; PH→PH, two weeks at high of POLA; PH→OL, first week at high POLA and second week at low of OPLA; PH→OH, first week at high of POLA and second week at high of OPLA.

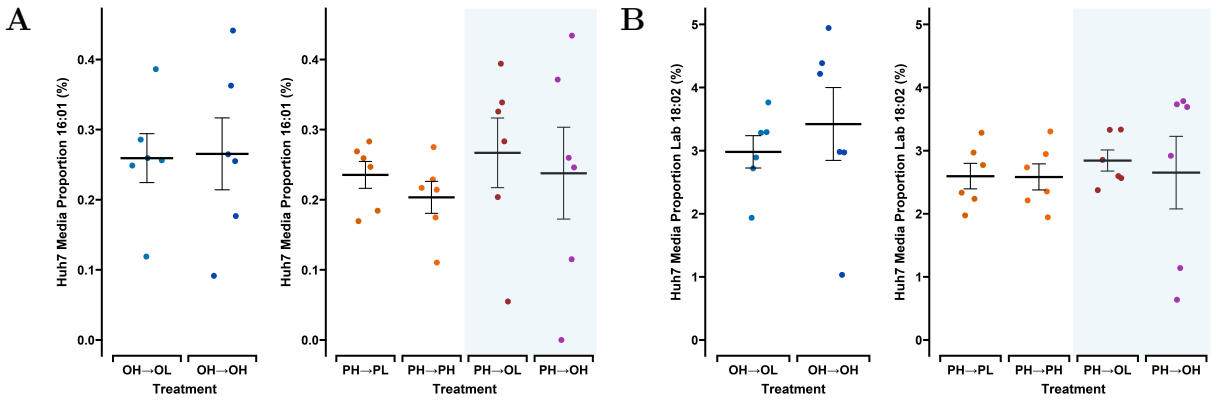


Figure A.12: Media Palmitoleate and linoleic acid. A) palmitoleate proportion of media FA B) Linoleic acid proportion of media FA. Data presented as mean +/- SD, n = 6 per treatment unless stated otherwise. Abbreviations: OH→OL, first week at high (800µM) and second week at low (200µM) of OPLA; OH→OH, two weeks at high of OPLA; PH→PL, first week at high and second week at low of POLA; PH→PH, two weeks at high of POLA; PH→OL, first week at high POLA and second week at low of OPLA; PH→OH, first week at high of POLA and second week at high of OPLA.

A.4 Supplementary Material for Chapter 5

A.4.1 Participant post parandial breath samples

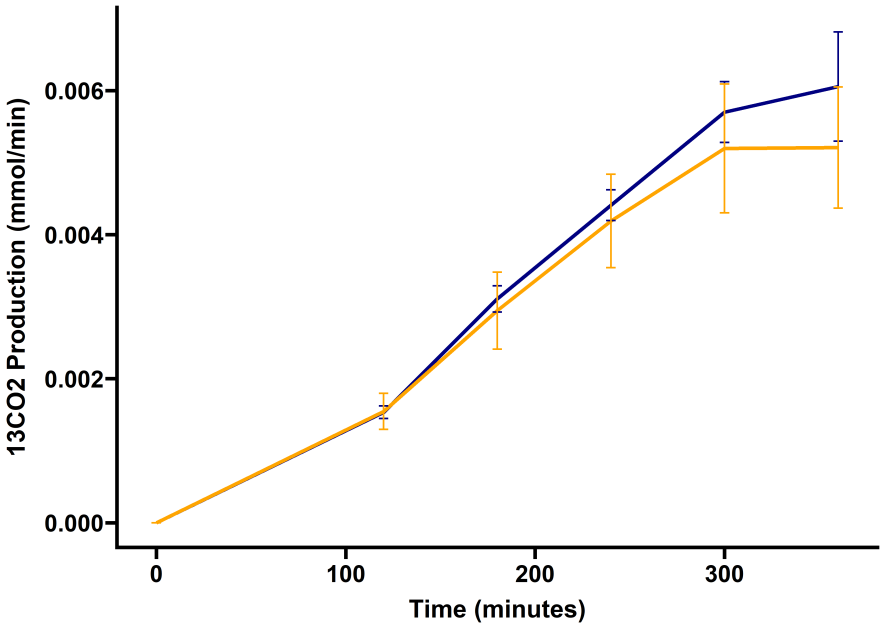


Figure A.13: Production of $^{13}CO_2$ in the breath over the post-prandial study day. Blue line indicates data from diet enriched in UNSFA and orange line indicates diet enriched in SFA. Data show mean +/- SD.

A.4.2 Participant insulin concentration

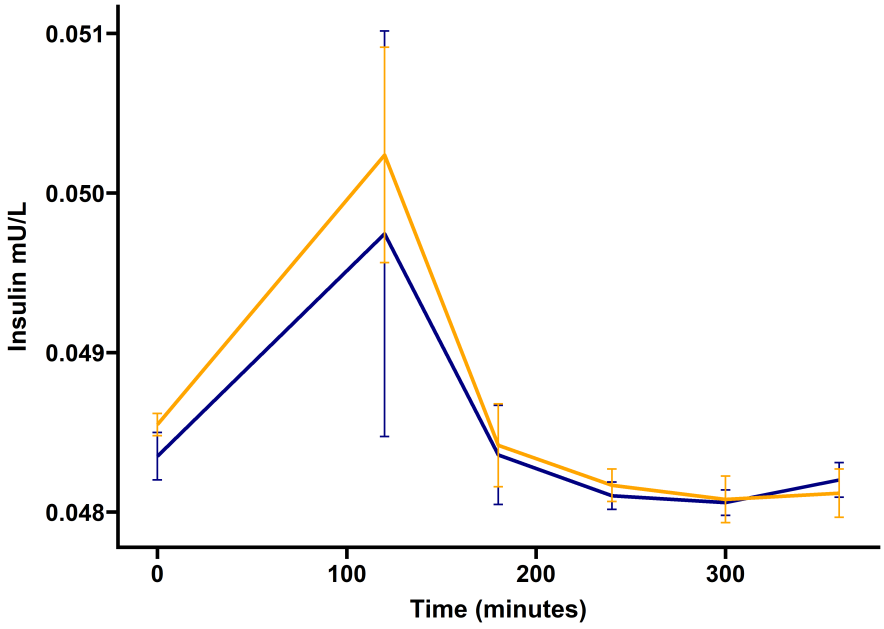


Figure A.14: Study day plasma insulin concentration. A) Plasma Insulin. Blue line indicates data from diet enriched in UNSFA and orange line indicates diet enriched in SFA. Data show mean +/- SD.

References

Aarsland, A., Chinkes, D., and Wolfe, R. R. (June 1997). "Hepatic and whole-body fat synthesis in humans during carbohydrate overfeeding." In: *The American journal of clinical nutrition* 65.6, pp. 1774–82.

Adiels, M., Olofsson, S. O., Taskinen, M. R., and Borén, J. (July 2008). "Overproduction of very low-density lipoproteins is the hallmark of the dyslipidemia in the metabolic syndrome". In: *Arteriosclerosis, thrombosis, and vascular biology* 28.7, pp. 1225–1236.

Adolph, T. E., Grander, C., Grabherr, F., and Tilg, H. (July 2017). "Adipokines and Non-Alcoholic Fatty Liver Disease: Multiple Interactions". In: *International Journal of Molecular Sciences 2017, Vol. 18, Page 1649* 18.8, p. 1649.

Agius, L. (Aug. 2008). *Glucokinase and molecular aspects of liver glycogen metabolism.*

Ahadi, M., Molooghi, K., Masoudifar, N., Namdar, A. B., Vossoughinia, H., and Farzanehfar, M. (June 2021). "A review of non-alcoholic fatty liver disease in non-obese and lean individuals". In: *Journal of gastroenterology and hepatology* 36.6, pp. 1497–1507.

Ahmed, H., Umar, M. I., Imran, S., Javaid, F., Syed, S. K., Riaz, R., and Hassan, W. (Feb. 2022). "TGF-β1 signaling can worsen NAFLD with liver fibrosis backdrop". In: *Experimental and molecular pathology* 124.

Ahrén, B. and Holst, J. J. (May 2001). "The cephalic insulin response to meal ingestion in humans is dependent on both cholinergic and noncholinergic mechanisms and is important for postprandial glycemia." In: *Diabetes* 50.5, pp. 1030–8.

Allain, C. C., Poon, L. S., Chan, C. S. G., Richmond, W., and Fu, P. C. (Apr. 1974). "Enzymatic Determination of Total Serum Cholesterol". In: *Clinical Chemistry* 20.4, pp. 470–475.

Alshawsh, M. A., Alsalahi, A., Alshehade, S. A., Saghir, S. A. M., Ahmeda, A. F., Zarzour, R. H. A., and Mahmoud, A. M. (Feb. 2022). "A Comparison of the Gene Expression Profiles of Non-Alcoholic Fatty Liver Disease between Animal Models of a High-Fat Diet and Methionine-Choline-Deficient Diet". In: *Molecules (Basel, Switzerland)* 27.3.

Alves-Bezerra, M. and Cohen, D. E. (Jan. 2018). "Triglyceride metabolism in the liver". In: *Comprehensive Physiology* 8.1, pp. 1–22.

Amara, U., Rittirsch, D., Flierl, M., Bruckner, U., Klos, A., Gebhard, F., Lambris, J. D., and Huber-Lang, M. (2008). "Interaction Between the Coagulation and Complement System". In: *Advances in experimental medicine and biology.* Vol. 632. NIH Public Access, pp. 68–76.

Anderson, J. J., Gray, S. R., Welsh, P., Mackay, D. F., Celis-Morales, C. A., Lyall, D. M., Forbes, J., Sattar, N., Gill, J. M., and Pell, J. P. (Apr. 2020). "The associations of sugar-sweetened, artificially sweetened and naturally sweet juices with all-cause mortality in 198,285 UK Biobank participants: a prospective cohort study". In: *BMC Medicine* 18.1.

Arendt, B. M., Comelli, E. M., Ma, D. W., Lou, W., Teterina, A., Kim, T., Fung, S. K., Wong, D. K., Mcgilvray, I., Fischer, S. E., and Allard, J. P. (May 2015). "Altered

hepatic gene expression in nonalcoholic fatty liver disease is associated with lower hepatic n-3 and n-6 polyunsaturated fatty acids". In: *Hepatology (Baltimore, Md.)* 61.5, pp. 1565–1578.

Arslanow, A., Teutsch, M., Walle, H., Grünhage, F., Lammert, F., and Stokes, C. S. (June 2016). "Short-Term Hypocaloric High-Fiber and High-Protein Diet Improves Hepatic Steatosis Assessed by Controlled Attenuation Parameter". In: *Clinical and Translational Gastroenterology* 7.6, e176.

Arulraj, R. and Neuberger, J. (Apr. 2011). "Liver transplantation: filling the gap between supply and demand." In: *Clinical medicine (London, England)* 11.2, pp. 194–8.

Baiceanu, A., Mesdom, P., Lagouge, M., and Foufelle, F. (Dec. 2016). *Endoplasmic reticulum proteostasis in hepatic steatosis.*

Bajt, M. L., Yan, H. M., Farhood, A., and Jaeschke, H. (Aug. 2008). "Plasminogen Activator Inhibitor-1 Limits Liver Injury and Facilitates Regeneration after Acetaminophen Overdose". In: *Toxicological Sciences* 104.2, p. 419.

Barrientos-Riosalido, A., Bertran, L., Vilaró-Blay, M., Aguilar, C., Martínez, S., Paris, M., Sabench, F., Riesco, D., Binetti, J., Castillo, D. D., Richart, C., and Auguet, T. (Mar. 2023). "The Role of Olfactomedin 2 in the Adipose Tissue-Liver Axis and Its Implication in Obesity-Associated Nonalcoholic Fatty Liver Disease". In: *International journal of molecular sciences* 24.6.

Berg, J. M., Tymoczko, J. L., Stryer, L., and Gatto, G. J. (2011). *Biochemistry*, p. 1224.

Bertran, L., Jorba-martin, R., Barrientos-riosalido, A., Portillo-carrasquer, M., Aguilar, C., Riesco, D., Martínez, S., Vives, M., Sabench, F., Castillo, D. D., Richart, C., and Auguet, T. (July 2022). "New Insights of OLFM2 and OLFM4 in Gut-Liver Axis and Their Potential Involvement in Nonalcoholic Fatty Liver Disease". In: *International journal of molecular sciences* 23.13.

Bharadwaj, K. G., Hiyama, Y., Hu, Y., Huggins, L. A., Ramakrishnan, R., Abumrad, N. A., Shulman, G. I., Blaner, W. S., and Goldberg, I. J. (Dec. 2010). "Chylomicron- and VLDL-derived lipids enter the heart through different pathways: in vivo evidence for receptor- and non-receptor-mediated fatty acid uptake." In: *The Journal of biological chemistry* 285.49, pp. 37976–86.

Bjornstad, P. and Eckel, R. H. (Oct. 2018). "Pathogenesis of Lipid Disorders in Insulin Resistance: A Brief Review". In: *Current diabetes reports* 18.12, p. 127.

Blenner, M. A., Dong, X., and Springer, T. A. (Feb. 2014). "Structural basis of regulation of von Willebrand factor binding to glycoprotein Ib". In: *The Journal of biological chemistry* 289.9, pp. 5565–5579.

Böhn, L., Störsrud, S., Liljebo, T., Collin, L., Lindfors, P., Törnblom, H., and Simrén, M. (Nov. 2015). "Diet low in FODMAPs reduces symptoms of irritable bowel syndrome as well as traditional dietary advice: a randomized controlled trial". In: *Gastroenterology* 149.6, pp. 1399–1407.

Borradaile, N. M., Han, X., Harp, J. D., Gale, S. E., Ory, D. S., and Schaffer, J. E. (Dec. 2006). "Disruption of endoplasmic reticulum structure and integrity in lipotoxic cell death". In: *Journal of Lipid Research* 47.12, pp. 2726–2737.

Botham, K. M., Avella, M., Cantafora, A., and Bravo, E. (Feb. 1999). "The effect of oestrogen on the metabolism of chylomicron cholesterol in the rat in vivo". In: *Biochemical Society Transactions* 27.1, A50–A50.

Bowerman, K. L., Knowles, S. C. L., Bradley, J. E., Baltrūnaitė, L., Lynch, M. D. J., Jones, K. M., and Hugenholtz, P. (Sept. 2021). "Effects of laboratory domestication on the rodent gut microbiome". In: *ISME Communications 2021 1:1* 1.1, pp. 1–14.

Britton, K. A. and Fox, C. S. (Dec. 2011). "Ectopic fat depots and cardiovascular disease." In: *Circulation* 124.24, pp. 837–41.

Buratta, S., Shimanaka, Y., Costanzi, E., Ni, S., Urbanelli, L., Kono, N., Morena, F., Sagini, K., Giovagnoli, S., Romani, R., Gargaro, M., Arai, H., and Emiliani, C. (123). "Lipotoxic stress alters the membrane lipid profile of extracellular vesicles released by Huh-7 hepatocarcinoma cells". In: *Scientific Reports* | 11, p. 4613.

Burdge, G. C., Wright, P., Jones, A. E., and Wootton, S. A. (Nov. 2000). "A method for separation of phosphatidylcholine, triacylglycerol, non-esterified fatty acids and cholesterol esters from plasma by solid-phase extraction." In: *The British journal of nutrition* 84.5, pp. 781–7.

Burnett, J. R., Hooper, A. J., and Hegele, R. A. (Mar. 1993). *Chylomicron Retention Disease*. University of Washington, Seattle.

Buzzetti, E., Pinzani, M., and Tsochatzis, E. A. (Aug. 2016). "The multiple-hit pathogenesis of non-alcoholic fatty liver disease (NAFLD)". In: *Metabolism: clinical and experimental* 65.8, pp. 1038–1048.

Cahill, G. F. (Aug. 2006). "Fuel Metabolism in Starvation". In: *Annual Review of Nutrition* 26.1, pp. 1–22.

Cai, W., Li, J., Shi, J., Yang, B., Tang, J., Truby, H., and Li, D. (Apr. 2018). "Acute metabolic and endocrine responses induced by glucose and fructose in healthy young subjects: A double-blinded, randomized, crossover trial". In: *Clinical nutrition (Edinburgh, Scotland)* 37.2, pp. 459–470.

Cargnoni, A., Farigu, S., Cotti Piccinelli, E., Bonassi Signoroni, P., Romele, P., Vanosi, G., Toschi, I., Cesari, V., Barros Sant'Anna, L., Magatti, M., Silini, A. R., and Parolini, O. (Feb. 2018). "Effect of human amniotic epithelial cells on pro-fibrogenic resident hepatic cells in a rat model of liver fibrosis". In: *Journal of Cellular and Molecular Medicine* 22.2, pp. 1202–1213.

Carotti, S., Aquilano, K., Zalfa, F., Ruggiero, S., Valentini, F., Zingariello, M., Francesconi, M., Perrone, G., Alletto, F., Antonelli-Incalzi, R., Picardi, A., Morini, S., Lettieri-Barbato, D., and Vespasiani-Gentilucci, U. (July 2020). "Lipophagy Impairment Is Associated With Disease Progression in NAFLD." In: *Frontiers in physiology* 11, p. 850.

Casares, D., Escribá, P. V., and Rosselló, C. A. (May 2019). "Membrane Lipid Composition: Effect on Membrane and Organelle Structure, Function and Compartmentalization and Therapeutic Avenues". In: *International Journal of Molecular Sciences* 20.9, p. 2167.

Chakrabarti, P., Kim, J. Y., Singh, M., Shin, Y.-K., Kim, J., Kumbrink, J., Wu, Y., Lee, M.-J., Kirsch, K. H., Fried, S. K., and Kandror, K. V. (Sept. 2013). "Insulin Inhibits Lipolysis in Adipocytes via the Evolutionarily Conserved mTORC1-Egr1-ATGL-Mediated Pathway". In: *Molecular and Cellular Biology* 33.18, p. 3659.

Chalasani, N., Younossi, Z., Lavine, J. E., Diehl, A. M., Brunt, E. M., Cusi, K., Charlton, M., and Sanyal, A. J. (June 2012). "The diagnosis and management of non-alcoholic fatty liver disease: Practice Guideline by the American Association for the Study of Liver Diseases, American College of Gastroenterology, and the American Gastroenterological Association". In: *Hepatology* 55.6, pp. 2005–2023.

Chávez, S. M., Poniachik, J. M., Urzua, Á. M., Roblero, J. P., Cattaneo, M. J., Jimenez, A. P., Carreño, L. E., and Cornejo, R. A. (Sept. 2021). "Acute liver failure due to herpes simplex virus: diagnostic clues and potential role of plasmapheresis: A case report". In: *Medicine* 100.35, E27139.

Chong, M. F., Fielding, B. A., and Frayn, K. N. (June 2007). "Mechanisms for the acute effect of fructose on postprandial lipemia". In: *The American journal of clinical nutrition* 85.6, pp. 1511–1520.

Choo, V. L., Viguiliouk, E., Blanco Mejia, S., Cozma, A. I., Khan, T. A., Ha, V., Wolever, T. M. S., Leiter, L. A., Vuksan, V., Kendall, C. W. C., Souza, R. J. de, Jenkins, D. J. A., and Sievenpiper, J. L. (Nov. 2018). "Food sources of fructose-containing sugars and glycaemic control: systematic review and meta-analysis of controlled intervention studies." In: *BMJ (Clinical research ed.)* 363, k4644.

Clark, J. M., Brancati, F. L., and Diehl, A. M. (May 2003). "The prevalence and etiology of elevated aminotransferase levels in the United States". In: *The American journal of gastroenterology* 98.5, pp. 960–967.

Clarke, G., Mao, J., Fan, Y., Hann, A., Gupta, A., Nutu, A., Buckel, E., Kayani, K., Murphy, N., Bangash, M. N., Casey, A. L., Wootton, I., Lawson, A. J., Dasari, B. V., Perera, M. T. P., Mergental, H., and Afford, S. C. (Nov. 2023). "N-acetylcysteine: a novel approach to methaemoglobinaemia in normothermic liver machine perfusion". In: *Scientific Reports 2023 13:1* 13.1, pp. 1–8.

Cobelli, C., Federspil, G., Pacini, G., Salvan, A., and Scandellari, C. (Feb. 1982). "An integrated mathematical model of the dynamics of blood glucose and its hormonal control". In: *Mathematical Biosciences* 58.1, pp. 27–60.

Cooper, A. D. (Nov. 1997). "Hepatic uptake of chylomicron remnants". In: *Journal of Lipid Research* 38.11, pp. 2173–2192.

Cooperberg, B. A. and Cryer, P. E. (Nov. 2010). "Insulin Reciprocally Regulates Glucagon Secretion in Humans". In: *Diabetes* 59.11, p. 2936.

Côté, I., Chapados, N. A., and Lavoie, J. M. (Nov. 2014). "Impaired VLDL assembly: a novel mechanism contributing to hepatic lipid accumulation following ovariectomy and high-fat/high-cholesterol diets?" In: *The British journal of nutrition* 112.10, pp. 1592–1600.

Cross, E., Dearlove, D. J., and Hodson, L. (Mar. 2023). "Nutritional regulation of hepatic de novo lipogenesis in humans". In: *Current opinion in clinical nutrition and metabolic care* 26.2, pp. 65–71.

Cunningham, R. P. and Porat-Shliom, N. (Sept. 2021). "Liver Zonation - Revisiting Old Questions With New Technologies". In: *Frontiers in physiology* 12.

Davis, C. G., Goldstein, J. L., Südhof, T. C., Anderson, R. G. W., Russell, D. W., and Brown, M. S. (Apr. 1987). "Acid-dependent ligand dissociation and recycling of LDL receptor mediated by growth factor homology region". In: *Nature* 326.6115, pp. 760–765.

Davis, C., Bryan, J., Hodgson, J., and Murphy, K. (Nov. 2015). "Definition of the Mediterranean Diet; a Literature Review". In: *Nutrients* 7.11, pp. 9139–9153.

DeFronzo, R. A. and Tripathy, D. (Nov. 2009). "Skeletal muscle insulin resistance is the primary defect in type 2 diabetes." In: *Diabetes care* 32 Suppl 2.Suppl 2, pp. 157–63.

Desai, A. J. and Miller, L. J. (Nov. 2018). "Changes in the plasma membrane in metabolic disease: impact of the membrane environment on G protein-coupled receptor structure and function". In: *British Journal of Pharmacology* 175.21, pp. 4009–4025.

Diard, P., Malewiak, M. I., Lagrange, D., and Griglio, S. (May 1994). "Hepatic lipase may act as a ligand in the uptake of artificial chylomicron remnant-like particles by isolated rat hepatocytes." In: *Biochemical Journal* 299.3, pp. 889–894.

Dibner, C., Schibler, U., and Albrecht, U. (Mar. 2010). "The mammalian circadian timing system: organization and coordination of central and peripheral clocks". In: *Annual review of physiology* 72, pp. 517–549.

Ding, C., Li, Y., Guo, F., Jiang, Y., Ying, W., Li, D., Yang, D., Xia, X., Liu, W., Zhao, Y., He, Y., Li, X., Sun, W., Liu, Q., Song, L., Zhen, B., Zhang, P., Qian, X., Qin, J., and He, F. (Oct. 2016). "A Cell-type-resolved Liver Proteome". In: *Molecular & Cellular Proteomics : MCP* 15.10, p. 3190.

Ding, L., Sun, W., Balaz, M., He, A., Klug, M., Wieland, S., Caiazzo, R., Raverdy, V., Pattou, F., Lefebvre, P., Lodhi, I. J., Staels, B., Heim, M., and Wolfrum, C. (Dec. 2021). "Peroxisomal β-oxidation acts as a sensor for intracellular fatty acids and regulates lipolysis". In: *Nature Metabolism 2021 3:12* 3.12, pp. 1648–1661.

Diraison, F., Yankah, V., Letexier, D., Dusserre, E., Jones, P., and Beylot, M. (Apr. 2003). "Differences in the regulation of adipose tissue and liver lipogenesis by carbohydrates in humans". In: *Journal of Lipid Research* 44.4, pp. 846–853.

Dixon, J. B. (Oct. 2010). "Mechanisms of chylomicron uptake into lacteals". In: *Annals of the New York Academy of Sciences* 1207.s1.

Donnelly, K. L., Smith, C. I., Schwarzenberg, S. J., Jessurun, J., Boldt, M. D., and Parks, E. J. (May 2005). "Sources of fatty acids stored in liver and secreted via lipoproteins in patients with nonalcoholic fatty liver disease". In: *The Journal of Clinical Investigation* 115.5, pp. 1343–1351.

Drewnowski, A. and Bellisle, F. (Mar. 2007). "Liquid calories, sugar, and body weight". In: *The American Journal of Clinical Nutrition* 85.3, pp. 651–661.

Du, D., Liu, C., Qin, M., Zhang, X., Xi, T., Yuan, S., Hao, H., and Xiong, J. (Feb. 2022). "Metabolic dysregulation and emerging therapeutical targets for hepatocellular carcinoma". In: *Acta Pharmaceutica Sinica B* 12.2, pp. 558–580.

Eckel-Mahan, K. L., Patel, V. R., De Mateo, S., Orozco-Solis, R., Ceglia, N. J., Sahar, S., Dilag-Penilla, S. A., Dyar, K. A., Baldi, P., and Sassone-Corsi, P. (Dec. 2013). "Reprogramming of the circadian clock by nutritional challenge". In: *Cell* 155.7, pp. 1464–1478.

Egnatchik, R. A., Leamy, A. K., Noguchi, Y., Shiota, M., and Young, J. D. (Feb. 2014). "Palmitate-induced activation of mitochondrial metabolism promotes oxidative stress and apoptosis in H4IIEC3 rat hepatocytes". In: *Metabolism: clinical and experimental* 63.2, pp. 283–295.

Eslam, M., Sanyal, A. J., George, J., Sanyal, A., Neuschwander-Tetri, B., Tiribelli, C., Kleiner, D. E., Brunt, E., Bugianesi, E., Yki-Järvinen, H., Grønbæk, H., Cortez-Pinto, H., Fan, J., Valenti, L., Abdelmalek, M., Romero-Gomez, M., Rinella, M., Arrese, M., Bedossa, P., Newsome, P. N., Anstee, Q. M., Jalan, R., Bataller, R., Loomba, R., Sookoian, S., Sarin, S. K., Harrison, S., Kawaguchi, T., Wong, V. W. S., Ratziu, V., Yilmaz, Y., and Younossi, Z. (May 2020). "MAFLD: A Consensus-Driven Proposed Nomenclature for Metabolic Associated Fatty Liver Disease". In: *Gastroenterology* 158.7, pp. 1999–2014.

Espinosa-Salas, S. and Gonzalez-Arias, M. (Aug. 2024). *Nutrition: Macronutrient Intake, Imbalances, and Interventions*. StatPearls Publishing.

Essman, M., Zimmer, C., Carpentier, F. D., Swart, E. C., and Taillie, L. S. (Dec. 2022). "Are intentions to change, policy awareness, or health knowledge related to changes in dietary intake following a sugar-sweetened beverage tax in South Africa? A before-and-after study". In: *The International Journal of Behavioral Nutrition and Physical Activity* 19.1, p. 136.

Evans, K., Kuusela, P. J., Cruz, M. L., Wilhelmova, I., Fielding, B. A., and Frayn, K. N. (May 1998). "Rapid chylomicron appearance following sequential meals: effects of second meal composition". In: *British Journal of Nutrition* 79.5, pp. 425–429.

Eykelenboom, M., Van Stralen, M. M., Olthof, M. R., Renders, C. M., and Steenhuis, I. H. (June 2021). "Public acceptability of a sugar-sweetened beverage tax and its associated factors in the Netherlands". In: *Public Health Nutrition* 24.8, p. 2354.

Fabbrini, E., Sullivan, S., and Klein, S. (Feb. 2010). "Obesity and nonalcoholic fatty liver disease: Biochemical, metabolic, and clinical implications". In: *Hepatology* 51.2, pp. 679–689.

Fan, Y., Liu, J., Miao, J., Zhang, X., Yan, Y., Bai, L., Chang, J., Wang, Y., Wang, L., Bian, Y., and Zhou, H. (Aug. 2021). "Anti-inflammatory activity of the Tongmai Yangxin pill in the treatment of coronary heart disease is associated with estrogen receptor and NF-κB signaling pathway". In: *Journal of ethnopharmacology* 276.

Feingold, K. R. (Jan. 2000). *Introduction to Lipids and Lipoproteins*. MDText.com, Inc.

Flessa, C. M., Kyrou, I., Nasiri-Ansari, N., Kaltsas, G., Kassi, E., and Randeva, H. S. (Oct. 2022). "Endoplasmic reticulum stress in nonalcoholic (metabolic associated) fatty liver disease (NAFLD/MAFLD)". In: *Journal of Cellular Biochemistry* 123.10, pp. 1585–1606.

Folch, J., Lees, M., and Slone, G. H. (1957). "A simple method for the isolation and purification of total lipides from animal tissues." In: *The Journal of biological chemistry* 226.1, pp. 497–509.

Foroughi, M., Maghsoudi, Z., Khayyatzadeh, S., Ghiasvand, R., Askari, G., and Iraj, B. (Feb. 2016). "Relationship between non-alcoholic fatty liver disease and inflammation in patients with non-alcoholic fatty liver". In: *Advanced Biomedical Research* 5.1, p. 28.

Fransen, M., Lismont, C., and Walton, P. (June 2017). "The Peroxisome-Mitochondria Connection: How and Why?" In: *International journal of molecular sciences* 18.6.

Freudenheim, J. L. (Feb. 1993). "A review of study designs and methods of dietary assessment in nutritional epidemiology of chronic disease." In: *The Journal of nutrition* 123.2 Suppl, pp. 401–5.

Friedman, S. L., Neuschwander-Tetri, B. A., Rinella, M., and Sanyal, A. J. (July 2018). "Mechanisms of NAFLD development and therapeutic strategies". In: *Nature medicine* 24.7, pp. 908–922.

Fu, S., Yang, L., Li, P., Hofmann, O., Dicker, L., Hide, W., Lin, X., Watkins, S. M., Ivanov, A. R., and Hotamisligil, G. S. (May 2011). "Aberrant lipid metabolism disrupts calcium homeostasis causing liver endoplasmic reticulum stress in obesity". In: *Nature* 473.7348, pp. 528–531.

Fu, X., Xing, L., Xu, W., and Shu, J. (July 2016). "Treatment with estrogen protects against ovariectomy-induced hepatic steatosis by increasing AQP7 expression". In: *Molecular Medicine Reports* 14.1, pp. 425–431.

Fuchs, A., Samovski, D., Smith, G. I., Cifarelli, V., Farabi, S. S., Yoshino, J., Pietka, T., Chang, S. W., Ghosh, S., Myckatyn, T. M., and Klein, S. (Sept. 2021). "Associations Among Adipose Tissue Immunology, Inflammation, Exosomes and Insulin Sensitivity in People With Obesity and Nonalcoholic Fatty Liver Disease". In: *Gastroenterology* 161.3, pp. 968–981.

Furlong, C. E., Marsillach, J., Jarvik, G. P., and Costa, L. G. (Nov. 2016). "Paraoxonases-1, -2 and -3: What are their functions?" In: *Chemico-biological interactions* 259.Pt B, pp. 51–62.

Gallego, S. F., Hermansson, M., Liebisch, G., Hodson, L., and Ejsing, C. S. (Dec. 2018). "Total Fatty Acid Analysis of Human Blood Samples in One Minute by High-Resolution Mass Spectrometry". In: *Biomolecules* 9.1, p. 7.

Gangl, A. and Ockner, R. K. (Apr. 1975). "Intestinal metabolism of plasma free fatty acids. Intracellular compartmentation and mechanisms of control." In: *The Journal of clinical investigation* 55.4, pp. 803–13.

Gao, D., Nong, S., Huang, X., Lu, Y., Zhao, H., Lin, Y., Man, Y., Wang, S., Yang, J., and Li, J. (Sept. 2010). "The effects of palmitate on hepatic insulin resistance are mediated by NADPH Oxidase 3-derived reactive oxygen species through JNK and p38MAPK pathways". In: *The Journal of biological chemistry* 285.39, pp. 29965–29973.

Garcia-Martinez, I., Alen, R., Pereira, L., Povo-Retana, A., Astudillo, A. M., Hitos, A. B., Gomez-Hurtado, I., Lopez-Collazo, E., Boscá, L., Francés, R., Lizasoain, I., Moro, M. Á., Balsinde, J., Izquierdo, M., and Valverde, Á. M. (Apr. 2023). "Saturated fatty acid-enriched small extracellular vesicles mediate a crosstalk inducing liver inflammation and hepatocyte insulin resistance". In: *JHEP Reports*, p. 100756.

Geidl-Flueck, B. and Gerber, P. A. (May 2023). "Fructose drives de novo lipogenesis affecting metabolic health". In: *The Journal of Endocrinology* 257.2.

Giammanco, A., Cefalù, A. B., Noto, D., and Averna, M. R. (2015). "The pathophysiology of intestinal lipoprotein production". In: *Frontiers in Physiology* 6.MAR, p. 61.

Girard, J., Perdereau, D., Foufelle, F., Prip-Buus, C., and Ferré, P. (Jan. 1994). "Regulation of lipogenic enzyme gene expression by nutrients and hormones". In: *FASEB journal : official publication of the Federation of American Societies for Experimental Biology* 8.1, pp. 36–42.

Gjorgjieva, M., Sobolewski, C., Dolicka, D., Correia De Sousa, M., and Foti, M. (Nov. 2019). "miRNAs and NAFLD: from pathophysiology to therapy". In: *Gut* 68.11, pp. 2065–2079.

Gomaraschi, M., Fracanzani, A. L., Dongiovanni, P., Pavanello, C., Giorgio, E., Da Dalt, L., Norata, G. D., Calabresi, L., Consonni, D., Lombardi, R., Branchi, A., and Fargion, S. (Dec. 2019). "Lipid accumulation impairs lysosomal acid lipase activity in hepatocytes: Evidence in NAFLD patients and cell cultures". In: *Biochimica et Biophysica Acta (BBA) - Molecular and Cell Biology of Lipids* 1864.12, p. 158523.

Gómez Candela, C., Bermejo López, L. M., and Loria Kohen, V. (Mar. 2011). "Importance of a balanced omega 6/omega 3 ratio for the maintenance of health: nutritional recommendations." In: *Nutricion hospitalaria* 26.2, pp. 323–9.

Goto, T., Lee, J. Y., Teraminami, A., Kim, Y. I., Hirai, S., Uemura, T., Inoue, H., Takahashi, N., and Kawada, T. (May 2011). "Activation of peroxisome proliferator-activated receptor-alpha stimulates both differentiation and fatty acid oxidation in adipocytes". In: *Journal of Lipid Research* 52.5, p. 873.

Green, C. J., Parry, S. A., Gunn, P. J., Ceresa, C. D., Rosqvist, F., Piché, M.-E., and Hodson, L. (Mar. 2020). "Studying non-alcoholic fatty liver disease: the ins and outs of in vivo, ex vivo and in vitro human models". In: *Hormone Molecular Biology and Clinical Investigation* 41.1.

Green, C. J., Pramfalk, C., Morten, K. J., and Hodson, L. (Jan. 2015). "From whole body to cellular models of hepatic triglyceride metabolism: man has got to know his limitations". In: *American journal of physiology. Endocrinology and metabolism* 308.1, E1–E20.

Guan, D., Xiong, Y., Borck, P. C., Jang, C., Doulias, P. T., Papazyan, R., Fang, B., Jiang, C., Zhang, Y., Briggs, E. R., Hu, W., Steger, D., Ischiropoulos, H., Rabinowitz, J. D., and Lazar, M. A. (Aug. 2018). "Diet-Induced Circadian Enhancer Remodeling Synchronizes Opposing Hepatic Lipid Metabolic Processes". In: *Cell* 174.4, pp. 831–842.

Gunn, P. J., Green, C. J., Pramfalk, C., and Hodson, L. (Dec. 2017). "In vitro cellular models of human hepatic fatty acid metabolism: Differences between Huh7 and HepG2 cell lines in human and fetal bovine culturing serum". In: *Physiological Reports* 5.24.

Gunn, P. J., Pramfalk, C., Millar, V., Cornfield, T., Hutchinson, M., Johnson, E. M., Nagarajan, S. R., Troncoso-Rey, P., Mithen, R. F., Pinnick, K. E., Traka, M. H., Green, C. J., and Hodson, L. (July 2020). "Modifying nutritional substrates induces macrovesicular lipid droplet accumulation and metabolic alterations in a cellular model of hepatic steatosis". In: *Physiological reports* 8.13.

Guo, Y., Yu, X., Rihani, K., Wang, Q. Y., and Rong, L. (Apr. 2004). "The role of a conserved acidic residue in calcium-dependent protein folding for a low density lipoprotein (LDL)-A module: implications in structure and function for the LDL receptor superfamily". In: *The Journal of biological chemistry* 279.16, pp. 16629–16637.

Gyori, B. M., Venkatachalam, G., Thiagarajan, P. S., Hsu, D., and Clement, M. V. (Jan. 2014). "OpenComet: An automated tool for comet assay image analysis". In: *Redox Biology* 2.1, pp. 457–465.

Hagenfeldt, L., Wahren, J., Pernow, B., and Räf, L. (Sept. 1972). "Uptake of individual free fatty acids by skeletal muscle and liver in man." In: *The Journal of clinical investigation* 51.9, pp. 2324–30.

Hamabe, A., Uto, H., Imamura, Y., Kusano, K., Mawatari, S., Kumagai, K., Kure, T., Tamai, T., Moriuchi, A., Sakiyama, T., Oketani, M., Ido, A., and Tsubouchi, H. (June 2011). "Impact of cigarette smoking on onset of nonalcoholic fatty liver disease over a 10-year period". In: *Journal of Gastroenterology* 46.6, pp. 769–778.

Han, H., Ge, X., Komakula, S. S. B., Desert, R., Das, S., Song, Z., Chen, W., Athavale, D., Gaskell, H., Lantvit, D., Guzman, G., and Nieto, N. (July 2023). "Macrophage-derived Osteopontin (SPP1) Protects From Nonalcoholic Steatohepatitis". In: *Gastroenterology* 165.1, pp. 201–217.

Hanson, R. and Owen, O. (Feb. 2013). "Gluconeogenesis". In: *Encyclopedia of Biological Chemistry*. Elsevier, pp. 381–386.

Hashidate-Yoshida, T., Harayama, T., Hishikawa, D., Morimoto, R., Hamano, F., Tokuoka, S. M., Eto, M., Tamura-Nakano, M., Yanobu-Takanashi, R., Mukumoto, Y., Kiyonari, H., Okamura, T., Kita, Y., Shindou, H., and Shimizu, T. (Apr. 2015). "Fatty acid remodeling by LPCAT3 enriches arachidonate in phospholipid membranes and regulates triglyceride transport." In: *eLife* 4.

Havel, R. J. and Hamilton, R. L. (Nov. 1988). "Hepatocytic lipoprotein receptors and intracellular lipoprotein catabolism". In: *Hepatology* 8.6, pp. 1689–1704.

He, M., Wang, C., Long, X. H., Peng, J. J., Liu, D. F., Yang, G. Y., Jensen, M. D., and Zhang, L. L. (Mar. 2020). "Mesencephalic astrocyte-derived neurotrophic factor ameliorates steatosis in HepG2 cells by regulating hepatic lipid metabolism". In: *World Journal of Gastroenterology* 26.10, p. 1029.

He, Y., Yang, W., Gan, L., Liu, S., Ni, Q., Bi, Y., Han, T., Liu, Q., Chen, H., Hu, Y., Long, Y., and Yang, L. (May 2021). "Silencing HIF-1α aggravates non-alcoholic fatty

liver disease in vitro through inhibiting PPAR-α/ANGPTL4 singling pathway". In: *Gastroenterologia y hepatologia* 44.5, pp. 355–365.

Herman, M. A. and Birnbaum, M. J. (Dec. 2021). "Molecular aspects of fructose metabolism and metabolic disease". In: *Cell metabolism* 33.12, pp. 2329–2354.

Herpen, N. A. van, Schrauwen-Hinderling, V. B., Schaart, G., Mensink, R. P., and Schrauwen, P. (Apr. 2011). "Three Weeks on a High-Fat Diet Increases Intrahepatic Lipid Accumulation and Decreases Metabolic Flexibility in Healthy Overweight Men". In: *The Journal of Clinical Endocrinology & Metabolism* 96.4, E691–E695.

Hesse, D., Jaschke, A., Chung, B., and Schürmann, A. (Feb. 2013). "Trans-Golgi proteins participate in the control of lipid droplet and chylomicron formation". In: *Bioscience Reports* 33.1, pp. 1–9.

Hirosawa, K., Fukami, T., Tashiro, K., Sakai, Y., Kisui, F., Nakano, M., and Nakajima, M. (Apr. 2021). "Role of Human Arylacetamide Deacetylase (AADAC) on Hydrolysis of Eslicarbazepine Acetate and Effects of AADAC Genetic Polymorphisms on Hydrolase Activity". In: *Drug metabolism and disposition: the biological fate of chemicals* 49.4, pp. 322–329.

Hirsch, D., Stahl, A., and Lodish, H. F. (July 1998). "A family of fatty acid transporters conserved from mycobacterium to man". In: *Proceedings of the National Academy of Sciences* 95.15, pp. 8625–8629.

Hirsova, P., Ibrahim, S. H., Krishnan, A., Verma, V. K., Bronk, S. F., Werneburg, N. W., Charlton, M. R., Shah, V. H., Malhi, H., and Gores, G. J. (Apr. 2016). "Lipid-Induced Signaling Causes Release of Inflammatory Extracellular Vesicles From Hepatocytes". In: *Gastroenterology* 150.4, pp. 956–967.

Hodson, L., Bickerton, A. S., McQuaid, S. E., Roberts, R., Karpe, F., Frayn, K. N., and Fielding, B. A. (Oct. 2007). "The contribution of splanchnic fat to VLDL triglyceride is greater in insulin-resistant than insulin-sensitive men and women: Studies in the postprandial state". In: *Diabetes* 56.10, pp. 2433–2441.

Hodson, L. and Gunn, P. J. (Sept. 2019). "The regulation of hepatic fatty acid synthesis and partitioning: the effect of nutritional state". In: *Nature Reviews Endocrinology 2019 15:12* 15.12, pp. 689–700.

Hodson, L., McQuaid, S. E., Karpe, F., Frayn, K. N., and Fielding, B. A. (Jan. 2009). "Differences in partitioning of meal fatty acids into blood lipid fractions: a comparison of linoleate, oleate, and palmitate". In: *American Journal of Physiology-Endocrinology and Metabolism* 296.1, E64–E71.

Hodson, L., Skeaff, C. M., and Fielding, B. A. (Sept. 2008). "Fatty acid composition of adipose tissue and blood in humans and its use as a biomarker of dietary intake". In: *Progress in Lipid Research* 47.5, pp. 348–380.

Hossain, N., Afendy, A., Stepanova, M., Nader, F., Srishord, M., Rafiq, N., Goodman, Z., and Younossi, Z. (Nov. 2009). "Independent Predictors of Fibrosis in Patients With Nonalcoholic Fatty Liver Disease". In: *Clinical Gastroenterology and Hepatology* 7.11, pp. 1224–1229.

Hotamisligil, G. S. (Dec. 2006). "Inflammation and metabolic disorders". In: *Nature* 444.7121, pp. 860–867.

Houttu, V., Csader, S., Nieuwdorp, M., Holleboom, A. G., and Schwab, U. (July 2021). "Dietary Interventions in Patients With Non-alcoholic Fatty Liver Disease: A Systematic Review and Meta-Analysis". In: *Frontiers in Nutrition* 8, p. 716783.

Huang, H., Cruz, W., Chen, J., and Zheng, G. (May 2015). "Learning from Biology: Synthetic Lipoproteins for Drug Delivery". In: *Wiley interdisciplinary reviews. Nanomedicine and nanobiotechnology* 7.3, p. 298.

Innerarity, T. L. (Dec. 2002). "Structural biology: LDL receptor's β-propeller displaces LDL". In: *Science* 298.5602, pp. 2337–2339.

Ipsen, D. H., Lykkesfeldt, J., and Tveden-Nyborg, P. (Sept. 2018). "Molecular mechanisms of hepatic lipid accumulation in non-alcoholic fatty liver disease". In: *Cellular and Molecular Life Sciences* 75.18, pp. 3313–3327.

Iqbal, J. and Hussain, M. M. (June 2009). "Intestinal lipid absorption". In: *American Journal of Physiology - Endocrinology and Metabolism* 296.6, E1183.

Jahn, D., Kircher, S., Hermanns, H. M., and Geier, A. (May 2019). "Animal models of NAFLD from a hepatologist's point of view". In: *Biochimica et biophysica acta. Molecular basis of disease* 1865.5, pp. 943–953.

Jang, C., Hui, S., Lu, W., Cowan, A. J., Morscher, R. J., Lee, G., Liu, W., Tesz, G. J., Birnbaum, M. J., and Rabinowitz, J. D. (Feb. 2018). "The Small Intestine Converts Dietary Fructose into Glucose and Organic Acids". In: *Cell metabolism* 27.2, p. 351.

Jonchere, V., Marisa, L., Greene, M., Virouleau, A., Buhard, O., Bertrand, R., Svrcek, M., Cervera, P., Goloudina, A., Guillerm, E., Coulet, F., Landman, S., Ratovomanana, T., Job, S., Ayadi, M., Elarouci, N., Armenoult, L., Merabtene, F., Dumont, S., Parc, Y., Lefèvre, J. H., André, T., Fléjou, J. F., Guilloux, A., Collura, A., Reyniès, A. de, and Duval, A. (Jan. 2018). "Identification of Positively and Negatively Selected Driver Gene Mutations Associated With Colorectal Cancer With Microsatellite Instability". In: *Cellular and molecular gastroenterology and hepatology* 6.3, pp. 277–300.

Jungermann, K. and Katz, N. (July 1989). "Functional specialization of different hepatocyte populations". In: *Physiological Reviews* 69.3, pp. 708–764.

Jungermann, K. and Kietzmann, T. (Feb. 2000). "Oxygen: Modulator of metabolic zonation and disease of the liver". In: *Hepatology* 31.2, pp. 255–260.

Kang, S. and Davis, R. A. (Dec. 2000). "Cholesterol and hepatic lipoprotein assembly and secretion". In: *Biochimica et biophysica acta* 1529.1-3, pp. 223–230.

Kargulewicz, A., Stankowiak-Kulpa, H., and Grzymisławski, M. (Mar. 2014). "Dietary recommendations for patients with nonalcoholic fatty liver disease". In: *Gastroenterology Review* 1.1, pp. 18–23.

Karim, G. and Bansal, M. B. (2023). "Resmetirom: An Orally Administered, Small-molecule, Liver-directed, β-selective THR Agonist for the Treatment of Non-alcoholic Fatty Liver Disease and Non-alcoholic Steatohepatitis". In: *European Endocrinology* 19.1, p. 60.

Karpe, F., Dickmann, J. R., and Frayn, K. N. (Oct. 2011). *Fatty acids, obesity, and insulin resistance: Time for a reevaluation.*

Kasper, H. (Jan. 1970). "Faecal Fat Excretion, Diarrhea, and Subjective Complaints with Highly Dosed Oral Fat Intake". In: *Digestion* 3.6, pp. 321–330.

Kassis, T., Yarlagadda, S. C., Kohan, A. B., Tso, P., Breedveld, V., and Dixon, J. B. (May 2016). "Postprandial lymphatic pump function after a high-fat meal: A characterization of contractility, flow, and viscosity". In: *American Journal of Physiology - Gastrointestinal and Liver Physiology* 310.10, G776–G789.

Katan, M. B., Brouwer, I. A., Clarke, R., Geleijnse, J. M., and Mensink, R. P. (Aug. 2010). "Saturated fat and heart disease". In: *The American journal of clinical nutrition* 92.2, pp. 459–460.

Kathiresan, S., Melander, O., Guiducci, C., Surti, A., Burtt, N. P., Rieder, M. J., Cooper, G. M., Roos, C., Voight, B. F., Havulinna, A. S., Wahlstrand, B., Hedner, T., Corella, D., Tai, E. S., Ordovas, J. M., Berglund, G., Vartiainen, E., Jousilahti, P., Hedblad, B., Taskinen, M.-R., Newton-Cheh, C., Salomaa, V., Peltonen, L.,

Groop, L., Altshuler, D. M., and Orho-Melander, M. (Feb. 2008). "Six new loci associated with blood low-density lipoprotein cholesterol, high-density lipoprotein cholesterol or triglycerides in humans." In: *Nature genetics* 40.2, pp. 189–97.

Kaur, S., Rawal, P., Siddiqui, H., Rohilla, S., Sharma, S., Tripathi, D. M., Baweja, S., Hassan, M., Vlaic, S., Guthke, R., Thomas, M., Dayoub, R., Bihari, C., Sarin, S. K., and Weiss, T. S. (Oct. 2019). "Increased Expression of RUNX1 in Liver Correlates with NASH Activity Score in Patients with Non-Alcoholic Steatohepatitis (NASH)". In: *Cells* 8.10.

Kawamoto, M., Yamaji, T., Saito, K., Shirasago, Y., Satomura, K., Endo, T., Fukasawa, M., Hanada, K., and Osada, N. (Oct. 2020). "Identification of Characteristic Genomic Markers in Human Hepatoma HuH-7 and Huh7.5.1-8 Cell Lines". In: *Frontiers in Genetics* 11, p. 546106.

Kegel, V., Deharde, D., Pfeiffer, E., Zeilinger, K., Seehofer, D., and Damm, G. (Mar. 2016). "Protocol for Isolation of Primary Human Hepatocytes and Corresponding Major Populations of Non-parenchymal Liver Cells". In: *Journal of visualized experiments : JoVE* 2016.109.

Keller, K. L., Liang, L. C., Sakimura, J., May, D., Van Belle, C., Breen, C., Driggin, E., Tepper, B. J., Lanzano, P. C., Deng, L., and Chung, W. K. (May 2012). "Common Variants in the CD36 Gene Are Associated With Oral Fat Perception, Fat Preferences, and Obesity in African Americans". In: *Obesity* 20.5, pp. 1066–1073.

Khatun, I., Clark, R. W., Vera, N. B., Kou, K., Erion, D. M., Coskran, T., Bobrowski, W. F., Okerberg, C., and Goodwin, B. (Feb. 2016). "Characterization of a Novel Intestinal Glycerol-3-phosphate Acyltransferase Pathway and Its Role in Lipid Homeostasis". In: *The Journal of Biological Chemistry* 291.6, p. 2602.

Kietzmann, T. (Apr. 2017). "Metabolic zonation of the liver: The oxygen gradient revisited". In: *Redox Biology* 11, pp. 622–630.

Kim, C. W., Addy, C., Kusunoki, J., Anderson, N. N., Deja, S., Fu, X., Burgess, S. C., Li, C., Chakravarthy, M., Previs, S., Milstein, S., Fitzgerald, K., Kelley, D. E., and Horton, J. D. (Aug. 2017). "Acetyl CoA Carboxylase Inhibition Reduces Hepatic Steatosis but Elevates Plasma Triglycerides in Mice and Humans: A Bedside to Bench Investigation". In: *Cell Metabolism* 26.2, pp. 394–406.

Kim, S., Hong, J., Jeon, R., and Kim, H. S. (Jan. 2016). "Adzuki bean ameliorates hepatic lipogenesis and proinflammatory mediator expression in mice fed a high-cholesterol and high-fat diet to induce nonalcoholic fatty liver disease". In: *Nutrition research (New York, N.Y.)* 36.1, pp. 90–100.

Kleiboeker, B. and Lodhi, I. J. (Nov. 2022). "Peroxisomal regulation of energy homeostasis: Effect on obesity and related metabolic disorders". In: *Molecular Metabolism* 65, p. 101577.

Kleiner, D. E., Brunt, E. M., Van Natta, M., Behling, C., Contos, M. J., Cummings, O. W., Ferrell, L. D., Liu, Y. C., Torbenson, M. S., Unalp-Arida, A., Yeh, M., McCullough, A. J., and Sanyal, A. J. (June 2005). "Design and validation of a histological scoring system for nonalcoholic fatty liver disease". In: *Hepatology (Baltimore, Md.)* 41.6, pp. 1313–1321.

Koh, H. C. E. and Mittendorfer, B. (Apr. 2021). "Adipose tissue lipolysis, plasma fatty acids, and glucose homeostasis in people with obesity: New pieces that help solve the puzzle". In: *eBioMedicine* 66, p. 103311.

Kohan, A. B., Wang, F., Lo, C.-M., Liu, M., and Tso, P. (Mar. 2015). "ApoA-IV: current and emerging roles in intestinal lipid metabolism, glucose homeostasis, and satiety."

In: *American journal of physiology. Gastrointestinal and liver physiology* 308.6, pp. 472–81.

Koska, J., Ozias, M. K., Deer, J., Kurtz, J., Salbe, A. D., Harman, S. M., and Reaven, P. D. (Nov. 2016). "A human model of dietary saturated fatty acid induced insulin resistance". In: *Metabolism: clinical and experimental* 65.11, pp. 1621–1628.

Koutoukidis, D. A., Astbury, N. M., Tudor, K. E., Morris, E., Henry, J. A., Noreik, M., Jebb, S. A., and Aveyard, P. (Sept. 2019). "Association of Weight Loss Interventions With Changes in Biomarkers of Nonalcoholic Fatty Liver Disease: A Systematic Review and Meta-analysis". In: *JAMA Internal Medicine* 179.9, pp. 1262–1271.

Krahmer, N., Guo, Y., Wilfling, F., Hilger, M., Lingrell, S., Heger, K., Newman, H. W., Schmidt-Supprian, M., Vance, D. E., Mann, M., Farese, R. V., and Walther, T. C. (Oct. 2011). "Phosphatidylcholine synthesis for lipid droplet expansion is mediated by localized activation of CTP:Phosphocholine cytidylyltransferase". In: *Cell Metabolism* 14.4, pp. 504–515.

Kumar, R., Porwal, Y. C., Dev, N., Kumar, P., Chakravarthy, S., and Kumawat, A. (Jan. 2020). "Association of high-sensitivity C-reactive protein (hs-CRP) with non-alcoholic fatty liver disease (NAFLD) in Asian Indians: A cross-sectional study." In: *Journal of family medicine and primary care* 9.1, pp. 390–394.

Lafontan, M. and Langin, D. (Sept. 2009). "Lipolysis and lipid mobilization in human adipose tissue". In: *Progress in lipid research* 48.5, pp. 275–297.

Lair, B., Laurens, C., Van Den Bosch, B., and Moro, C. (Sept. 2020). "Novel Insights and Mechanisms of Lipotoxicity-Driven Insulin Resistance". In: *International Journal of Molecular Sciences* 21.17, p. 6358.

Lee, W. N., Bassilian, S., Ajie, H. O., Schoeller, D. A., Edmond, J., Bergner, E. A., and Byerley, L. O. (May 1994). "In vivo measurement of fatty acids and cholesterol synthesis using D2O and mass isotopomer analysis". In: *American Journal of Physiology-Endocrinology and Metabolism* 266.5, E699–E708.

Lee, Y. H., Jang, H. J., Kim, S., Choi, S. S., Khim, K. W., Eom, H. J., Hyun, J., Shin, K. J., Chae, Y. C., Kim, H., Park, J., Park, N. H., Woo, C. Y., Hong, C. H., Koh, E. H., Nam, D., and Choi, J. H. (Dec. 2021). "Hepatic MIR20B promotes nonalcoholic fatty liver disease by suppressing PPARA". In: *eLife* 10.

Lennon, H., Sperrin, M., Badrick, E., and Renehan, A. G. (Sept. 2016). "The Obesity Paradox in Cancer: a Review". In: *Current Oncology Reports* 18.9, p. 56.

Lewis, G. F., O'Meara, N. M., Soltys, P. A., Blackman, J. D., Iverius, P. H., Pugh, W. L., Getz, G. S., and Polonsky, K. S. (Apr. 1991). "Fasting hypertriglyceridemia in noninsulin-dependent diabetes mellitus is an important predictor of postprandial lipid and lipoprotein abnormalities." In: *The Journal of clinical endocrinology and metabolism* 72.4, pp. 934–44.

Lewis, G. F., Carpentier, A., Adeli, K., and Giacca, A. (Apr. 2002). "Disordered Fat Storage and Mobilization in the Pathogenesis of Insulin Resistance and Type 2 Diabetes". In: *Endocrine Reviews* 23.2, pp. 201–229.

Li, B., Yan, N., Jiang, H., Cui, M., Wu, M., Wang, L., Mi, B., Li, Z., Shi, J., Fan, Y., Azalati, M. M., Li, C., Chen, F., Ma, M., Wang, D., and Ma, L. (Mar. 2023). "Consumption of sugar sweetened beverages, artificially sweetened beverages and fruit juices and risk of type 2 diabetes, hypertension, cardiovascular disease, and mortality: A meta-analysis." In: *Frontiers in nutrition* 10, p. 1019534.

Li, S., Cao, M., Yang, C., Zheng, H., and Zhu, Y. (Oct. 2020). "Association of sugar-sweetened beverage intake with risk of metabolic syndrome among children and adolescents in urban China". In: *Public Health Nutrition* 23.15, p. 2770.

Li, Y. H. and Liu, L. (Aug. 2014). "Apolipoprotein E synthesized by adipocyte and apolipoprotein E carried on lipoproteins modulate adipocyte triglyceride content". In: *Lipids in Health and Disease* 13.1.

Lin, Y., Feng, X., Cao, X., Miao, R., Sun, Y., Li, R., Ye, J., and Zhong, B. (Nov. 2022). "Age patterns of nonalcoholic fatty liver disease incidence: heterogeneous associations with metabolic changes". In: *Diabetology & Metabolic Syndrome* 14.1, p. 181.

Lindenmeyer, C. C. and McCullough, A. J. (Feb. 2018). "The Natural History of Nonalcoholic Fatty Liver Disease—An Evolving View". In: *Clinics in Liver Disease* 22.1, pp. 11–21.

Liu, S., Brown, J. D., Stanya, K. J., Homan, E., Leidl, M., Inouye, K., Bhargava, P., Gangl, M. R., Dai, L., Hatano, B., Hotamisligil, G. S., Saghatelian, A., Plutzky, J., and Lee, C.-H. (Oct. 2013). "A diurnal serum lipid integrates hepatic lipogenesis and peripheral fatty acid use." In: *Nature* 502.7472, pp. 550–4.

Liu, Y., Yu, F., Han, Y., Li, Q., Cao, Z., Xiang, X., Jiang, S., Wang, X., Lu, J., Lai, R., Wang, H., Cai, W., Bao, S., and Xie, Q. (Nov. 2016). "SUMO-specific protease 3 is a key regulator for hepatic lipid metabolism in non-alcoholic fatty liver disease". In: *Scientific Reports* 6.1, p. 37351.

Lo, V., Erickson, B., Thomason-Hughes, M., Ko, K. W., Dolinsky, V. W., Nelson, R., and Lehner, R. (Feb. 2010). "Arylacetamide deacetylase attenuates fatty-acid-induced triacylglycerol accumulation in rat hepatoma cells". In: *Journal of lipid research* 51.2, pp. 368–377.

Loneker, A. E., Alisafaei, F., Kant, A., Li, D., Janmey, P. A., Shenoy, V. B., and Wells, R. G. (Apr. 2023). "Lipid droplets are intracellular mechanical stressors that impair hepatocyte function". In: *Proceedings of the National Academy of Sciences* 120.16, e2216811120.

Long, J.-K., Dai, W., Zheng, Y.-W., and Zhao, S.-P. (June 2019). "miR-122 promotes hepatic lipogenesis via inhibiting the LKB1/AMPK pathway by targeting Sirt1 in non-alcoholic fatty liver disease." In: *Molecular medicine (Cambridge, Mass.)* 25.1, p. 26.

López-Soldado, I., Avella, M., and Botham, K. M. (Feb. 2009a). "Differential influence of different dietary fatty acids on very low-density lipoprotein secretion when delivered to hepatocytes in chylomicron remnants". In: *Metabolism: clinical and experimental* 58.2, pp. 186–195.

— (2009b). "Suppression of VLDL secretion by cultured hepatocytes incubated with chylomicron remnants enriched in n-3 polyunsaturated fatty acids is regulated by hepatic nuclear factor-4alpha". In: *Biochimica et biophysica acta* 1791.12, pp. 1181–1189.

Lowry, O., Rosebrough, N., Farr, A. L., and Randall, R. (Nov. 1951). "Protein measurement with the folin phenol reagent". In: *Journal of Biological Chemistry* 193.1, pp. 265–275.

Luo, L. and Liu, M. (Dec. 2016). "Adipose tissue in control of metabolism". In: *Journal of Endocrinology* 231.3, R77–R99.

Luukkonen, P. K., Sädevirta, S., Zhou, Y., Kayser, B., Ali, A., Ahonen, L., Lallukka, S., Pelloux, V., Gaggini, M., Jian, C., Hakkarainen, A., Lundbom, N., Gylling, H., Salonen, A., Oresic, M., Hyötyläinen, T., Orho-Melander, M., Rissanen, A., Gastaldelli, A., Clément, K., Hodson, L., and Yki-Järvinen, H. (Aug. 2018). "Saturated Fat Is More Metabolically Harmful for the Human Liver Than Unsaturated Fat or Simple Sugars". In: *Diabetes care* 41.8, pp. 1732–1739.

Luukkonen, P. K., Zhou, Y., Sädevirta, S., Leivonen, M., Arola, J., Orešič, M., Hyötyläinen, T., and Yki-Järvinen, H. (May 2016). "Hepatic ceramides dissociate steatosis and insulin resistance in patients with non-alcoholic fatty liver disease". In: *Journal of hepatology* 64.5, pp. 1167–1175.

Machado, M. V. and Cortez-Pinto, H. (Sept. 2014). *Non-alcoholic fatty liver disease: What the clinician needs to know.*

Maersk, M., Belza, A., Stødkilde-Jørgensen, H., Ringgaard, S., Chabanova, E., Thomsen, H., Pedersen, S. B., Astrup, A., and Richelsen, B. (Feb. 2012). "Sucrose-sweetened beverages increase fat storage in the liver, muscle, and visceral fat depot: a 6-mo randomized intervention study". In: *The American journal of clinical nutrition* 95.2, pp. 283–289.

Malehmir, M., Pfister, D., Gallage, S., Szydlowska, M., Inverso, D., Kotsiliti, E., Leone, V., Peiseler, M., Surewaard, B. G., Rath, D., Ali, A., Wolf, M. J., Drescher, H., Healy, M. E., Dauch, D., Kroy, D., Krenkel, O., Kohlhepp, M., Engleitner, T., Olkus, A., Sijmonsma, T., Volz, J., Deppermann, C., Stegner, D., Helbling, P., Nombela-Arrieta, C., Rafiei, A., Hinterleitner, M., Rall, M., Baku, F., Borst, O., Wilson, C. L., Leslie, J., O'Connor, T., Weston, C. J., Adams, D. H., Sheriff, L., Teijeiro, A., Prinz, M., Bogeska, R., Anstee, N., Bongers, M. N., Notohamiprodjo, M., Geisler, T., Withers, D. J., Ware, J., Mann, D. A., Augustin, H. G., Vegiopoulos, A., Milsom, M. D., Rose, A. J., Lalor, P. F., Llovet, J. M., Pinyol, R., Tacke, F., Rad, R., Matter, M., Djouder, N., Kubes, P., Knolle, P. A., Unger, K., Zender, L., Nieswandt, B., Gawaz, M., Weber, A., and Heikenwalder, M. (Apr. 2019). "Platelet GPIbα is a mediator and potential interventional target for NASH and subsequent liver cancer". In: *Nature Medicine 2019 25:4* 25.4, pp. 641–655.

Malhi, H. and Kaufman, R. J. (Apr. 2011). "Endoplasmic reticulum stress in liver disease". In: *Journal of Hepatology* 54.4, pp. 795–809.

Malik, V. S. and Hu, F. B. (Apr. 2022). "The role of sugar-sweetened beverages in the global epidemics of obesity and chronic diseases". In: *Nature Reviews. Endocrinology* 18.4, p. 205.

Manco, R. and Itzkovitz, S. (Feb. 2021). "Liver zonation". In: *Journal of Hepatology* 74.2, pp. 466–468.

Mann, J. P., Romeo, S., and Valenti, L. (Dec. 2022). "Lipid droplets as the genetic nexus of fatty liver". In: *Liver International* 42.12, pp. 2594–2596.

Manore, M. M. (Aug. 2005). "Exercise and the Institute of Medicine recommendations for nutrition." In: *Current sports medicine reports* 4.4, pp. 193–8.

Mansbach, C. M. and Siddiqi, S. A. (Mar. 2010). "The biogenesis of chylomicrons". In: *Annual review of physiology* 72, pp. 315–333.

Marchesini, G., Day, C. P., Dufour, J. F., Canbay, A., Nobili, V., Ratziu, V., Tilg, H., Roden, M., Gastaldelli, A., Yki-Järvinen, H., Schick, F., Vettor, R., Frühbeck, G., and Mathus-Vliegen, L. (May 2016). "EASL-EASD-EASO Clinical Practice Guidelines for the Management of Non-Alcoholic Fatty Liver Disease". In: *Obesity Facts* 9.2, p. 65.

Mashek, D. G., Cui, W., Shang, L., and Najt, C. P. (Feb. 2020). "Hepatic Lipid Droplets in Liver Function and Disease". In: *The Liver*. Wiley, pp. 245–254.

Mashek, D. G., Khan, S. A., Sathyanarayan, A., Ploeger, J. M., and Franklin, M. P. (Sept. 2015). "Hepatic lipid droplet biology: Getting to the root of fatty liver". In: *Hepatology* 62.3, pp. 964–967.

Mattes, R. D. (Feb. 2009a). "Brief oral stimulation, but especially oral fat exposure, elevates serum triglycerides in humans". In: *American Journal of Physiology - Gastrointestinal and Liver Physiology* 296.2, pp. 365–371.

Mattes, R. D. (Aug. 2009b). "Is there a fatty acid taste?" In: *Annual review of nutrition* 29, pp. 305–327.

Maury, E., Ramsey, K. M., and Bass, J. (Feb. 2010). "Circadian rhythms and metabolic syndrome: from experimental genetics to human disease". In: *Circulation research* 106.3, pp. 447–462.

Mauvais-Jarvis, F. (Jan. 2011). "Estrogen and androgen receptors: regulators of fuel homeostasis and emerging targets for diabetes and obesity". In: *Trends in endocrinology and metabolism: TEM* 22.1, pp. 24–33.

Meer, R. W. van der, Hammer, S., Lamb, H. J., Frölich, M., Diamant, M., Rijzewijk, L. J., Roos, A. de, Romijn, J. A., and Smit, J. W. A. (July 2008). "Effects of Short-Term High-Fat, High-Energy Diet on Hepatic and Myocardial Triglyceride Content in Healthy Men". In: *The Journal of Clinical Endocrinology & Metabolism* 93.7, pp. 2702–2708.

Mei, S., Ni, H. M., Manley, S., Bockus, A., Kassel, K. M., Luyendyk, J. P., Copple, B. L., and Ding, W. X. (Nov. 2011). "Differential roles of unsaturated and saturated fatty acids on autophagy and apoptosis in hepatocytes". In: *The Journal of pharmacology and experimental therapeutics* 339.2, pp. 487–498.

Mensink, R. P. and Katan, M. B. (Aug. 1992). "Effect of dietary fatty acids on serum lipids and lipoproteins. A meta-analysis of 27 trials." In: *Arteriosclerosis and thrombosis : a journal of vascular biology* 12.8, pp. 911–9.

Menzel, J., Longree, A., Abraham, K., Schulze, M. B., and Weikert, C. (July 2022). "Dietary and Plasma Phospholipid Profiles in Vegans and Omnivores-Results from the RBVD Study". In: *Nutrients* 14.14.

Mergental, H., Laing, R. W., Kirkham, A. J., Clarke, G., Boteon, Y. L., Barton, D., Neil, D. A., Isaac, J. R., Roberts, K. J., Abradelo, M., Schlegel, A., Dasari, B. V., Ferguson, J. W., Cilliers, H., Morris, C., Friend, P. J., Yap, C., Afford, S. C., Perera, M. T. P., and Mirza, D. F. (Jan. 2024). "Discarded livers tested by normothermic machine perfusion in the VITTAL trial: Secondary end points and 5-year outcomes". In: *Liver transplantation : official publication of the American Association for the Study of Liver Diseases and the International Liver Transplantation Society* 30.1, pp. 30–45.

Michelotti, G. A., Machado, M. V., and Diehl, A. M. (Oct. 2013). "NAFLD, NASH and liver cancer". In: *Nature Reviews Gastroenterology & Hepatology 2013 10:11* 10.11, pp. 656–665.

Milger, K., Herrmann, T., Becker, C., Gotthardt, D., Zickwolf, J., Ehehalt, R., Watkins, P. A., Stremmel, W., and Füllekrug, J. (Nov. 2006). "Cellular uptake of fatty acids driven by the ER-localized acyl-CoA synthetase FATP4". In: *Journal of cell science* 119.Pt 22, pp. 4678–4688.

Mills, I. G., Jones, A. T., and Clague, M. J. (Jan. 1999). "Regulation of endosome fusion." In: *Molecular membrane biology* 16.1, pp. 73–9.

Mishra, A., Iyer, S., Kesarwani, A., Baligar, P., Arya, S. P., Arindkar, S., Kumar, M. J., Upadhyay, P., Majumdar, S. S., and Nagarajan, P. (Aug. 2016). "Role of antigen presenting cell invariant chain in the development of hepatic steatosis in mouse model". In: *Experimental cell research* 346.2, pp. 188–197.

Miyata, M., Matsushita, K., Shindo, R., Shimokawa, Y., Sugiura, Y., and Yamashita, M. (June 2020). "Selenoneine Ameliorates Hepatocellular Injury and Hepatic Steatosis in a Mouse Model of NAFLD". In: *Nutrients* 12.6.

Moravcová, A., Červinková, Z., Kučera, O., Mezera, V., Rychtrmoc, D., and Lotková, H. (2015). "The effect of oleic and palmitic acid on induction of steatosis and

cytotoxicity on rat hepatocytes in primary culture." In: *Physiological research* 64.Suppl 5, pp. 627–36.

Mortazavi, A., Williams, B. A., McCue, K., Schaeffer, L., and Wold, B. (July 2008). "Mapping and quantifying mammalian transcriptomes by RNA-Seq". In: *Nature methods* 5.7, pp. 621–628.

Mortimer, B.-C., Beveridge, D. J., Martins, I. J., and Redgrave, T. G. (Dec. 1995). "Intracellular Localization and Metabolism of Chylomicron Remnants in the Livers of Low Density Lipoprotein Receptor-deficient Mice and ApoE-deficient Mice". In: *Journal of Biological Chemistry* 270.48, pp. 28767–28776.

Müller, A., Niederstadt, L., Jonas, W., Yi, C. X., Meyer, F., Wiedmer, P., Fischer, J., Grötzinger, C., Schürmann, A., Tschöp, M., Kleinau, G., Grüters, A., Krude, H., and Biebermann, H. (Aug. 2016). "Ring finger protein 11 inhibits melanocortin 3 and 4 receptor signaling". In: *Frontiers in Endocrinology* 7.AUG, p. 109.

Mundi, M. S., Velapati, S., Patel, J., Kellogg, T. A., Abu Dayyeh, B. K., and Hurt, R. T. (Feb. 2020). "Evolution of NAFLD and Its Management". In: *Nutrition in Clinical Practice* 35.1, pp. 72–84.

Nagarajan, S. R., Cross, E., Johnson, E., Sanna, F., Daniels, L. J., Ray, D. W., and Hodson, L. (Oct. 2022). "Determining the temporal, dose, and composition effects of nutritional substrates in an in vitro model of intrahepatocellular triglyceride accumulation". In: *Physiological reports* 10.20.

Nagarajan, S. R., Paul-Heng, M., Krycer, J. R., Fazakerley, D. J., Sharland, A. F., and Hoy, A. J. (Apr. 2019). "Lipid and glucose metabolism in hepatocyte cell lines and primary mouse hepatocytes: a comprehensive resource for in vitro studies of hepatic metabolism". In: *American Journal of Physiology-Endocrinology and Metabolism* 316.4, E578–E589.

Nagrath, D., Xu, H., Tanimura, Y., Zuo, R., Berthiaume, F., Avila, M., Yarmush, R., and Yarmush, M. L. (July 2009). "Metabolic Preconditioning of Donor Organs: Defatting Fatty Livers by Normothermic Perfusion Ex Vivo". In: *Metabolic engineering* 11.4-5, p. 274.

Nakabayashi, H., Taketa, K., Yamane, T., Miyazaki, M., Miyano, K., and Sato, J. (1984). "Phenotypical stability of a human hepatoma cell line, HuH-7, in long-term culture with chemically defined medium". In: *GANN Japanese Journal of Cancer Research* 75.2, pp. 151–158.

Nakajima, K., Nakano, T., Tokita, Y., Nagamine, T., Inazu, A., Kobayashi, J., Mabuchi, H., Stanhope, K. L., Havel, P. J., Okazaki, M., Ai, M., and Tanaka, A. (July 2011). "Postprandial lipoprotein metabolism; VLDL vs chylomicrons". In: *Clinica Chimica Acta; International Journal of Clinical Chemistry* 412.15-16, p. 1306.

Natarajan, V., Moeller, M., Casey, C. A., Harris, E. N., and Kidambi, S. (Jan. 2020). "Matrix Stiffness Regulates Liver Sinusoidal Endothelial Cell Function Mimicking Responses in Fatty Liver Disease". In: *bioRxiv*, p. 2020.01.27.921353.

Neuschwander-Tetri, B. A. (Aug. 2010). "Hepatic lipotoxicity and the pathogenesis of nonalcoholic steatohepatitis: The central role of nontriglyceride fatty acid metabolites". In: *Hepatology* 52.2, pp. 774–788.

Newton, D. F. and Mansbach, C. M. (Oct. 1978). "beta-Sitosterol as a nonabsorbable marker of dietary lipid absorption in man". In: *Clinica chimica acta; international journal of clinical chemistry* 89.2, pp. 331–339.

Nielsen, S. and Karpe, F. (Aug. 2012). "Determinants of VLDL-triglycerides production". In: *Current opinion in lipidology* 23.4, pp. 321–326.

Nielsen, T. S., Jessen, N., Jørgensen, J. O. L., Møller, N., and Lund, S. (June 2014). "Dissecting adipose tissue lipolysis: molecular regulation and implications for metabolic disease". In: *Journal of Molecular Endocrinology* 52.3, R199–R222.

Nissar, A. U., Sharma, L., and Tasduq, S. A. (Aug. 2015). "Palmitic acid induced lipotoxicity is associated with altered lipid metabolism, enhanced CYP450 2E1 and intracellular calcium mediated ER stress in human hepatoma cells". In: *Toxicology Research* 4.5, pp. 1344–1358.

Niu, L., Geyer, P. E., Wewer Albrechtsen, N. J., Gluud, L. L., Santos, A., Doll, S., Treit, P. V., Holst, J. J., Knop, F. K., Vilsbøll, T., Junker, A., Sachs, S., Stemmer, K., Müller, T. D., Tschöp, M. H., Hofmann, S. M., and Mann, M. (Mar. 2019). "Plasma proteome profiling discovers novel proteins associated with non-alcoholic fatty liver disease". In: *Molecular systems biology* 15.3.

Obradovic, M., Sudar-Milovanovic, E., Soskic, S., Essack, M., Arya, S., Stewart, A. J., Gojobori, T., and Isenovic, E. R. (May 2021). "Leptin and Obesity: Role and Clinical Implication". In: *Frontiers in Endocrinology* 12.

Ong, J. P., Pitts, A., and Younossi, Z. M. (Oct. 2008). "Increased overall mortality and liver-related mortality in non-alcoholic fatty liver disease". In: *Journal of Hepatology* 49.4, pp. 608–612.

Paddon-Jones, D., Westman, E., Mattes, R. D., Wolfe, R. R., Astrup, A., and Westerterp-Plantenga, M. (May 2008). "Protein, weight management, and satiety". In: *The American journal of clinical nutrition* 87.5.

Pais, R., Barritt, A. S., Calmus, Y., Scatton, O., Runge, T., Lebray, P., Poynard, T., Ratziu, V., and Conti, F. (Dec. 2016). "NAFLD and liver transplantation: Current burden and expected challenges". In: *Journal of hepatology* 65.6, p. 1245.

Palmisano, B. T., Zhu, L., and Stafford, J. M. (2017). "Role of Estrogens in the Regulation of Liver Lipid Metabolism". In: *Advances in experimental medicine and biology*. Vol. 1043. Adv Exp Med Biol, pp. 227–256.

Papandreou, C., Bullò, M., Tinahones, F. J., Martínez-González, M. Á., Corella, D., Fragkiadakis, G. A., López-Miranda, J., Estruch, R., Fitó, M., and Salas-Salvadó, J. (Sept. 2017). "Serum metabolites in non-alcoholic fatty-liver disease development or reversion; a targeted metabolomic approach within the PREDIMED trial". In: *Nutrition & metabolism* 14.1.

Papatheodoridi, M. and Cholongitas, E. (Jan. 2018). "Diagnosis of Non-alcoholic Fatty Liver Disease (NAFLD): Current Concepts". In: *Current pharmaceutical design* 24.38, pp. 4574–4586.

Parini, P., Johansson, L., Bröijersén, A., Angelin, B., and Rudling, M. (Feb. 2006). "Lipoprotein profiles in plasma and interstitial fluid analyzed with an automated gel-filtration system". In: *European Journal of Clinical Investigation* 36.2, pp. 98–104.

Parker, H. M., Johnson, N. A., Burdon, C. A., Cohn, J. S., O'Connor, H. T., and George, J. (Apr. 2012). "Omega-3 supplementation and non-alcoholic fatty liver disease: A systematic review and meta-analysis". In: *Journal of Hepatology* 56.4, pp. 944–951.

Parks, E. J., Krauss, R. M., Christiansen, M. P., Neese, R. A., and Hellerstein, M. K. (1999). "Effects of a low-fat, high-carbohydrate diet on VLDL-triglyceride assembly, production, and clearance". In: *Journal of Clinical Investigation* 104.8, pp. 1087–1096.

Parry, S. A. and Hodson, L. (2017). "Influence of dietary macronutrients on liver fat accumulation and metabolism." In: *Journal of investigative medicine : the official publication of the American Federation for Clinical Research* 65.8, pp. 1102–1115.

Parry, S. A., Rosqvist, F., Mozes, F. E., Cornfield, T., Hutchinson, M., Piche, M.-E., Hülsmeier, A. J., Hornemann, T., Dyson, P., and Hodson, L. (May 2020a). "Intrahepatic Fat and Postprandial Glycemia Increase After Consumption of a Diet Enriched in Saturated Fat Compared With Free Sugars." In: *Diabetes care* 43.5, pp. 1134–1141.

Parry, S. A., Rosqvist, F., Cornfield, T., Barrett, A., and Hodson, L. (Mar. 2021). "Oxidation of dietary linoleate occurs to a greater extent than dietary palmitate in vivo in humans". In: *Clinical nutrition (Edinburgh, Scotland)* 40.3, pp. 1108–1114.

Parry, S. A., Turner, M. C., and Hodson, L. (Nov. 2020b). "Lifestyle interventions affecting hepatic fatty acid metabolism". In: *Current opinion in clinical nutrition and metabolic care* 23.6, pp. 373–379.

Pelsers, M. M. A. L., Namiot, Z., Kisielewski, W., Namiot, A., Januszkiewicz, M., Hermens, W. T., and Glatz, J. F. C. (Oct. 2003). "Intestinal-type and liver-type fatty acid-binding protein in the intestine. Tissue distribution and clinical utility." In: *Clinical biochemistry* 36.7, pp. 529–35.

Pepin, A., Stanhope, K. L., and Imbeault, P. (May 2019). "Are Fruit Juices Healthier Than Sugar-Sweetened Beverages? A Review". In: *Nutrients* 11.5.

Perez-Pozo, S. E., Schold, J., Nakagawa, T., Sánchez-Lozada, L. G., Johnson, R. J., and Lillo, J. L. (Mar. 2010). "Excessive fructose intake induces the features of metabolic syndrome in healthy adult men: role of uric acid in the hypertensive response". In: *International journal of obesity (2005)* 34.3, pp. 454–461.

Perla, F. M., Prelati, M., Lavorato, M., Visicchio, D., and Anania, C. (June 2017). "The Role of Lipid and Lipoprotein Metabolism in Non-Alcoholic Fatty Liver Disease." In: *Children (Basel, Switzerland)* 4.6, p. 46.

Peter, A., Cegan, A., Wagner, S., Elcnerova, M., Königsrainer, A., Königsrainer, I., Häring, H.-U., Schleicher, E. D., and Stefan, N. (Feb. 2011). "Relationships between hepatic stearoyl-CoA desaturase-1 activity and mRNA expression with liver fat content in humans". In: *American Journal of Physiology-Endocrinology and Metabolism* 300.2, E321–E326.

Piché, M.-E., Parry, S. A., Karpe, F., and Hodson, L. (Jan. 2018). "Chylomicron-Derived Fatty Acid Spillover in Adipose Tissue: A Signature of Metabolic Health?" In: *The Journal of clinical endocrinology and metabolism* 103.1, pp. 25–34.

Pietrantoni, D. and Mayrovitz, H. N. (July 2022). "The Impacts of Sugar-Sweetened Beverages (SSB) on Cardiovascular Health". In: *Cureus* 14.7.

Pompey, S., Zhao, Z., Luby-Phelps, K., and Michaely, P. (Mar. 2013). "Quantitative fluorescence imaging reveals point of release for lipoproteins during LDLR-dependent uptake". In: *Journal of Lipid Research* 54.3, pp. 744–753.

Ponz de Leon, M., Iori, R., Barbolini, G., Pompei, G., Zaniol, P., and Carulli, N. (July 1982). "Influence of Small-Bowel Transit Time on Dietary Cholesterol Absorption in Human Beings". In: *New England Journal of Medicine* 307.2, pp. 102–103.

Pramfalk, C., Jakobsson, T., Verzijl, C. R., Minniti, M. E., Obensa, C., Ripamonti, F., Olin, M., Pedrelli, M., Eriksson, M., and Parini, P. (June 2020). "Generation of new hepatocyte-like in vitro models better resembling human lipid metabolism". In: *Biochimica et biophysica acta. Molecular and cell biology of lipids* 1865.6.

Ramos, M. J., Bandiera, L., Menolascina, F., and Fallowfield, J. A. (Jan. 2022). "In vitro models for non-alcoholic fatty liver disease: Emerging platforms and their applications". In: *iScience* 25.1, p. 103549.

Ray, K. (Nov. 2013). *NAFLD - The next global epidemic.*

Raymond, T. L., Reynolds, S. A., and Swanson, J. A. (Mar. 1986). "Turnover of low-density lipoprotein isolated from interstitial inflammatory fluid of the rabbit". In: *Inflammation* 10.1, pp. 93–98.

Redgrave, T. G., Maranhao, R. C., Tercyak, A. M., Lincoln, E. C., and Brunengraber, H. (Feb. 1988). "Uptake of artificial model remnant lipoprotein emulsions by the perfused rat liver". In: *Lipids* 23.2, pp. 101–105.

Ren, H., Hu, F., Wang, D., Kang, X., Feng, X., Zhang, L., Zhou, B., Liu, S., and Yuan, G. (Aug. 2021). "Sirtuin 2 Prevents Liver Steatosis and Metabolic Disorders by Deacetylation of Hepatocyte Nuclear Factor 4α". In: *Hepatology (Baltimore, Md.)* 74.2, p. 723.

Rich, N. E., Oji, S., Mufti, A. R., Browning, J. D., Parikh, N. D., Odewole, M., Mayo, H., and Singal, A. G. (Feb. 2018). "Racial and Ethnic Disparities in Nonalcoholic Fatty Liver Disease Prevalence, Severity, and Outcomes in the United States: A Systematic Review and Meta-analysis". In: *Clinical Gastroenterology and Hepatology* 16.2, pp. 198–210.

Richieri, G., Ogata, R., and Kleinfeld, A. (Sept. 1994). "Equilibrium constants for the binding of fatty acids with fatty acid-binding proteins from adipocyte, intestine, heart, and liver measured with the fluorescent probe ADIFAB." In: *Journal of Biological Chemistry* 269.39, pp. 23918–23930.

Rinella, M. E., Lazarus, J. V., Ratziu, V., Francque, S. M., Sanyal, A. J., Kanwal, F., Romero, D., Abdelmalek, M. F., Anstee, Q. M., Arab, J. P., Arrese, M., Bataller, R., Beuers, U., Boursier, J., Bugianesi, E., Byrne, C. D., Castro Narro, G. E., Chowdhury, A., Cortez-Pinto, H., Cryer, D. R., Cusi, K., El-Kassas, M., Klein, S., Eskridge, W., Fan, J., Gawrieh, S., Guy, C. D., Harrison, S. A., Kim, S. U., Koot, B. G., Korenjak, M., Kowdley, K. V., Lacaille, F., Loomba, R., Mitchell-Thain, R., Morgan, T. R., Powell, E. E., Roden, M., Romero-Gómez, M., Silva, M., Singh, S. P., Sookoian, S. C., Spearman, C. W., Tiniakos, D., Valenti, L., Vos, M. B., Wong, V. W. S., Xanthakos, S., Yilmaz, Y., Younossi, Z., Hobbs, A., Villota-Rivas, M., and Newsome, P. N. (Dec. 2023). "A multisociety Delphi consensus statement on new fatty liver disease nomenclature". In: *Journal of hepatology* 79.6, pp. 1542–1556.

Robertson, M. D., Parkes, M., Warren, B. F., Ferguson, D. J., Jackson, K. G., Jewell, D. P., and Frayn, K. N. (June 2003). "Mobilisation of enterocyte fat stores by oral glucose in humans". In: *Gut* 52.6, p. 834.

Robinson, M. D. and Oshlack, A. (Mar. 2010). "A scaling normalization method for differential expression analysis of RNA-seq data". In: *Genome Biology* 11.3, pp. 1–9.

Rodríguez, A., Marinelli, R. A., Tesse, A., Frühbeck, G., and Calamita, G. (Nov. 2015). "Sexual Dimorphism of Adipose and Hepatic Aquaglyceroporins in Health and Metabolic Disorders." In: *Frontiers in endocrinology* 6, p. 171.

Rong, X., Wang, B., Dunham, M. M., Hedde, P. N., Wong, J. S., Gratton, E., Young, S. G., Ford, D. A., and Tontonoz, P. (Mar. 2015). "Lpcat3-dependent production of arachidonoyl phospholipids is a key determinant of triglyceride secretion." In: *eLife* 4.4.

Rosqvist, F., Iggman, D., Kullberg, J., Cedernaes, J., Johansson, H.-E., Larsson, A., Johansson, L., Ahlström, H., Arner, P., Dahlman, I., and Risérus, U. (July 2014). "Overfeeding polyunsaturated and saturated fat causes distinct effects on liver and visceral fat accumulation in humans." In: *Diabetes* 63.7, pp. 2356–68.

Ruderman, N. B., Saha, A. K., and Kraegen, E. W. (Dec. 2003). *Minireview: Malonyl CoA, AMP-Activated Protein Kinase, and Adiposity.*

Ryan, M. C., Itsiopoulos, C., Thodis, T., Ward, G., Trost, N., Hofferberth, S., O'Dea, K., Desmond, P. V., Johnson, N. A., and Wilson, A. M. (July 2013). "The Mediterranean diet improves hepatic steatosis and insulin sensitivity in individuals with non-alcoholic fatty liver disease". In: *Journal of Hepatology* 59.1, pp. 138–143.

Saito, M., Hanson, P. I., and Schlesinger, P. (Sept. 2007). "Luminal Chloride-dependent Activation of Endosome Calcium Channels". In: *Journal of Biological Chemistry* 282.37, pp. 27327–27333.

Saltiel, A. R. and Kahn, C. R. (Dec. 2001). "Insulin signalling and the regulation of glucose and lipid metabolism". In: *Nature* 414.6865, pp. 799–806.

Sampson, E. J., Baird, M. A., Burtis, C. A., Smith, E. M., Witte, D. L., and Bayse, D. D. (June 1980). "A coupled-enzyme equilibrium method for measuring urea in serum: optimization and evaluation of the AACC study group on urea candidate reference method." In: *Clinical Chemistry* 26.7, pp. 816–826.

Santhekadur, P. K., Kumar, D. P., and Sanyal, A. J. (Feb. 2018). "Preclinical models of non-alcoholic fatty liver disease". In: *Journal of hepatology* 68.2, pp. 230–237.

Sarkar, A., Ye, A., and Singh, H. (Oct. 2016). "On the role of bile salts in the digestion of emulsified lipids". In: *Food Hydrocolloids* 60, pp. 77–84.

Schindelin, J., Arganda-Carreras, I., Frise, E., Kaynig, V., Longair, M., Pietzsch, T., Preibisch, S., Rueden, C., Saalfeld, S., Schmid, B., Tinevez, J.-Y., White, D. J., Hartenstein, V., Eliceiri, K., Tomancak, P., and Cardona, A. (July 2012). "Fiji: an open-source platform for biological-image analysis". In: *Nature Methods* 9.7, pp. 676–682.

Schmidt, N. H., Svendsen, P., Albarrán-Juárez, J., Moestrup, S. K., and Bentzon, J. F. (Feb. 2021). "High-fructose feeding does not induce steatosis or non-alcoholic fatty liver disease in pigs". In: *Scientific Reports 2021 11:1* 11.1, pp. 1–10.

Schneider, C. A., Rasband, W. S., and Eliceiri, K. W. (June 2012). "NIH Image to ImageJ: 25 years of image analysis". In: *Nature Methods 2012 9:7* 9.7, pp. 671–675.

Schutz, Y. (Sept. 1995). "Macronutrients and energy balance in obesity". In: *Metabolism* 44.SUPPL. 3, pp. 7–11.

Šeda, O., Cahová, M., Míková, I., Šedová, L., Daňková, H., Heczková, M., Brátová, M., Ďásková, N., Erhartová, D., Čapek, V., Chylíková, B., and Trunečka, P. (Apr. 2019). "Hepatic Gene Expression Profiles Differentiate Steatotic and Non-steatotic Grafts in Liver Transplant Recipients." In: *Frontiers in endocrinology* 10, p. 270.

Semmler, G., Datz, C., Reiberger, T., and Trauner, M. (Oct. 2021). "Diet and exercise in NAFLD/NASH: Beyond the obvious". In: *Liver international : official journal of the International Association for the Study of the Liver* 41.10, pp. 2249–2268.

Setyaningsih, W. A. W., Sari, D. C. R., Romi, M. M., and Arfian, N. (May 2021). "Liver fibrosis associated with adipose tissue and liver inflammation in an obesity model." In: *The Medical journal of Malaysia* 76.3, pp. 304–310.

Shimomura, I., Bashmakov, Y., and Horton, J. D. (Oct. 1999). "Increased levels of nuclear SREBP-1c associated with fatty livers in two mouse models of diabetes mellitus". In: *The Journal of biological chemistry* 274.42, pp. 30028–30032.

Simonian, H. P., Kresge, K. M., Boden, G. H., and Parkman, H. P. (June 2005). "Differential effects of sham feeding and meal ingestion on ghrelin and pancreatic polypeptide levels: evidence for vagal efferent stimulation mediating ghrelin release1". In: *Neurogastroenterology & Motility* 17.3, pp. 348–354.

Sinha, N., Suarez-Diez, M., Van Schothorst, E. M., Keijer, J., Dos Santos, V. A., and Hooiveld, G. J. (Aug. 2017). "Predicting the murine enterocyte metabolic response to

diets that differ in lipid and carbohydrate composition". In: *Scientific Reports 2017 7:1* 7.1, pp. 1–11.

Snel, M., Jonker, J. T., Schoones, J., Lamb, H., Roos, A. de, Pijl, H., Smit, J. W. A., Meinders, A. E., and Jazet, I. M. (2012). "Ectopic fat and insulin resistance: pathophysiology and effect of diet and lifestyle interventions." In: *International journal of endocrinology* 2012, p. 983814.

Sokoła-Wysoczańska, E., Wysoczański, T., Wagner, J., Czyż, K., Bodkowski, R., Lochyński, S., and Patkowska-Sokoła, B. (Oct. 2018). "Polyunsaturated Fatty Acids and Their Potential Therapeutic Role in Cardiovascular System Disorders—A Review". In: *Nutrients* 10.10, p. 1561.

Sookoian, S. and Pirola, C. J. (Feb. 2023). "Genetics in non-alcoholic fatty liver disease: The role of risk alleles through the lens of immune response." In: *Clinical and molecular hepatology* 29, S184–S195.

— (Mar. 2017). "Genetic predisposition in nonalcoholic fatty liver disease". In: *Clinical and Molecular Hepatology* 23.1, pp. 1–12.

Sousa-Victor, P., Neves, J., Cedron-Craft, W., Ventura, P. B., Liao, C. Y., Riley, R. R., Soifer, I., Bruggen, N. van, Kolumam, G. A., Villeda, S. A., Lamba, D. A., and Jasper, H. (Feb. 2019). "MANF regulates metabolic and immune homeostasis in ageing and protects against liver damage". In: *Nature metabolism* 1.2, pp. 276–290.

Stahl, A., Hirsch, D. J., Gimeno, R. E., Punreddy, S., Ge, P., Watson, N., Patel, S., Kotler, M., Raimondi, A., Tartaglia, L. A., and Lodish, H. F. (Sept. 1999). "Identification of the major intestinal fatty acid transport protein." In: *Molecular cell* 4.3, pp. 299–308.

Steiner, G. and Lewis, G. (July 1996). "Hyperinsulinemia and Triglyceride-Rich Lipoproteins". In: *Diabetes* 45.Supplement_3, S24–S26.

Stirling, D. R., Swain-Bowden, M. J., Lucas, A. M., Carpenter, A. E., Cimini, B. A., and Goodman, A. (Dec. 2021). "CellProfiler 4: improvements in speed, utility and usability". In: *BMC Bioinformatics* 22.1, pp. 1–11.

Su, R. C., Lad, A., Breidenbach, J. D., Blomquist, T. M., Gunning, W. T., Dube, P., Kleinhenz, A. L., Malhotra, D., Haller, S. T., and Kennedy, D. J. (Dec. 2019). "Hyperglycemia induces key genetic and phenotypic changes in human liver epithelial HepG2 cells which parallel the Leprdb/J mouse model of non-alcoholic fatty liver disease (NAFLD)". In: *PLoS ONE* 14.12.

Su, W., Wang, Y., Jia, X., Wu, W., Li, N., Tian, X., Li, S., Wang, C., Xu, H., Cao, J., Han, Q., Xu, S., Chen, Y., Zhong, Y., Zhang, X., Liu, P., Gustafsson, J. Å., and Guan, Y. (Aug. 2014). "Comparative proteomic study reveals 17β-HSD13 as a pathogenic protein in nonalcoholic fatty liver disease". In: *Proceedings of the National Academy of Sciences of the United States of America* 111.31, pp. 11437–11442.

Subudhi, S., Drescher, H. K., Dichtel, L. E., Bartsch, L. M., Chung, R. T., Hutter, M. M., Gee, D. W., Meireles, O. R., Witkowski, E. R., Gelrud, L., Masia, R., Osganian, S. A., Gustafson, J. L., Rwema, S., Bredella, M. A., Bhatia, S. N., Warren, A., Miller, K. K., Lauer, G. M., and Corey, K. E. (Jan. 2022). "Distinct Hepatic Gene-Expression Patterns of NAFLD in Patients With Obesity". In: *Hepatology Communications* 6.1, p. 77.

Sveinbjornsson, G., Ulfarsson, M. O., Thorolfsdottir, R. B., Jonsson, B. A., Einarsson, E., Gunnlaugsson, G., Rognvaldsson, S., Arnar, D. O., Baldvinsson, M., Bjarnason, R. G., Eiriksdottir, T., Erikstrup, C., Ferkingstad, E., Halldorsson, G. H., Helgason, H., Helgadottir, A., Hindhede, L., Hjorleifsson, G., Jones, D., Knowlton, K. U., Lund, S. H., Melsted, P., Norland, K., Olafsson, I., Olafsson, S.,

Oskarsson, G. R., Ostrowski, S. R., Pedersen, O. B., Snaebjarnarson, A. S., Sigurdsson, E., Steinthorsdottir, V., Schwinn, M., Thorgeirsson, G., Thorleifsson, G., Jonsdottir, I., Bundgaard, H., Nadauld, L., Bjornsson, E. S., Rulifson, I. C., Rafnar, T., Norddahl, G. L., Thorsteinsdottir, U., Sulem, P., Gudbjartsson, D. F., Holm, H., and Stefansson, K. (Nov. 2022). "Multiomics study of nonalcoholic fatty liver disease". In: *Nature Genetics* 54.11, pp. 1652–1663.

Tabas, I., Lim, S., Xu, X. X., and Maxfield, F. R. (Sept. 1990). "Endocytosed beta-VLDL and LDL are delivered to different intracellular vesicles in mouse peritoneal macrophages." In: *The Journal of cell biology* 111.3, pp. 929–40.

Takahashi, S. (June 2017). "Triglyceride Rich Lipoprotein -LPL-VLDL Receptor and Lp(a)-VLDL Receptor Pathways for Macrophage Foam Cell Formation." In: *Journal of atherosclerosis and thrombosis* 24.6, pp. 552–559.

Teng, M. L., Ng, C. H., Huang, D. Q., Chan, K. E., Tan, D. J., Lim, W. H., Yang, J. D., Tan, E., and Muthiah, M. D. (Feb. 2023). "Global incidence and prevalence of nonalcoholic fatty liver disease". In: *Clinical and Molecular Hepatology* 29.Suppl, S32.

Teufel, A., Itzel, T., Erhart, W., Brosch, M., Wang, X. Y., Kim, Y. O., Schönfels, W. von, Herrmann, A., Brückner, S., Stickel, F., Dufour, J. F., Chavakis, T., Hellerbrand, C., Spang, R., Maass, T., Becker, T., Schreiber, S., Schafmayer, C., Schuppan, D., and Hampe, J. (Sept. 2016). "Comparison of Gene Expression Patterns Between Mouse Models of Nonalcoholic Fatty Liver Disease and Liver Tissues From Patients". In: *Gastroenterology* 151.3, pp. 513–525.

Thampy, K. G. and Wakil, S. J. (1988). "Regulation of Acetyl-coenzyme A Carboxylase 11". In: *Journal of Biological Chemistry* 263.13, pp. 6454–6458.

Tian, L., Prasad, N., and Jang, Y. Y. (July 2016). "In Vitro Modeling of Alcohol-Induced Liver Injury using Human-Induced Pluripotent Stem Cells". In: *Methods in Molecular Biology* 1353, pp. 271–283.

Timlin, M. T. and Parks, E. J. (Jan. 2005). "Temporal pattern of de novo lipogenesis in the postprandial state in healthy men." In: *The American journal of clinical nutrition* 81.1, pp. 35–42.

Titchenell, P. M., Lazar, M. A., and Birnbaum, M. J. (July 2017). "Unraveling the Regulation of Hepatic Metabolism by Insulin". In: *Trends in endocrinology and metabolism: TEM* 28.7, pp. 497–505.

Titchenell, P. M., Quinn, W. J., Lu, M., Chu, Q., Lu, W., Li, C., Chen, H., Monks, B. R., Chen, J., Rabinowitz, J. D., and Birnbaum, M. J. (June 2016). "Direct Hepatocyte Insulin Signaling Is Required for Lipogenesis but Is Dispensable for the Suppression of Glucose Production". In: *Cell Metabolism* 23.6, pp. 1154–1166.

Tollin, C., Ericsson, M., Johnson, O., and Backman, C. (Jan. 1985). "Clearance of triglycerides from the circulation and its relationship to serum lipoproteins: influence of age and sex". In: *Scandinavian Journal of Clinical and Laboratory Investigation* 45.8, pp. 679–684.

Townsend, L. K., Medak, K. D., Peppler, W. T., Meers, G. M., Rector, R. S., LeBlanc, P. J., and Wright, D. C. (July 2019). "High-saturated-fat diet-induced obesity causes hepatic interleukin-6 resistance via endoplasmic reticulum stress." In: *Journal of lipid research* 60.7, pp. 1236–1249.

Tran, T. T. T., Poirier, H., Clément, L., Nassir, F., Pelsers, M. M., Petit, V., Degrace, P., Monnot, M. C., Glatz, J. F., Abumrad, N. A., Besnard, P., and Niot, I. (July 2011). "Luminal lipid regulates CD36 levels and downstream signaling to stimulate chylomicron synthesis". In: *The Journal of biological chemistry* 286.28, pp. 25201–25210.

Trefts, E., Gannon, M., and Wasserman, D. H. (Nov. 2017). *The liver*.

Tso, P. and Balint, J. A. (June 1986). "Formation and transport of chylomicrons by enterocytes to the lymphatics." In: *The American journal of physiology* 250.6 Pt 1, pp. 715–26.

Unger, A. L., Torres-Gonzalez, M., and Kraft, J. (Sept. 2019). "Dairy Fat Consumption and the Risk of Metabolic Syndrome: An Examination of the Saturated Fatty Acids in Dairy". In: *Nutrients* 11.9.

Valenti, L., Tripodi, A., La Mura, V., Pelusi, S., Bianco, C., Scalambrino, E., Margarita, S., Malvestiti, F., Ronzoni, L., Clerici, M., D'Ambrosio, R., Fraquelli, M., Carpani, R., Prati, D., and Peyvandi, F. (Dec. 2022). "Clinical and genetic determinants of the fatty liver-coagulation balance interplay in individuals with metabolic dysfunction." In: *JHEP reports : innovation in hepatology* 4.12, p. 100598.

Varlamov, O. (May 2017). "Western-style diet, sex steroids and metabolism". In: *Biochimica et biophysica acta. Molecular basis of disease* 1863.5, pp. 1147–1155.

Vega-López, S., Venn, B. J., and Slavin, J. L. (Oct. 2018). "Relevance of the Glycemic Index and Glycemic Load for Body Weight, Diabetes, and Cardiovascular Disease". In: *Nutrients* 10.10.

Vekemans, K. and Braet, F. (Sept. 2005). "Structural and functional aspects of the liver and liver sinusoidal cells in relation to colon carcinoma metastasis". In: *World Journal of Gastroenterology : WJG* 11.33, p. 5095.

Verweij, N., Haas, M. E., Nielsen, J. B., Sosina, O. A., Kim, M., Akbari, P., De, T., Hindy, G., Bovijn, J., Persaud, T., Miloscio, L., Germino, M., Panagis, L., Watanabe, K., Mbatchou, J., Jones, M., LeBlanc, M., Balasubramanian, S., Lammert, C., Enhörning, S., Melander, O., Carey, D. J., Still, C. D., Mirshahi, T., Rader, D. J., Parasoglou, P., Walls, J. R., Overton, J. D., Reid, J. G., Economides, A., Cantor, M. N., Zambrowicz, B., Murphy, A. J., Abecasis, G. R., Ferreira, M. A., Smagris, E., Gusarova, V., Sleeman, M., Yancopoulos, G. D., Marchini, J., Kang, H. M., Karalis, K., Shuldiner, A. R., Della Gatta, G., Locke, A. E., Baras, A., and Lotta, L. A. (July 2022). " Germline Mutations in CIDEB and Protection against Liver Disease ". In: *New England Journal of Medicine* 387.4, pp. 332–344.

Vilar-Gomez, E., Martinez-Perez, Y., Calzadilla-Bertot, L., Torres-Gonzalez, A., Gra-Oramas, B., Gonzalez-Fabian, L., Friedman, S. L., Diago, M., and Romero-Gomez, M. (Aug. 2015). "Weight Loss Through Lifestyle Modification Significantly Reduces Features of Nonalcoholic Steatohepatitis". In: *Gastroenterology* 149.2, pp. 367–378.

Virović-Jukić, L., Stojsavljević-Shapeski, S., Forgač, J., Kukla, M., and Mikolašević, I. (Feb. 2021). "Non-alcoholic fatty liver disease – a procoagulant condition?" In: *Croatian Medical Journal* 62.1, p. 25.

Vlachos, D., Malisova, S., Lindberg, F. A., and Karaniki, G. (June 2020). "Glycemic Index (GI) or Glycemic Load (GL) and Dietary Interventions for Optimizing Postprandial Hyperglycemia in Patients with T2 Diabetes: A Review". In: *Nutrients* 12.6.

Vusse, G. J. van der (May 2009). "Albumin as Fatty Acid Transporter". In: *Drug Metabolism and Pharmacokinetics* 24.4, pp. 300–307.

Walle, P., Takkunen, M., Männistö, V., Vaittinen, M., Lankinen, M., Kärjä, V., Käkelä, P., Ågren, J., Tiainen, M., Schwab, U., Kuusisto, J., Laakso, M., and Pihlajamäki, J. (May 2016). "Fatty acid metabolism is altered in non-alcoholic steatohepatitis independent of obesity". In: *Metabolism: clinical and experimental* 65.5, pp. 655–666.

Wanders, R. J., Baes, M., Ribeiro, D., Ferdinandusse, S., and Waterham, H. R. (Jan. 2023). "The physiological functions of human peroxisomes". In: *Physiological reviews* 103.1, pp. 957–1024.

Wang, D., Wei, Y., and Pagliassotti, M. J. (Feb. 2006). "Saturated fatty acids promote endoplasmic reticulum stress and liver injury in rats with hepatic steatosis". In: *Endocrinology* 147.2, pp. 943–951.

Wang, T. Y., Liu, M., Portincasa, P., and Wang, D. Q. (Nov. 2013). "New insights into the molecular mechanism of intestinal fatty acid absorption". In: *European journal of clinical investigation* 43.11, p. 1203.

Wang, Y., Chen, C., Chen, J., Sang, T., Peng, H., Lin, X., Zhao, Q., Chen, S., Eling, T., and Wang, X. (June 2022). "Overexpression of NAG-1/GDF15 prevents hepatic steatosis through inhibiting oxidative stress-mediated dsDNA release and AIM2 inflammasome activation". In: *Redox biology* 52.

Weber, F., Treeck, O., Mester, P., and Buechler, C. (Feb. 2023). "Expression and Function of BMP and Activin Membrane-Bound Inhibitor (BAMBI) in Chronic Liver Diseases and Hepatocellular Carcinoma". In: *International journal of molecular sciences* 24.4.

Weston, S. R., Leyden, W., Murphy, R., Bass, N. M., Bell, B. P., Manos, M. M., and Terrault, N. A. (Feb. 2005). "Racial and ethnic distribution of nonalcoholic fatty liver in persons with newly diagnosed chronic liver disease." In: *Hepatology (Baltimore, Md.)* 41.2, pp. 372–9.

White, J. S., Basu, S., Kaplan, S., Madsen, K. A., Villas-Boas, S. B., and Schillinger, D. (Apr. 2023). "Evaluation of the sugar-sweetened beverage tax in Oakland, United States, 2015–2019: A quasi-experimental and cost-effectiveness study". In: *PLOS Medicine* 20.4, pp. 2015–2019.

Wilfling, F., Wang, H., Haas, J. T., Krahmer, N., Gould, T. J., Uchida, A., Cheng, J. X., Graham, M., Christiano, R., Fröhlich, F., Liu, X., Buhman, K. K., Coleman, R. A., Bewersdorf, J., Farese, R. V., and Walther, T. C. (Feb. 2013). "Triacylglycerol synthesis enzymes mediate lipid droplet growth by relocalizing from the ER to lipid droplets". In: *Developmental Cell* 24.4, pp. 384–399.

Wilson, C. G., Tran, J. L., Erion, D. M., Vera, N. B., Febbraio, M., and Weiss, E. J. (Feb. 2016). "Hepatocyte-Specific Disruption of CD36 Attenuates Fatty Liver and Improves Insulin Sensitivity in HFD-Fed Mice". In: *Endocrinology* 157.2, pp. 570–585.

Wolfe, R. R. (Mar. 1998). "Metabolic interactions between glucose and fatty acids in humans." In: *The American journal of clinical nutrition* 67.3 Suppl, 519S–526S.

Worm, N. (May 2020). "Beyond Body Weight-Loss: Dietary Strategies Targeting Intrahepatic Fat in NAFLD". In: *Nutrients* 12.5, p. 1316.

Xiang, C., Du, Y., Meng, G., Yi, L. S., Sun, S., Song, N., Zhang, X., Xiao, Y., JieWan, J., Yi, Z., Liu, Y., Xie, B., Wu, M., Shu, J., Sun, D., Jia, J., Liang, Z., Sun, D., Huang, Y., Shi, Y., Xu, J., Lu, F., Li, C., Xiang, K., Yuan, Z., Lu, S., and Deng, H. (2019). "Long-term functional maintenance of primary human hepatocytes in vitro". In: *Science (New York, N.Y.)* 364.6438, pp. 399–402.

Xiao, C., Stahel, P., and Lewis, G. F. (Jan. 2019). "Regulation of Chylomicron Secretion: Focus on Post-Assembly Mechanisms". In: *Cellular and Molecular Gastroenterology and Hepatology* 7.3, pp. 487–501.

Xiao, Y., Liu, D., Cline, M. A., and Gilbert, E. R. (Dec. 2020). *Chronic stress, epigenetics, and adipose tissue metabolism in the obese state.*

Xu, G., Wu, M., Zhang, J., Guo, F., Liu, Y., Gong, J., Yan, F., and Yan, J. (Sept. 2023). "Interferon-γ mediating overexpression of polymeric immunoglobulin receptor in grass

carp (Ctenopharyngodon idellus) liver cells". In: *Developmental & Comparative Immunology* 146, p. 104746.

Yamauchi, T. and Kadowaki, T. (Feb. 2013). "Adiponectin receptor as a key player in healthy longevity and obesity-related diseases". In: *Cell metabolism* 17.2, pp. 185–196.

Yan, J., Liu, Q., Tang, Q., Zhang, J., Jing, X., Xia, Y., Xu, Y., Li, J., Li, Y., and He, J. (June 2022). "Mesencephalic astrocyte-derived neurotrophic factor alleviates non-alcoholic steatohepatitis induced by Western diet in mice". In: *The FASEB Journal* 36.6, e22349.

Yao, X., Xia, F., Tang, W., Xiao, C., Yang, M., and Zhou, B. (Feb. 2018). "Isobaric tags for relative and absolute quantitation (iTRAQ)-based proteomics for the investigation of the effect of Hugan Qingzhi on non-alcoholic fatty liver disease in rats". In: *Journal of Ethnopharmacology* 212, pp. 208–215.

Yin, C., Evason, K. J., Asahina, K., and Stainier, D. Y. (May 2013). "Hepatic stellate cells in liver development, regeneration, and cancer". In: *The Journal of Clinical Investigation* 123.5, p. 1902.

Yki-Järvinen, H., Luukkonen, P. K., Hodson, L., and Moore, J. B. (Nov. 2021). "Dietary carbohydrates and fats in nonalcoholic fatty liver disease". In: *Nature reviews. Gastroenterology & hepatology* 18.11, pp. 770–786.

Younossi, Z. M., Blissett, D., Blissett, R., Henry, L., Stepanova, M., Younossi, Y., Racila, A., Hunt, S., and Beckerman, R. (Nov. 2016a). "The economic and clinical burden of nonalcoholic fatty liver disease in the United States and Europe". In: *Hepatology* 64.5, pp. 1577–1586.

Younossi, Z. M., Gramlich, T., Matteoni, C. A., Boparai, N., and McCullough, A. J. (Mar. 2004). "Nonalcoholic fatty liver disease in patients with type 2 diabetes". In: *Clinical Gastroenterology and Hepatology* 2.3, pp. 262–265.

Younossi, Z. M., Koenig, A. B., Abdelatif, D., Fazel, Y., Henry, L., and Wymer, M. (July 2016b). "Global epidemiology of nonalcoholic fatty liver disease-Meta-analytic assessment of prevalence, incidence, and outcomes". In: *Hepatology (Baltimore, Md.)* 64.1, pp. 73–84.

Yu, S., Li, C., Ji, G., and Zhang, L. (Nov. 2021). "The Contribution of Dietary Fructose to Non-alcoholic Fatty Liver Disease". In: *Frontiers in Pharmacology* 12, p. 783393.

Zechner, R., Madeo, F., and Kratky, D. (Aug. 2017). "Cytosolic lipolysis and lipophagy: two sides of the same coin". In: *Nature Reviews Molecular Cell Biology 2017 18:11* 18.11, pp. 671–684.

Zeilinger, K., Freyer, N., Damm, G., Seehofer, D., and Knöspel, F. (Sept. 2016). "Cell sources for in vitro human liver cell culture models". In: *Experimental biology and medicine (Maywood, N.J.)* 241.15, pp. 1684–1698.

Zeissig, S., Dougan, S. K., Barral, D. C., Junker, Y., Chen, Z., Kaser, A., Ho, M., Mandel, H., McIntyre, A., Kennedy, S. M., Painter, G. F., Veerapen, N., Besra, G. S., Cerundolo, V., Yue, S., Beladi, S., Behar, S. M., Chen, X., Gumperz, J. E., Breckpot, K., Raper, A., Baer, A., Exley, M. A., Hegele, R. A., Cuchel, M., Rader, D. J., Davidson, N. O., and Blumberg, R. S. (Aug. 2010). "Primary deficiency of microsomal triglyceride transfer protein in human abetalipoproteinemia is associated with loss of CD1 function". In: *The Journal of Clinical Investigation* 120.8, p. 2889.

Zeng, H., Qin, H., Liao, M., Zheng, E., Luo, X., Xiao, A., Li, Y., Chen, L., Wei, L., Zhao, L., Ruan, X. Z., Yang, P., and Chen, Y. (Mar. 2022). "CD36 promotes de novo lipogenesis in hepatocytes through INSIG2-dependent SREBP1 processing". In: *Molecular metabolism* 57.

Zhang, D. and Yin, L. (Jan. 2015). "Transcriptional regulation of de novo lipogenesis in liver". In: *Hepatic De Novo Lipogenesis and Regulation of Metabolism*. Springer International Publishing, pp. 1–31.

Zhang, F., Zarkada, G., Han, J., Li, J., Dubrac, A., Ola, R., Genet, G., Boyé, K., Michon, P., Künzel, S. E., Camporez, J. P., Singh, A. K., Fong, G. H., Simons, M., Tso, P., Fernández-Hernando, C., Shulman, G. I., Sessa, W. C., and Eichmann, A. (Aug. 2018). "Lacteal junction zippering protects against diet-induced obesity". In: *Science* 361.6402, pp. 599–603.

Zhang, L., Wang, P., Shi, M., Fang, Z., Ji, J., Liao, X., Hu, X., and Chen, F. (June 2020). "The modulation of Luffa cylindrica (L.) Roem supplementation on gene expression and amino acid profiles in liver for alleviating hepatic steatosis via gut microbiota in high-fat diet-fed mice: insight from hepatic transcriptome analysis". In: *The Journal of nutritional biochemistry* 80.

Zhang, Y. L., Hernandez-Ono, A., Ko, C., Yasunaga, K., Huang, L. S., and Ginsberg, H. N. (Apr. 2004). "Regulation of hepatic apolipoprotein B-lipoprotein assembly and secretion by the availability of fatty acids. I. Differential response to the delivery of fatty acids via albumin or remnant-like emulsion particles". In: *The Journal of biological chemistry* 279.18, pp. 19362–19374.

Zhao, Z. and Michaely, P. (Aug. 2009). "The role of calcium in lipoprotein release by the low-density lipoprotein receptor". In: *Biochemistry* 48.30, pp. 7313–7324.